PRE-STACK MIGRATION IN TWO AND THREE DIMENSIONS

PROEFSCHRIFT ter verkrijging van
de graad van doctor in de
technische wetenschappen
aan de Technische Hogeschool Delft,
op gezag van de Rector Magnificus,
prof.dr. J.M. Dirken,
in het openbaar te
verdedigen ten overstaan
van het College van Dekanen op
donderdag 6 februari 1986
te 16.00 uur door

CORNELIS PIETER ARIE WAPENAAR

geboren te Vlaardingen
natuurkundig ingenieur

BIBLIOTHEEK TECHNISCHE UNIVERSITEIT
Prom[illegible]plein 1
DELFT

Gebotekst Zoetermeer/1986

TR diss
1471

Dit proefschrift is goedgekeurd door de promotor
prof.dr.ir. A.J. Berkhout

Ter nagedachtenis van mijn vader

PREFACE

The main purpose of the research project which led to this thesis, was to develop three-dimensional (3-D) seismic migration techniques. From a theoretical point of view 3-D migration is not much more complicated than 2-D migration. However, the problems related to the practical implementation of 'just one more dimension' are significant.

In 1982, when this project was initiated, the group of Seismics and Acoustics did not have the appropriate computer facilities at its disposal, so a seismic work-station, dedicated to heavy migration tasks, had to be developed. In the meantime, I had the opportunity to reflect on seismic techniques in general and on pre-stack migration in particular. The results of these reflections are presented in the theoretical chapters of this thesis and in two geophysical journals. By the time that the work-station was operational my promotor and I decided that the emphasis of the 3-D migration research should be shifted from post-stack (pseudo zero-offset) towards pre-stack (genuine multi-offset) applications in order to meet the ever increasing needs of the seismic industry. Again there was the problem how to implement one more (offset) dimension.

Therefore, in January 1986, we initiated a new project, sponsored by the seismic industry, on 3-D target oriented migration (TRITON). With this project we aim to solve the 3-D pre-stack migration problem. The results of an extensive feasibility study, carried out with the aid of the seismic work-station as well as a Cray XMP computer, are presented in the final chapter of this thesis.

I would like to take the opportunity to thank my family and all my friends and colleagues for their moral support. In particular I wish to express my sincere gratitude to my promotor, professor Berkhout, for his ever continuing enthusiasm, which has been very stimulating throughout my stay in his research group. Also many thanks are due to Jan Ridder for his professional advice in hardware affairs and to Edo Bergsma and Rob Verschoor for developing the seismic work-station.

I am very much obliged to various people in our group who developed much of the software; in particular I refer to the excellent work of Niels Kinneging and Gerrit Blacquière, who are presently my colleagues in the TRITON project, and Yann Parrod, who visited our group, sponsored by Elf Aquitaine.

I thank the people in the project groups of Jan Vogel and Gerard Faber for providing the facilities for the watertank experiment; in particular I must mention Theo Modderman who carried out the measurements.
I thank Bram de Knegt of the drawing department for his enthusiastic support, Mr. A.R. Suiters of the photographic department and Mrs. Gerda Boone of 'Gebotekst' for preparing the final manuscript. Finally I would like to thank our secretary Mrs. Hanneke Mulder for her friendly support and all the type-writing during my stay in the group.
The investigations were supported by the Netherlands Foundation for Earth Science Research (AWON) with financial aid from the Netherlands Technology Foundation (STW, grant DGE 14.0169). Computational support was given by Cray Research, Inc.

Delft, February 1986

CONTENTS

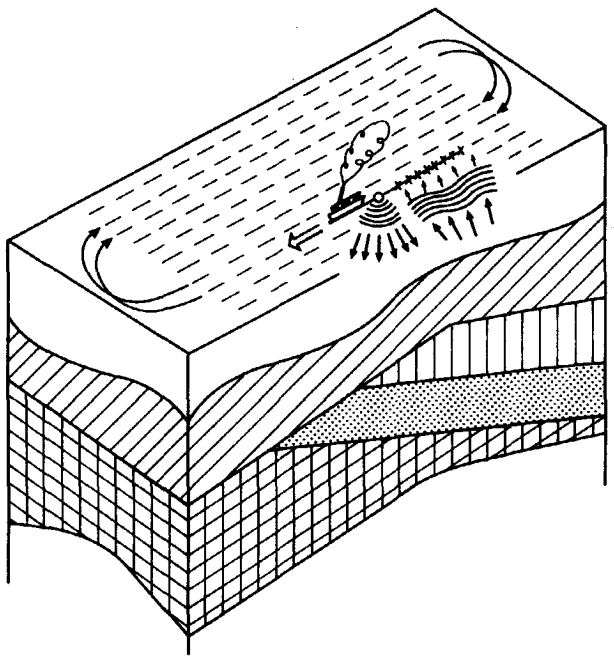

Figure I-1: In 3-D seismics, data are often gathered along straight lines. Along each line many seismic experiments are carried out for different positions of the seismic source. In each seismic experiment many seismic signals are registered by the seismic detectors.

a. A typical 3-D marine survey.

CHAPTER I

GENERAL ASPECTS OF SEISMIC INVERSION

I.1 INTRODUCTION

Exploration seismology is based on analysis of seismic waves reflected from different layers in the earth's subsurface. Seismic waves, radiated by a seismic source into the subsurface, encounter discontinuities between the layers and are partially reflected back to the surface. The returning reflected waves, which contain indirect information on the elastic parameters of the subsurface, are detected and stored on magnetic tapes. Generally many seismic experiments are carried out for different positions of the seismic source. A typical three-dimensional (3-D) marine survey is visualized in Figure I-1a. A schematic representation of seismic data acquisition is shown in Figure I-1b.

Historically, two diverging approaches to seismic inversion have been developed: inversion in terms of '**inverse scattering**' aims at resolving the elastic parameters of the earth's subsurface from seismic measurements; inversion in terms of '**seismic migration**' aims at resolving a structural image of the subsurface from seismic measurements (see Figure I-1c).

The inverse scattering approach is rigorously founded on the principles of wave theory. However, in many schemes strongly simplifying assumptions are made with respect to the elastic parameters of the earth's subsurface: in 'Born inversion' often a homogeneous background medium is assumed.

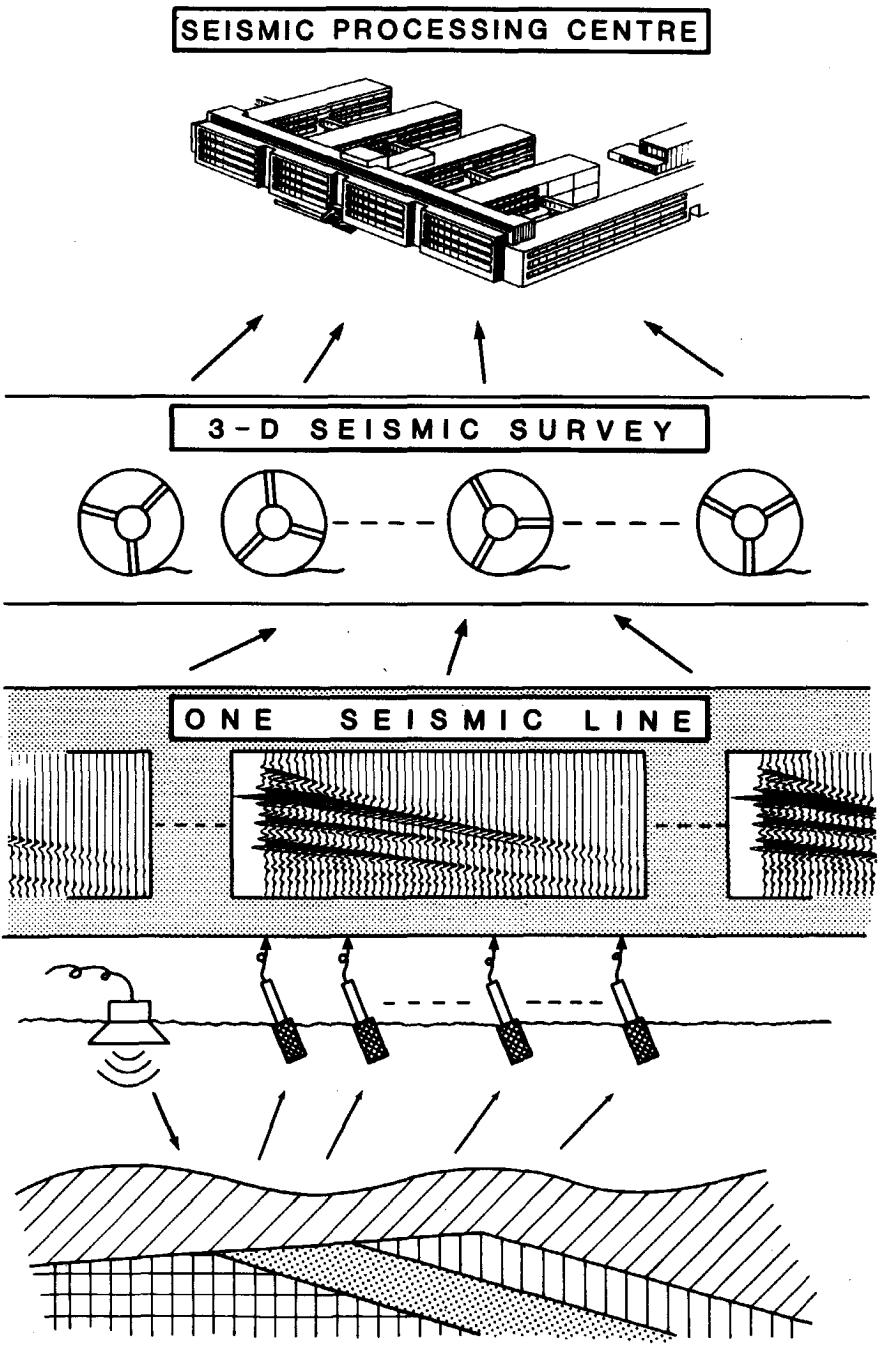

Figure I-1: (continued)

b. Schematic representation of seismic data acquisition.

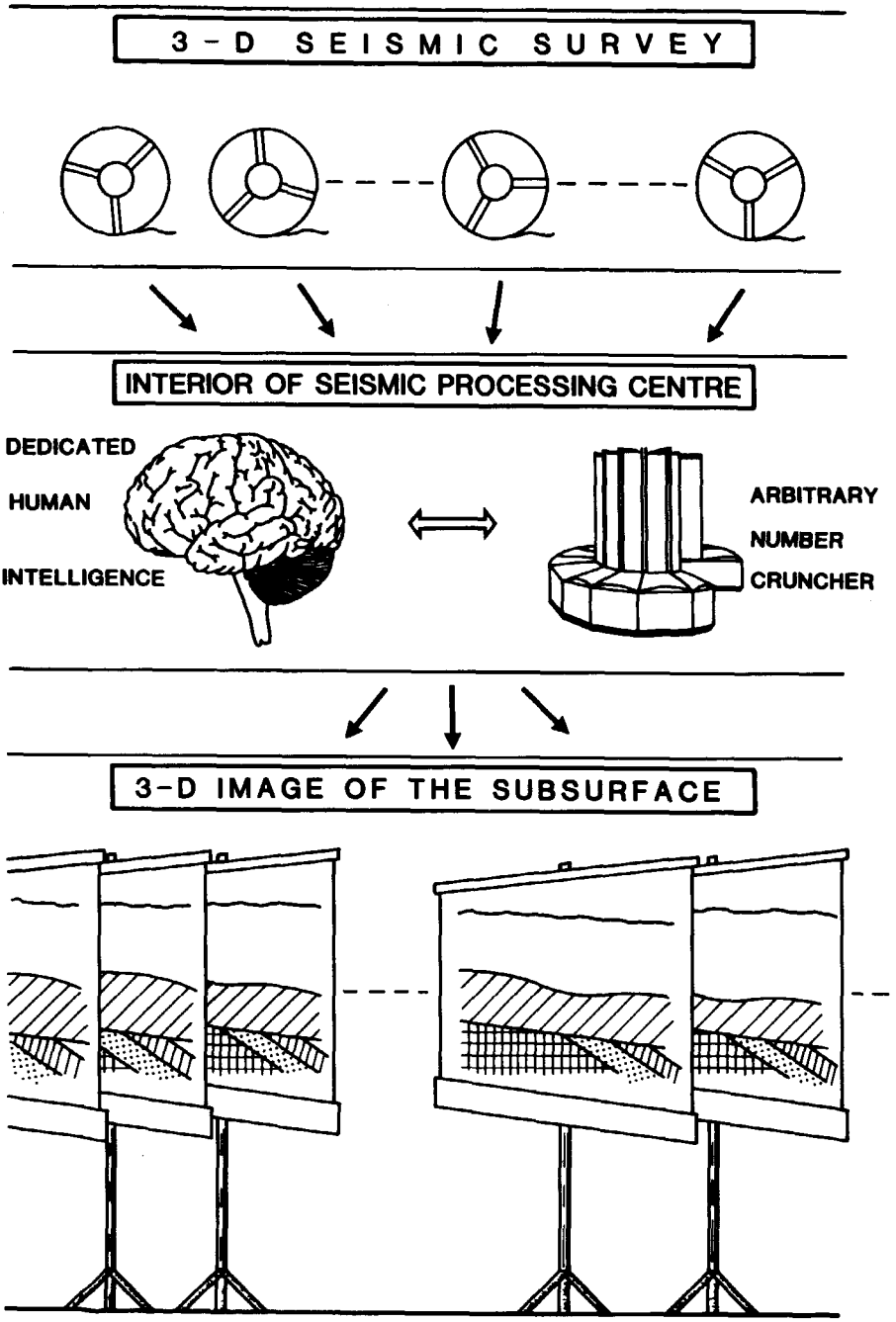

Figure I-1: (continued)

c. Schematic representation of seismic inversion (in terms of seismic migration).

The seismic migration approach, on the other hand, accounts for the complex geology of the earth's subsurface. In post-stack migration, however, strongly simplifying assumptions are made with respect to the propagation mechanism of seismic waves through the subsurface: it is assumed that the waves are generated by secondary sources in the subsurface ('exploding reflectors'), and that these waves travel with half the actual propagation velocity. In spite of these simplifications, post-stack migration is widely applied by the oil industries because it has proved itself a successful tool in the search for oil and gas.

In the last decades most of the large obvious oil and gas fields have been found and new, more sophisticated seismic inversion techniques are required to explore fields in complex subsurface structures. It is argued by Berkhout (1986) that major improvements of seismic inversion schemes can only be accomplished by thoroughly reconsidering the underlying assumptions. He discusses a new approach to seismic inversion in which seismic migration and inverse scattering converge to two equivalent interchangeable sub-processes. In this introductory chapter the basics of this approach are outlined and several new aspects are introduced. It is argued that full pre-stack migration in two or three dimensions (the subject of this thesis) is a very promising seismic inversion technique.

I.2 INVERSE SCATTERING VERSUS SEISMIC MIGRATION

Irrespective of the approach to seismic inversion it is always necessary to make some assumptions concerning the elastic parameters of the subsurface. In the following we assume that the medium can be described completely in terms of the bulk compression modulus K, the shear modulus μ and the mass density ρ*.

*) Actually we should speak of the mechanical parameters, because the mass density is not an elastic parameter. It is common practice in seismics, however, to speak of the **elastic** parameters K, μ and ρ of a solid, opposed to the **acoustic** parameters K and ρ of a liquid. An equivalent alternative set of parameters to describe the medium, which is frequently used in seismic practice, consists of the compressional wave velocity c_P, the shear wave velocity c_S and the mass density ρ for a solid, opposed to c_P and ρ for a liquid.

No further approximation is made if we define the elastic parameters as a superposition of background and deviation parameters, according to

$$K = \bar{K} + \Delta K,$$
$$\mu = \bar{\mu} + \Delta\mu,$$
$$\rho = \bar{\rho} + \Delta\rho.$$

A very natural choice is a geologically oriented background or reference medium (Berkhout, 1984b), which implies that the deviation parameters can be kept small. Such a geologically oriented background medium is called the elastic **macro** model of the subsurface. An example is given in Figure I-2. Notice that within each macro layer the background medium parameters $\bar{K}$, $\bar{\mu}$ and $\bar{\rho}$ may be functions of the spatial coordinates x, y and z. (For comparison, many Born-type inverse scattering techniques assume a homogeneous background medium and small deviation parameters, which is far from geologic reality). The deviation parameters ΔK, $\Delta\mu$ and $\Delta\rho$, which are also functions of the spatial

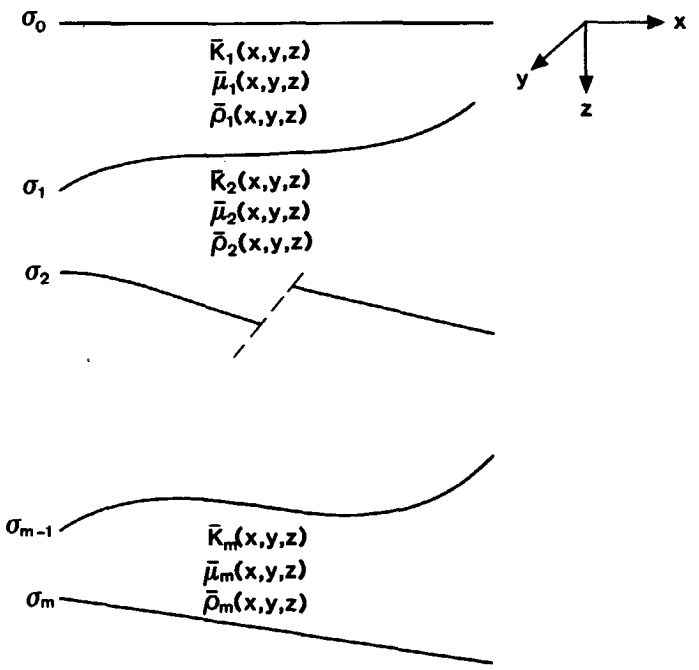

Figure I-2: An example of an elastic macro model of the subsurface.

coordinates, define the elastic **micro*** model of the subsurface. With these assumptions, the properties of the reflected waves are determined by two properties of the subsurface:

1. The **propagation** properties, which depend mainly on the elastic macro parameters of the medium (background parameters).
2. The **reflectivity** properties, which depend mainly on the elastic micro parameters of the medium (detailed deviation parameters).

The seismic inversion problem can now be sub-divided into two steps:

1. Inversion for the **macro parameters** of the subsurface (determination of the propagation properties).
2. Inversion for the **detail** in the subsurface (elimination of the propagation properties).

The macro subsurface model and the detailed inversion result define together the full solution of the seismic inversion problem (see Figure I-3).

The two inversion steps discussed above require completely different approaches.

Most existing inversion techniques for the parameters of the **macro** subsurface model are based on reflection information (in terms of traveltimes) of the main reflecting boundaries between the macro layers. These so called 'tomographic' techniques, which use phase information rather than amplitude information, invert for the propagation velocity only. A discussion is beyond the scope of this thesis. The reader is referred to Dix (1955), Taner and Koehler (1969), Hubral (1976), Krey (1976), Gjøystdal and Ursin (1981), Van der Made et al. (1984) and Wapenaar and Berkhout (1985).

Inversion for the **detail** can be carried out in two different ways:

a. Inverse scattering (generalized Born inversion).
b. Seismic migration.

---

*) In this thesis the adjective 'micro' is used to distinguish the **detailed** subsurface information (details smaller than the seismic wavelength) from the background medium.

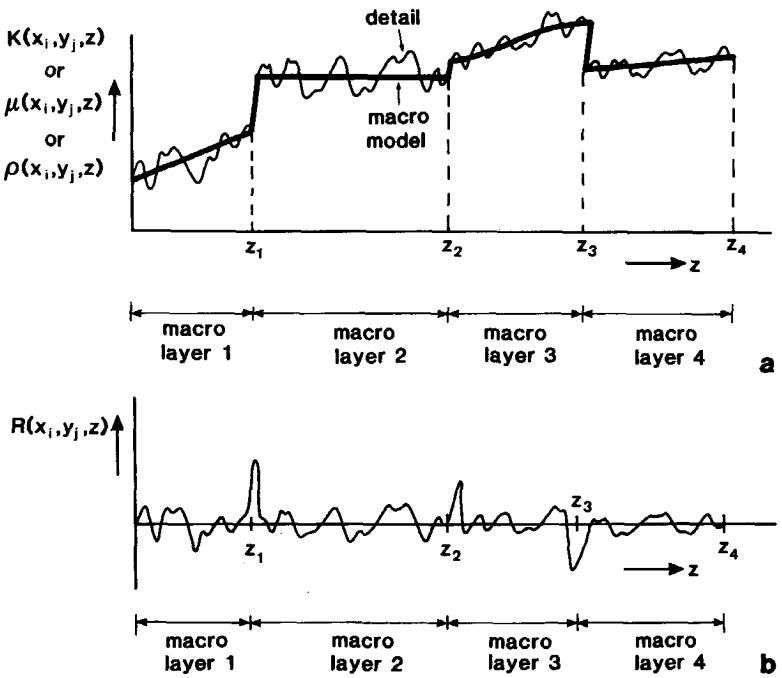

Figure I-3: The solution of the seismic inversion problem consists of a macro subsurface model and a distribution of local deviations ('detail').

a. In the inverse scattering approach, the detail is described in terms of the elastic parameters.

b. In the seismic migration approach, the detail is described in terms of the reflectivity.

The relation between these two approaches has been elegantly described by Berkhout (1984b). Both processes invert propagation operators for the elimination of propagation effects between the surface and the depth level of interest. The inversion must be carried out in a band-limited way. Both inversion processes require a macro subsurface model as input. The inverse scattering process computes the detailed elastic properties of the medium (Figure I-3a). On the other hand, the output of the seismic migration process consists of the detailed reflectivity distribution of the subsurface (Figure I-3b). In this thesis only the seismic migration approach is discussed. For discussions on inverse scattering the reader is referred to Cohen and Bleistein (1979), Clayton and Stolt (1981), Raz (1981), Weglein (1982), Berkhout (1984b), Cheng and Coen (1984) and Tarantola (1984).

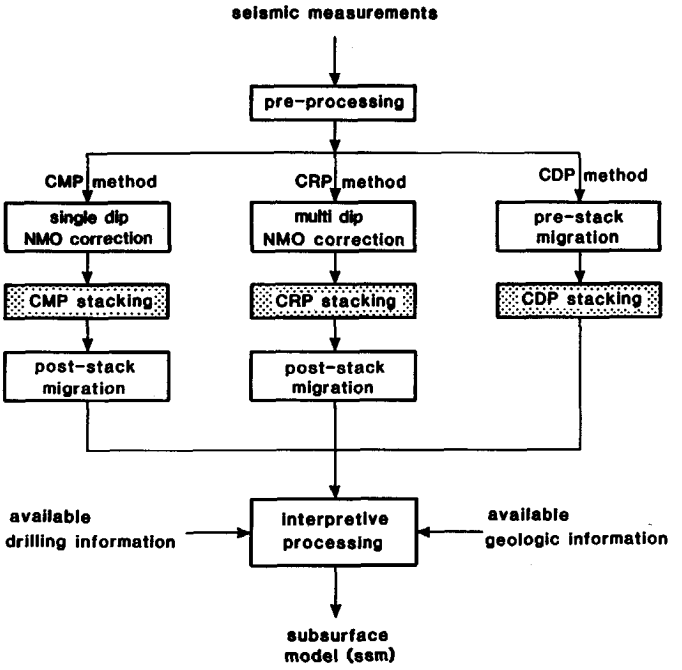

Figure I-4: Basic elements of the seismic processing scheme, consisting of pre-processing, stacking and migration (or vice versa), and interpretive processing.

I.3 CMP VERSUS CDP PROCESSING

In this section we briefly review the basic elements of seismic processing. In particular we pay attention to the various approaches to seismic migration. Our discussion is based on the scheme, shown in Figure I-4.

Irrespective of the approach to seismic migration it is always necessary to perform some pre-processing to the seismic data prior to migration. An important pre-processing step which improves the vertical resolution significantly is deconvolution. A discussion is beyond the scope of this thesis. The interested reader is referred to Wiener (1949), Berkhout (1977), Treitel and Lines (1982), Robinson (1984) and Ziolkowski (1984).

Seismic migration can be carried out in three different ways:

i. Conventional common-midpoint (CMP) method (post-stack migration).

ii. Common-reflectionpoint (CRP) method (partial pre-stack migration).
iii. Common-depthpoint (CDP) method (full pre-stack migration).

A discussion of the various approaches to migration follows below. Irrespective of the approach, however, the output is always a **band-limited** representation of the reflectivity distribution in the earth's subsurface. Further interpretive processing is required in order to obtain a high resolution depth model. This is not further discussed in this thesis. A very promising interpretive processing technique is described by Van Riel and Berkhout (1985). Their method is based on parametric inversion for the detail: by involving additional information (drilling information, geologic information) in the inversion process, a depth model with a resolution beyond the seismic bandwidth can be obtained.

We now consider the three approaches to seismic migration in more detail.

In the conventional CMP method data are re-ordered around surface midpoints into CMP gathers. In each CMP gather the data are normal-moveout (NMO) corrected (traveltime correction) and stacked in order to perform data reduction and to improve the signal to noise ratio. Subsequently the stacked data (pseudo zero-offset (ZO) data) are migrated (post-stack migration) in order to collapse diffraction energy (improvement of lateral resolution) and to correctly position ('migrate') reflection energy. This method, which was originally designed in the early sixties, is computationally manageable with mini computers. The main drawback, however, are the assumptions underlying the stacking procedure: it is assumed that CMP gathers are CRP gathers. This assumption is satisfied when both the macro and the micro subsurface model are approximately horizontally layered. Conflicting dips and diffraction energy cannot be properly handled by the NMO correction. Figure I-5a shows a situation where the CMP principle is approximately valid (small reflectionpoint smear, hyperbolic traveltimes). Figure I-5b shows a situation where the CMP principle fails (large reflectionpoint smear, non-hyperbolic traveltimes). A further discussion on the conventional CMP method is beyond the scope of this thesis. The interested reader is referred to Robinson and Treitel (1980) and Sheriff and Geldart (1983).

In the CRP method the NMO correction is performed as a function of dip by means of a partial pre-stack migration procedure (dip dependent NMO correction is also known as dip-moveout (DMO) correction). Next the data are stacked,

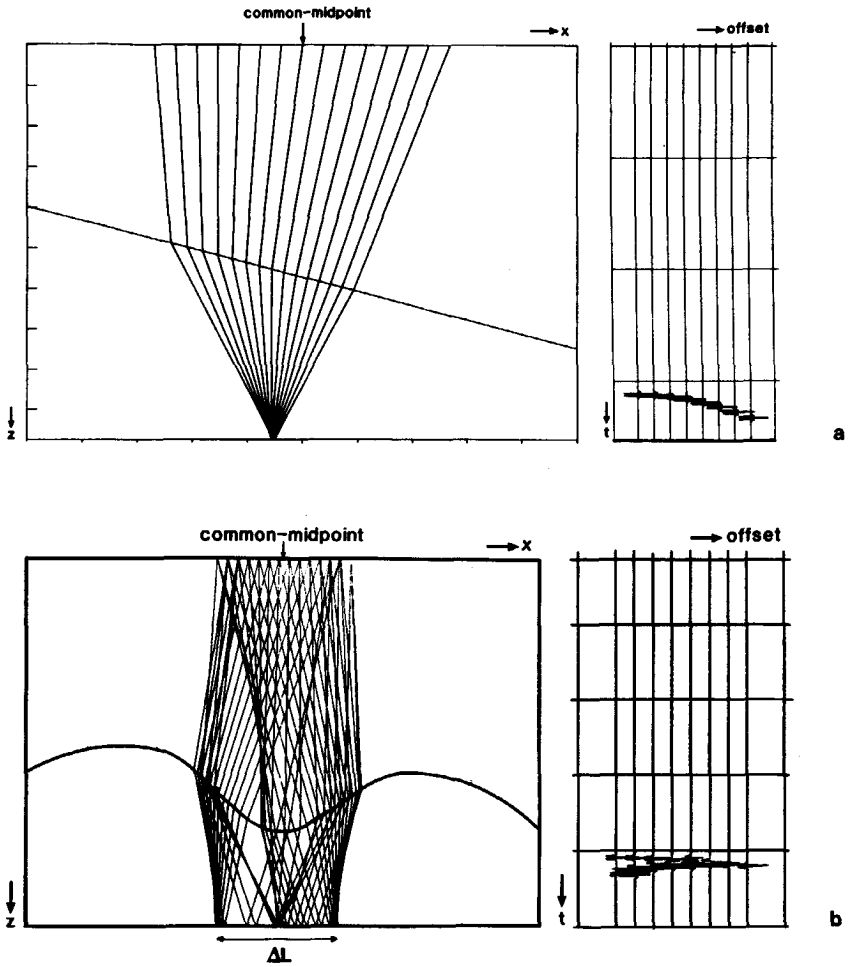

Figure I-5: a. CMP gather with acceptable reflectionpoint smear (hyperbolic traveltime curve).
b. CMP gather with unacceptable reflectionpoint smear (non-hyperbolic traveltime curve).

followed by post-stack migration. This method, which was developed in the seventies and in the early eighties, has become very popular because of its efficiency on one hand and its flexibility on the other hand: only the macro subsurface model is assumed to be approximately horizontally layered (hyperbolic traveltime approximation). Conflicting dips and diffraction energy in the

micro subsurface model are properly handled by the DMO correction. Also the CRP method is not further discussed in this thesis. The reader is referred to Yilmaz and Claerbout (1980), Bolondi et al. (1984) and Hale (1984).

In the CDP method the data are collected per source position in common-shotpoint (CSP) gathers. The data are migrated in the field coordinate system per CSP gather (pre-stack migration by single-shot record inversion (SSRI), Berkhout, 1984a, and De Graaff, 1984). Optionally, the migrated data can be re-ordered into true CDP gathers, where residual NMO corrections can be applied if the input macro subsurface model was slightly in error. Subsequently, the migrated data are stacked (true CDP stacking). Conflicting dips and diffraction energy are properly handled. This method, which was developed in the early eighties, is a sophisticated multi-experiment, multi-offset seismic inversion technique with very promising capabilities with respect to the exploration of oil and gas fields in complex subsurface structures. Geologically oriented macro subsurface models (see Figure I-2) can be handled because the migration process is carried out in the field coordinate system. Hence, the hyperbolic traveltime assumption is released. The CDP method is further discussed in chapter II and the remainder of this thesis is dedicated to new techniques based on the CDP method.

Finally we give an example to demonstrate the differences in the resolving power of the three migration techniques. Figure I-6a shows a single diffractor in a homogeneous medium. Synthetic shot records were generated at the surface of this model (not shown in the figure).

Conventional CMP stacking, followed by post-stack migration, yields the depth section shown in Figure I-6b. The low resolution is due to the fact that the NMO correction does not properly account for diffraction energy.

CRP stacking yields high quality zero-offset data, because the DMO correction properly handles diffraction energy in case of a constant velocity medium. A migrated zero-offset section is shown in Figure I-6c. Note that the resolution improved significantly compared to Figure I-6b.

Pre-stack migration of the shot records followed by CDP stacking yields the depth section shown in Figure I-6d. Note the excellent imaging quality of this multi-experiment, multi-offset seismic inversion technique.

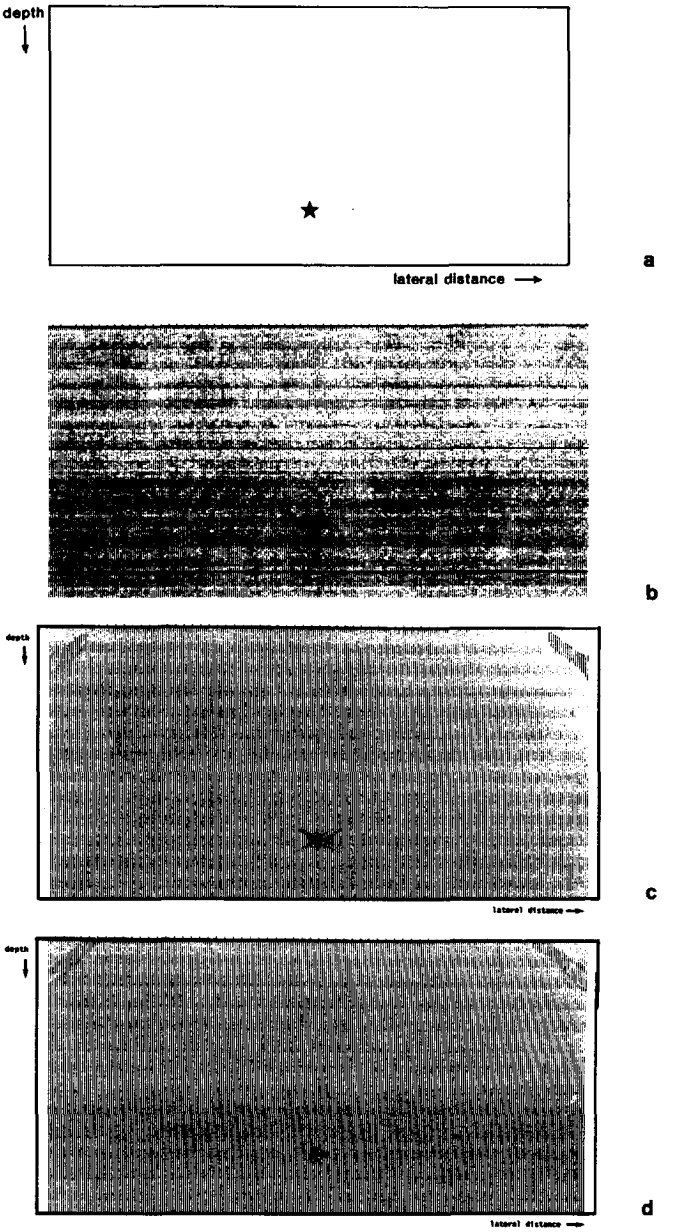

Figure I-6: a. Single diffractor model.
b. Migration result according to the CMP method.
c. (Simulated) migration result according to the CRP method.
d. Migration result according to the CDP method.
(By courtesy of M.P. de Graaff)

I.4 ONE-WAY VERSUS TWO-WAY WAVE EQUATION MIGRATION

Irrespective of the approach to seismic migration, the two basic ingredients are always:

1. Wave field extrapolation.
2. Imaging.

Particularly with respect to wave field extrapolation many techniques have been developed and it is expected that many new techniques will be developed in future. Wave field extrapolation techniques can be sub-divided into two classes:

a. One-way extrapolation techniques.
b. Two-way extrapolation techniques.

Most approaches to seismic wave field extrapolation are based on the assumption that the downgoing source wave field and the upgoing reflected wave field may be treated independently. This **one-way** approach has theoretical drawbacks (the one-way wave equations are not exact) and in practical implementations for inhomogeneous macro models the solution is highly affected by numerical inaccuracy (limited dip-angle performance). The basic concepts of the one-way approach to wave field extrapolation are reviewed in chapter III, where also a new method is suggested for the incorporation of critical angle events in pre-stack migration, assuming a 1-D (vertically) inhomogeneous macro subsurface model.

A more fundamental approach to wave field extrapolation is based on the **two-way** wave equation. This approach does not have the theoretical drawbacks of the one-way approach because the two-way wave equation is exact (in linear acoustics) and thus all fundamental wave phenomena are included. Furthermore, in practical implementations for inhomogeneous macro models the solutions may be very accurate (high dip-angle performance). In the early eighties there has been an increasing interest in the development of migration schemes based on the two-way wave equation. However, up to the present day only the post-stack approach to two-way wave equation migration has been seriously explored. Several high dip-angle migration schemes have been developed (Kosloff and

Baysal, 1983; McMechan, 1983). In most cases these schemes are fit into CMP-oriented processing techniques, thus degrading the two-way solution to a one-way approach (exploding reflector assumption). In fact, several tricks must be done to suppress fundamental wave phenomena, such as multiple reflections, in order to make these schemes work (Baysal et al., 1984). Therefore we refer to this CMP oriented solution of the two-way wave equation as the 'pseudo' two-way approach.

If we want to explore the capabilities of the two-way wave equation fully, the natural way to go is to choose for the CDP oriented processing sequence, because full pre-stack migration by SSRI and CDP stacking is applied in field coordinates to individual seismic experiments (CSP gathers), which obey the two-way wave equation. In chapter IV the principles are discussed of a new pre-stack migration technique based on the 'true' two-way approach. It is concluded that all (acoustic) wave phenomena can be properly handled when the geologically oriented 1-D, 2-D or 3-D inhomogeneous macro subsurface model is accurately known.

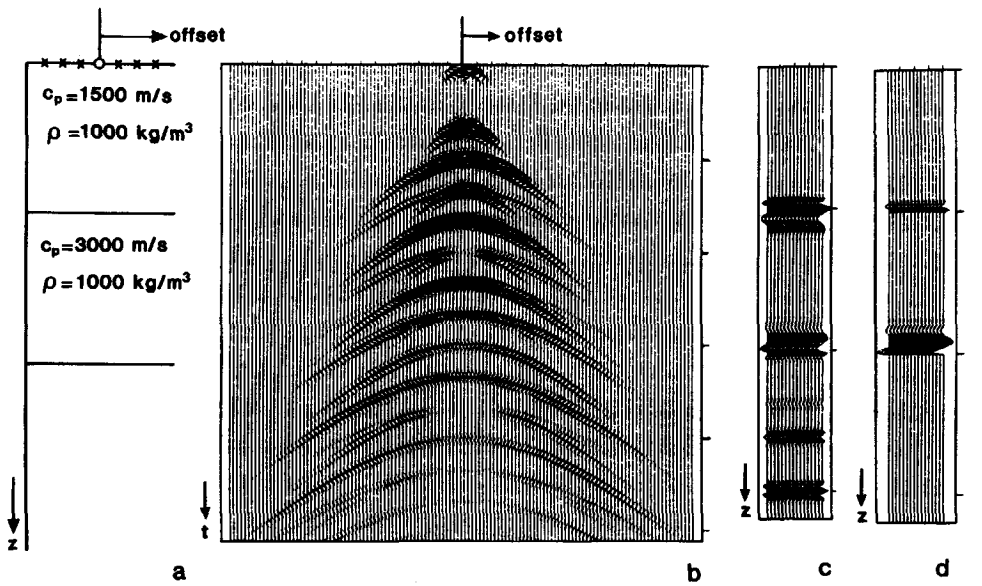

Figure I-7: a. Two layer model.
b. CSP gather.
c. One-way migration result.
d. Two-way migration result.

Finally we give an example to demonstrate the differences with respect to multiple handling of one-way and two-way wave equation migration schemes. Figure I-7a shows a two-layer model. A synthetic shot record was generated using a two-way extrapolation technique (Figure I-7b). Notice that besides the two primary reflections several multiple reflections are present in these data.

Pre-stack migration by SSRI, based on the one-way wave equations, yields the depth section shown in Figure I-7c. The two reflectors are properly imaged. However, many 'ghost-images' occur due to the fact that the one-way wave equations do not account for multiple reflected energy.

Pre-stack migration by SSRI, based on the two-way wave equation, yields the depth section shown in Figure I-7d. Notice that this image accurately matches the subsurface model of Figure I-7a.

I.5 ACOUSTIC VERSUS ELASTIC WAVE EQUATION MIGRATION

On basis of the propagation mechanism, seismic wave types are often sub-divided into two classes:

a. Dilatational or compressional waves.
b. Distortional or shear waves.

The particle motion associated to dilatational or compressional waves is rotation-free. In special cases (for instance plane waves) this means that the particle motion is perpendicular to the wave fronts (longitudinal waves). The particle motion associated to distortional or shear waves is divergence-free. In special cases (for instance plane waves) this means that the particle motion is tangential to the wave fronts (transversal waves).
Generally a seismic wave is neither purely a dilatational wave nor a distortional wave, or in other words, compressional and shear waves are generally interrelated. The main interaction (wave conversion) takes place at the major layer interfaces (the boundaries in the macro subsurface model), particularly for steep incidence angles. Most seismic sources generate mainly compressional waves (apart from surface waves, which do not propagate into the earth) and in many seismic data acquisition configurations, waves with steep propagation angles are not recorded (short offsets). Therefore the contribution of reflected shear waves may often be neglected in seismic inversion

techniques. In this case the inversion scheme may be based on the acoustic wave equation* which is significantly less complicated than the full elastic wave equation. Most of the material presented in this thesis is based on the acoustic wave equation. Hence, it is assumed that the macro subsurface model may be fully described by the constrained compression modulus $\overline{K}_c$ and the mass density $\overline{\rho}$, or, equivalently, by the compressional wave velocity $\overline{c}_p$ and the mass density $\overline{\rho}$.

In the seventies and in the early eighties there has been an increasing interest in large offset data acquisition techniques because large offset data may contain wide-angle information (angle dependent reflection amplitudes, refraction arrivals, etc.) which is not recorded by small offset data acquisition techniques. In large offset data the effects of wave conversion cannot be neglected any longer and therefore seismic inversion should be based on the full elastic wave equation. (The full elastic wave equation describes compressional as well as shear waves in solid media such as rock layers in which shear stresses may play an important role). Because practically all operational seismic inversion techniques are based on the CMP principle, in which converted waves are suppressed by CMP stacking, no full elastic migration results have been presented sofar in seismic literature. Again, CDP oriented processing is the way to go, also for full elastic migration, because the stacking procedure is carried out after migration. Particularly, full pre-stack migration according to the full elastic two-way approach is very attractive when both compressional and shear waves must be considered, because wave conversion is properly described by the full elastic two-way wave equation. In chapter V the principles of a new full elastic migration technique are discussed.

Finally we give an example to demonstrate the differences with respect to wave conversion handling of acoustic and full elastic wave equation migration

---

*) Actually the acoustic wave equation describes compressional waves in fluid media such as gasses and liquids in which the shear modulus μ is negligible. However, when we replace the bulk compression modulus K by the constrained compression modulus $K_c = K + 4\mu/3$, then, under some conditions (see also chapter III), the acoustic wave equation may be applied for compressional waves in solid media as well.

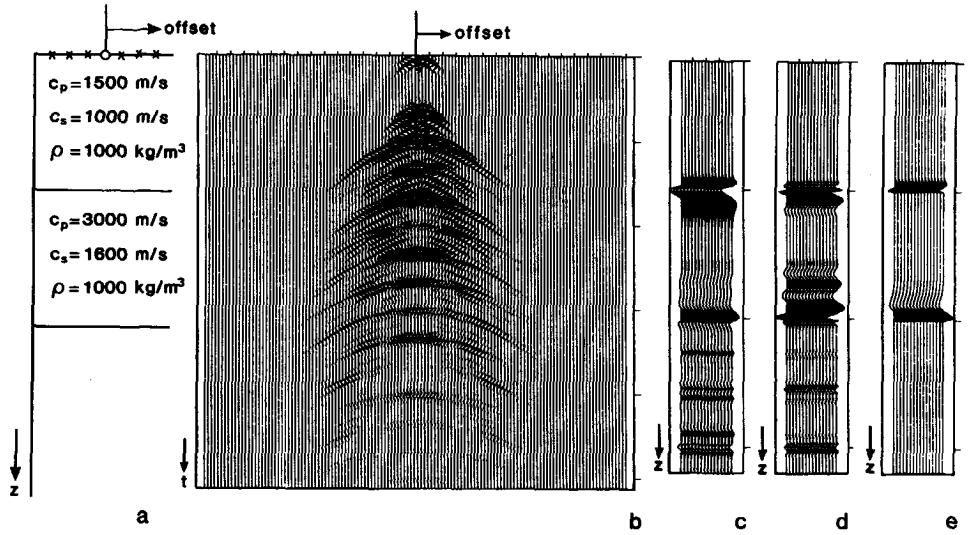

Figure I-8: a. Solid two-layer model.
b. CSP gather.
c. Acoustic one-way migration result.
d. Acoustic two-way migration result.
e. Full elastic two-way migration result.

schemes. Figure I-8a shows a solid two-layer model. A synthetic shot record was generated using a full elastic two-way extrapolation technique (Figure I-8b). Notice that besides the two primary reflections several multiple reflected and converted waves are present in these data.

Pre-stack migration by SSRI, based on the acoustic wave equation, yields the depth sections shown in Figure I-8c (acoustic one-way result) and Figure I-8d (acoustic two-way result). The two reflectors are properly imaged. However, many 'ghost-images' occur, even in the two-way result, due to the fact that the acoustic wave equation does not account for converted waves.

Pre-stack migration by SSRI, based on the full elastic two-way wave equation, yields the depth section shown in Figure I-8e. Notice that this image accurately matches the subsurface model of Figure I-8a.

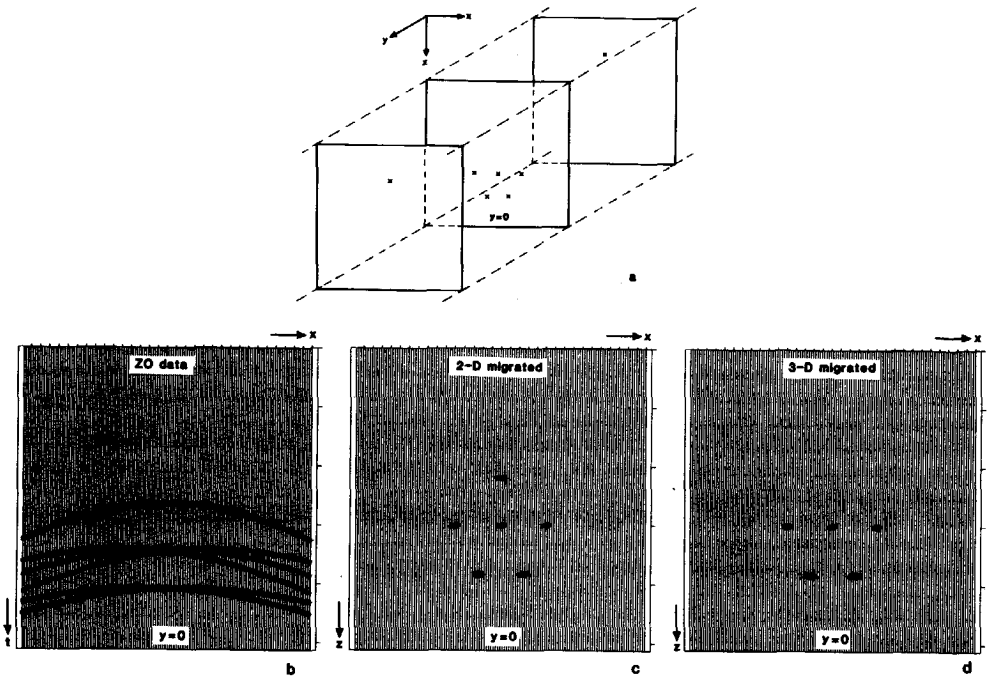

Figure I-9: a. 3-D multi diffractor model.
b. 2-D slice (y=o) of 3-D ZO gather.
c. 2-D migration result.
d. 2-D slice of 3-D migration result.

I.6 2-D VERSUS 3-D MIGRATION

In many practical situations seismic data acquisition is carried out along a straight line. Subsequently, seismic migration is carried out only for a vertical cross-section of the earth's subsurface below the acquisition line. In this case seismic inversion becomes a two-dimensional (2-D) technique. This may be very attractive from a computational point of view, however, the earth is three-dimensional (3-D). Particularly in areas with complicated structures, 2-D migration techniques give a poor image of the subsurface. Actually, 2-D migration techniques may only be used when both the macro and the micro subsurface model approximately satisfy the 2-D assumption, that is, when the elastic parameters depend on two spatial coordinates only. Unfortunately this assumption is rarely met in practice and therefore the reliability of many 2-D migration results is questionable.

The need for 3-D migration techniques is illustrated with a simple ZO data example. Figure I-9a shows a 3-D multi-diffractor model. A synthetic 3-D ZO gather was generated at the surface. A 2-D slice of these data (for y=o) is shown in Figure I-9b. Notice that all diffractors of the 3-D model are present in this 2-D data slice.

2-D ZO migration, applied to the 2-D ZO gather of Figure I-9b, yields the depth section shown in Figure I-9c. The five 'in-plane' diffractors are properly imaged. However, also a 'ghost-image' occurs, due to the fact that the 2-D algorithm does not properly account for 'out-of-plane' events.

3-D ZO migration, applied to the whole 3-D ZO gather, yields a 3-D depth section. A 2-D slice of this depth section (for y=o) is shown in Figure I-9d. Notice that this image accurately matches the 2-D slice (y=o) of the subsurface model, shown in Figure I-9a.

In the seventies and the early eighties much effort has been spent in the development of both 3-D data acquisition and 3-D inversion techniques. Up to the present day, however, only the 3-D extension of the conventional CMP method has got serious attention. Apart from the drawbacks of the CMP method which were already mentioned in the previous sections, an additional problem arises in the 3-D situation: particularly in marine applications one common midpoint does not exist and some pre-processing is needed to generate artificial midpoints ('binning'). Hence, in many situations 3-D processing may neither represent a CDP nor a CMP technique. In addition, 3-D post-stack migration is generally applied as two separate 2-D migration processes in perpendicular directions. This is an economic solution but in the seismic application it is not correct because it assumes a homogeneous macro subsurface model. Most of above mentioned problems also apply for the 3-D extension of the CRP method (partial pre-stack migration). However, this approach should certainly be explored because of its higher accuracy (better dip handling) in comparison with the conventional CMP method on one hand and because of its higher efficiency in comparison with the CDP method (full pre-stack migration) on the other hand. In this thesis the 3-D versions of the CMP and the CRP methods are not further discussed. The reader is referred to French (1975), Gardner et al. (1978), Ristow (1980), Gibson et al. (1983), Jakubowicz and Levin (1983), Hale (1983), and Schultz and Lau (1984).

Full 3-D pre-stack migration according to the CDP method (pre-stack migration by SSRI and CDP stacking) appears to be the natural way to perform seismic inversion because a 3-D geologically oriented macro subsurface model may be chosen. Also the binning problem is evaded because independent seismic experiments are migrated in the field coordinate system. However, even with nowadays fast vector computers full 3-D pre-stack migration is still unthinkable because of the enormous amount of data to be processed.
For instance, a typical 3-D marine survey (see also Figure I-1) consists of

200 seismic lines,
200 shot records per seismic line,
100 traces per shot record,
2000 samples per trace,
4 bytes per sample,

hence, the total survey contains 32 Gbyte of data. It is obvious that, given the limitations of computer hardware, a more practical view to 3-D pre-stack migration is required. In chapter VI an efficient, **target oriented,** 3-D pre-stack migration algorithm is discussed and preliminary results on both synthetic and scale model data are presented.

I.7 OUTLINE OF THIS THESIS

In chapter II the principle of pre-stack migration by SSRI and CDP stacking is reviewed. As was argued in this introduction, pre-stack migration by SSRI can be based either on the one-way wave equations or on the acoustic or full elastic two-way wave equation. Therefore three chapters are dedicated to various aspects of wave field extrapolation techniques. In chapter III methods using the acoustic one-way wave equations are discussed. In chapter IV methods using the acoustic two-way wave equation are discussed and in chapter V methods using the full elastic two-way wave equation are discussed. The theory in chapters III to V is set up for the greater part in three dimensions, whereas the examples demonstrate applications in two dimensions. Practical aspects with respect to pre-stack migration in three dimensions are discussed in the final chapter VI. Conclusions are illustrated on a 3-D real data example, the data being generated in a model tank.

CHAPTER II

PRINCIPLE OF FULL PRE-STACK MIGRATION BY SINGLE-SHOT RECORD INVERSION AND COMMON-DEPTHPOINT STACKING

II.1 INTRODUCTION

It was argued in the introductory chapter that common-depthpoint (CDP) oriented pre-stack migration, as proposed by Berkhout (1984a), is the most promising approach to seismic inversion for the detail, particularly for complicated subsurface geometries.

The main purpose of this chapter is to give the reader who is not familiar with the CDP method an impression of the mechanism and the underlying principles. The method is explained on the basis of a matrix formulation of a 2-D model of seismic records, however, the computational diagrams presented in sections II.3 and II.4 are in principle applicable for 2-D as well as 3-D situations. No attempt is made to give a rigorous discussion on the matrix formalism itself; therefore the reader is referred to Berkhout (1982). We adopt this symbolic notation because it postpones the choice which wave equation to solve, so we can fully concentrate on the CDP technique itself. In the subsequent chapters various solutions of different wave equations (one-way acoustic, two-way acoustic, two-way full elastic) are put forward which fit in with the scheme discussed in this chapter. The outline of this chapter is as follows. In section II.2 the 2-D model of seismic shot records is briefly discussed. In section II.3 it is argued that, ideally, full pre-stack true amplitude migration is carried out by multi-experiment, multi-offset inversion. In the following we refer to this method as multi-shot record inversion (MSRI). The scheme is based on straightforward inversion of the forward model of all shot records in a seismic line, but is not very practical for various reasons. In

section II.4 we come to the actual subject of this chapter, namely full pre-stack migration by single-shot record inversion (SSRI) and CDP stacking. It is argued that this scheme is very attractive because of its high flexibility. The data can be migrated per common-shotpoint (CSP) record (single-experiment, multi-offset inversion), followed by true CDP stacking. Finally, in section II.5 the different approaches to full pre-stack migration are compared and it is investigated under which conditions the proposed SSRI scheme represents true amplitude migration.

II.2 TWO-DIMENSIONAL MODEL OF SEISMIC SHOT RECORDS

If we make use of the matrix notation an elegant expression can be given for the measurements of one seismic experiment, that is, the data of one CSP record. The formulation is a monochromatic one (the circular frequency ω is a parameter) and divides the physical process in four parts.

1. **Downward propagation**

$$\vec{S}^{+}(z_i) = \mathbf{W}(z_i, z_o)\vec{S}^{+}(z_o). \qquad \text{(II-1)}$$

The vector $\vec{S}^{+}(z_o)$ describes the downgoing source wave field at the surface z_o, each element representing one lateral x position. In case of a point source at $x=x_m$, the m'th element of vector $\vec{S}^{+}(z_o)$ contains the source function $S(\omega)$, while the other elements are zero.
Matrix $\mathbf{W}(z_i, z_o)$ describes how the source wave field propagates from the surface to depth level z_i, each column representing the spatial impulse response corresponding to one source position at the surface. Vector $\vec{S}^{+}(z_i)$ represents the downward traveling source wave field at depth level z_i.

2. **Reflection**

$$\vec{P}^{-}(z_i) = \mathbf{R}(z_i)\vec{S}^{+}(z_i). \qquad \text{(II-2)}$$

The reflectivity matrix $\mathbf{R}(z_i)$ describes how the downward traveling source wave field at depth level z_i is transformed into the upward traveling reflected wave field $\vec{P}^{-}(z_i)$.

3. **Upward propagation**

$$\vec{P}^{-}(z_o) = \sum_{i=1}^{I} \mathbf{W}(z_o,z_i)\vec{P}^{-}(z_i). \qquad \text{(II-3)}$$

Matrix $\mathbf{W}(z_o,z_i)$ describes how the reflected wave field propagates from depth level z_i to the surface z_o. Vector $\vec{P}^{-}(z_o)$ represents the sum of the reflected wave fields from all depth levels of interest $(z_1,z_2,\ldots z_I)$ at the surface z_o.

4. **Detection**

$$\vec{P}^{-}_{CSP}(z_o) = \mathbf{D}(z_o)\vec{P}^{-}(z_o). \qquad \text{(II-4)}$$

Matrix $\mathbf{D}(z_o)$ describes how the upgoing wave field $\vec{P}^{-}(z_o)$ is detected at the surface, each row defining the detector array ('field pattern') at one lateral position. In case of identical omni-directional single-detector elements, $\mathbf{D}(z_o)$ represents a unit matrix, weighted by a frequency dependent factor $D(\omega)$. Vector $\vec{P}^{-}_{CSP}(z_o)$ represents the detected upgoing wave field in a CSP record.

Above expressions can be elegantly combined into one equation

$$\vec{P}^{-}_{CSP}(z_o) = \mathbf{D}(z_o)\sum_{i=1}^{I}\left[\mathbf{W}(z_o,z_i)\mathbf{R}(z_i)\mathbf{W}(z_i,z_o)\right]\vec{S}^{+}(z_o). \qquad \text{(II-5)}$$

Figure II-1 gives a schematic illustration.

Because seismic migration aims at determining the reflectivity of the subsurface, some attention need be paid to the properties of reflectivity matrix $\mathbf{R}(z_i)$. Each row of this matrix represents an operator which defines angle dependent reflection at one lateral position. In case of 'locally reacting' reflectors the operator is represented by a spatial delta function, so $\mathbf{R}(z_i)$ is a diagonal matrix. An example of a locally reacting reflector is an interface between two homogeneous liquids which have a density contrast only. Here locally reacting is equivalent to angle independent reflecting. Unfortunately the locally reacting assumption is not valid in many practical situations, so matrix $\mathbf{R}(z_i)$ generally exhibits a band structure. It is shown in the following sections that band matrix $\mathbf{R}(z_i)$ can be resolved from the seismic data both by **'full pre-stack migration by multi-shot record inversion'**

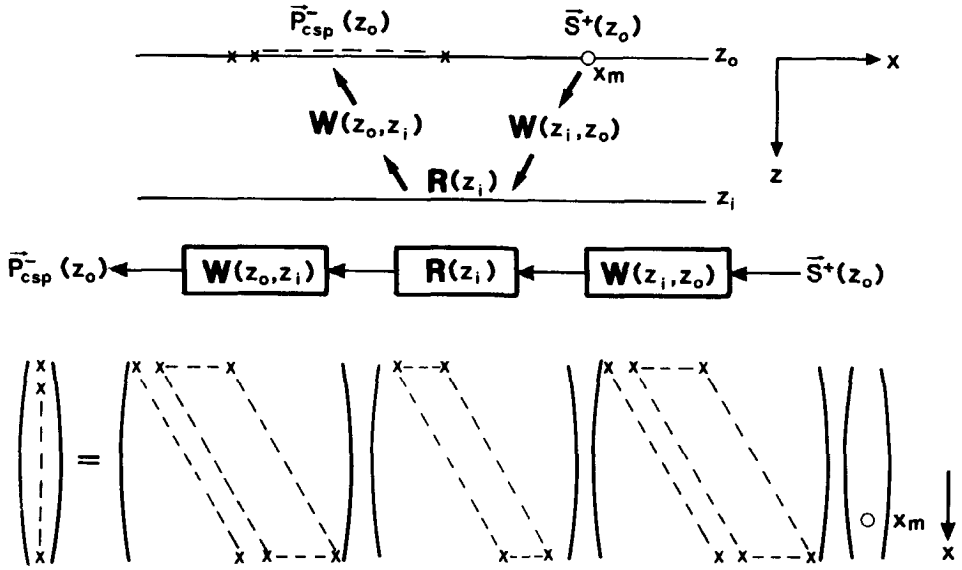

Figure II-1: Basic model for the seismic response from depth level z_i (no field patterns).

as well as by **'full pre-stack migration by single-shot record inversion and common-depthpoint stacking'**. Seismic interpreters are generally satisfied if the reflectivity information of each subsurface depthpoint is represented by its zero-offset (ZO) reflection coefficient only. This means that after miration only the diagonal elements of $\mathbf{R}(z_i)$ need be selected, yielding the wide-angle ZO reflectivity matrix $\mathbf{R}_{ZO}(z_i)$, which summarizes the reflectivity properties of depth level z_i.

II.3 FULL PRE-STACK MIGRATION BY MULTI-SHOT RECORD INVERSION

The forward model for one seismic experiment can be summarized according to relation (II-5) by

$$\vec{P}^-_{CSP}(z_o) = \mathbf{D}(z_o)\mathbf{X}(z_o)\vec{S}^+(z_o), \qquad \text{(II-6a)}$$

where

$$\mathbf{X}(z_o) = \sum_i \left[\mathbf{W}(z_o,z_i)\mathbf{R}(z_i)\mathbf{W}(z_i,z_o)\right]. \qquad \text{(II-6b)}$$

In relation (II-6a), $\vec{P}^{-}_{CSP}$ describes the seismic measurements, $\mathbf{D}$ and $\vec{S}$ represent acquisition parameters, while $\mathbf{X}$ describes the medium, that is, each column of $\mathbf{X}$ represents the spatial impulse response of the medium, corresponding to one source position at the surface. In relation (II-6b), the matrices $\mathbf{W}$ describe the propagation properties of the macro subsurface model, while $\mathbf{R}$ describes the reflectivity properties of both the macro and the micro subsurface model. The inverse problem in terms of seismic migration can be formulated as follows:

> given the seismic measurements, the acquisition parameters and the macro subsurface model, determine the reflectivity of the subsurface.

Obviously, inversion of relation (II-6) is an ill-posed problem: the measurements are given by **one vector**, while the reflectivity is described by **many matrices**. First we extend shot record model (II-6) to the model for a multi-shot record data set. This can be easily done by extending the source vector $\vec{S}^{+}(z_o)$ to a source matrix $\mathbf{S}^{+}(z_o)$. Each column of source matrix $\mathbf{S}^{+}(z_o)$ defines one source vector, corresponding to one source (array) at the surface. Similarly, the response vector $\vec{P}^{-}_{CSP}(z_o)$ is replaced by a response matrix $\mathbf{P}^{-}_{MSP}(z_o)$, where the sub-script MSP denotes 'multi-shotpoint record'. Each column of response matrix $\mathbf{P}^{-}_{MSP}(z_o)$ defines one response vector due to one source vector. The seismic data matrix $\mathbf{P}^{-}_{MSP}(z_o)$ contains the monochromatic information of all shot records which define one seismic line. Relation (II-6) may now be rewritten as

$$\mathbf{P}^{-}_{MSP}(z_o) = \mathbf{D}(z_o)\mathbf{X}(z_o)\mathbf{S}^{+}(z_o). \qquad \text{(II-7)}$$

Notice that we have obtained a situation for which the **acquisition parameters** can be removed from the data by matrix inversion. A rigorous treatment is beyond the scope of this thesis. We discuss a simplified situation by considering identical, equidistantly spaced point sources, characterized by $S(\omega)$, and identical, equidistantly spaced omni-directional single-detector elements, characterized by $D(\omega)$. In this case both $\mathbf{S}^{+}$ and $\mathbf{D}$ represent weighted unit matrices, so equation (II-7) may be written as

$$\mathbf{P}^{-}_{MSP}(z_o) = [D(\omega)S(\omega)]\mathbf{X}(z_o). \qquad \text{(II-8)}$$

Notice that $\mathbf{X}(z_o)$ can be resolved from the measured data $\mathbf{P}^{-}_{MSP}(z_o)$ in a

band-limited way. This **deconvolution** procedure is actually a pre-processing step prior to migration (see also Figure I-4). The actual migration objective is to eliminate the **propagation effects** from $\mathbf{X}(z_o)$ in order to obtain the undistorted reflectivity information. Therefore we consider for the moment the response from one depth level only, that is, we assume that $\mathbf{X}(z_o)$ is given by

$$\mathbf{X}(z_o) = \mathbf{W}(z_o,z_i)\mathbf{R}(z_i)\mathbf{W}(z_i,z_o). \qquad \text{(II-9)}$$

If we define matrices $\mathbf{F}(z_o,z_i)$ and $\mathbf{F}(z_i,z_o)$ such that

$$\mathbf{W}(z_i,z_o)\,\mathbf{F}(z_o,z_i) = \mathbf{I}, \qquad \text{(II-10a)}$$

$$\mathbf{F}(z_i,z_o)\mathbf{W}(z_o,z_i) = \mathbf{I}, \qquad \text{(II-10b)}$$

where $\mathbf{I}$ represents the unit matrix, then relation (II-9) can be inverted according to

$$\mathbf{R}(z_i) = \mathbf{F}(z_i,z_o)\mathbf{X}(z_o)\,\mathbf{F}(z_o,z_i). \qquad \text{(II-11)}$$

In practice conditions (II-10a) and (II-10b) can never be satisfied, so inversion should be carried out in a spatially band-limited way. A practical solution is found as follows.

1. Define the least-squares inversion of $\mathbf{W}(z_i,z_o)$ as

$$\mathbf{F}(z_o,z_i) = \left[\mathbf{W}^{*T}(z_i,z_o)\mathbf{W}(z_i,z_o)\right]^{-1}\mathbf{W}^{*T}(z_i,z_o), \qquad \text{(II-12a)}$$

   where T denotes matrix transposition and where * denotes complex conjugation. This relation, which is exact for square matrices, states that matrix inversion can be carried out in two steps: first mainly a **phase** correction is applied by zero-phasing operator $\mathbf{W}^{*T}(z_i,z_o)$; next mainly an **amplitude** correction is applied by inverse operator $\left[\mathbf{W}^{*T}(z_i,z_o)\mathbf{W}(z_i,z_o)\right]^{-1}$. Particularly the amplitude correction is difficult because it requires matrix inversion. This problem may be partly bypassed, however, as is shown in the next step.
2. Assume that the amplitude effects of upward propagation are inversely proportional to the amplitude effects of downward propagation, according to

$$\mathbf{W}^{T}(z_o,z_i) \approx \left[\mathbf{W}(z_i,z_o)\mathbf{W}^{*T}(z_i,z_o)\right]^{-1}\mathbf{W}(z_i,z_o), \qquad \text{(II-12b)}$$

or

$$\mathbf{W}^{*T}(z_i,z_o) \approx \left[\mathbf{W}^{*T}(z_i,z_o)\mathbf{W}(z_i,z_o)\right]\mathbf{W}^{*}(z_o,z_i). \qquad \text{(II-12c)}$$

3. Substitute relation (II-12c) into (II-12a), yielding

$$\mathbf{F}(z_o,z_i) \approx \mathbf{W}^{*}(z_o,z_i). \qquad \text{(II-13a)}$$

A similar relation can be found for matrix $\mathbf{F}(z_i,z_o)$:

$$\mathbf{F}(z_i,z_o) \approx \mathbf{W}^{*}(z_i,z_o). \qquad \text{(II-13b)}$$

Relation (II-13) describes the **'matched filter'** approach to inverse wave field extrapolation. It is shown by Berkhout (1982) for a **homogeneous** macro model that these very simple inverse operators are exact within the spatial bandwidth of propagating waves. In addition, as is shown in sections III.5 and III.7 of this thesis, the matched filter approach is also exact (within the spatial bandwidth of propagating waves) both in amplitude and phase, in case of a 1-D inhomogeneous macro model, assuming the medium parameters vary smoothly with depth. In case of 2-D and 3-D inhomogeneous macro subsurface models assumption (II-12b) breaks down, so inversion should preferably be carried out according to (II-12a) in some stable sense. However, the matched filter approach to inverse wave field extrapolation represents an interesting compromise of accuracy and efficiency and is therefore often applied in seismic practice, also for 2-D and 3-D inhomogeneous macro models. A further discussion of the matched filter approach is beyond the scope of this thesis. In the following we use the symbol $\mathbf{F}$ for general **band-limited** inverse extrapolation operators. Whenever the matched filter approach is assumed this is explicitly stated.

In conclusion, inversion result $\mathbf{R}(z_i)$, as defined by relation (II-11), is correct in **amplitude** as well as in **phase** within the limitations imposed by the temporal and spatial seismic bandwidth. Hence, the angle dependent reflection operators, represented by the rows of matrix $\mathbf{R}(z_i)$, can be properly determined from the surface data.

If we now consider again the response from many depth levels, that is, if we assume that $\mathbf{X}(z_o)$ is given by

$$\mathbf{X}(z_o) = \sum_j \left[\mathbf{W}(z_o,z_j)\mathbf{R}(z_j)\mathbf{W}(z_j,z_o)\right], \qquad \text{(II-14)}$$

then inversion algorithm (II-11) should be replaced by

$$\mathbf{X}(z_i) = \mathbf{F}(z_i,z_o)\mathbf{X}(z_o)\,\mathbf{F}(z_o,z_i). \qquad \text{(II-15)}$$

Substituting (II-14) into (II-15) yields

$$\mathbf{X}(z_i) = \sum_j \left[\mathbf{F}(z_i,z_o)\mathbf{W}(z_o,z_j)\mathbf{R}(z_j)\mathbf{W}(z_j,z_o)\,\mathbf{F}(z_o,z_i)\right], \qquad \text{(II-16a)}$$

or

$$\mathbf{X}(z_i) = \mathbf{R}(z_i) + \sum_{j\neq i}[\ldots]. \qquad \text{(II-16b)}$$

According to relation (II-16b) the total response $\mathbf{X}(z_i)$ at depth level z_i consists of two parts: the undistorted reflectivity $\mathbf{R}(z_i)$, from which all propagation effects have been properly removed by zero-phasing inverse operators $\mathbf{F}(z_o,z_i)$ and $\mathbf{F}(z_i,z_o)$, and an extra term which contains amplitude and phase distorted reflectivity information from all other depth levels. Apparently additional information is required to resolve the reflectivity $\mathbf{R}(z_i)$ from the total response $\mathbf{X}(z_i)$ at the current depth level. If we keep in mind that above mentioned zero-phasing property for $\mathbf{R}(z_i)$ holds for all frequencies, while the phase distortion in the extra term is different for different frequencies, then it is clear that a summation over all frequencies within the seismic bandwidth, according to

$$\langle\mathbf{R}(z_i)\rangle = \frac{\Delta\omega}{2\pi}\sum_{\omega}\mathbf{X}(z_i), \qquad \text{(II-17)}$$

yields a good estimate of the reflectivity, because all terms $\mathbf{R}(z_i)$ add up coherently while the extra terms interfere destructively ($\Delta\omega$ denotes the circular frequency sampling interval). The process described by (II-17), is called **imaging.**

Notice that relation (II-17) may also be interpreted as a (discrete) inverse Fourier transform from frequency to time, where the inverse transformed function is calculated for zero-time only (see also relation (III-3b), for t=o). This can be physically well understood: matrix $\mathbf{X}(z_i)$ describes the

general relation between downgoing and upgoing waves at depth z_i, while reflectivity matrix $\mathbf{R}(z_i)$ describes the time-coincidence of downgoing and upgoing waves at depth z_i.

Summarizing, in this section we have shown that a good estimate of the subsurface reflectivity can be obtained from many monochromatic MSP records at different frequencies. Practical seismic measurements always contain broad-band information, so the required monochromatic MSP records can be easily obtained by Fourier transform. The scheme for full pre-stack migration by multi-shot record inversion (MSRI) can be summarized as follows.

1. **Partly compensation for the acquisition limitations** at the surface z_o by inverting relation (II-8)

$$\mathbf{P}^{-}_{MSP}(z_o) = [D(\omega)S(\omega)]\mathbf{X}(z_o) \qquad \text{(II-18)}$$

in a band-limited way (deconvolution).

2. **Inverse wave field extrapolation** to all depth levels z_i. Non-recursive inverse wave field extrapolation is described by relation (II-15). Recursive inverse wave field extrapolation can be formally described by

$$\mathbf{X}(z_i) = \mathbf{F}(z_i, z_{i-1})\mathbf{X}(z_{i-1})\mathbf{F}(z_{i-1}, z_i). \qquad \text{(II-19)}$$

3. **Imaging** by summing over all frequencies, according to relation (II-17), yielding the reflectivity matrix at depth level z_i:

$$\langle \mathbf{R}(z_i) \rangle = \frac{\Delta\omega}{2\pi} \sum_{\omega} \mathbf{X}(z_i). \qquad \text{(II-20)}$$

As we stated in the previous section, for seismic interpretation it is often sufficient if we select the diagonal elements of matrix $\langle \mathbf{R}(z_i) \rangle$, yielding the wide-angle ZO reflection matrix $\langle \mathbf{R}_{ZO}(z_i) \rangle$, to summarize the reflectivity at depth level z_i.

Step 1 is a pre-processing step; steps 2 and 3 describe the actual migration procedure.

A computational diagram of this multi-experiment, multi-offset seismic migration scheme is presented in Figure II-2. Because the procedure is carried out in field coordinates, the inverse wave field extrapolation operators can be

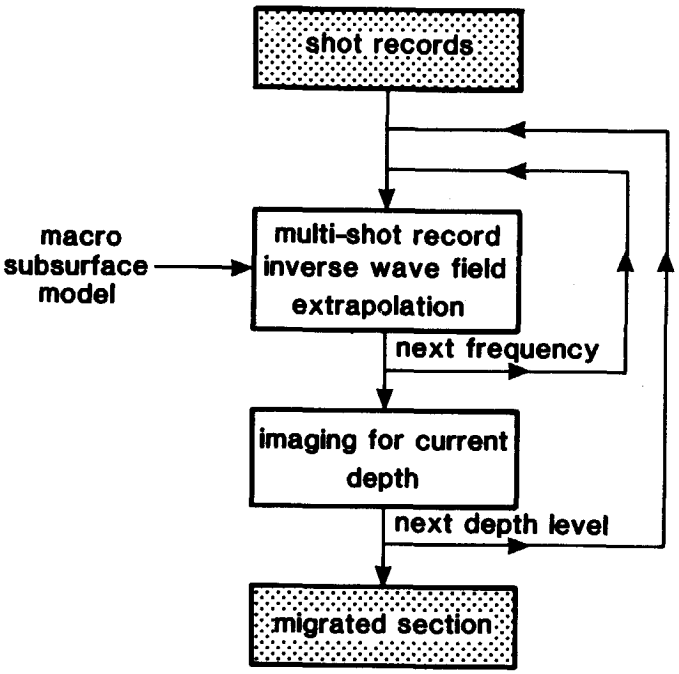

Figure II-2: Computational diagram for full pre-stack migration by multi shot record inversion (MSRI).

optimumly designed for a geologically oriented macro subsurface model. Hence, assuming that the proper operators are used, non-hyperbolic traveltimes are allowed and **true amplitude** migration is accomplished. The main disadvantage of the scheme is the cumbersome data management: all shot records must be available at the same time to carry out inverse wave field extrapolation. Furthermore the scheme does not cope with errors in the description of the macro subsurface model. Finally we remark that the scheme is essentially based on the one-way equations. In the next section we discuss an alternative true amplitude migration scheme which does not suffer from these practical drawbacks.

II.4 FULL PRE-STACK MIGRATION BY SINGLE-SHOT RECORD INVERSION AND COMMON-DEPTHPOINT STACKING

We consider again the forward model for one seismic experiment

$$\vec{P}^{-}_{CSP}(z_o) = \mathbf{D}(z_o)\mathbf{X}(z_o)\vec{S}^{+}(z_o), \tag{II-21a}$$

where

$$\mathbf{X}(z_o) = \sum_i \left[\mathbf{W}(z_o,z_i)\mathbf{R}(z_i)\mathbf{W}(z_i,z_o)\right]. \tag{II-21b}$$

Unlike in the previous section, where we extended this model to a multi-record data set, here we discuss migration by single-shot record inversion (SSRI) and CDP stacking. If we assume the same source and detector properties as in the previous section then relation (II-21a) can be rewritten as

$$\vec{P}^{-}_{CSP}(z_o) = [D(\omega)S(\omega)]\,\mathbf{X}(z_o)\vec{S}^{+}_{o}(z_o). \tag{II-22}$$

Here $\vec{S}^{+}_{o}(z_o)$ represents a unit source vector. Acquisition parameters and medium parameters can be separately described as follows:

$$\vec{P}^{-}_{CSP}(z_o) = [D(\omega)S(\omega)]\vec{P}^{-}_{o}(z_o), \tag{II-23a}$$

where

$$\vec{P}^{-}_{o}(z_o) = \mathbf{X}(z_o)\vec{S}^{+}_{o}(z_o). \tag{II-23b}$$

Notice that according to (II-23a), $\vec{P}^{-}_{o}(z_o)$ can be resolved from the measured data $\vec{P}^{-}_{CSP}(z_o)$ in a band-limited way (deconvolution). Apparently the acquisition parameters cannot be fully eliminated because the source wave field is characterized by a unit vector rather than a unit matrix. In the following we discuss inversion of relation (II-23b). The sub-script 'o', which denotes that the response is due to a unit source, is deleted for notational convenience. Similarly as in the previous section we consider for the moment the response from one depth level only, that is, we assume that $\vec{P}^{-}(z_o) = \mathbf{X}(z_o)\vec{S}^{+}(z_o)$ is given by

$$\vec{P}^{-}(z_o) = \mathbf{W}(z_o,z_i)\mathbf{R}(z_i)\mathbf{W}(z_i,z_o)\vec{S}^{+}(z_o). \tag{II-24}$$

Compensation for the propagation effects between the surface and depth level z_i is described by

$$\vec{S}^{+}(z_i) = \mathbf{W}(z_i,z_o)\vec{S}^{+}(z_o), \qquad \text{(II-25a)}$$

$$\vec{P}^{-}(z_i) = \mathbf{F}(z_i,z_o)\vec{P}^{-}(z_o). \qquad \text{(II-25b)}$$

Relation (II-25a) describes forward extrapolation of the downgoing source wave field and relation (II-25b) describes inverse extrapolation of the upgoing detected wave field. Given the downgoing source wave field $\vec{S}^{+}(z_i)$ and the upgoing reflected wave field $\vec{P}^{-}(z_i)$ at depth level z_i, then reflection matrix $\mathbf{R}(z_i)$ should be resolved from relation (II-2):

$$\vec{P}^{-}(z_i) = \mathbf{R}(z_i)\vec{S}^{+}(z_i). \qquad \text{(II-26)}$$

Notice that for arbitrary $\mathbf{R}(z_i)$, (generally $\mathbf{R}(z_i)$ has a band-structure), this problem is ill-posed. One particular solution is given by

$$<\mathbf{R}(z_i)> = \vec{P}^{-}(z_i)\left[\left(\vec{S}^{+}(z_i)\right)^{*T}\vec{S}^{+}(z_i)\right]^{-1}\left(\vec{S}^{+}(z_i)\right)^{*T}, \qquad \text{(II-27a)}$$

or

$$<\mathbf{R}(z_i)> = \frac{1}{s^2}\vec{P}^{-}(z_i)\left(\vec{S}^{+}(z_i)\right)^{*T}, \qquad \text{(II-27b)}$$

with

$$s^2 = ||\vec{S}^{+}(z_i)||^2, \qquad \text{(II-27c)}$$

which can be easily verified by substituting this solution into (II-26). It should be kept in mind that this solution is non-unique. In the following section, however, it is shown that the inversion approach, as described by (II-27), is a good choice.

Notice that this inversion is stable because $\vec{S}^{+}(z_i)$ describes the response of a unit source. In case of a **homogeneous macro model** the scaling factor s^2 approaches unity.

As we mentioned before, it is often sufficient if the reflectivity information of each subsurface depthpoint is represented by its zero-offset reflection coefficient only. This means that only the diagonal of $<\mathbf{R}(z_i)>$ need be calculated. According to (II-27) each diagonal element of $<\mathbf{R}(z_i)>$ is obtained by multiplying one element of vector $\vec{P}^{-}(z_i)$ by the complex conjugated of the

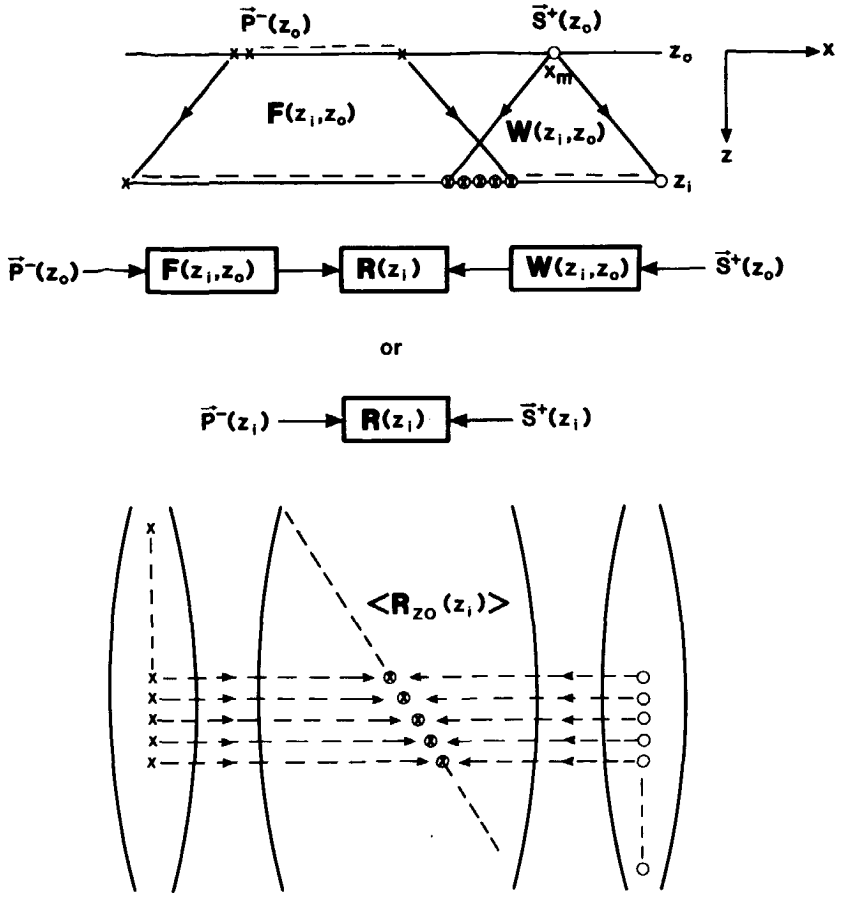

Figure II-3: Migration of a single seismic response from depth level z_i. The ZO reflectivity matrix at depth z_i follows from the downward extrapolated source and detector vectors at z_i.

corresponding element of (scaled) vector $\vec{S}^+(z_i)$. The results can be placed in a diagonal ZO reflection matrix $<\mathbf{R}_{ZO}(z_i)>$. Figure II-3 gives a schematic illustration.

To formulate the computation of the ZO reflectivity, a scalar notation is more appropriate. If we drop the matrix notation, then the wave vectors $\vec{P}^-(z_i)$ and $\vec{S}^+(z_i)$ should be replaced by the wave functions $P^-(x,z_i,\omega)$ and $S^+(x,z_i,\omega)$, respectively, while the diagonal matrix $<\mathbf{R}_{ZO}(z_i)>$ should be replaced by the ZO reflectivity function $<R_{ZO}(x,z_i,\omega)>$. According to relation (II-27) we may write for this ZO reflectivity function

$$\langle R_{ZO}(x,z_i,\omega)\rangle = \frac{1}{s^2} P^-(x,z_i,\omega)\Big(S^+(x,z_i,\omega)\Big)^*. \qquad \text{(II-28)}$$

Notice that relation (II-28) represents the frequency domain formulation for a scaled **correlation** of the downgoing source wave and the reflected upgoing waves at depth level z_i.

We now consider again the response from many depth levels, that is, we assume that $\vec{P}^-(z_o)$ is given by

$$\vec{P}^-(z_o) = \sum_i \Big[\mathbf{W}(z_o,z_i)\mathbf{R}(z_i)\mathbf{W}(z_i,z_o)\Big]\vec{S}^+(z_o), \qquad \text{(II-29)}$$

where $\vec{S}^+(z_o)$ represents a unit source vector. Again, elimination of the propagation effects between the surface and depth level z_i is described by relation (II-25), yielding $\vec{S}^+(z_i)$ and $\vec{P}^-(z_i)$, however, because many depth levels are involved now, reflection matrix $\mathbf{R}(z_i)$ should not be resolved from (II-26) but from

$$\vec{P}^-(z_i) = \mathbf{X}(z_i)\vec{S}^+(z_i), \qquad \text{(II-30a)}$$

with

$$\mathbf{X}(z_i) = \mathbf{R}(z_i) + \sum_{j\neq i} [\ldots], \qquad \text{(II-30b)}$$

see also relation (II-16). Notice that the inverse problem is ill-posed for two reasons:

1. Response matrix $\mathbf{X}(z_i)$ cannot be resolved from relation (II-30a) because $\mathbf{X}(z_i)$ is a full matrix.
2. Reflection matrix $\mathbf{R}(z_i)$ cannot be resolved from relation (II-30b) because this relation describes the response from all depth levels.

In accordance with (II-27), one particular solution of (II-30a) is given by

$$\langle \mathbf{X}(z_i)\rangle = \frac{1}{s^2} \vec{P}^-(z_i)\Big(\vec{S}^+(z_i)\Big)^{*T}, \qquad \text{(II-31)}$$

with s^2 given by (II-27c). Optionally, the ZO response matrix $\langle \mathbf{X}_{ZO}(z_i)\rangle$ is obtained by selecting the diagonal elements from the full response matrix $\langle \mathbf{X}(z_i)\rangle$. If we drop the matrix notation, then the ZO response

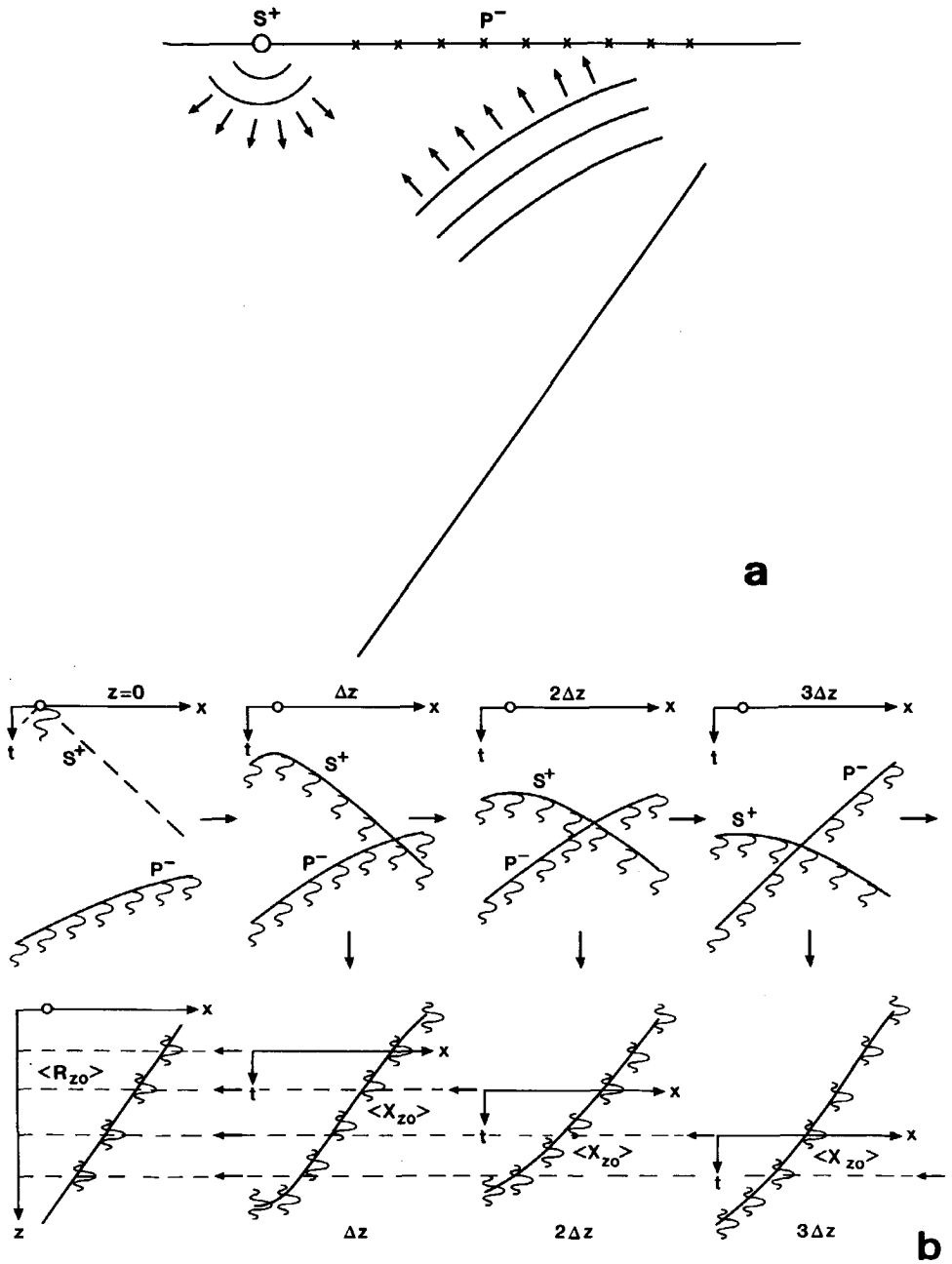

Figure II-4: Example showing the mechanism of pre-stack migration of one seismic experiment.

a. Subsurface configuration

b. Extrapolation, correlation and imaging for various depths.

$\langle X_{Z0}(x,z_i,\omega)\rangle$ may be expressed as

$$\langle X_{Z0}(x,z_i,\omega)\rangle = \frac{1}{s^2} P^-(x,z_i,\omega)\left(S^+(x,z_i,\omega)\right)^*. \qquad \text{(II-32)}$$

Relation (II-30b) can be inverted similarly as in the previous section by imaging, that is, by summing over all frequencies within the seismic bandwidth, according to

$$\langle \mathbf{R}(z_i)\rangle = \frac{\Delta\omega}{2\pi} \sum_{\omega} \langle \mathbf{X}(z_i)\rangle. \qquad \text{(II-33a)}$$

If we are interested in the Z0 reflectivity function, imaging is described by

$$\langle R_{Z0}(x,z_i)\rangle = \frac{\Delta\omega}{2\pi} \sum_{\omega} \langle X_{Z0}(x,z_i,\omega)\rangle. \qquad \text{(II-33b)}$$

Notice that relation (II-33) represents an inverse Fourier transform for zero time (t=o) only.

In order to discuss some aspects related to the mechanism of the SSRI method, we consider the configuration shown in Figure II-4a, that is, we consider the seismic response from one strongly dipping reflector. A superposition of the downgoing source wave S^+ and the upgoing detected wave P^- is presented in the space-time (x,t) domain in the upper left frame of Figure II-4b. The downward extrapolated results at depths Δz, $2\Delta z$ and $3\Delta z$, respectively, are shown in the upper frames of Figure II-4b, while the correlated data $\langle X_{Z0}\rangle$ are shown in the corresponding lower frames. Obviously these single-fold Z0 data are not exact: the dipping plane reflector appears slightly curved in the lower x,t-panels. Imaging involves computing the zero-time component of the Z0 impulse response in order to resolve the Z0 reflectivity of the current depth level. The Z0 reflectivity $\langle R_{Z0}\rangle$ for all depths is shown in the lower left frame of Figure II-4b. This single-fold Z0 reflectivity function in the x,z domain clearly represents the dipping plane reflector.

One important remark need be made with respect to spatial aliasing. In conventional CMP oriented processing the spatial sampling interval of the stacked data (pseudo Z0 data) is **half** the detector spacing. This sampling interval reduction (spatial interpolation) is necessary because the stacked data are migrated using half the propagation velocity (exploding reflector model), which means that the apparent wavelength is also reduced by a factor

two. In the CDP oriented processing method, as described in this section, the source and detector data are extrapolated using the true propagation velocity. However, after correlating the extrapolated source and detector data in order to obtain ZO data, the apparent dips are roughly doubled. This can be clearly seen in Figure II-4b, particularly by comparing the dips of P^- and $\langle X_{ZO} \rangle$ at depth $2\Delta z$. If the migrated data must be further processed then spatial aliasing should be avoided by spatially interpolating the extrapolated source and detector data **before** correlation. In this case the spatial sampling interval of the migrated data is the same for both CMP as well as CDP oriented processing techniques.

Sofar we discussed migration of one single shot record only. Because we solved an ill-posed problem the result depends highly on the input data. Generally many shot records are available which may be individually migrated, using above described procedure. The resulting zero-offset reflectivity functions $\langle R_{ZO}(x,z) \rangle_m$ may be summed, yielding a **wide-angle** zero-offset reflectivity function, according to

$$\langle R_{ZO}^{CDP}(x,z) \rangle = \sum_m \langle R_{ZO}(x,z) \rangle_m , \qquad \text{(II-34)}$$

where the super-script CDP denotes that the data have been stacked per common-depthpoint **after** migration. The principle of this procedure, which we call 'CDP stacking', is shown in Figure II-5.

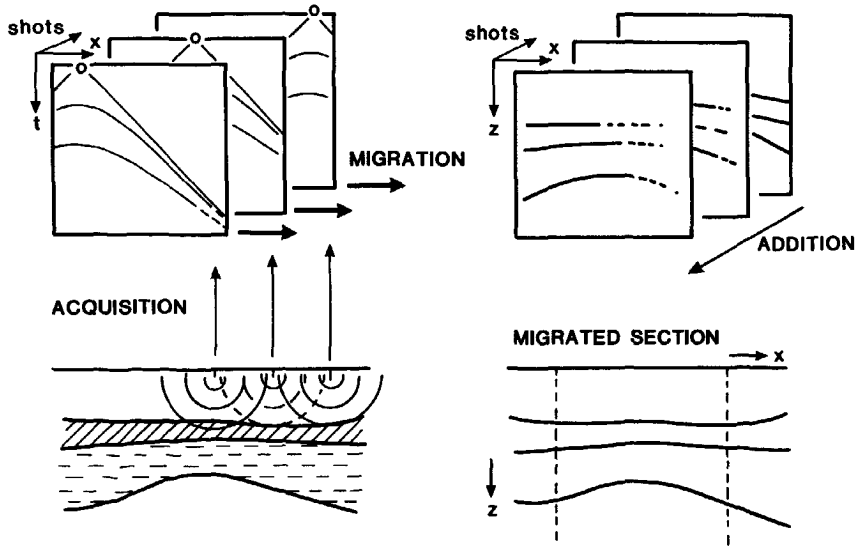

Figure II-5: Principle of CDP stacking after migration.

Sofar we discussed migration in two dimensions only. The scheme can be easily extended to three dimensions. Therefore a symbolic convolutional notation is more appropriate: we replace wave vectors by two-dimensional wave functions of the x and y coordinates, while matrix multiplications are replaced by two-dimensional, space-variant, spatial convolutions along the x and y coordinates (Berkhout, 1982), denoted by the symbol *. Full 3-D pre-stack migration by SSRI and CDP stacking can now be summarized as follows.

1. **Partly compensation for the acquisition limitations at the surface z_o.** The boundary condition $P^-_{mn}(x,y,z_o,\omega)$ follows by inverting

$$P^-_{CSP,mn}(x,y,z_o,\omega) = [D(\omega)S(\omega)]P^-_{mn}(x,y,z_o,\omega) \qquad \text{(II-35a)}$$

in a band-limited way. Here $P^-_{CSP,mn}$ represents the measured upgoing pressure wave in CSP gather mn. The boundary condition $S^+_{mn}(x,y,z_o,\omega)$, which describes a unit source at (x_m,y_n,z_o), is simply given by

$$S^+_{mn}(x,y,z_o,\omega) = \delta(x-x_m)\delta(y-y_n). \qquad \text{(II-35b)}$$

2. **Downward wave field extrapolation** to all depth levels z_i. Non-recursive 2-D wave field extrapolation is described by relation (II-25). Recursive 3-D wave field extrapolation can be formally described by

$$S^+_{mn}(x,y,z_i,\omega) = W(x,y,z_i,z_{i-1},\omega) * S^+_{mn}(x,y,z_{i-1},\omega), \qquad \text{(II-36a)}$$

$$P^-_{mn}(x,y,z_i,\omega) = F(x,y,z_i,z_{i-1},\omega) * P^-_{mn}(x,y,z_{i-1},\omega). \qquad \text{(II-36b)}$$

3. **Correlation** of the downgoing source wave and the upgoing reflected waves, yielding the single-fold ZO impulse response at depth level z_i

$$\langle X_{ZO}(x,y,z_i,\omega)\rangle_{mn} = \frac{1}{s^2_{mn}} P^-_{mn}(x,y,z_i,\omega)[S^+_{mn}(x,y,z_i,\omega)]^*, \qquad \text{(II-37a)}$$

where

$$s^2_{mn} = \int\int S^+_{mn}(x,y,z_i,\omega)[S^+_{mn}(x,y,z_i,\omega)]^* dxdy. \qquad \text{(II-37b)}$$

4. **Imaging** by summing over all frequencies, yielding the single-fold ZO reflectivity at depth level z_i

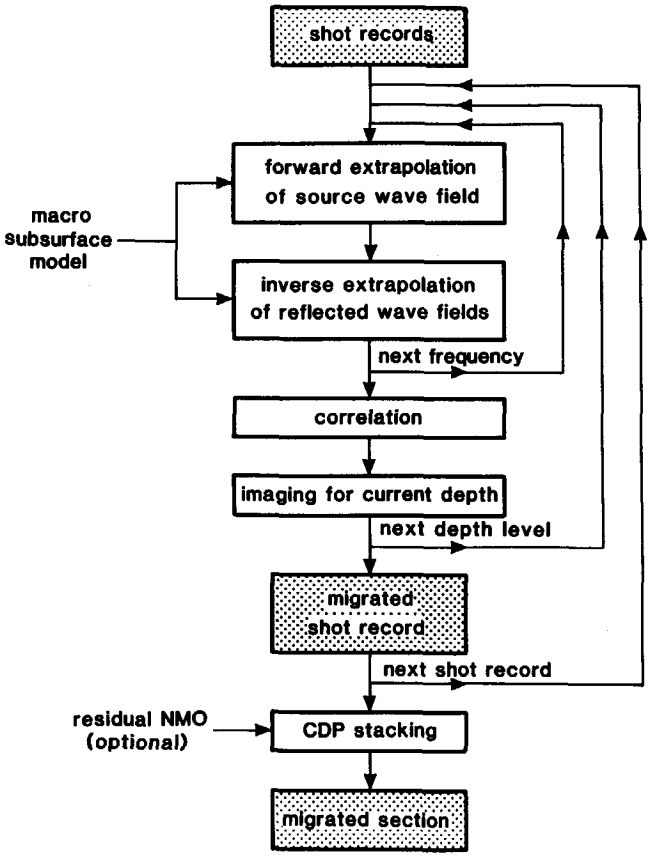

Figure II-6: Computational diagram for shot record oriented pre-stack migration.

$$\langle R_{Z0}(x,y,z_i)\rangle_{mn} = \frac{\Delta\omega}{2\pi} \sum_{\omega} \langle X_{Z0}(x,y,z_i,\omega)\rangle_{mn}. \qquad \text{(II-38)}$$

5. **CDP stacking** by summing all single-fold Z0 reflectivity functions, yielding the multi-fold wide-angle Z0 reflectivity at depth level z_i

$$\langle R^{CDP}_{Z0}(x,y,z_i)\rangle = \sum_{m} \sum_{n} \langle R_{Z0}(x,y,z_i)\rangle_{mn}. \qquad \text{(II-39)}$$

Step 1 is a pre-processing step; steps 2, 3, 4 and 5 describe the actual migration procedure. A computational diagram of this migration scheme is presented in Figure II-6. Notice that, similar as in full pre-stack migration by MSRI, migration by SSRI is carried out in field coordinates, so the wave

field extrapolation operators can be optimumly designed for a geologically oriented macro subsurface model, hence, **non-hyperbolic traveltimes** are allowed. In addition, it is shown in the next section that under certain conditions the result of the scheme presented in this section equals the result of full pre-stack migration by MSRI. Hence, under certain conditions, full pre-stack migration by SSRI and CDP stacking represents **true amplitude** migration. Furthermore the scheme has many attractive features.

Because shot records are migrated independently, any data acquisition configuration can be handled. This is particularly advantageous for 3-D applications because 3-D data are generally not gathered on a regular 2-D grid. The method is not restricted to surface data acquisition. Also vertical seismic profile (VSP) migration can be carried out by SSRI and CDP stacking. Another attractive feature is that the scheme easily copes with errors in the description of the macro subsurface model, because the data are stacked per CDP **after** migration. If the individual shot records are migrated erroneously due to errors in the macro subsurface model, then the data in a (2-D) CDP gather,

$$\langle R_{ZO}(x_j,z)\rangle_m, \quad (j \text{ is fixed, } m \text{ is a variable})$$

are not properly aligned, so a **residual NMO correction** may be applied before the CDP stack is carried out. Of course this approach is only valid for limited errors in the macro subsurface model. When these limits are exceeded, the macro model must be updated and the migration procedure should be repeated.

Another advantage of the scheme is that downward wave field extrapolation may be based on all types of wave equations. Sofar we considered independent forward extrapolation of the primary downgoing source wave and inverse extrapolation of the primary upgoing reflected waves, based on the one-way wave equations. Various aspects of the one-way approach are discussed in chapter III. Alternatively, downward extrapolation may also be based on the two-way wave equation, which describes the propagation of all primary and **multiple reflected** downgoing and upgoing waves simultaneously. Downward extrapolation can even be based on the full elastic two-way wave equation, which describes the propagation of all primary, multiple reflected and **converted** downgoing and upgoing waves simultaneously. Various aspects of the two-way approach are discussed in chapter IV for the acoustic case, and in chapter V for the full elastic case.

Finally, it should be noted that the sequence of the five processing steps, as described above, is not unique. Various alternative processing sequences can be

designed, depending on the migration objective. Generality can be gained for the cost of loss of efficiency, when the following (2-D) procedure is followed:

1. Partly compensation for the acquisition limitations (as above).
2. Downward wave field extrapolation (as above).
3. Correlation, according to relation (II-31), yielding the single-fold **full** response matrix $\langle \mathbf{X}(z_i) \rangle_m$.
4. CDP stacking, by summing all single-fold full response matrices, yielding the wide-angle multi-fold full response matrix $\mathbf{X}^{CDP}(z_i)$.
5. Imaging, by summing all frequency components of the multi-fold full response matrix, yielding the multi-fold **wide-angle** reflectivity matrix $\langle \mathbf{R}^{CDP}(z_i) \rangle$, optionally followed by selecting the diagonal elements, yielding the multi-fold wide-angle ZO reflectivity matrix $\langle \mathbf{R}^{CDP}_{ZO}(z_i) \rangle$, or, dropping the matrix notation, $\langle R^{CDP}_{ZO}(x,z_i) \rangle$.

It is obvious that the final result $\langle R^{CDP}_{ZO}(x,z_i) \rangle$ is the same as the one obtained by (II-34). However, as is shown in the next section, under certain conditions also the intermediate result $\mathbf{X}^{CDP}(z_i)$ is the same as the one obtained by (II-19) in the MSRI scheme. Hence, by means of SSRI and CDP stacking, true amplitude multi-fold full response data sets $\mathbf{X}^{CDP}(z_i)$ can be generated for arbitrary depth levels. Particularly for 3-D applications it is very attractive from a computational point of view to generate (parts of) these full response data sets for the macro layer boundaries only and to apply computationally cheaper procedures inside (some of) the macro layers. This is discussed in more detail in chapter VI.

Summarizing, full pre-stack migration by SSRI and CDP stacking is a promising technique with the following characteristic properties

- non-hyperbolic traveltimes are allowed,
- true amplitude migration may be accomplished,
- any data acquisition configuration is allowed (3-D, VSP, etc.),
- small errors in the macro subsurface model can be compensated,
- any type of wave equation can be used (one-way, two-way, full elastic, etc.),
- many variants can be designed, depending of the migration objective (angle dependent reflectivity, full response data sets at the major interfaces, etc.).

II.5 A COMPARISON OF THE DIFFERENT APPROACHES TO FULL PRE-STACK MIGRATION

Full pre-stack migration by SSRI and CDP stacking in its general form can be summarized by the following steps (we consider the 2-D scheme).

1. Partly compensation for the acquisition limitations.
2. Downward wave field extrapolation.
3. Correlation, yielding $\langle \mathbf{X}(z_i) \rangle_m$.
4. CDP stacking, yielding $\mathbf{X}^{CDP}(z_i)$.
5. Imaging, yielding $\langle \mathbf{R}^{CDP}(z_i) \rangle$ or $\langle \mathbf{R}^{CDP}_{Z0}(z_i) \rangle$.

On the other hand, full pre-stack migration by MSRI may be summarized by

1. Partly compensation for the acquisition limitations.
2. Inverse wave field extrapolation, yielding $\mathbf{X}(z_i)$.
3. Imaging, yielding $\langle \mathbf{R}(z_i) \rangle$ or $\langle \mathbf{R}_{Z0}(z_i) \rangle$.

In this section we analyse both procedures step by step and compare the results. Since the final step is the same in both procedures it is sufficient to compare the full response matrices $\mathbf{X}^{CDP}(z_i)$ and $\mathbf{X}(z_i)$. First we analyse pre-stack migration by SSRI and CDP stacking, and adapt the notation to make the comparison possible.

We consider non-recursive relations (II-25a) and (II-25b):

$$\vec{S}^{+}_{m}(z_i) = \mathbf{W}(z_i, z_o)\vec{S}^{+}_{m}(z_o), \qquad \text{(II-40a)}$$

$$\vec{P}^{-}_{m}(z_i) = \mathbf{F}(z_i, z_o)\vec{P}^{-}_{m}(z_o), \qquad \text{(II-40b)}$$

where m denotes the shot record number. Remember that $\vec{S}^{+}_{m}(z_o)$ represents a **unit** source vector, while $\vec{P}^{-}_{m}(z_o)$ is related to the measured data $\vec{P}^{-}_{CSP,m}(z_o)$ according to relation (II-23a):

$$\vec{P}^{-}_{CSP,m}(z_o) = [D(\omega)S(\omega)]\vec{P}^{-}_{m}(z_o). \qquad \text{(II-40c)}$$

We now define matrices $\mathbf{S}^{+}_{m}$ and $\mathbf{P}^{-}_{m}$ with zero-columns except for both columns m, which contain vectors $\vec{S}^{+}_{m}$ and $\vec{P}^{-}_{m}$, respectively, and rewrite relations (II-40a) and (II-40b) as

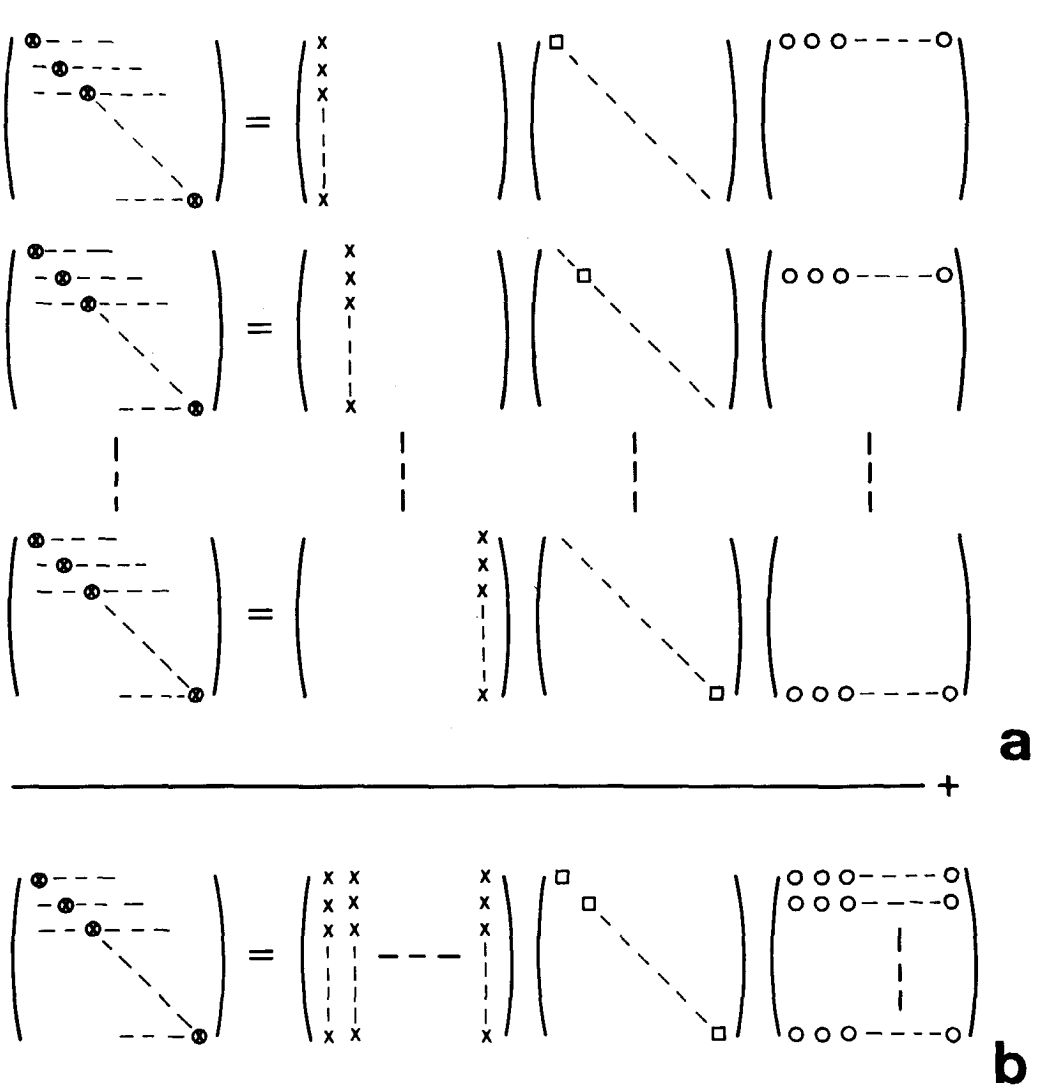

Figure II-7: A comparison of two approaches to pre-stack migration.

a. Pre-stack migration by SSRI (relation (II-43b) for various shot records).

b. Full pre-stack migration by MSRI (relation (II-48b)).

$$\mathbf{S}_m^+(z_i) = \mathbf{W}(z_i, z_o)\,\mathbf{S}_m^+(z_o), \tag{II-41a}$$

$$\mathbf{P}_m^-(z_i) = \mathbf{F}(z_i, z_o)\,\mathbf{P}_m^-(z_o). \tag{II-41b}$$

Following solution (II-27), we define a matrix $\mathbf{G}_m(z_i)$ according to

$$\mathbf{G}_m(z_i) = \left(\mathbf{S}_m^+(z_i)\right)^{*T} \mathbf{S}_m^+(z_i). \tag{II-42a}$$

Notice that $\mathbf{G}_m(z_i)$ contains zero-elements except for the m'th diagonal element, which represents the scaling factor s_m^2, so

$$\mathbf{G}_m(z_i) = \begin{pmatrix} \ddots & & \\ & s_m^2 & \\ & & \ddots \end{pmatrix}, \tag{II-42b}$$

with

$$s_m^2 = \left(\vec{S}_m^+(z_i)\right)^{*T} \vec{S}_m^+(z_i) = ||\vec{S}_m^+(z_i)||^2. \tag{II-42c}$$

Finally we define a matrix $\mathbf{C}_m(z_i)$ which contains zero-elements except for the m'th diagonal element, which represents the reciprocal of the scaling factor s_m^2, so

$$\mathbf{C}_m(z_i) = \begin{pmatrix} \ddots & & \\ & s_m^{-2} & \\ & & \ddots \end{pmatrix}. \tag{II-42d}$$

With these definitions relation (II-31)

$$\langle \mathbf{X}(z_i) \rangle_m = \frac{1}{s_m^2} \vec{P}_m^-(z_i) \left(\vec{S}_m^+(z_i)\right)^{*T} \tag{II-43a}$$

can be rewritten as

$$\langle \mathbf{X}(z_i) \rangle_m = \mathbf{P}_m^-(z_i) \mathbf{C}_m(z_i) \left(\mathbf{S}_m^+(z_i)\right)^{*T}. \tag{II-43b}$$

Relation (II-43b) is schematically shown for various m in Figure II-7a. The multi-fold full response matrix $\mathbf{X}^{CDP}(z_i)$ is obtained by CDP stacking, according to

$$\mathbf{X}^{CDP}(z_i) = \sum_m \langle \mathbf{X}(z_i) \rangle_m, \tag{II-44a}$$

or

$$\mathbf{X}^{CDP}(z_i) = \sum_m \left[\mathbf{P}_m^-(z_i) \mathbf{C}_m(z_i) \left(\mathbf{S}_m^+(z_i)\right)^{*T}\right]. \tag{II-44b}$$

Sofar we considered full pre-stack migration by SSRI and CDP stacking. Let us now consider again full pre-stack migration by MSRI. First we define downgoing source wave fields and upgoing reflected wave fields according to

$$\mathbf{S}^{+}(z_i) = \mathbf{W}(z_i,z_o)\,\mathbf{S}^{+}(z_o), \tag{II-45a}$$

$$\mathbf{P}^{-}(z_i) = \mathbf{F}(z_i,z_o)\,\mathbf{P}^{-}(z_o), \tag{II-45b}$$

where $\mathbf{S}^{+}(z_o)$ represents a unit source matrix and where $\mathbf{P}^{-}(z_o)$ is related to the measured data $\mathbf{P}^{-}_{MSP}(z_o)$ by

$$\mathbf{P}^{-}_{MSP}(z_o) = [D(\omega)S(\omega)]\,\mathbf{P}^{-}(z_o). \tag{II-45c}$$

According to relation (II-8) matrix $\mathbf{P}^{-}(z_o)$ equals the spatial impulse response matrix $\mathbf{X}(z_o)$. We may now rewrite relations (II-45a) and (II-45b) as

$$\mathbf{S}^{+}(z_i) = \mathbf{W}(z_i,z_o), \tag{II-46a}$$

$$\mathbf{P}^{-}(z_i) = \mathbf{F}(z_i,z_o)\mathbf{X}(z_o). \tag{II-46b}$$

In addition we define matrices $\mathbf{G}(z_i)$ and $\mathbf{C}(z_i)$ according to

$$\mathbf{G}(z_i) = \left(\mathbf{S}^{+}(z_i)\right)^{*T}\mathbf{S}^{+}(z_i), \tag{II-47a}$$

$$\mathbf{C}(z_i) = \left(\mathbf{G}(z_i)\right)^{-1}, \tag{II-47b}$$

hence

$$\left(\mathbf{S}^{+}(z_i)\right)^{-1} = \mathbf{C}(z_i)\left(\mathbf{S}^{+}(z_i)\right)^{*T}. \tag{II-47c}$$

With these definitions, keeping in mind that $\mathbf{F}(z_o,z_i)$ is defined as the inverse of $\mathbf{S}^{+}(z_i) = \mathbf{W}(z_i,z_o)$, we may rewrite relation (II-15), given by

$$\mathbf{X}(z_i) = \mathbf{F}(z_i,z_o)\mathbf{X}(z_o)\,\mathbf{F}(z_o,z_i)$$

as

$$\mathbf{X}(z_i) = \mathbf{P}^{-}(z_i)\left(\mathbf{S}^{+}(z_i)\right)^{-1}, \tag{II-48a}$$

or

$$\mathbf{X}(z_i) = \mathbf{P}^{-}(z_i)\mathbf{C}(z_i)\left(\mathbf{S}^{+}(z_i)\right)^{*T}. \qquad \text{(II-48b)}$$

Relation (II-48b) is schematically shown in Figure II-7b, assuming $\mathbf{C}(z_i)$ may be represented by a diagonal matrix.

Our aim is to investigate under which conditions matrix $\mathbf{X}^{CDP}(z_i)$, obtained by SSRI and CDP stacking according to relation (II-44b), equals matrix $\mathbf{X}(z_i)$, obtained by MSRI according to relation (II-48b).

Assuming a regular acquisition grid, the matrices at the surface z_o are related by

$$\mathbf{S}^{+}(z_o) = \sum_m \mathbf{S}_m^{+}(z_o), \qquad \text{(II-49a)}$$

$$\mathbf{P}^{-}(z_o) = \sum_m \mathbf{P}_m^{-}(z_o). \qquad \text{(II-49b)}$$

Straightforward application of relations (II-41) and (II-45) yields similar relations for the matrices at depth level z_i

$$\mathbf{S}^{+}(z_i) = \sum_m \mathbf{S}_m^{+}(z_i), \qquad \text{(II-49c)}$$

$$\mathbf{P}^{-}(z_i) = \sum_m \mathbf{P}_m^{-}(z_i). \qquad \text{(II-49d)}$$

Assuming matrix $\mathbf{G}(z_i)$ represents a diagonal matrix we find the following relation between $\mathbf{G}_m(z_i)$, as defined by (II-42a), and $\mathbf{G}(z_i)$, as defined by (II-47a):

$$\mathbf{G}(z_i) = \sum_m \mathbf{G}_m(z_i), \qquad \text{(II-50a)}$$

or

$$\mathbf{G}(z_i) = \begin{pmatrix} s_1^2 & & & \\ & \ddots & & \\ & & s_m^2 & \\ & & & \ddots \\ & & & & s_M^2 \end{pmatrix}, \qquad \text{(II-50b)}$$

(see also appendix A). Consequently, for matrix $\mathbf{C}(z_i)$, which is defined as the inverse of $\mathbf{G}(z_i)$, we may write

$$\mathbf{C}(z_i) = \sum_m \mathbf{C}_m(z_i), \qquad \text{(II-50c)}$$

or

$$\mathbf{C}(z_i) = \begin{pmatrix} s_1^{-2} & & & \\ & \ddots & & \\ & & s_m^{-2} & \\ & & & \ddots \\ & & & & s_M^{-2} \end{pmatrix} \qquad \text{(II-50d)}$$

With relations (II-49) and (II-50) the full response matrix $\mathbf{X}(z_i)$, given by (II-48b), can be written as

$$\mathbf{X}(z_i) = \left[\sum_m \mathbf{P}_m^-(z_i)\right]\left[\sum_m \mathbf{C}_m(z_i)\right]\left[\sum_m \left(\mathbf{S}_m^+(z_i)\right)^{*T}\right]. \qquad \text{(II-51a)}$$

In Figure II-7 it is made plausible that this relation may also be written as

$$\mathbf{X}(z_i) = \sum_m \left[\mathbf{P}_m^-(z_i)\mathbf{C}_m(z_i)\left(\mathbf{S}_m^+(z_i)\right)^{*T}\right]. \qquad \text{(II-51b)}$$

The proof is given in appendix A. Comparing (II-51b) with the definition of $\mathbf{X}^{CDP}(z_i)$ in (II-44b) yields

$$\mathbf{X}(z_i) = \mathbf{X}^{CDP}(z_i). \qquad \text{(II-52)}$$

Hence, we have shown that full pre-stack migration by SSRI and CDP stacking is equivalent with **true amplitude** full pre-stack migration by MSRI if we may make some particular assumptions on

- the data acquisition configuration at the surface,
- the illuminating source wave field in the subsurface.

With respect to the first assumption we remark that in full pre-stack migration by MSRI it is assumed that the data are gathered on a regular grid. On the other hand, in full pre-stack migration by SSRI and CDP stacking, seismic records are migrated independently so they may have random positions at the surface, which is very attractive from a practical point of view, particularly for 3-D applications. However, the classification 'true amplitude migration' is correct only when the individually migrated seismic records are gathered on a regular grid as in full pre-stack migration by MSRI. With respect to the second assumption we remark that in full pre-stack migration by MSRI the matrix product

$$\mathbf{G}(z_i) = \left(\mathbf{S}^{+}(z_i)\right)^{*T}\mathbf{S}^{+}(z_i)$$

is inverted (see relation (II-47b)), which means that generally all illuminating source wave fields must be available simultaneously. Only when $\mathbf{G}(z_i)$ is a **diagonal** matrix, inversion can be carried out per diagonal element $s_m^2 = ||\vec{S}_m^{+}(z_i)||^2$, so per illuminating source wave field as in full pre-stack migration by SSRI and CDP stacking.

The character of matrix $\mathbf{G}(z_i)$ depends on the properties of the macro subsurface model between the surface and depth level z_i. We consider three cases.

i. The macro subsurface model is homogeneous. In this case matrix $\mathbf{G}(z_i)$ is a unit matrix, within the limitations imposed by the spatial bandwidth of propagating waves (matched filter approach). Hence, for a homogeneous macro subsurface model the two approaches to full pre-stack migration are equivalent. Notice that the scaling factor s_m^{-2} in SSRI need not be applied because it approaches unity.

ii. The macro subsurface model is 1-D inhomogeneous, that is, the medium parameters are a function of depth only. In this case the character of the illuminating source wave field in the subsurface is independent of the source position at the surface, hence, the elements of $\mathbf{G}(z_i)$ are constant along the diagonal. However, matrix $\mathbf{G}(z_i)$ is not purely a diagonal matrix, hence, the two approaches to full pre-stack migration are not fully equivalent. In SSRI the effect of the scaling factor s_m^{-2} (which is constant for all m) is an energy correction for the illuminating wave fields.

iii. The macro subsurface model is arbitrarily inhomogeneous. In this case matrix $\mathbf{G}(z_i)$ may deviate significantly from a diagonal matrix, hence, the two approaches to full pre-stack migration are no longer equivalent. Ideally, true inversion (**not** the matched filter approach) should be applied in pre-stack migration by MSRI. Amplitude errors (**no** positioning errors) are made in pre-stack migration by SSRI and CDP stacking. However, compared with practical pre-stack migration schemes known in seismic literature, the (source dependent) energy correction factor s_m^{-2}, as suggested in this chapter, means an improvement with respect to the amplitude handling of migration schemes for arbitrarily inhomogeneous macro subsurface models.

Finally, we give an example to demonstrate the mechanism of SSRI and CDP stacking. We consider the configuration shown in Figure II-8a, that is, we consider the seismic response from four point-diffractors. Three 'split-spread' CSP records for different source positions are presented in the space-time (x,t) domain in Figure II-8b. After downward extrapolation to the level of the upper diffractors, the source and detector data are correlated, yielding single-fold ZO responses $\langle X_{ZO} \rangle$. These responses are presented with a floating time reference in the space-time domain in Figure II-8c. To enhance several artefacts, the amplitudes in this display were clipped at -20 dB (relative to the maximum amplitude). Obviously these single-fold ZO gathers are not exact: the three diffractors at the current extrapolation level are focussed but not well resolved, while the lower diffractor is represented by three different time-reversed hyperbolae. This was expected because single-shot records were inverted.

We now consider the effect of CDP stacking after SSRI. The upper left frame of Figure II-8d shows the 8-fold CDP stacked ZO response X_{ZO}^{CDP}. Notice that all individual inversion results can be clearly distinguished in this figure (the amplitudes were clipped at -32 dB). This effect is also known as spatial aliasing: the source spacing at the surface is significantly larger than half the dominant wavelength. The effect of reducing the source spacing is shown in the other frames of Figure II-8d for, respectively, 16-fold, 32-fold and 64-fold CDP stacked ZO data X_{ZO}^{CDP}. Notice that particularly the lower right frame shows high quality ZO data: the three diffractors at the current extrapolation level are properly focussed and well resolved, and the lower diffractor is clearly represented by a hyperbola, confirming that the CDP stacked data X_{ZO}^{CDP} represent **wide-angle** ZO data. The remaining artefacts, which are visible because the amplitudes are clipped in this display, are due to the limited temporal and spatial bandwidth.

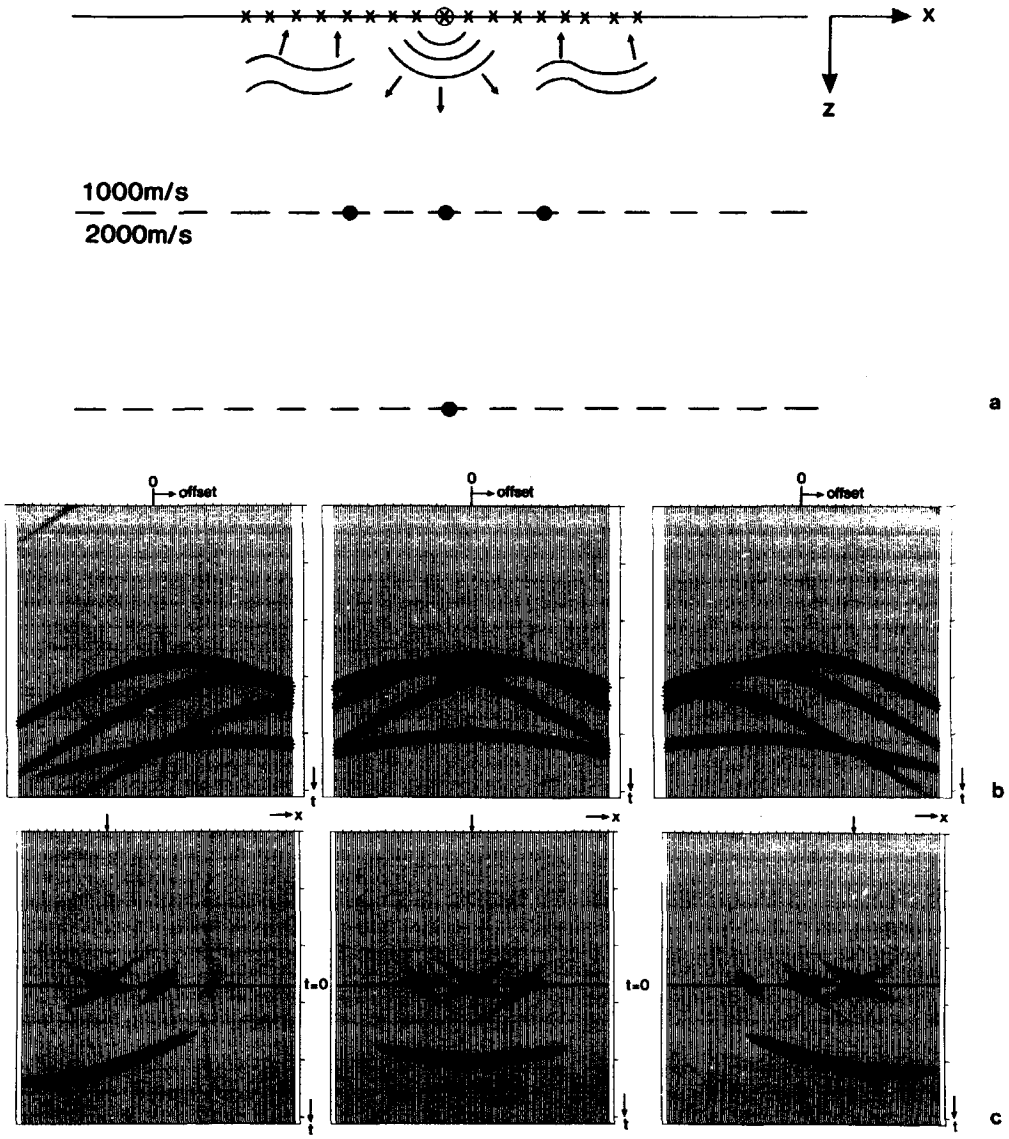

Figure II-8: Example showing the mechanism of SSRI and CDP stacking.

a. Subsurface configuration

b. Three CSP gathers.

c. Corresponding downward extrapolated single-fold ZO responses (the source positions at the surface are indicated by arrows).

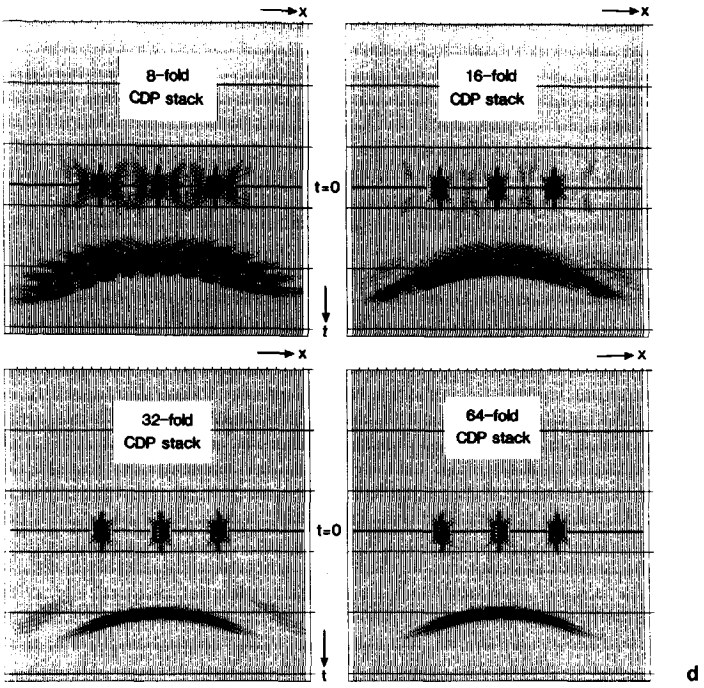

Figure II-8 (continued)

d. Multi-fold CDP stacked ZO data.

CHAPTER III

WAVE FIELD EXTRAPOLATION TECHNIQUES, INCLUDING CRITICAL ANGLE EVENTS, BASED ON THE ACOUSTIC ONE-WAY WAVE EQUATIONS

III.1 INTRODUCTION

Both in modeling and migration schemes, wave field extrapolation operators play an important role. In depth extrapolation techniques these operators describe the propagation effects of the wave field from one depth level to another. For this purpose a horizontally layered **computational** model is often chosen, as shown in Figure III-1. Notice that we consider the acoustic case. It should be stressed that the depth levels $z_o, z_1, z_2 \cdots z_{i-1}, z_i, \cdots z_I$ generally do not

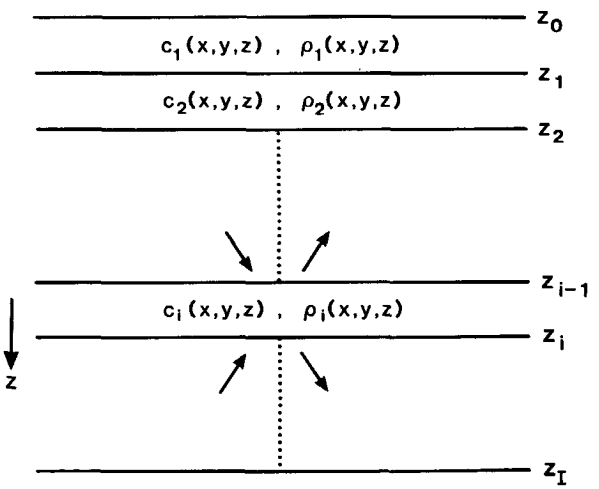

Figure III-1: Computationally convenient acoustic subsurface model for depth extrapolation techniques.

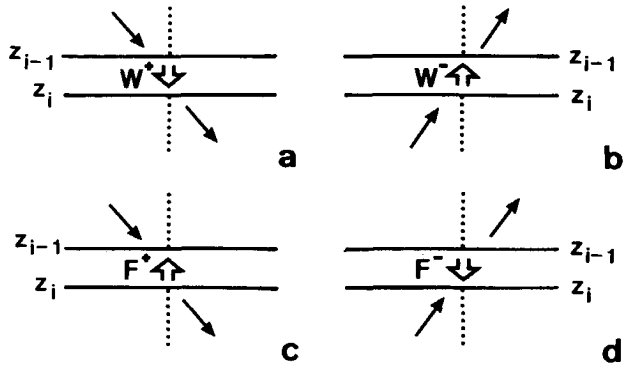

Figure III-2: In the one-way approach to wave field extrapolation downgoing and upgoing waves are treated independently.
a. Forward extrapolation of downgoing waves
b. Forward extrapolation of upgoing waves
c. Inverse extrapolation of downgoing waves
d. Inverse extrapolation of upgoing waves

coincide with the reflecting boundaries in the macro subsurface model. As a consequence, the medium parameters c and ρ (compressional wave velocity and mass density; for notational convenience we delete the bars above symbols which describe the macro subsurface model) between two depth levels may be arbitrary functions of the spatial coordinates (x,y,z). Most approaches to wave field extrapolation are based on the assumption that the downgoing source wave field and the upgoing reflected wave field may be treated independently. This **one-way approach** is extensively discussed by Berkhout (1982). In the frequency domain the one-way operations can be formulated in terms of spatial convolutions. We consider four cases.

i. **Forward extrapolation of downgoing waves** P^+ (the positive z-axis is pointing downward) is symbolically described by

$$P^+(z_i) = W^+(z_i,z_{i-1}) * P^+(z_{i-1}), \qquad \text{(III-1a)}$$

see also Figure III-2a. (For notational convenience we abbreviate wave functions $P(x,y,z,\omega)$ as $P(z)$ or P; the symbol * denotes spatial convolutions along the x and y coordinates).

ii. **Forward extrapolation of upgoing waves** P^- is symbolically described by

$$P^-(z_{i-1}) = W^-(z_{i-1},z_i) * P^-(z_i), \qquad \text{(III-1b)}$$

see also Figure III-2b.

iii. **Inverse extrapolation of downgoing waves** P^+ is symbolically described by

$$P^+(z_{i-1}) = F^+(z_{i-1},z_i) * P^+(z_i), \qquad \text{(III-1c)}$$

see also Figure III-2c.

iv. **Inverse extrapolation of upgoing waves** P^- is symbolically described by

$$P^-(z_i) = F^-(z_i,z_{i-1}) * P^-(z_{i-1}), \qquad \text{(III-1d)}$$

see also Figure III-2d.

Various expressions for the one-way operators W^+, W^-, F^+ and F^- are discussed further on in this chapter.
In case of arbitrarily inhomogeneous media, the one-way approach is only justified for waves traveling with limited propagation angles, in seismic literature referred to as sub-critical angle events. The wave equations which govern these sub-critical angle events are commonly known as **the one-way wave equations** for downgoing and upgoing waves. In this chapter we briefly review the one-way wave equations, the underlying assumptions and the solutions. Furthermore a discussion of the physical interpretation is presented.

The treatment of waves with large propagation angles is significantly different from the treatment of sub-critical events. In literature much attention has been paid to the behaviour of the wave field in the vicinity of so called turning points. An extensive historical survey is presented by McHugh (1971). At a turning point the propagation direction of the energy flow of an incident wave field is fully changed from downwards into upwards or vice versa, due to a vertical gradient in the propagation velocity. In the following, such events are referred to as 'critical'. Unlike sub-critical angle data, the treatment of seismic data including critical angle events is rather complicated, because propagating downgoing and upgoing waves are **coupled** near the turning point. This implies that modeling and migration schemes for sub-critical angle data cannot simply be extended for the incorporation of critical angle events if the

coupling of propagating downgoing and upgoing waves is neglected. Several alternative modeling approaches have been proposed, based on the WKBJ-technique, which give an adequate treatment of critical angle events. Although satisfactory for modeling, these approaches are not suitable for migration applications. In this chapter we discuss an alternative subdivision of the total wave field near the turning point into downgoing and upgoing waves. Based on this approach, we define one-way forward and inverse wave field extrapolation operators which include critical angle events for 1-D (vertically) inhomogeneous media. Applications of these operators in modeling and migration schemes are also discussed in this chapter. In chapter IV we compare the one-way results with two-way wave field extrapolation operators which include critical events for arbitrarily inhomogeneous media.

III.2 GENERAL ASPECTS OF THE ACOUSTIC WAVE EQUATION

For loss-less inhomogeneous fluids the linearized equation of motion reads, for the source-free situation,

$$\frac{1}{\rho}\nabla p = -\frac{\partial \vec{v}}{\partial t}, \tag{III-2a}$$

and the linearized stress-strain relation reads

$$K\nabla.\vec{v} = -\frac{\partial p}{\partial t}. \tag{III-2b}$$

Here $p=p(x,y,z,t)$ represents the acoustic pressure as a function of the spatial coordinates (x,y,z) and time t, and $\vec{v}=\vec{v}(x,y,z,t)$ represents the particle velocity, also as a function of space and time. Furthermore, $\rho=\rho(x,y,z)$ describes the space dependent mass density in equilibrium and $K=K(x,y,z)$ describes the space dependent bulk compression modulus. The temporal Fourier transformation of a function $f(x,y,z,t)$ from time to frequency we define as

$$F(x,y,z,\omega) = \int_{-\infty}^{\infty} f(x,y,z,t)e^{-j\omega t}dt, \tag{III-3a}$$

and its inverse as

$$f(x,y,z,t) = \frac{1}{2\pi}\int_{-\infty}^{\infty} F(x,y,z,\omega)e^{+j\omega t}d\omega. \tag{III-3b}$$

Here ω represents the radial frequency. With these definitions the equation of motion in the frequency domain reads

$$\frac{1}{\rho} \nabla P = -j\omega \vec{V}, \qquad \text{(III-4a)}$$

and the stress-strain relation in the frequency domain reads

$$K \nabla . \vec{V} = -j\omega P, \qquad \text{(III-4b)}$$

where $P=P(x,y,z,\omega)$ represents the temporal Fourier transform of the acoustic pressure $p=p(x,y,z,t)$ and where $\vec{V}=\vec{V}(x,y,z,\omega)$ represents the temporal Fourier transform of the particle velocity $\vec{v}=\vec{v}(x,y,z,t)$. Relations (III-4a) and (III-4b) can be combined into the well-known frequency domain representation of the acoustic wave equation

$$\rho \nabla (\frac{1}{\rho} \nabla P) + k^2 P = o, \qquad \text{(III-5a)}$$

where

$$k = \omega / c \qquad \text{(III-5b)}$$

with

$$c = \sqrt{K/\rho}. \qquad \text{(III-5c)}$$

Here $c=c(x,y,z)$ describes the space dependent propagation velocity. Wave equation (III-5) is valid for **inhomogeneous liquids** in which shear stresses cannot exist (the shear modulus μ equals zero). It is shown, however, in chapter V that similar wave equations hold for (independent) compressional and shear waves in **homogeneous solids.** For instance, P in relation (III-5) may represent the (scalar) potential for the particle velocity of dilatational or compressional waves in homogeneous solids when the propagation velocity c is replaced by c_p, given by

$$c_p = \sqrt{(\lambda + 2\mu)/\rho}. \qquad \text{(III-6a)}$$

Here the Lamé constants λ and μ are related to K and Poisson's ratio σ according to

$$K = \lambda + 2\mu/3, \qquad \text{(III-6b)}$$

$$\sigma = \tfrac{1}{2}\lambda/(\lambda + \mu). \qquad \text{(III-6c)}$$

(Notice that in liquids the shear modulus μ vanishes (μ=o), so K=λ and σ=½). If we define a constrained compression modulus K_c, according to

$$K_c = K + 4\mu/3, \tag{III-7a}$$

then it follows that the velocity c_p of compressional waves in solids can be written in a similar form as the velocity c in liquids, according to

$$c_p = \sqrt{K_c/\rho}. \tag{III-7b}$$

Hence, assuming that wave conversion may be neglected, all the results obtained from the **acoustic** wave equation in chapters III and IV can be directly translated to compressional waves in solids when the bulk compression modulus K is replaced by the constrained compression modulus K_c. This constrained acoustic approach is exact for homogeneous solids, where wave conversion cannot occur, while it is approximately valid for weakly inhomogeneous solids. The constrained acoustic approach breaks down in strongly inhomogeneous solids, where wave conversion cannot be neglected any longer. In this case the full elastic approach, as discussed in chapter V, must be followed.

We consider again acoustic wave equation (III-5). In order to describe wave field extrapolation along the depth coordinate we separate z-derivatives from x and y-derivatives according to

$$\rho \frac{\partial}{\partial z}\left(\frac{1}{\rho}\frac{\partial P}{\partial z}\right) = -k^2 P - \rho \frac{\partial}{\partial x}\left(\frac{1}{\rho}\frac{\partial P}{\partial x}\right) - \rho \frac{\partial}{\partial y}\left(\frac{1}{\rho}\frac{\partial P}{\partial y}\right). \tag{III-8}$$

Because seismic data are always band-limited, the z-derivatives can be expressed as a lateral **convolution operator** working on P at depth level z, according to

$$\rho \frac{\partial}{\partial z}\left(\frac{1}{\rho}\frac{\partial P}{\partial z}\right) = -H_2 * P, \tag{III-9a}$$

where

$$H_2(x,y,z,\omega) = \left[k^2 d_o(x,y) + d_2(x) + d_2(y) - \frac{\partial \ln\rho}{\partial x} d_1(x) - \frac{\partial \ln\rho}{\partial y} d_1(y)\right]_z. \tag{III-9b}$$

Relation (III-9) represents a space variant spatial convolution along the x and y coordinates. The operators $d_m(x)$ and $d_m(y)$ represent **space invariant** band-limited spatial differentiation operators with respect to x and y

respectively, where m represents the order of differentiation; operator $d_o(x,y)$ represents a spatial delta function:

$$d_o(x,y) = \delta(x)\delta(y). \qquad \text{(III-9c)}$$

The parameters k^2, $\partial \ln\rho/\partial x$ and $\partial \ln\rho/\partial y$ represent **space variant** weighting factors which should be applied after the differentiations have been carried out. The **spatially band-limited** operators $d_m(x)$ and $d_m(y)$ can be designed via the wavenumber domain. Therefore we define the double spatial Fourier transform of a function $F(x,y,z,\omega)$ as

$$\tilde{F}(k_x,k_y,z,\omega) = \iint_{-\infty}^{\infty} F(x,y,z,\omega)e^{j(k_x x+k_y y)}dxdy \qquad \text{(III-10a)}$$

and its inverse as

$$F(x,y,z,\omega) = (\frac{1}{2\pi})^2 \iint_{-\infty}^{\infty} \tilde{F}(k_x,k_y,z,\omega)e^{-j(k_x x+k_y y)}dk_x dk_y . \qquad \text{(III-10b)}$$

Here the wavenumbers k_x and k_y represent the horizontal components of the wave vector $\vec{k}$. With these definitions the differentiations

$$\frac{\partial^m}{\partial x^m} F(x,y,z,\omega) \qquad \text{(III-11a)}$$

and

$$\frac{\partial^m}{\partial y^m} F(x,y,z,\omega) \qquad \text{(III-11b)}$$

in the space-frequency domain correspond to the following multiplications in the wavenumber-frequency domain

$$(-jk_x)^m \tilde{F}(k_x,k_y,z,\omega) \qquad \text{(III-11c)}$$

and

$$(-jk_y)^m \tilde{F}(k_x,k_y,z,\omega) \qquad \text{(III-11d)}$$

respectively. The band-limited versions of $(-jk_x)^m$ and $(-jk_y)^m$ for m=2 are schematically presented in Figure III-3a. The corresponding band-limited

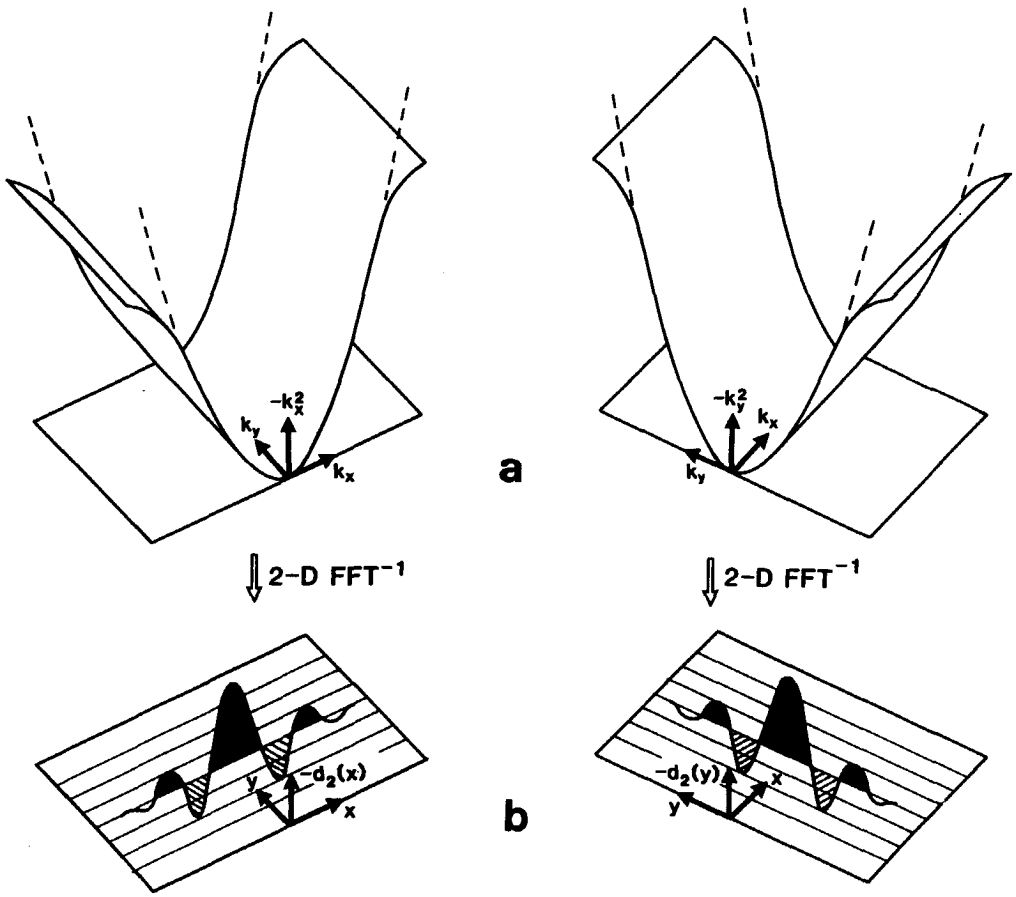

Figure III-3: Spatially band-limited differentiation operators.
a. Representation in the wavenumber domain.
b. Representation in the space domain.

differentiation operators $d_m(x)$ and $d_m(y)$ for m=2 (which are obtained after a double inverse Fourier transformation) are shown in Figure III-3b. Note that $d_m(x)$ and $d_m(y)$ represent **one-dimensional** convolution operators. For a rigorous discussion on the effects of band-limitation the reader is referred to Berkhout (1982). In the following, whenever appropriate, band-limitation is assumed without notification.

In its present formulation, wave equation (III-9) is not yet suitable for wave field extrapolation because it is a second order differential equation. In

principle there are two ways to transform this wave equation into easily manageable first order differential equations:

i. Decomposition of the total wave field into "downgoing" and "upgoing" waves P^+ and P^-:

$$P = P^+ + P^- \tag{III-11}$$

such that

$$\frac{\partial P^+}{\partial z} = -jH_1^+ * P^+, \tag{III-12a}$$

$$\frac{\partial P^-}{\partial z} = +jH_1^- * P^-. \tag{III-12b}$$

ii. Reformulation of the scalar wave equation into a matrix equation

$$\frac{\partial}{\partial z}\begin{bmatrix} P \\ \frac{1}{\rho}\frac{\partial P}{\partial z} \end{bmatrix} = \begin{bmatrix} 0 & \rho d_o^* \\ \frac{-1}{\rho}H_2^* & 0 \end{bmatrix}\begin{bmatrix} P \\ \frac{1}{\rho}\frac{\partial P}{\partial z} \end{bmatrix}. \tag{III-13}$$

In (III-12) we symbolically formulated **one-way wave equations.** The definition of operators H_1^+ and H_1^- depends on the approach to decomposition. In section III.4 we discuss the conventional approach where H_1^+ and H_1^- cannot be decoupled for critical angle events. In section III.7 we introduce an alternative approach where H_1^+ and H_1^- decouple for sub-critical as well as critical angle events in 1-D inhomogeneous media.

In (III-13) we formulated the matrix representation of the **two-way wave equation.** This equation is exact; hence it is valid for sub-critical as well as critical angle events in arbitrarily inhomogeneous fluid-like media. Solutions are discussed in chapter IV.

III.3 ACOUSTIC ONE-WAY WAVE EQUATIONS FOR A HOMOGENEOUS MEDIUM

In a homogeneous medium, equation (III-9) can be simplified to

$$\frac{\partial P}{\partial z} = \pm jH_1 * P, \tag{III-14a}$$

where the **square-root operator** H_1 is implicitly defined according to

$$H_1 * H_1 = H_2. \qquad \text{(III-14b)}$$

We now study the propagation direction of P. Therefore we choose $j=+\sqrt{-1}$. With definition (III-10), in the wavenumber-frequency domain equation (III-14) reads

$$\frac{\partial \tilde{P}}{\partial z} = \pm j\tilde{H}_1 \tilde{P}, \qquad \text{(III-15a)}$$

where the transformed square-root operator $\tilde{H}_1$ is explicitly defined according to

$$\tilde{H}_1^2 = \tilde{H}_2, \qquad \text{(III-15b)}$$

or

$$\tilde{H}_1 = k_z = \sqrt{k^2 - k_x^2 - k_y^2}, \qquad \text{(III-15c)}$$

or, in spherical coordinates

$$\tilde{H}_1 = k \cos\theta, \qquad \text{(III-15d)}$$

where θ is the angle between the propagation direction and the z-axis (Berkhout, 1982). The solution of wave equation (III-15a) is given by

$$\tilde{P}(z) = \tilde{W}(z,z_o)\tilde{P}(z_o), \qquad \text{(III-16a)}$$

with

$$\tilde{W}(z,z_o) = \exp(\pm j\tilde{H}_1 \Delta z), \qquad \text{(III-16b)}$$

$$\Delta z = z - z_o. \qquad \text{(III-16c)}$$

When we consider propagating waves ($\tilde{H}_1^2 \geq o$), it follows that $-j\tilde{H}_1$ refers to downgoing waves, because the argument of $\tilde{W}$ decreases with depth. Similarly, $+j\tilde{H}_1$ refers to upgoing waves. For **forward** one-way wave field extrapolation, operator $\tilde{W}$ is generally rewritten as

$$\tilde{W}(z,z_o) = \exp(-j\tilde{H}_1 |\Delta z|). \qquad \text{(III-16d)}$$

Notice that this formulation applies for forward extrapolation of downgoing waves ($\Delta z > o$), as well as for upgoing waves ($\Delta z < o$). The operator $\tilde{W}$, as defined by (III-16d), is commonly known as the phase-shift operator (Gazdag, 1978). The

inverse double spatial Fourier transform of relation (III-16a) is given by

$$P(z) = W(z,z_o) * P(z_o), \qquad \text{(III-17)}$$

where W represents the well-known Rayleigh II operator (Schneider, 1978). Note that relation (III-17) describes wave field extrapolation in the z-direction; the convolution is carried out in the x and y-directions. The operators W and $\tilde{W}$ are extensively discussed for both propagating and evanescent waves by Berkhout (1982). Furthermore it is shown by Berkhout that the spatially band-limited **inverse** one-way wave field extrapolation operators can be well approximated by the complex conjugated of the forward operators W and $\tilde{W}$.

Summarizing, conformable to (III-12a,b) in a **homogeneous medium** the one-way wave equations for downgoing and upgoing waves P^+ and P^- read

$$\frac{\partial P^+}{\partial z} = -jH_1^+ * P^+, \qquad \text{(III-18a)}$$

$$\frac{\partial P^-}{\partial z} = +jH_1^- * P^-, \qquad \text{(III-18b)}$$

respectively, with

$$H_1^+ = H_1^- = H_1, \qquad \text{(III-18c)}$$

where H_1 is the **square-root operator** as defined by (III-14b). Notice that these relations are exact. Furthermore, conformable to (III-1), solutions of (III-18a) and (III-18b) for forward extrapolation are given by

$$P^+(z_i) = W^+(z_i,z_{i-1}) * P^+(z_{i-1}), \qquad \text{(III-19a)}$$

$$P^-(z_{i-1}) = W^-(z_{i-1},z_i) * P^-(z_i), \qquad \text{(III-19b)}$$

respectively, with

$$W^+ = W^- = W,$$

where W is the Rayleigh II operator. Finally, relations (III-19a) and (III-19b) can be inverted in a spatially band-limited way according to

$$P^+(z_{i-1}) = F^+(z_{i-1},z_i) * P^+(z_i), \qquad \text{(III-19c)}$$

$$P^-(z_i) = F^-(z_i,z_{i-1}) * P^-(z_{i-1}), \qquad \text{(III-19d)}$$

respectively, with

$$F^+ = F^- = W^*,$$

where the superscript * denotes complex conjugation.

III.4 ACOUSTIC ONE-WAY WAVE EQUATIONS FOR AN ARBITRARILY INHOMOGENEOUS MEDIUM

In an arbitrarily inhomogeneous medium one-way wave equations (III-18a) and (III-18b) do not hold. It has been shown by Brekhovskikh (1980), amongst others, that decomposition into downgoing and upgoing waves is not uniquely defined. Here we extend the approach which is usually followed for 1-D (vertically) inhomogeneous media to arbitrarily inhomogeneous media. In section III.7 we discuss an alternative decoupling approach which properly incorporates critical angle events in 1-D inhomogeneous media.

In the following we choose the decomposition such that the particle velocity of our choice of the downgoing wave is related to the pressure of this downgoing wave only. A similar choice is taken for the upgoing wave. For the **total** wave field we have the following relations between particle velocity and pressure

$$-\frac{\partial P}{\partial z} = j\omega\rho V_z, \qquad \text{(III-20a)}$$

$$H_2 * P = j\omega\rho \frac{\partial V_z}{\partial z}, \qquad \text{(III-20b)}$$

where relation (III-20a) describes the z-component of the equation of motion (III-4a) (V_z: z-component of particle velocity $\vec{V}$), and where relation (III-20b) is obtained after substituting the x and y-components of the equation of motion into the stress-strain relation (III-4b). Notice that relations (III-20a) and (III-20b) are consistent with wave equation (III-9).
Now we **define** "downgoing" and "upgoing" waves such that (according to the homogeneous situation)

$$j\omega\rho\, V_z^+ \overset{\text{def}}{=\!=} + jH_1 * P^+, \tag{III-21a}$$

$$j\omega\rho\, V_z^- \overset{\text{def}}{=\!=} - jH_1 * P^-, \tag{III-21b}$$

where

$$H_1 * H_1 = H_2, \tag{III-21c}$$

with H_2 defined by relation (III-9b). If we also demand that

$$P = P^+ + P^-, \tag{III-22a}$$

$$V_z = V_z^+ + V_z^-, \tag{III-22b}$$

then substitution into the modified equation of motion (III-20a) yields

$$\frac{\partial}{\partial z}(P^+ + P^-) = -jH_1 * (P^+ - P^-), \tag{III-23a}$$

while substitution into the modified stress-strain relation (III-20b) yields

$$H_2 * (P^+ + P^-) = j\rho \frac{\partial}{\partial z}\left[\frac{1}{\rho} H_1 * (P^+ - P^-)\right], \tag{III-23b}$$

or

$$\frac{\partial}{\partial z}(P^+ - P^-) = -jH_1 * (P^+ + P^-) - H_{-1} * \left[\rho \frac{\partial}{\partial z}(\frac{1}{\rho} H_1)\right] * (P^+ - P^-), \tag{III-23c}$$

where

$$H_{-1} * H_1 = \delta(x)\delta(y). \tag{III-23d}$$

Addition of relations (III-23a) and (III-23c) yields

$$\frac{\partial P^+}{\partial z} = -jH_1 * P^+ - \tfrac{1}{2}H_{-1} * \left[\rho \frac{\partial}{\partial z}(\frac{1}{\rho} H_1)\right] * (P^+ - P^-). \tag{III-24a}$$

Substraction of relations (III-23a) and (III-23c) yields

$$\frac{\partial P^-}{\partial z} = jH_1 * P^- + \tfrac{1}{2}H_{-1} * \left[\rho \frac{\partial}{\partial z}(\frac{1}{\rho} H_1)\right] * (P^+ - P^-). \tag{III-24b}$$

Notice that these relations are exact, but our choice of downgoing and upgoing waves are coupled by the reflectivity properties of the medium. The relations

(III-24a,b) can be written conformable to (III-12a,b), when we define

$$P = P^+ + P^- = [\delta(x)\delta(y) + \Gamma^+] * P^+ \qquad \text{(III-25a)}$$

for downward propagation, and

$$P = P^+ + P^- = [\delta(x)\delta(y) + \Gamma^-] * P^- \qquad \text{(III-25b)}$$

for upward propagation. Now the one-way wave equations read

$$\frac{\partial P^+}{\partial z} = -jH_1^+ * P^+, \qquad \text{(III-26a)}$$

$$\frac{\partial P^-}{\partial z} = +jH_1^- * P^-, \qquad \text{(III-26b)}$$

where the operators H_1^+ and H_1^- are defined as

$$jH_1^+ = jH_1 + \tfrac{1}{2}H_{-1} * [\rho \frac{\partial}{\partial z}(\frac{1}{\rho} H_1)] * [\delta(x)\delta(y) - \Gamma^+], \qquad \text{(III-26c)}$$

$$jH_1^- = jH_1 - \tfrac{1}{2}H_{-1} * [\rho \frac{\partial}{\partial z}(\frac{1}{\rho} H_1)] * [\delta(x)\delta(y) - \Gamma^-]. \qquad \text{(III-26d)}$$

Notice that the coupling of these one-way wave equations is described by the operators Γ^+ and Γ^-. In the following we consider three cases in which the one-way wave equations decouple.

A. The medium parameters are functions of the lateral coordinates only, that is, $c=c(x,y)$, $\rho=\rho(x,y)$. For this situation relations (III-26a) and (III-26b) decouple since H_1^+ and H_1^- both simplify to H_1. Notice that this decoupling is exact. A special case was already found in section III.3 for a homogeneous medium.

B. Only primary waves are considered, that is, Γ^+ and Γ^- are neglected in relations (III-25a) and (III-25b). The one-way wave equations (III-26a) and (III-26b) decouple because the coupling operators Γ^+ and Γ^- in relations (III-26c) and (III-26d) are absent. This approach is valid for sub-critical angle events only, as is shown in section III.5.

C. Multiple reflections are incorporated in the primary waves, as described by relations (III-25a) and (III-25b). Now a general solution cannot be given. In section III.7 we discuss a special case which is based on the WKBJ approach with a particular choice of downgoing and upgoing waves,

which, well away from the critical region, reduce to the P^+ and P^- terms as defined above, for $\Gamma^+ = \Gamma^- = o$. This approach enables decoupled one-way wave equations to be constructed for sub-critical as well as critical angle events in 1-D (vertically) inhomogeneous media.

III.5 SOLUTION OF THE ACOUSTIC ONE-WAY WAVE EQUATIONS FOR SUB-CRITICAL ANGLE EVENTS

The least complicated case of decoupled downgoing and upgoing waves in inhomogeneous media occurs when the medium parameters are functions of the horizontal coordinates only, as was shown in the previous section (case A). For this situation the decoupled one-way wave equations read

$$\frac{\partial P^+}{\partial z} = -jH_1 * P^+, \qquad \text{(III-27a)}$$

and

$$\frac{\partial P^-}{\partial z} = jH_1 * P^-. \qquad \text{(III-27b)}$$

Assuming that the derivatives $\partial^n P^+/\partial z^n$ exist and are continuous between z_{i-1} and z, we can define forward one-way wave field extrapolation of downgoing waves by means of the following Taylor series summation

$$P^+(z) = \sum_{n=o}^{\infty} \frac{\Delta z^n}{n!} \left[\frac{\partial^n P^+}{\partial z^n}\right]_{z_{i-1}}, \qquad \text{(III-28)}$$

with $\Delta z = z - z_{i-1} \geq o$, or, with one-way wave equation (III-27a),

$$P^+(z_i) = W^+(z_i, z_{i-1}) * P^+(z_{i-1}), \qquad \text{(III-29a)}$$

where

$$W^+(z_i, z_{i-1}) = \sum_{n=o}^{\infty} \frac{\Delta z^n}{n!} (-j)^n H_n, \qquad \text{(III-29b)}$$

with $\Delta z = z_i - z_{i-1} \geq o$ and with H_n defined recursively by

$$H_n = H_1 * H_{n-1}, \qquad \text{(III-29c)}$$

$$H_{n-1} = H_1 * H_{n-2}, \qquad \text{(III-29d)}$$

etc. and

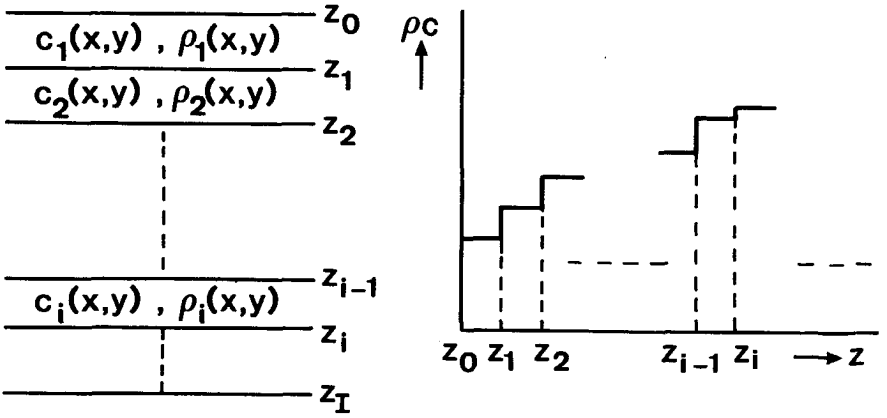

Figure III-4: Computationally convenient acoustic subsurface model for recursive wave field extrapolation based on the one-way wave equations.

$$H_o = d_o(x,y) = \delta(x)\delta(y). \qquad \text{(III-29e)}$$

Similarly, forward one-way wave field extrapolation of upgoing waves is described by

$$P^-(z_{i-1}) = W^-(z_{i-1},z_i) * P^-(z_i), \qquad \text{(III-29f)}$$

where

$$W^-(z_{i-1},z_i) = \sum_{n=o}^{\infty} \frac{(-\Delta z)^n}{n!} j^n H_n. \qquad \text{(III-29g)}$$

Notice that for this situation $W^+(z_i,z_{i-1})$ equals $W^-(z_{i-1},z_i)$. In practical implementation the scheme should be applied recursively for small steps Δz. The total error per extrapolation step depends on two different sub-errors:

1. The error in the estimates of the derivatives with respect to z. This error is due to the implicit character of the square-root operator H_1, which should be expanded for practical implementation.
2. The error due to the truncation of the Taylor series.

For a detailed discussion the reader is referred to Berkhout (1982). For two-way extrapolation the Taylor series summation approach is extensively discussed in chapter IV. Above operators can be elegantly used for recursive one-way wave field extrapolation in arbitrarily inhomogeneous macro subsurface

models. Therefore we choose a computational model, as shown in Figure III-4, that is, we assume that in the i'th layer, with $z_{i-1} \leq z < z_i$, the medium parameters may be approximated by

$$c_i = c_i(x,y), \tag{III-30a}$$

$$\rho_i = \rho_i(x,y). \tag{III-30b}$$

This assumption is justified when the layers are chosen sufficiently thin. Recursive extrapolation of **primary** data can now be defined according to

$$P^+(z_m) = W^+(z_m,z_o) * P^+(z_o), \tag{III-31a}$$

$$P^-(z_o) = W^-(z_o,z_m) * P^-(z_m), \tag{III-31b}$$

where the operators $W^+(z_m,z_o)$ and $W^-(z_o,z_m)$ are given by

$$W^+(z_m,z_o) = W^+(z_m,z_{m-1}) * T^+(z_{m-1}) * \ldots T^+(z_1) * W^+(z_1,z_o), \tag{III-31c}$$

$$W^-(z_o,z_m) = W^-(z_o,z_1) * T^-(z_1) * \ldots T^-(z_{m-1}) * W^-(z_{m-1},z_m). \tag{III-31d}$$

Here T^+ and T^- represent transmission operators, which account for the discontinuity of the medium parameters at the (computational) layer interfaces. A discussion of these operators, which are often neglected in practical implementation, is beyond the scope of this thesis. The basic relation for modeling of primary data reads (see also section II.2)

$$P^-(z_o) = \sum_m \left[W^-(z_o,z_m) * R(z_m) * W^+(z_m,z_o)\right] * P^+(z_o), \tag{III-31e}$$

where $R(z_m)$ represents the reflectivity operator at depth $z=z_m$. Since multiple reflections are neglected, relations (III-31a) and (III-31b) are not exact. In order to quantify the approximation, we consider the relations in the wavenumber-frequency domain, assuming a 1-D inhomogeneous medium:

$$\hat{P}^+(z_m) = \hat{W}^+(z_m,z_o)\hat{P}^+(z_o), \tag{III-32a}$$

$$\hat{P}^-(z_o) = \hat{W}^-(z_o,z_m)\hat{P}^-(z_m), \tag{III-32b}$$

with

$$\tilde{W}^{+}(z_m,z_o) = \tilde{W}^{+}(z_m,z_{m-1})\tilde{T}^{+}(z_{m-1})\ldots\tilde{T}^{+}(z_1)\tilde{W}^{+}(z_1,z_o), \qquad \text{(III-32c)}$$

$$\tilde{W}^{-}(z_o,z_m) = \tilde{W}^{-}(z_o,z_1)\tilde{T}^{-}(z_1)\ldots\tilde{T}^{-}(z_{m-1})\tilde{W}^{-}(z_{m-1},z_m). \qquad \text{(III-32d)}$$

Assuming the 1-D inhomogeneous medium is continuously layered, then, according to appendix B, these operators can be written as

$$\tilde{W}^{+}(z_m,z_o) = \sqrt{\frac{\rho(z_m)\tilde{H}_1(z_o)}{\rho(z_o)\tilde{H}_1(z_m)}}\ \exp\int_{z_o}^{z_m} -j\tilde{H}_1(z)dz, \qquad \text{(III-33a)}$$

$$\tilde{W}^{-}(z_o,z_m) = \sqrt{\frac{\rho(z_o)\tilde{H}_1(z_m)}{\rho(z_m)\tilde{H}_1(z_o)}}\ \exp\int_{z_m}^{z_o} +j\tilde{H}_1(z)dz, \qquad \text{(III-33b)}$$

with

$$\tilde{H}_1^2(z) = \left(\omega^2/c^2(z)\right) - k_x^2 - k_y^2 > 0 \text{ for } z_o < z < z_m. \qquad \text{(III-33c)}$$

Notice that, **by definition,** relations (III-32a) and (III-32b), with operators $\tilde{W}^{+}(z_m,z_o)$ and $\tilde{W}^{-}(z_o,z_m)$ given by relations (III-33a) and (III-33b), describe wave field extrapolation of **primary** propagating waves in continuously layered media. From these relations it follows that primary downgoing and upgoing waves in continuously layered media may be defined for variable z according to

$$\tilde{P}^{+}(z) = \tilde{C}^{+}\left(\frac{\tilde{H}_1(z)}{\rho(z)}\right)^{-\frac{1}{2}}\ \exp\int_{z_o}^{z} -j\tilde{H}_1(z')dz', \qquad \text{(III-34a)}$$

$$\tilde{P}^{-}(z) = \tilde{C}^{-}\left(\frac{\tilde{H}_1(z)}{\rho(z)}\right)^{-\frac{1}{2}}\ \exp\int_{z_1}^{z} +j\tilde{H}_1(z')dz', \qquad \text{(III-34b)}$$

where $\tilde{C}^{+}$, $\tilde{C}^{-}$, z_o,z_1 are arbitrary constants. Differentiation with respect to z yields

$$\frac{\partial\tilde{P}^{+}}{\partial z} = \left[-j\tilde{H}_1 - \tfrac{1}{2}\left(\frac{\tilde{H}_1}{\rho}\right)^{-1}\frac{\partial}{\partial z}\left(\frac{\tilde{H}_1}{\rho}\right)\right]\tilde{P}^{+}, \qquad \text{(III-35a)}$$

$$\frac{\partial \tilde{\vec{P}}}{\partial z} = \left[+j\tilde{H}_1 - \tfrac{1}{2}\left(\frac{\tilde{H}_1}{\rho}\right)^{-1} \frac{\partial}{\partial z}\left(\frac{\tilde{H}_1}{\rho}\right)\right] \tilde{\vec{P}}. \qquad \text{(III-35b)}$$

Notice that these relations represent the spatial Fourier transforms of one-way wave equations (III-26a) and (III-26b), without the coupling operators $\tilde{\Gamma}^{+}$ and $\tilde{\Gamma}^{-}$ (case B).

Multiplication by $1/\rho$ and again differentiation with respect to z yields

$$-\rho \frac{\partial}{\partial z}\left(\frac{1}{\rho}\frac{\partial \tilde{\vec{P}}^{+}}{\partial z}\right) = [\tilde{H}_2 - \tilde{E}_c - E_\rho]\tilde{\vec{P}}^{+}, \qquad \text{(III-36a)}$$

with

$$\tilde{E}_c = -\frac{1}{4\tilde{H}_2}\frac{\partial^2 \tilde{H}_2}{\partial z^2} + \frac{5}{16}\left(\frac{1}{\tilde{H}_2}\frac{\partial \tilde{H}_2}{\partial z}\right)^2, \qquad \text{(III-36b)}$$

$$E_\rho = \frac{1}{2\rho}\frac{\partial^2 \rho}{\partial z^2} - \frac{3}{4}\left(\frac{1}{\rho}\frac{\partial \rho}{\partial z}\right)^2. \qquad \text{(III-36c)}$$

Notice that this relation represents the spatial Fourier transform of two-way wave equation (III-9), assuming

$$|\tilde{E}_c + E_\rho| << |\tilde{H}_2|. \qquad \text{(III-36d)}$$

We may conclude that **recursive** wave field extrapolation of primary waves, as described by (III-31), is not justified when condition (III-36d) is violated. Notice that this occurs when $\tilde{H}_2 \to 0$ ($\tilde{E}_c \to \infty$). Since $\tilde{H}_2 = \tilde{H}_1^2 = k^2 \cos^2\theta$, recursive relations (III-31a) and (III-31b) are invalid for critical angle events ($\theta \to 90°$).

Relations (III-34a) and (III-34b) can be found directly from the two-way wave equation following the approach suggested by Liouville (1837) and Green (1837). They assumed a solution $\exp[\Phi(z)]$ and solved a non-linear differential equation in $\Phi(z)$ assuming $|\partial_z^2 \Phi| << |\partial_z \Phi|^2$. Various other authors solved the two-way wave equation iteratively. Amongst others, Bremmer (1951) and Brekhovskikh (1980) showed that relations (III-34a) and (III-34b) represent the zeroth order solution of an iterative procedure, the so-called geometrical optics approach. For a seismological application the reader is referred to Chapman (1976). In the following, relations (III-34a) and (III-34b) are called the "LG approximation" (for "Liouville-Green") for subcritical angle events. In seismic literature, these relations are commonly known as the WKB or WKBJ

approximation, referring to papers by Wentzel (1926), Kramers (1926), Brillouin (1926) and Jeffreys (1924). However, the extra important item introduced by these authors is a technique to connect LG approximations for $\tilde{H}_2>0$ with LG approximations for $\tilde{H}_2<0$ by means of an approximation which is valid for $\tilde{H}_2 \to 0$. Therefore, following Olver (1974), we reserve the name WKBJ approach for methods which properly handle sub-critical as well as critical angle events. This is discussed in section III.6.

Finally, we present closed expressions for the LG-operators $\tilde{W}^+(z_i,z_{i-1})$ and $\tilde{W}^-(z_{i-1},z_i)$. Assuming that the operator $\tilde{H}_2$ may be linearized according to

$$\tilde{H}_2(z) = \tilde{H}_1^2(z) = \tilde{H}_1^2(z_{i-1}) + (z-z_{i-1})\chi_i, \text{ for } z_{i-1}<z<z_i, \qquad \text{(III-37)}$$

then the LG-operators for sub-critical angle events are given by

$$\tilde{W}^+(z_i,z_{i-1}) = \sqrt{\frac{\rho(z_i)\tilde{H}_1(z_{i-1})}{\rho(z_{i-1})\tilde{H}_1(z_i)}}\exp\left[-j\,\frac{2}{3\chi_i}\left\{\tilde{H}_2^{3/2}(z_i)-\tilde{H}_2^{3/2}(z_{i-1})\right\}\right], \qquad \text{(III-38a)}$$

$$\tilde{W}^-(z_{i-1},z_i) = \sqrt{\frac{\rho(z_{i-1})\tilde{H}_1(z_i)}{\rho(z_i)\tilde{H}_1(z_{i-1})}}\exp\left[-j\,\frac{2}{3\chi_i}\left\{\tilde{H}_2^{3/2}(z_i)-\tilde{H}_2^{3/2}(z_{i-1})\right\}\right]. \qquad \text{(III-38b)}$$

The inverse operators for propagating waves are given by

$$\tilde{F}^+(z_{i-1},z_i) = [\tilde{W}^+(z_i,z_{i-1})]^{-1} = [\tilde{W}^-(z_{i-1},z_i)]^*, \qquad \text{(III-39a)}$$

$$\tilde{F}^-(z_i,z_{i-1}) = [\tilde{W}^-(z_{i-1},z_i)]^{-1} = [\tilde{W}^+(z_i,z_{i-1})]^*. \qquad \text{(III-39b)}$$

For small χ_i the complex exponential function in both (III-38a) and (III-38b) can be written as

$$\left[1-\tfrac{1}{4}j\chi_i\,\Delta z^2\tilde{H}_1^{-1}(z_{i-1})\right]\exp[-j\tilde{H}_1(z_{i-1})\Delta z], \qquad \text{(III-40)}$$

with $\Delta z = z_i - z_{i-1}$. For $\chi_i = 0$ this expression corresponds to the phase-shift operator for homogeneous media, as discussed in section III.3.

Summarizing, in this section we discussed a wave field extrapolation algorithm for propagating waves. Lateral variations of c and ρ can be properly incorporated because the algorithm is based on exact one-way wave equations. Vertical

variations of c and ρ can be incorporated by applying the scheme recursively. By taking the stepsize sufficiently small, this approach is correct for primary waves within the seismic bandwidth. The solution is not valid for critical angle events since multiple reflections are neglected. For 1-D inhomogeneous media the recursive approach complies with the LG approximation. The condition for this approximation is quantified by inequality (III-36d).

In the seismic literature several approaches have been suggested for the incorporation of multiple reflections. Berkhout (1982) discussed a recursive scheme for discretely layered 3-D inhomogeneous media. A feed-back system at each layer interface generates an infinite number of multiple reflections. On the other hand, Chapman (1976) discussed an iterative scheme for continuously layered 1-D inhomogeneous media. In each successive iteration step a new order of multiple reflections is generated. The WKBJ technique, discussed in the next section, takes automatically into account all multiple reflections within the critical region ($\tilde{H}_2 \rightarrow 0$).

III.6 THE WKBJ TECHNIQUE FOR CRITICAL ANGLE EVENTS

In the previous section we have seen that the conventional approach to wave field extrapolation fails for critical angle events because multiple reflections are neglected. In order to satisfy the two-way wave equation, an infinite number of multiple reflections should be incorporated, which is not very attractive from a practical point of view. In this section we discuss an alternative solution for 1-D inhomogeneous media, suggested by Wentzel (1926), Kramers (1926), Brillouin (1926) and Jeffreys (1924).

In the wavenumber-frequency domain wave equation (III-9) reads

$$\frac{\partial^2}{\partial z^2}\left(\frac{\tilde{P}}{\sqrt{\rho}}\right) = -\tilde{H}_2\left(\frac{\tilde{P}}{\sqrt{\rho}}\right), \qquad \text{(III-41a)}$$

with

$$\tilde{H}_2 = \tilde{H}_2(z) = \frac{\omega^2}{c^2(z)} - k_x^2 - k_y^2, \qquad \text{(III-41b)}$$

assuming $|E_\rho| \ll k^2$, with E_ρ defined by relation (III-36c). For large $|\tilde{H}_2|$, solutions are given by the LG-approximations (III-34a) and (III-34b). Problems occur for $|\tilde{H}_2| \rightarrow 0$, where the LG solutions grow out of bounds. An acceptable solution for all $\tilde{H}_2$ can be found with the WKBJ technique, which involves the following steps (see also McHugh, 1971).

1. Assume $\tilde{H}_2(z)$ may be linearized for small $|z-z_t|$, where z_t is the turning point of equation (III-41a):

$$\tilde{H}_2(z) \approx (z-z_t)\chi, \tag{III-42a}$$

with

$$\chi = \frac{\partial \tilde{H}_2}{\partial z}\Big|_{z_t} = -2\left(\frac{\omega^2}{c^3(z_t)}\right)\frac{\partial c(z)}{\partial z}\Big|_{z_t}. \tag{III-42b}$$

2. Expand the LG approximations (III-34a) and (III-34b) under assumption (III-42).

3. Replace equation (III-41a) under assumption (III-42) by the Airy equation

$$\frac{\partial^2 \tilde{\Psi}}{\partial \zeta^2} - \zeta \tilde{\Psi} = 0, \tag{III-43a}$$

where

$$\tilde{\Psi} = \tilde{P}/\sqrt{\rho} \tag{III-43b}$$

is the scaled pressure and

$$\zeta = -(z-z_t)\chi^{1/3} \tag{III-43c}$$

is the scaled depth. Solutions are given by the Airy functions $Ai(\zeta)$, $Bi(\zeta)$, see Appendix C.

4. Choose linear combinations of LG-solutions and Airy functions such that the LG-expansions match the asymptotic Airy expansions at both sides of the turning point z_t.

We discuss this method with the aid of an example. Consider a 1-D inhomogeneous medium, with velocity $c(z)$ constant for $z<z_o$ and increasing monotonously with depth for $z \geq z_o$. Assume a downgoing plane-wave $\tilde{P}^+(z_o)$ incident at $z=z_o$, with propagation angle θ_o, so $\tilde{H}_2(z_o) = \omega^2 c^{-2}(z_o)\cos^2\theta_o$. According to relation (III-41b) $\tilde{H}_2(z)$ decreases monotonously with depth for $z \geq z_o$. We assume that the condition $|\tilde{E}_c + E_\rho| << |\tilde{H}_2|$ is violated in the region $z_1<z<z_2$ and that in this region a turning point is present at $z=z_t$, that is, $\tilde{H}_2(z_t) = 0$. Furthermore we assume that $\tilde{H}_2(z)$ may be linearized in the region $z_1 \leq z \leq z_2$, according to $\tilde{H}_2(z) \approx (z-z_t)\chi$. Notice that χ is negative. The operator $\tilde{H}_2(z)$ is shown in Figure III-5a.

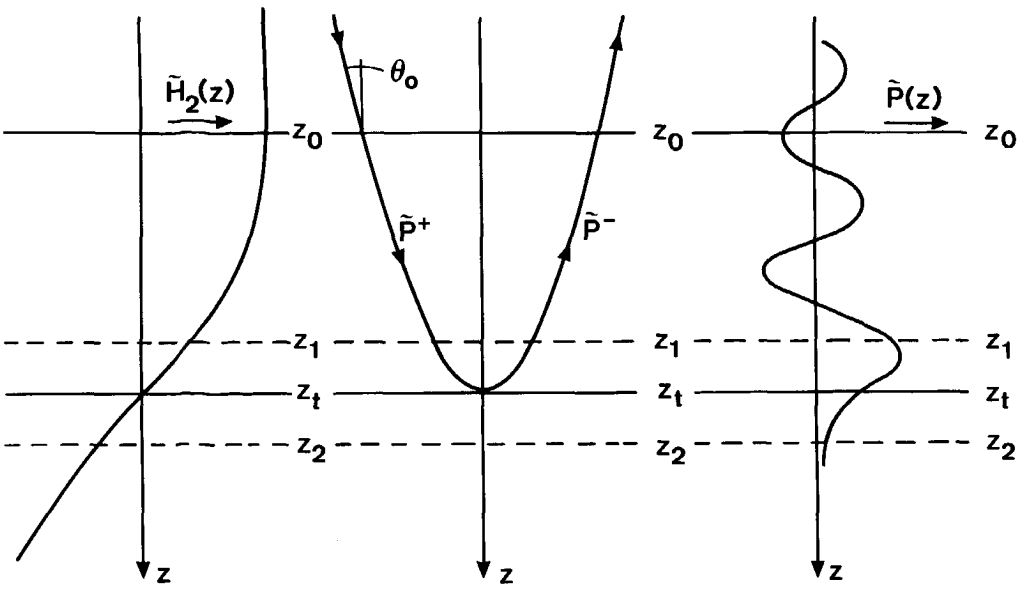

Figure III-5: Critical angle events in a 1-D inhomogeneous macro subsurface model.

a. The operator $\tilde{H}_2(z)$, including a turning point at $z=z_t$.

b. Ray representation.

c. The total wave field $\tilde{P}(z)$.

We assume that for $z_o \leq z \leq z_1$ the total wave field is given by the superposition of a downgoing and an upgoing wave (see Figure III-5b), so

$$\tilde{P}(z) = \tilde{P}^+(z) + \tilde{P}^-(z), \qquad \text{(III-44a)}$$

where $\tilde{P}^+(z)$ and $\tilde{P}^-(z)$ are given by the LG-solutions (III-34a) and (III-34b):

$$\tilde{P}^+(z) = \tilde{C}^+\left(\frac{\tilde{H}_1(z)}{\rho(z)}\right)^{-\frac{1}{2}} \exp \int_{z_o}^{z} -j\tilde{H}_1(z')dz', \qquad \text{(III-44b)}$$

$$\tilde{P}^-(z) = \tilde{C}^-\left(\frac{\tilde{H}_1(z)}{\rho(z)}\right)^{-\frac{1}{2}} \exp \int_{z_1}^{z} +j\tilde{H}_1(z')dz'. \qquad \text{(III-44c)}$$

The amplitudes $\tilde{C}^+$ and $\tilde{C}^-$ are given by

$$\tilde{C}^+ = (\tilde{H}_1(z_o)/\rho(z_o))^{\frac{1}{2}}\tilde{P}^+(z_o), \tag{III-45a}$$

$$\tilde{C}^- = (\tilde{H}_1(z_1)/\rho(z_1))^{\frac{1}{2}}\tilde{P}^-(z_1), \tag{III-45b}$$

where $\tilde{P}^+(z_o)$ is the incident wave. Our aim is to determine $\tilde{P}^-(z_1)$ and to study the total wave field near the turning point $z=z_t$.

Around z_1 the LG-solutions can be approximated by

$$\tilde{P}^+(z) = \tilde{D}^+\left(\frac{\tilde{H}_1(z)}{\rho(z)}\right)^{-\frac{1}{2}} \exp\left[-j\,\frac{2}{3\chi}\,\tilde{H}_2^{3/2}(z)\right], \tag{III-46a}$$

$$\tilde{P}^-(z) = \tilde{D}^-\left(\frac{\tilde{H}_1(z)}{\rho(z)}\right)^{-\frac{1}{2}} \exp\left[+j\,\frac{2}{3\chi}\,\tilde{H}_2^{3/2}(z)\right], \tag{III-46b}$$

with

$$\tilde{D}^+ = \left(\tilde{H}_1(z_1)/\rho(z_1)\right)^{\frac{1}{2}} \exp[+j\,\tfrac{2}{3\chi}\tilde{H}_2^{3/2}(z_1)]\tilde{P}^+(z_1), \tag{III-46c}$$

$$\tilde{D}^- = \left(\tilde{H}_1(z_1)/\rho(z_1)\right)^{\frac{1}{2}} \exp[-j\,\tfrac{2}{3\chi}\tilde{H}_2^{3/2}(z_1)]\tilde{P}^-(z_1), \tag{III-46d}$$

where $\tilde{P}^+(z_1)$ and $\tilde{P}^-(z_1)$ satisfy LG-solutions (III-44b) and (III-44c). Around z_1, expansions (III-46a) and (III-46b) should match a linear combination of the asymptotic expansions ($\zeta \to -\infty$) of the Airy functions $Ai(\zeta)$ and $Bi(\zeta)$, according to

$$\rho^{-\frac{1}{2}}(z)[\tilde{P}^+(z) + \tilde{P}^-(z)] = \tilde{Q}_A Ai(\zeta) + \tilde{Q}_B Bi(\zeta), \text{ for } z \to z_1. \tag{III-47}$$

At the other side of the turning point, around z_2, the same linear combination of Airy functions, expanded for $\zeta\to\infty$, should again match LG-solutions. We shall not discuss this in detail. We only remark that the radiation condition requires that $\tilde{Q}_B$ is zero, since $Bi(\zeta)$ is exponentially growing for positive ζ (see relation (C-5c)). We may conclude that for $z>z_t$ the wave field is proportional to the exponentially decaying function $Ai(\zeta)$ and its corresponding LG-solution away from the turning point. In the following we leave the evanescent field for $z>z_t$ out of consideration.

With the asymptotic expansion of Ai(ζ), (see relation (C-6a)), it follows from relation (III-47), with $\tilde{Q}_B = 0$, that $\tilde{D}^-$ and $\tilde{Q}_A$ are given by

$$\tilde{D}^- = j\tilde{D}^+ \qquad \text{(III-48a)}$$

$$\tilde{Q}_A = (1+j)\sqrt{2\pi}|\chi|^{-1/6}\tilde{D}^+. \qquad \text{(III-48b)}$$

From relations (III-46a), (III-46b) and (III-48a) it follows that

$$\tilde{P}^-(z_1) = j \exp[+2j \frac{2}{3\chi}\tilde{H}_2^{3/2}(z_1)]\tilde{P}^+(z_1). \qquad \text{(III-49)}$$

In the next section we present a more elegant representation of this relation. Apparently total reflection occurs from the region around the turning point. Since $\tilde{D}^- = j\tilde{D}^+$, the conclusion is sometimes drawn that a phase shift of $\pi/2$ occurs at the turning point. Since expressions (III-46a) and (III-46b) are not valid at the turning point, this conclusion is premature, as is seen in the next section.

Finally, we conclude that the total wave field in the region $z_1 < z < z_2$ is given by

$$\tilde{P}(z) = \sqrt{\rho(z)}\ \tilde{Q}_A \mathrm{Ai}(\zeta). \qquad \text{(III-50)}$$

The total wave field for all z is shown schematically in Figure III-5c. We observe a standing wave before the turning point ($z \leq z_t$), and an evanescent wave beyond the turning point ($z > z_t$). In the above example we assumed a simplified earth model with a for all depths monotonous continuous velocity function c(z), which means that there are no reflecting interfaces, and that only one turning point is present in the whole depth range. For seismic applications we assume that the above described WKBJ-technique may be applied **locally** when the velocity function c(z) is monotonous continuous at least in the critical region around the turning point.

Summarizing, the WKBJ approach is suitable for modeling applications of critical angle events in 1-D inhomogeneous media. In its present formulation, the WKBJ approach is not suitable for migration applications of critical angle events since in the critical region the **total** wave field is considered. Therefore we propose a different way of decomposition in the critical region which properly includes critical angle events.

III.7 THE WKBJ ONE-WAY WAVE EQUATIONS FOR CRITICAL ANGLE EVENTS

In the previous section we have seen that in the vicinity of a turning point the total wave field may be described in terms of the Airy function $Ai(\zeta)$. For propagating waves, $\zeta \leq 0$, we formally define a choice of downgoing and upgoing waves according to

$$\tilde{P}^{+}(z) = \tfrac{1}{2}\sqrt{\rho(z)}\ \tilde{Q}_A[Ai(\zeta) + j\frac{\chi}{|\chi|}Bi(\zeta)], \qquad \text{(III-51a)}$$

$$\tilde{P}^{-}(z) = \tfrac{1}{2}\sqrt{\rho(z)}\ \tilde{Q}_A[Ai(\zeta) - j\frac{\chi}{|\chi|}Bi(\zeta)]. \qquad \text{(III-51b)}$$

These wave functions have also been used by Kennett and Illingworth (1981) for **modeling** applications. In this section we discuss wave field extrapolation operators, based on above wave functions, which can be used for modeling as well as **migration** applications. Notice that the total wave field, given by

$$\tilde{P}(z) = \tilde{P}^{+}(z) + \tilde{P}^{-}(z) = \sqrt{\rho(z)}\ \tilde{Q}_A Ai(\zeta), \qquad \text{(III-52)}$$

satisfies the wave equation, so critical angle events are properly incorporated in $\tilde{P}^{+}$ and $\tilde{P}^{-}$. In the following, italic type symbols refer to the incorporation of critical angle events in primary waves. We now prove that $\tilde{P}^{+}$ and $\tilde{P}^{-}$ represent suitable choices for downgoing and upgoing waves, respectively. For a wave in the positive z direction, the phase should decrease with increasing z, that is, the derivative with respect to z of the argument of $\tilde{P}^{+}$ should be negative. Using relation (C-3) we find

$$\frac{\partial}{\partial z}[\mathrm{Imag}(\tilde{P}^{+})/\mathrm{Real}(\tilde{P}^{+})] = \frac{\partial}{\partial z}\left[\frac{\chi}{|\chi|}Bi(\zeta)/Ai(\zeta)\right] = -|\chi|^{1/3}\frac{\pi^{-1}}{Ai^{2}(\zeta)} < 0. \qquad \text{(III-53)}$$

We may conclude that $\tilde{P}^{+}$ indeed represents a downgoing wave for all $\zeta \leq o$, where $\zeta = o$ represents the turning point. In a similar way it can be shown that $\tilde{P}^{-}$ represents an upgoing wave. Substitution of the asymptotic expansions of $Ai(\zeta)$ and $Bi(\zeta)$ for $\zeta \to -\infty$ (see relations (C-6a) and (C-6c)) in relations (III-51a) and (III-51b) with $\chi < 0$, yields LG-approximations (III-46a) and (III-46b).

Differentiation of $\tilde{P}^{+}$ and $\tilde{P}^{-}$ with respect to z yields

$$\frac{\partial \tilde{P}^{+}}{\partial z} = -\tilde{H}_1^{+}\tilde{P}^{+}, \qquad \text{(III-54a)}$$

$$\frac{\partial \tilde{\tilde{P}}}{\partial z} = +j\tilde{\tilde{H}}_1\tilde{\tilde{P}}, \qquad \text{(III-54b)}$$

with

$$\tilde{\tilde{H}}_1^{+} = \frac{j}{2\rho}\frac{\partial \rho}{\partial z} - \left(\chi^{1/3}\right)\frac{\left\{-\frac{\chi}{|\chi|}\pi^{-1} + jAi(\zeta)A\dot{i}(\zeta)+jBi(\zeta)B\dot{i}(\zeta)\right\}}{Ai^2(\zeta) + Bi^2(\zeta)}, \qquad \text{(III-54c)}$$

$$\tilde{\tilde{H}}_1^{-} = \frac{-j}{2\rho}\frac{\partial \rho}{\partial z} - \left(\chi^{1/3}\right)\frac{\left\{-\frac{\chi}{|\chi|}\pi^{-1} - jAi(\zeta)A\dot{i}(\zeta)-jBi(\zeta)B\dot{i}(\zeta)\right\}}{Ai^2(\zeta) + Bi^2(\zeta)}, \qquad \text{(III-54d)}$$

where the primes denote differentiation with respect to ζ. Notice that, unlike $\tilde{\tilde{P}}^{+}$ and $\tilde{\tilde{P}}^{-}$, $\tilde{\tilde{P}}^{+}$ and $\tilde{\tilde{P}}^{-}$ satisfy **decoupled** one-way wave equations, conformable to relation (III-12), without any further approximation. Consequently, all multiple reflections of the conventional approach are incorporated in the primary waves $\tilde{\tilde{P}}^{+}$ and $\tilde{\tilde{P}}^{-}$. The underlying assumption is that the medium parameters are specified in a given depth interval around the turning point.

At the turning point, $z=z_t$ (or $\zeta=0$), the ratio of $\tilde{\tilde{P}}^{-}$ and $\tilde{\tilde{P}}^{+}$ is given by (see also relation (C-4a)):

$$\frac{\tilde{\tilde{P}}^{-}(z_t)}{\tilde{\tilde{P}}^{+}(z_t)} = \frac{Ai(0) - j\frac{\chi}{|\chi|}Bi(0)}{Ai(0) + j\frac{\chi}{|\chi|}Bi(0)} = \exp\left(-j\frac{\chi}{|\chi|}\frac{2\pi}{3}\right). \qquad \text{(III-55)}$$

Notice that total reflection occurs at the turning point with a phase-shift of $2\pi/3$.

From expressions (III-51a) and (III-51b) wave field extrapolation operators for $\tilde{\tilde{P}}^{+}$ and $\tilde{\tilde{P}}^{-}$ can be defined according to

$$\tilde{\tilde{P}}^{+}(z_i) = \tilde{\tilde{W}}^{+}(z_i, z_{i-1})\tilde{\tilde{P}}^{+}(z_{i-1}), \qquad \text{(III-56a)}$$

$$\tilde{\tilde{P}}^{-}(z_{i-1}) = \tilde{\tilde{W}}^{-}(z_{i-1}, z_i)\tilde{\tilde{P}}^{-}(z_i), \qquad \text{(III-56b)}$$

with

$$\tilde{\tilde{W}}^{+}(z_i, z_{i-1}) = \sqrt{\frac{\rho(z_i)}{\rho(z_{i-1})}}\left[\frac{Ai(\zeta_i) + j\frac{\chi}{|\chi|}Bi(\zeta_i)}{Ai(\zeta_{i-1}) + j\frac{\chi}{|\chi|}Bi(\zeta_{i-1})}\right], \qquad \text{(III-56c)}$$

$$\tilde{W}^{-}(z_{i-1},z_i) = \sqrt{\frac{\rho(z_{i-1})}{\rho(z_i)}}\left[\frac{Ai(\zeta_{i-1}) - j\frac{\chi}{|\chi|}Bi(\zeta_{i-1})}{Ai(\zeta_i) - j\frac{\chi}{|\chi|}Bi(\zeta_i)}\right], \qquad \text{(III-56d)}$$

$$\zeta_{i-1} = -\chi^{1/3}(z_{i-1} - z_t), \qquad \text{(III-56e)}$$

$$\zeta_i = -\chi^{1/3}(z_i - z_t), \qquad \text{(III-56f)}$$

where both z_{i-1} and z_i are in the vicinity of the turning point z_t, with $z_i > z_{i-1}$. Operators (III-56c) and (III-56d) we call the WKBJ operators. The inverse operators are given by

$$\tilde{F}^{+}(z_{i-1},z_i) = [\tilde{W}^{+}(z_i,z_{i-1})]^{-1} = [\tilde{W}^{-}(z_{i-1},z_i)]^{*}, \qquad \text{(III-57a)}$$

$$\tilde{F}^{-}(z_i,z_{i-1}) = [\tilde{W}^{-}(z_{i-1},z_i)]^{-1} = [\tilde{W}^{+}(z_i,z_{i-1})]^{*}. \qquad \text{(III-57b)}$$

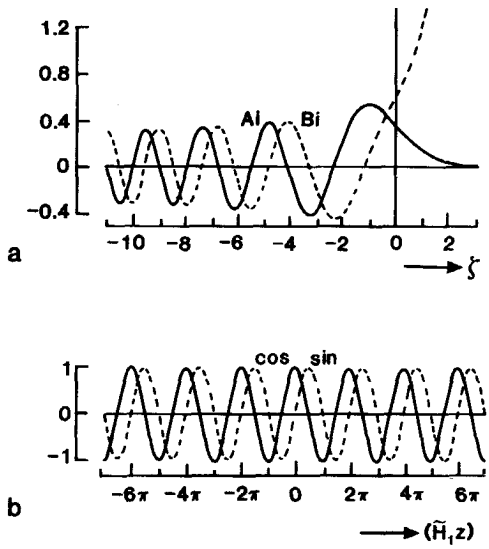

Figure III-6: a. Graphical representation of the Airy functions Ai(ζ) and Bi(ζ). Notice that ζ represents scaled depth: $\zeta = -\chi^{1/3}(z-z_t)$. The turning point depth $z=z_t$ corresponds to $\zeta = 0$.

b. For comparison, graphical representation of the goniometric functions $\cos(\tilde{H}_1 z)$ and $\sin(\tilde{H}_1 z)$.

Away from the turning point, the WKBJ-operators $\tilde{W}^{+}(z_i,z_{i-1})$ and $\tilde{W}^{-}(z_{i-1},z_i)$ reduce to the LG-operators $\tilde{W}^{+}(z_i,z_{i-1})$ and $\tilde{W}^{-}(z_{i-1},z_i)$, given by relations (III-38a) and (III-38b). With linearization assumption (III-37), these LG-operators are approximate solutions of the Airy equation as well. In fact they represent the leading term of an asymptotic expansion of the WKBJ-operators. A method which uses Airy's equation close to as well as away from the turning point is sometimes called a uniform asymptotic approach to the turning point problem. A rigorous mathematical treatment of the uniform solution is given by a.o. Wasow (1965).

Notice that for $\chi = 0$ critical angle events do not occur; the WKBJ operators $\tilde{W}^{+}(z_i,z_{i-1})$ and $\tilde{W}^{-}(z_{i-1},z_i)$ then reduce to the phase-shift operators for homogeneous layers, as can be seen from relations (III-38a), (III-38b) and (III-40). For comparison, the phase-shift operators can be written in a similar way as relations (III-56c) and (III-56d), according to

$$\tilde{W}^{+}(z_i,z_{i-1}) = \frac{\cos(\tilde{H}_1 z_i) - j\,\sin(\tilde{H}_1 z_i)}{\cos(\tilde{H}_1 z_{i-1}) - j\,\sin(\tilde{H}_1 z_{i-1})}, \qquad \text{(III-58a)}$$

$$\tilde{W}^{-}(z_{i-1},z_i) = \frac{\cos(\tilde{H}_1 z_{i-1}) + j\,\sin(\tilde{H}_1 z_{i-1})}{\cos(\tilde{H}_1 z_i) + j\,\sin(\tilde{H}_1 z_i)}. \qquad \text{(III-58b)}$$

Notice that $\tilde{W}^{+}(z_i,z_{i-1})$ equals $\tilde{W}^{-}(z_{i-1},z_i)$. The strong resemblance between the WKBJ operators $\tilde{W}^{\pm}$ and the phase shift operators $\tilde{W}^{\pm}$ is visualized in Figure III-6, where the Airy functions Ai and Bi are compared with the goniometric functions cos and sin respectively.

Summarizing, in this section we introduced an alternative approach to the decomposition of the total wave field near a turning point into downgoing and upgoing waves $\tilde{P}^{+}$ and $\tilde{P}^{-}$.

In the conventional approach $\tilde{P}^{+}$ and $\tilde{P}^{-}$ are coupled for all z, according to relations (III-24a) and (III-24b). Particularly in the vicinity of the turning point this coupling may not be neglected. The exact solution requires the incorporation of an infinite number of multiple reflections.

In our alternative approach $\tilde{P}^{+}$ and $\tilde{P}^{-}$ are coupled at the turning point z_t only. This coupling is described by relation (III-55). The exact solution in the critical region is simply given by $\tilde{P} = \tilde{P}^{+} + \tilde{P}^{-}$.

All multiple reflections of the conventional approach are incorporated in the primary waves $\tilde{P}^{+}$ and $\tilde{P}^{-}$, or in other words, critical angle events are incorporated in $\tilde{P}^{+}$ and $\tilde{P}^{-}$.

Finally we consider again the example which was discussed in the previous section. With the decomposition introduced in this section we may replace relation (III-49) by

$$\tilde{P}^{-}(z_1) = \tilde{W}^{-}(z_1,z_t)\tilde{R}(z_t)\tilde{W}^{+}(z_t,z_1)\tilde{P}^{+}(z_1) \qquad \text{(III-59a)}$$

with

$$\tilde{R}(z_t) = \exp(j2\pi/3), \qquad \text{(III-59b)}$$

where we made use of the fact that around z_1, $\tilde{P}^{+}(z)$ and $\tilde{P}^{-}(z)$ match the asymptotic expansions of $\tilde{P}^{+}(z)$ and $\tilde{P}^{-}(z)$, respectively. Relation (III-59) is fully equivalent with relation (III-49). However, the formulation of (III-59) allows a physical interpretation which links up with the conception of one-way wave propagation. For modeling applications this means that primary waves including critical angle events can be treated independently from interface related multiples ('long period multiples'). For migration purposes one-way formulation (III-59) can be easily inverted. With the aid of inverse operators (III-57a) and (III-57b) the reflectivity at the turning point can be determined from the downward extrapolated pressure data. Modeling and migration schemes based on the one-way formulation of critical angle events are discussed in sections III.8 and III.9, respectively.

The operators derived in this section are valid in 1-D inhomogeneous media only. In multi-dimensional linearized inversion schemes, as well as in migration schemes, they may describe the propagation of the reference wave field in a 1-D inhomogeneous macro subsurface model. Furthermore it is assumed that no reflecting interfaces are present in the critical region around the turning point. Due to this assumption the applicability of the WKBJ operators is restricted to simplified earth models with vanishing velocity gradients at macro layer interfaces.

In chapter IV we discuss another approach to wave field extrapolation of sub-critical as well as critical angle events, which is based on the two-way wave equation. In the two-way approach arbitrary depth models can be handled, while lateral variations can be incorporated as well.

III.8 PRE-STACK MODELING SCHEME BASED ON THE WKBJ ONE-WAY WAVE EQUATIONS

It has been shown in chapter II that a seismic experiment can be elegantly described by a sequence of independent one-way processes, which is schematically represented by

$$S^+ \rightarrow W^+ \rightarrow R \rightarrow W^- \rightarrow D \rightarrow P^-_{CSP}. \qquad \text{(III-60)}$$

A wave field, generated by sources S^+ at the surface, propagates downward into the earth, which is described by one-way wave field extrapolation operator W^+. In the subsurface this wave field is reflected, described by R, and propagates upward to the surface again, described by one-way operator W^-. At the surface the wave field is registered by detectors D, resulting in a seismic section P^-_{CSP} (one common-shotpoint gather). This simplified model is valid for sub-critical angle events only, because interaction between downgoing and upgoing waves is neglected in the one-way wave field extrapolation operators W^+ and W^-. Various expressions for these one-way operators have been discussed in section III.5. Based on model (III-60), Berkhout (1982) discussed modeling as well as migration schemes for sub-critical data in 1-D, 2-D and 3-D inhomogeneous media. In section III.7 we modified this model such that critical angle events may be included in 1-D inhomogeneous media. This is schematically represented by

$$S^+ \rightarrow W^+ \rightarrow R \rightarrow W^- \rightarrow D \rightarrow P^-_{CSP}. \qquad \text{(III-61)}$$

Here W^+ and W^- represent WKBJ one-way wave field extrapolation operators which include sub-critical as well as critical angle events, while R describes the reflectivity at the turning point. In this section we discuss a recursive modeling scheme based on the WKBJ one-way equations for 1-D inhomogeneous media. We consider a horizontally layered medium consisting of M (vertically inhomogeneous) **macro** layers, as is shown in Figure III-7. We assume homogeneous half spaces for $z<z_0$ and $z \geq z_M$. In macro layer m+1, with $z_m \leq z < z_{m+1}$, the propagation velocity and the density are given by $c_{m+1}(z)$ and $\rho_{m+1}(z)$, respectively. These are continuous monotonous functions of depth, with vanishing gradients in the vicinity of the interfaces. Notice that the concept 'vicinity of an interface' is related to the seismic frequency content. This means that the assumed gradient free area around the interfaces is proportional to the largest local wave length under consideration.

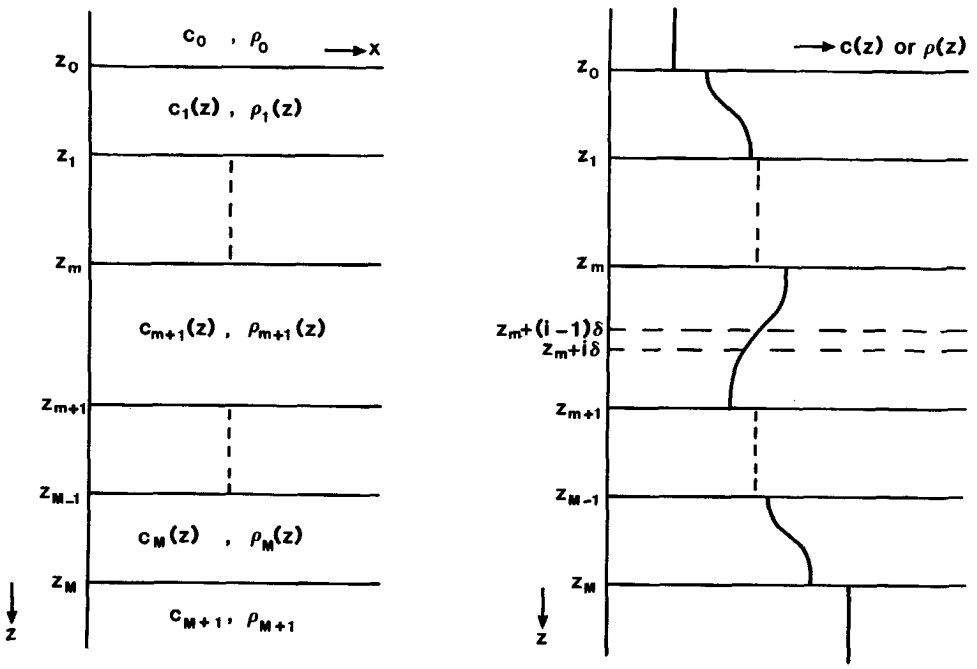

Figure III-7: Acoustic model of the subsurface for the one-way wave equation modeling scheme which includes critical angle events.

In the wavenumber-frequency domain (k_x, k_y, ω), modeling consists of the following steps

1. Given the plane-wave (PW) impulse response $\tilde{X}(z_{m+1})$ for the lower half space $z \geq z_{m+1}$, then the **primary** waves including critical angle events in macro layer m+1 can be modeled according to

$$\tilde{X}^{(o)}(z_m) = \tilde{W}^-(z_m, z_{m+1})\left[\tilde{X}(z_{m+1}-\varepsilon) + \tilde{R}(z_{m+1})\right]\tilde{W}^+(z_{m+1}, z_m), \quad \text{(III-62)}$$

   with $\varepsilon \to o$. The extrapolation operators $\tilde{W}^+$ and $\tilde{W}^-$ as well as the reflection operator $\tilde{R}$ are discussed below.

2. Given $\tilde{X}^{(o)}(z_m)$, then the (long period) **multiples** related to macro layer interface $z=z_m$ can be **optionally** included according to

$$\tilde{X}(z_m) = [1 - \tilde{X}^{(o)}(z_m)\tilde{R}^-(z_m)]^{-1}\tilde{X}^{(o)}(z_m). \quad \text{(III-63)}$$

   Multiple generation, as described by relation (III-63), is schematically shown in Figure III-8. Notice that the reflection operator

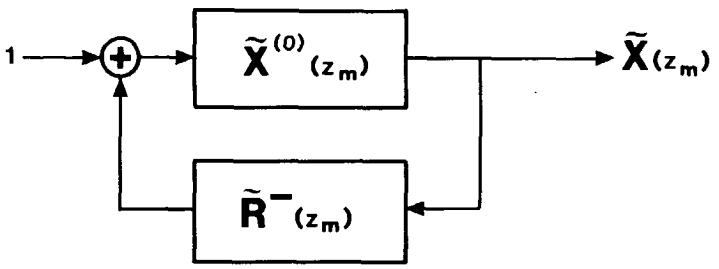

Figure III-8: Feed-back system for multiple generation at macro layer interface m.

$\tilde{R}^{-}(z_m) = -\tilde{R}(z_m)$ describes reflection at the lower side of interface z_m.

Steps 1 and 2, which describe the total modeling procedure for macro layer m+1, should be applied recursively.

3. The procedure (for each k_x, k_y and ω-value) starts at the shallowest level z_t where total reflection occurs, or at the maximum depth $z=z_M$ if total reflection does not occur.
4. When the surface $z=z_o$ has been reached, then the source and detector properties can be included, according to

$$\tilde{P}^{-}_{CSP}(z_o) = \tilde{D}(z_o)\tilde{X}(z_o)\tilde{S}^{+}(z_o), \qquad \text{(III-64)}$$

where $\tilde{S}^{+}(z_o)$ represents the downgoing source pressure wave, $\tilde{D}(z_o)$ represents the detector transfer function and $\tilde{P}^{-}_{CSP}(z_o)$ represents the detected upgoing pressure wave in a common-shotpoint gather in the wavenumber-frequency domain.
5. When this modeling procedure has been applied for all wavenumbers and frequencies, then the space-time data (one shot record) are obtained after inverse temporal and spatial Fourier transforms (see relations (III-3b) and (III-10b)).

Discussion.

The extrapolation operators $\tilde{W}$ in relation (III-62) are composed of N sub-operators, according to

$$\tilde{W}^{+}(z_{m+1},z_m) = \prod_{i=1}^{N} \tilde{W}^{+}(z_m + i\delta, z_m + (i-1)\delta), \qquad \text{(III-65a)}$$

$$\tilde{W}^{-}(z_m,z_{m+1}) = \prod_{i=1}^{N} \tilde{W}^{-}(z_m + (i-1)\delta, z_m + i\delta), \qquad \text{(III-65b)}$$

with $\delta=(z_{m+1}-z_m)/N$. Assuming that in each **micro** layer $(z_m+(i-1)\delta \leq z < z_m+i\delta)$ the operator $\tilde{H}_2(z)=\omega^2/c^2(z)-k_x^2-k_y^2$ may be linearized in z, then the sub-operators represent LG-operators for sub-critical angle events, given by relations (III-38a,b), if $\tilde{H}_2(z)$ is sufficiently large positive, while they represent WKBJ operators $\tilde{W}^{+}$ and $\tilde{W}^{-}$ for critical angle events, given by relations (III-56c,d), if $\tilde{H}_2(z)$ is small positive. Notice that we assume propagating waves for $z_m \leq z < z_{m+1}$.

An expression for $\tilde{X}(z_{m+1}-\varepsilon)$, $\varepsilon \to o$, in relation (III-62), is given by

$$\lim_{\varepsilon \to o} \tilde{X}(z_{m+1}-\varepsilon) = \tilde{T}^{-}(z_{m+1})\tilde{X}(z_{m+1})\tilde{T}^{+}(z_{m+1}), \qquad \text{(III-66a)}$$

$$\tilde{T}^{+-}(z_{m+1}) = 1 \pm \tilde{R}(z_{m+1}), \qquad \text{(III-66b)}$$

where $\tilde{T}^{+}$, $\tilde{T}^{-}$ and $\tilde{R}$ describe the transmission and reflection properties of the interface, with $\tilde{R}$ given by relation (B-3b).

The shallowest level z_t where total reflection occurs, as introduced in step 3, can represent either an interface or a turning point. In the latter case, z_t generally lays inside a macro layer $(z_m<z_t<z_{m+1})$, with $\tilde{H}_2(z_t)=o$. Now the recursive procedure starts with

$$\tilde{X}^{(o)}(z_m) = \tilde{W}^{-}(z_m,z_t)\tilde{R}(z_t)\tilde{W}^{+}(z_t,z_m), \qquad \text{(III-67)}$$

where $\tilde{R}(z_t)$ describes the reflectivity at the turning point, given by relation (III-59b), while the operators $\tilde{W}^{+}$ and $\tilde{W}^{-}$ are again composed of LG and WKBJ operators, similar as in relation (III-65).

Notice that in the critical angle modeling scheme as introduced in this section, evanescent waves are neglected. This is justified because

- macro layers are considered,
- the velocity gradients vanish in the vicinity of the interfaces, so no turning points are present in this area,

- the velocity functions are continuous monotonous, so not more than one turning point is present in each macro-layer.

A similar **modeling** scheme for piece-wise smooth models is presented by Kennett and Illingworth (1981). The main difference of both approaches lies in the formulation. It was not our intention to present an improved modeling approach. However, because our approach is basically founded on model (III-61):

$$S^{+} \rightarrow W^{+} \rightarrow R \rightarrow W^{-} \rightarrow D \rightarrow P^{-}_{CSP}$$

it provides an excellent starting point for the critical angle **migration** scheme, as discussed in the next section.
For more complicated 1-D inhomogeneous velocity models, a two-way wave equation modeling scheme is preferred. This is discussed in chapter IV, where also a numerical example is given for the more general case.

III.9 PRE-STACK MIGRATION SCHEME BASED ON THE WKBJ ONE-WAY WAVE EQUATIONS

It has been shown in chapter II that full pre-stack migration by single-shot record inversion (SSRI) and common-depthpoint (CDP) stacking is in principle based on inversion of one-way model (III-60). The reflectivity R should be estimated from the downward extrapolated source and detector data, which is schematically represented by

$$S^{+} \rightarrow W^{+} \rightarrow \langle R \rangle \leftarrow F^{-} \leftarrow D^{-1} \leftarrow P^{-}_{CSP}. \qquad \text{(III-68)}$$

Here operator W^{+} simulates the downward propagation effects of the source wave field from the surface into the subsurface, while F^{-} eliminates the upward propagation effects of the reflected waves from the subsurface to the surface. This pre-stack migration scheme is valid for sub-critical data in 1-D, 2-D and 3-D inhomogeneous macro subsurface models. Practical results on 2-D synthetic and real data are presented by De Graaff (1984). Practical aspects with respect to 3-D applications are discussed in chapter VI of this thesis.
In this section we discuss a pre-stack migration scheme, based on modified one-way model (III-61), which is valid for sub-critical as well as critical angle events in 1-D inhomogeneous macro subsurface models. This is schematically represented by

$$S^{+} \rightarrow W^{+} \rightarrow \langle R \rangle \leftarrow F^{-} \leftarrow D^{-1} \leftarrow P^{-}_{CSP}, \qquad \text{(III-69)}$$

As opposed to the procedure discussed in section II.4, we follow a somewhat different procedure, because we are particularly interested in angle dependent turning point problems. The whole procedure is carried out per angle of incidence in the wavenumber-frequency domain, while the zero-offset (ZO) imaging step is replaced by a plane-wave (PW) imaging step, as discussed below. Furthermore, because we consider 1-D inhomogeneous media, the procedure need be applied for one CSP gather only, so the CDP stacking procedure is deleted.

When interface related (long period) multiples as well as transmission effects are neglected, then the modeling scheme, as discussed in the previous section, can be summarized by

$$\tilde{P}^{-}_{CSP}(z_o) = \tilde{D}(z_o)\tilde{X}(z_o)\tilde{S}^{+}(z_o), \qquad \text{(III-70a)}$$

where

$$\tilde{X}(z_o) = \sum_m \tilde{W}^{-}(z_o,z_m)\tilde{R}(z_m)\tilde{W}^{+}(z_m,z_o). \qquad \text{(III-70b)}$$

The non-recursive operators $\tilde{W}^{+}(z_m,z_o)$ and $\tilde{W}^{-}(z_o,z_m)$ are composed of many sub-operators $\tilde{W}^{+}(z_m+i\delta,z_m+(i-1)\delta)$ and $\tilde{W}^{-}(z_m+(i-1)\delta,z_m+i\delta)$ for micro layers (see Figure III-7), which may represent either LG operators $\tilde{W}^{+}$ and $\tilde{W}^{-}$ or WKBJ operators $\tilde{W}^{+}$ and $\tilde{W}^{-}$. The reflection operator $\tilde{R}(z_m)$ can either describe reflection at an interface z_m between two macro layers, or total reflection $\tilde{R}(z_t)$ at a turning point z_t inside a macro layer. According to this model, the forward extrapolated source wave follows from

$$\tilde{S}^{+}(z_m+i\delta) = \tilde{W}^{+}(z_m+i\delta,z_o)\tilde{S}^{+}(z_o) \qquad \text{(III-71a)}$$

while the inverse extrapolated detected wave follows from

$$\tilde{P}^{-}(z_m+i\delta) = [\tilde{D}(z_o)\tilde{W}^{-}(z_o,z_m+i\delta)]^{-1}\tilde{P}^{-}_{CSP}(z_o). \qquad \text{(III-71b)}$$

From relations (III-70) and (III-71) it follows that the PW impulse response at $z=z_m+i\delta$ may be written as

$$\begin{aligned}\tilde{X}(z_m+i\delta) &\triangleq \tilde{P}^{-}(z_m+i\delta)/\tilde{S}^{+}(z_m+i\delta)\\ &= [\tilde{W}^{-}(z_o,z_m+i\delta)]^{-1}\tilde{X}(z_o)[\tilde{W}^{+}(z_m+i\delta,z_o)]^{-1}, \qquad \text{(III-72a)}\end{aligned}$$

where $\tilde{X}(z_o)$ is implicitely defined by relation (III-70a). Relation (III-72a) describes **non-recursive** downward extrapolation of the PW impulse response. On the other hand, **recursive** downward extrapolation of the PW impulse response is described by

$$\tilde{X}(z_m+i\delta) = [\tilde{W}^-(z_m+(i-1)\delta,z_m+i\delta)]^{-1}\tilde{X}(z_m+(i-1)\delta)[\tilde{W}^+(z_m+i\delta,z_m+(i-1)\delta)]^{-1}. \quad \text{(III-72b)}$$

Using these results, we propose the following single-shot record pre-stack migration scheme, which includes critical angle events, based on the WKBJ one-way wave equations.

1. Given the PW impulse response $\tilde{X}(z_m+(i-1)\delta)$, then downward extrapolation can be applied, according to

$$\tilde{X}(z_m+i\delta) = \tilde{F}^-(z_m+i\delta,z_m+(i-1)\delta)\,\tilde{X}(z_m+(i-1)\delta)\,\tilde{F}^+(z_m+(i-1)\delta,z_m+i\delta),$$

with (III-73a)

$$\tilde{F}^+(z_m+(i-1)\delta,z_m+i\delta) = [\tilde{W}^+]^{-1} = [\tilde{W}^-(z_m+(i-1)\delta,z_m+i\delta)]^*, \quad \text{(III-73b)}$$

$$\tilde{F}^-(z_m+i\delta,z_m+(i-1)\delta) = [\tilde{W}^-]^{-1} = [\tilde{W}^+(z_m+i\delta,z_m+(i-1)\delta)]^*. \quad \text{(III-73c)}$$

2. PW imaging can be applied, according to

$$\langle\tilde{R}(p_x,p_y,z_m+i\delta)\rangle = \frac{\Delta\omega}{2\pi}\sum_{\omega}{}' \tilde{X}(k_x,k_y,z_m+i\delta,\omega), \quad \text{(III-74)}$$

where the symbol $\sum'$ denotes that the summation is carried out for constant $p_x=k_x/\omega$ and $p_y=k_y/\omega$, and where $\Delta\omega$ represents the circular frequency sampling interval.

Steps 1 and 2, which describe the total migration procedure for one micro-layer, should be applied recursively.

3. The procedure starts at the surface z_o, where $\tilde{X}(z_o)$ is estimated from the CSP gather $\tilde{P}_{CSP}(z_o)$ by inverting relation (III-70a) in a band-limited way (deconvolution). Notice that, although only one seismic record is considered, this inversion problem is well-posed because the spatial impulse response of a 1-D inhomogeneous medium is space-invariant.

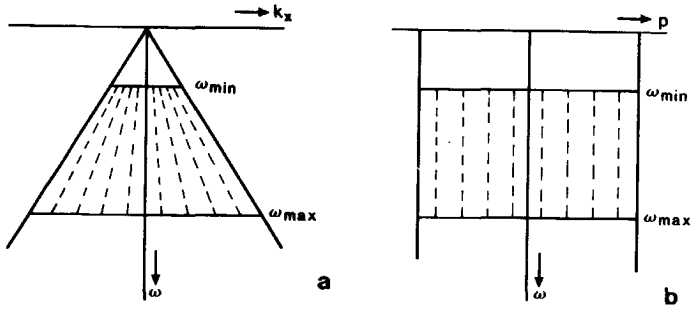

Figure III-9: Two approaches to the same plane wave imaging principle.
a. Summation along lines of constant k_x/ω in the k_x,ω-domain.
b. Summation along lines of constant p in the p,ω-domain.

4. The procedure stops at the shallowest level where total reflection occurs, or at the maximum depth $z=z_M$ if total reflection does not occur.

Discussion.

In the procedure described above it is assumed that the CSP gather has been transformed to the wavenumber-frequency domain. Both the extrapolation (step 1) and imaging (step 2) take place in the wavenumber-frequency domain. Assuming a 2-D situation, imaging for constant $p=k_x/\omega$ is visualized in Figure III-9a. Alternatively, the original CSP gather can be slant-stacked (p,τ-transformation; see Diebold and Stoffa, 1981), followed by a temporal Fourier transform, yielding the CSP-gather in the ray parameter-frequency domain (p,ω). Now, in the operators for downward extrapolation (step 1), k_x should be replaced by $p\omega$. Imaging for constant p (step 2) is visualized in Figure III-9b. In both approaches the final migration output should be identical and represent the reflectivity distribution in the ray parameter-depth domain (p,z).

Example.

We consider the 1-D inhomogeneous subsurface configuration shown in Figure III-10a. A CSP-gather was modeled, using a modeling scheme based on the two-way wave equation (see also the next chapter, Figure IV-13). A ray-representation of the main events is shown in Figure III-10b. Figure III-10c shows the slant-stacked data in the p,τ domain, while Figure III-10d shows the migrated data in the p,z domain. The horizontal events (2,4) represent the reflecting interfaces between the macro layers, while the curved events (1,3) represent

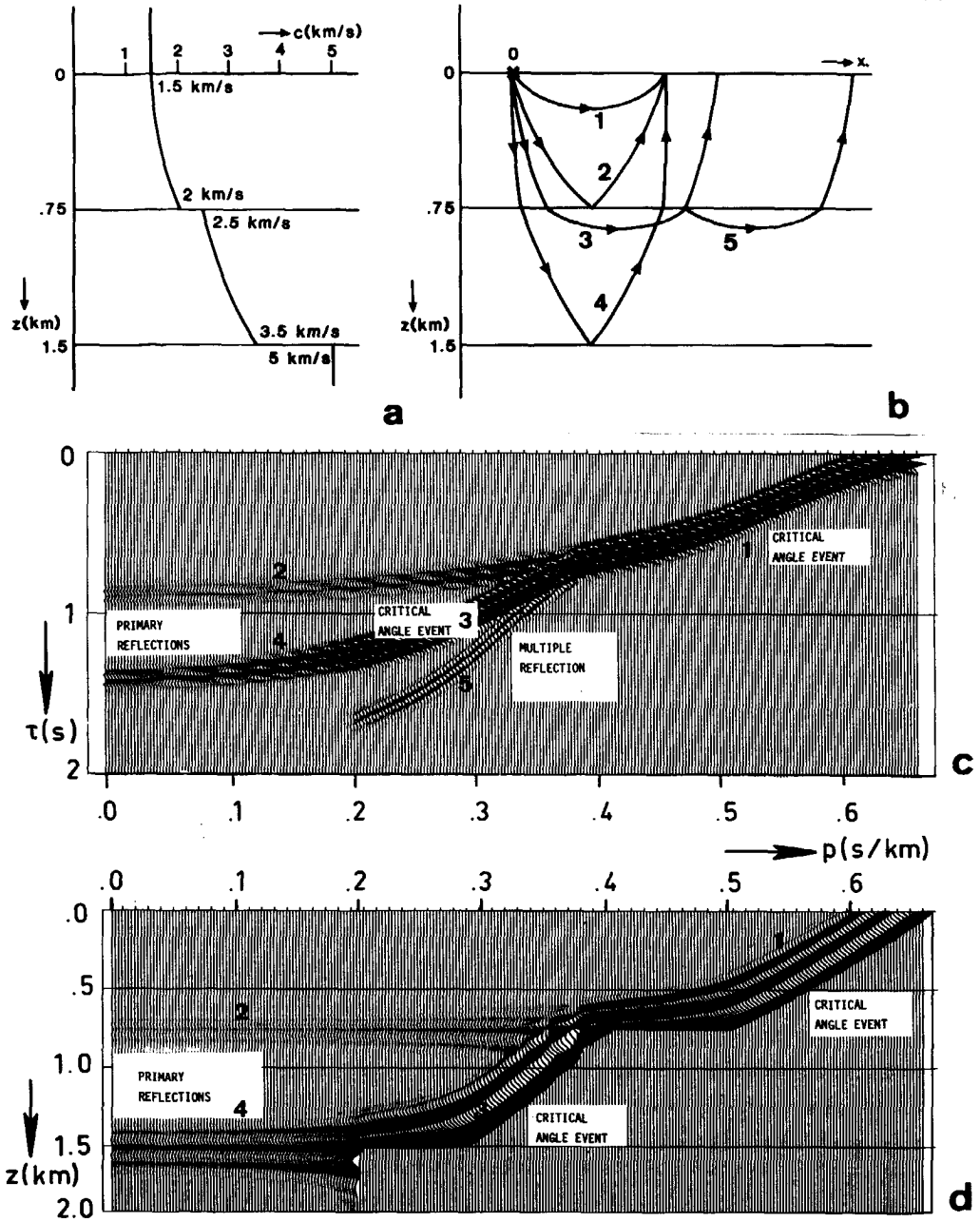

Figure III-10: Migration of critical angle data, based on the WKBJ one-way wave equations.

a. Subsurface velocity model (the density is constant).

b. Ray-representation of the main events.

c. Slant stacked CSP gather in the p,τ domain.

d. Migrated CSP gather in the p,z domain.

the angle dependent turning point effects. (Notice that the multiple reflected critical angle event (5) is not present in the migrated data because the migration procedure stops at the shallowest turning point; see step 4). A further interpretation of Figure III-10d is presented in the next section.

Finally we remark that we derived this migration scheme from the simplified modeling scheme (III-70), where it is assumed that velocity gradients vanish in the vicinity of interfaces and where interface related multiple reflections are neglected. For migration applications sufficient accuracy is obtained also when the velocity gradients do not vanish, like in Figure III-10a. A correct handling of interface related multiple reflections in migration can in principle be accomplished by an iterative scheme, which should be based on inversion of the modeling scheme as discussed in the previous section. A discussion is beyond the scope of this thesis. Berkhout (1982) gives an iterative migration scheme which properly handles multiple reflections of sub-critical angle events in 2-D and 3-D inhomogeneous media. An interesting alternative approach to the multiple problem, based on the two-way wave equation, is discussed in chapter IV.

III.10 INVERSION SCHEME FOR THE MACRO SUBSURFACE MODEL BASED ON THE WKBJ ONE-WAY WAVE EQUATIONS

A typical property of many inversion techniques for the macro subsurface model is that the abrupt changes of the medium parameters may be well retrieved from the data while inversion of the gradual changes is highly inaccurate. The reason for this is that most inversion techniques make use of sub-critical angle data only, which contain only **average propagation** information of the gradual transition zones: waves reflected by a major boundary below a gradual transition zone are transmitted through this zone. **Local reflection** information of a gradual transition zone may be obtained by involving critical angle events in the inversion process: critical angle waves are reflected at turning points inside a gradual transition zone. In this section we discuss a simple inversion scheme, based on the WKBJ one-way wave equations, for the velocity of a 1-D inhomogeneous macro subsurface model.

Consider again the migrated data of Figure III-10d. As we mentioned in section III-9, the curved lines in the rayparameter-depth domain (p,z) represent the angle dependent turning point effects. For the ray parameter we may write

$$p = k_x/\omega = (k_x/k(z_o))/c(z_o) = \sin\theta(z_o)/c(z_o), \qquad \text{(III-75a)}$$

or, with Snell's law,

$$p = \sin\theta(z)/c(z), \qquad \text{(III-75b)}$$

where $\theta(z)$ represents the depth dependent propagation angle. At a turning point the propagation angle $\theta(z_t)$ equals 90 degrees, so

$$p = 1/c(z_t). \qquad \text{(III-75c)}$$

This means that the turning point reflection curves in the migrated data of Figure III-10d may be interpreted as (reciprocal) velocity profiles in the slowness-depth domain (c^{-1},z), see also Figure III-11c. In other words, velocity information of a gradual transition zone may be obtained directly from migrated data which contain critical angle events. Unfortunately this velocity information should be available beforehand in order to perform the migration properly. Using an incorrect **input** velocity profile for migration yields an incorrect (reciprocal) **output** velocity profile in the slowness-depth domain. The velocity inversion procedure described in this section aims at deriving the **true** velocity profile from the input and output velocity profiles in a non-iterative way. Clayton and McMechan (1981) proposed an inversion scheme, based on iterative migration, where the migration input velocity profile in each iteration step equals the average of the input and output velocity profiles of the previous step. In their migration algorithm use is made of the **one-way** phase-shift operator. The inversion scheme is terminated when the output velocity profile matches the input velocity profile.

Based on the migration scheme presented in section III.9, we propose the following **recursive** velocity inversion scheme.

1. Given the downward extrapolated data at macro layer interface z_m, then migration can be applied for macro layer m+1, according to the algorithm described in section III.9, using an estimated migration input velocity profile $c'_{m+1}(z)$.
2. The output velocity profile $c''_{m+1}(z)$ can be measured from the migrated data, for instance by means of coherence calculations. From $c'_{m+1}(z)$ and $c''_{m+1}(z)$ the true velocity $c(z)$ may be estimated. We consider two cases:

i. Similar as in the non-recursive procedure of Clayton and McMechan we may write for our recursive inversion procedure

$$\hat{c}_{m+1}(z) = \tfrac{1}{2}[c'_{m+1}(z) + c''_{m+1}(z)]. \qquad \text{(III-76a)}$$

Notice that this relation is biased (see Appendix D). Steps 1 and 2i should be applied iteratively, with $[c'_{m+1}(z)]_{new}=[\hat{c}_{m+1}(z)]_{old}$. The iterative procedure stops when

$$|c'_{m+1}(z) - c''_{m+1}(z)| < \varepsilon, \qquad \text{(III-76b)}$$

where ε represents a threshold level.

ii. Assuming $c^{-2}_{m+1}(z)$ is linear inside the macro layer, then the unbiased true velocity follows directly from $c'_{m+1}(z)$ and $c''_{m+1}(z)$, as is shown in Appendix D. Here it is assumed that $c_{m+1}(z_m)$ is known. This value can be obtained directly from the downward extrapolated data at interface z_m.

3. Having determined the velocity profile $c_{m+1}(z)$, then the data can be downward extrapolated to interface z_{m+1}, using either a one-way or a two-way wave field extrapolation operator which includes critical angle events.

Steps 1, 2 and 3, which describe the total inversion procedure for macro layer m+1, should be applied recursively.

4. The procedure starts at the surface $z=z_o$, assuming an initial estimate $c'(z)$ is available for all z.
5. The procedure stops at $z=z_M$.

Discussion.

Compared to the scheme proposed by Clayton and McMechan, notice the following refinements

- Sub-critical as well as critical angle events are properly incorporated both in the migration step (step 1) and in the downward extrapolation step (step 3).
- Because the scheme is applied recursively for macro layers, less iteration steps are required, because biased relation (III-76a) is not applied for the entire medium, but for macro layers only (step 2i). Under a special assumption convergence already occurs after one iteration step (step 2ii).

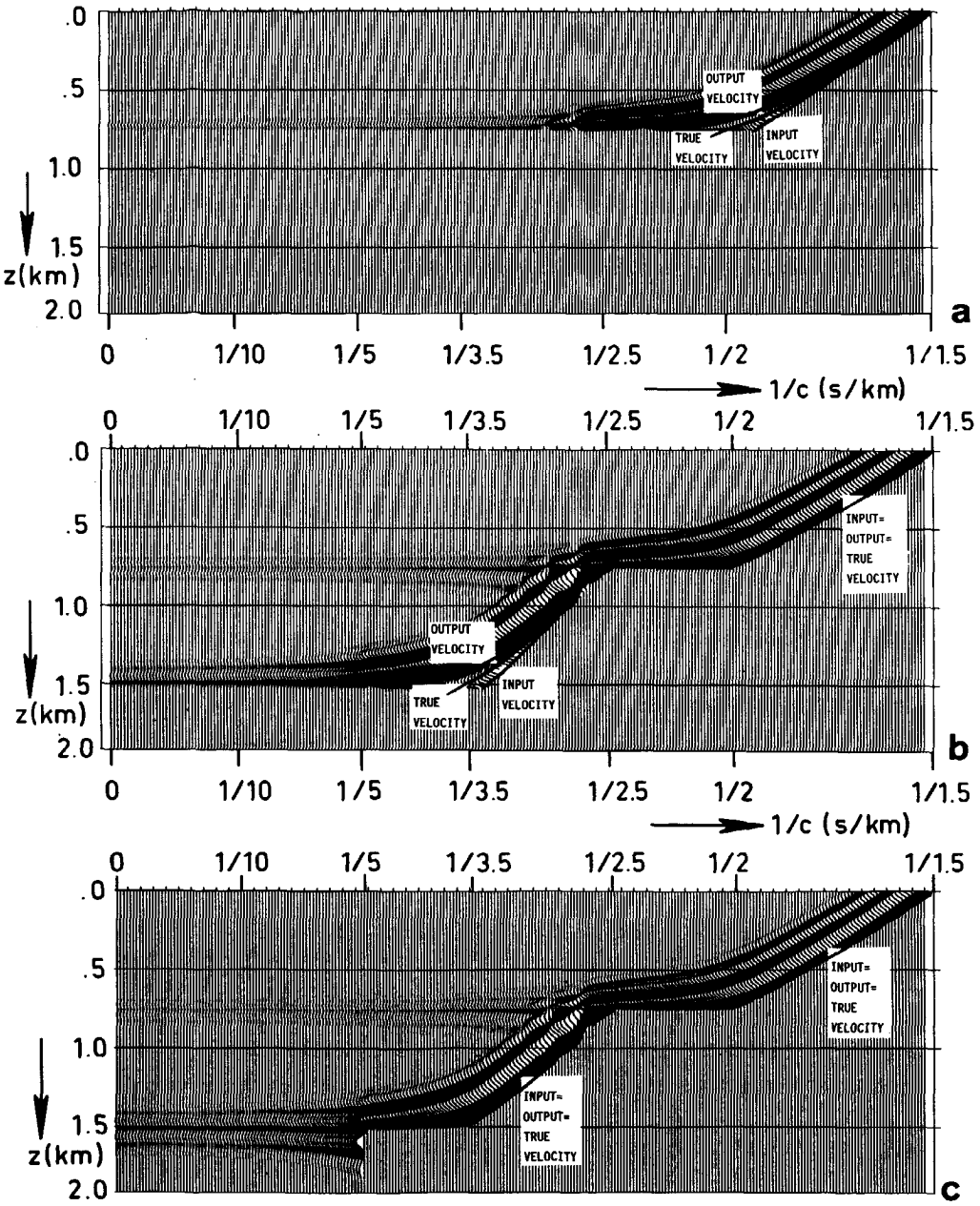

Figure III-11: Recursive velocity inversion for the macro subsurface model.

a. The first macro layer is undermigrated.

b. The first macro layer is correctly migrated, the second macro layer is undermigrated.

c. Both macro layers are correctly migrated.

Example.
Figure III-11a shows the first macro layer of the migrated CSP gather. Because the migration velocity was too low, the input and output velocity profiles do not match. Following the procedure described in Appendix D the true velocity profile for the first macro layer can be found directly. In Figure III-11b, the first macro layer was migrated, using the correct velocity profile, while the second macro layer was under-migrated. Again the true velocity can be found directly from the input and output velocity profiles. Finally, Figure III-11c shows the correctly migrated data for both macro layers. Notice that the migrated sub-critically reflected energy is perfectly aligned, which accounts for the correctness of the **average velocity** of the macro layers. In addition, notice that the output velocity profile, represented by the migrated critically reflected energy, matches the input velocity profile for the entire depth range. This accounts for the correctness of the **local velocity** inside the macro layers as well.

III.11 CONCLUDING REMARKS

In principle there are two approaches to modify the acoustic wave equation such that wave field extrapolation operators along the depth coordinate can be derived:

i. Decomposition into two first order one-way wave equations for P^+ and P^- respectively.

ii. Reformulation into a first order two-way matrix wave equation for $[P, \rho^{-1}\partial P/\partial z]^T$.

In this chapter we discussed methods using the one-way wave equations. We have derived two coupled equations for P^+ and P^- which are exact for all propagation angles. We discussed three decoupling approaches:

A. The **medium is approximated** by a sequence of layers where in each layer the medium parameters are functions of the lateral coordinates only. In this case the one-way wave equations decouple exactly in each layer. The formal solution per layer can be formulated in terms of wave field extrapolation operators based on Taylor series expansion. If the layer thickness is chosen sufficiently small, then a continuously layered medium can be simulated. Recursive one-way wave field extrapolation of primary waves in a finely discretized medium is valid for sub-critical angle events only.

B. The **one-way wave equations are approximated** by neglecting the coupling operators Γ^+ and Γ^-. This decoupling approach is valid for sub-critical

angle events only. For continuously layered media approaches A and B yield identical solutions. For 1-D inhomogeneous continuously layered media solutions are given by the Liouville-Green approximations.

C. For critical angle events the **operator H_2 is linearized** in depth. Based on the WKBJ approach the total wave field can be decomposed into a new choice of downgoing and upgoing primary waves P^+ and P^- which correctly include critical angle events in 1-D inhomogeneous continuously layered media.

Pre-stack migration based on the acoustic one-way wave equations is in principle founded on the following simplified inversion of a seismic experiment:

$$S^+ \rightarrow W^+ \rightarrow \langle R \rangle \leftarrow F^- \leftarrow D^{-1} \leftarrow P^-_{CSP}. \qquad \text{(III-77)}$$

The theory is extensively discussed by Berkhout (1982, 1984a) and in chapter II of this thesis. For sub-critical angle events the technique is applicable for 1-D, 2-D and 3-D inhomogeneous macro subsurface models (De Graaff, 1984, and chapter VI of this thesis).

Pre-stack migration based on the acoustic WKBJ one-way wave equations is in principle founded on the following modified inversion of a seismic experiment

$$S^+ \rightarrow W^+ \rightarrow \langle R \rangle \leftarrow F^- \leftarrow D^{-1} \leftarrow P^-_{CSP} \quad , \qquad \text{(III-78)}$$

where the italic type symbols refer to the incorporation of critical angle events. The theory is extensively discussed in this chapter. The technique is applicable for sub-critical as well as critical angle events in 1-D inhomogeneous macro subsurface models and can be advantageously used in a velocity inversion scheme for the macro subsurface model. A pre-stack migration technique which is applicable for sub-critical as well as critical angle events in 1-D, 2-D and 3-D inhomogeneous macro subsurface models is discussed in the next chapter.

CHAPTER IV

WAVE FIELD EXTRAPOLATION TECHNIQUES, INCLUDING CRITICAL ANGLE EVENTS, BASED ON THE ACOUSTIC TWO-WAY WAVE EQUATION

IV.1 INTRODUCTION

In chapter III acoustic one-way wave field extrapolation techniques were discussed, assuming a computationally convenient acoustic macro subsurface model, as shown in Figure IV-1. It was shown that the conventional one-way approach breaks down for strong vertical velocity gradients and large propagation angles (critical angle events). Interestingly, lateral gradients do not introduce any theoretical complications. Also we discussed an extension to

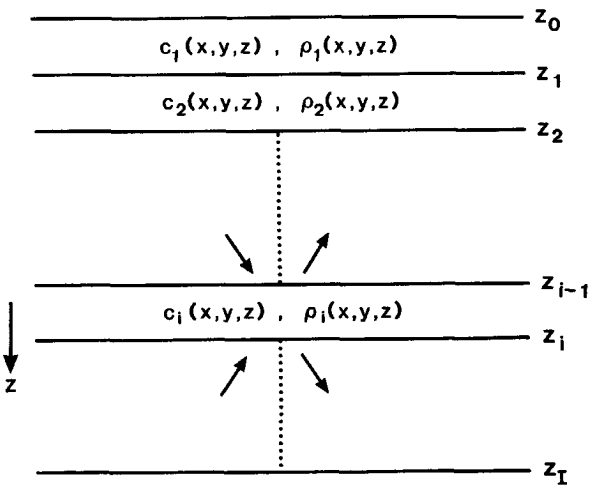

Figure IV-1: Computationally convenient acoustic macro subsurface model for depth extrapolation techniques (one-way and two-way).

the one-way approach which is suitable for critical angle events as well. However, for this extension we had to assume that the medium parameters are a function of depth only.

In this chapter we discuss a more fundamental approach to wave field extrapolation which evades many of the problems typical for the one-way approach. We consider extrapolation of the **total** wave field, described in terms of P and $\rho^{-1}\partial_z P$, again assuming the computational model of Figure IV-1. Because the total wave field is a superposition of downgoing and upgoing waves we may also speak of **two-way** wave field extrapolation. As opposed to one-way techniques it is important to realize that no assumptions need be made on the separability of downgoing and upgoing waves. In the frequency domain the two-way operations can be formulated in terms of spatial convolutions. We consider two cases

i. **Upward extrapolation of the total wave field** $[P,\rho^{-1}\partial_z P]^T$ is symbolically described in matrix notation by

$$\begin{bmatrix} P(z_{i-1}) \\ \frac{1}{\rho}\frac{\partial P}{\partial z}\Big|_{z_{i-1}} \end{bmatrix} = \begin{bmatrix} W_I(z_{i-1},z_i)^* & W_{II}(z_{i-1},z_i)^* \\ W_{III}(z_{i-1},z_i)^* & W_{IV}(z_{i-1},z_i)^* \end{bmatrix} \begin{bmatrix} P(z_i) \\ \frac{1}{\rho}\frac{\partial P}{\partial z}\Big|_{z_i} \end{bmatrix}, \quad \text{(IV-1a)}$$

or, in abbreviated form, by

$$\vec{Q}(z_{i-1}) = W(z_{i-1},z_i)\vec{Q}(z_i), \quad \text{(IV-1b)}$$

see also Figure IV-2a.

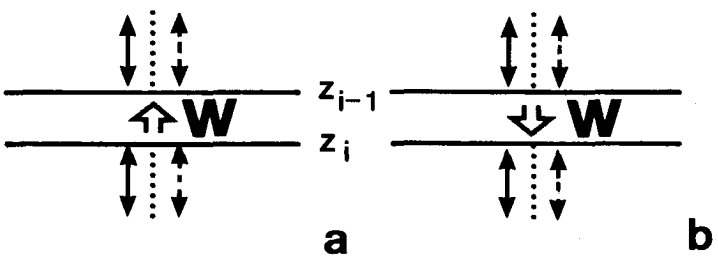

Figure IV-2: In the two-way approach to wave field extrapolation downgoing and upgoing waves are treated simultaneously

a. Upward extrapolation of the total wave field

b. Downward extrapolation of the total wave field

ii. **Downward extrapolation of the total wave field** $[P,\rho^{-1}\partial_z P]^T$ is symbolically described in matrix notation by

$$\begin{bmatrix} P(z_i) \\ \frac{1}{\rho}\frac{\partial P}{\partial z}\Big|_{z_i} \end{bmatrix} = \begin{bmatrix} W_I(z_i,z_{i-1})^* & W_{II}(z_i,z_{i-1})^* \\ W_{III}(z_i,z_{i-1})^* & W_{IV}(z_i,z_{i-1})^* \end{bmatrix} \begin{bmatrix} P(z_{i-1}) \\ \frac{1}{\rho}\frac{\partial P}{\partial z}\Big|_{z_{i-1}} \end{bmatrix}, \quad \text{(IV-1c)}$$

or, in abbreviated form, by

$$\vec{Q}(z_i) = \mathbf{W}(z_i,z_{i-1})\vec{Q}(z_{i-1}), \quad \text{(IV-1d)}$$

see also Figure IV-2b.

Various expressions for the two-way operator $\mathbf{W}$ are presented further on in this chapter. Notice that upward and downward two-way wave field extrapolation are fundamentally equivalent: in both cases downgoing and upgoing waves are extrapolated simultaneously.
In this chapter the two-way wave equation and its solutions are extensively reviewed and compared with the one-way solutions. It is shown that multiple reflections, critical angle events and transmission effects may all be included in the two-way wave field extrapolation operators for arbitrarily inhomogeneous acoustic macro subsurface models. Applications of these operators in modeling and migration schemes are also discussed in this chapter. In chapter V we discuss the extension of this approach for the incorporation of wave conversion in inhomogeneous full elastic macro subsurface models.

IV.2 A COMPARISON OF THE ONE-WAY AND THE TWO-WAY APPROACH

In the frequency domain, the matrix formulation of the two-way wave equation for inhomogeneous liquids reads

$$\frac{\partial \vec{Q}}{\partial z} = \mathbf{A}\vec{Q}, \quad \text{(IV-2a)}$$

where

$$\mathbf{A} = \begin{bmatrix} o & \rho d_o^* \\ -\frac{1}{\rho}H_2^* & o \end{bmatrix}, \quad \text{(IV-2b)}$$

and

$$\vec{Q} = \begin{bmatrix} P \\ \frac{1}{\rho}\frac{\partial P}{\partial z} \end{bmatrix}, \qquad \text{(IV-2c)}$$

with

$$H_2(x,y,z,\omega) = \left[k^2 d_o(x,y) + d_2(x) + d_2(y) - \frac{\partial \ln\rho}{\partial x} d_1(x) - \frac{\partial \ln\rho}{\partial y} d_1(y)\right]_z, \qquad \text{(IV-2d)}$$

and

$$d_o(x,y) = \delta(x)\delta(y), \qquad \text{(IV-2e)}$$

see also section III.2. Notice that two-way wave equation (IV-2) requires one boundary condition for the wave vector $\vec{Q}$ only.
If we define operators H_1 and H_{-1} such that

$$H_1 * H_1 = H_2, \qquad \text{(IV-3a)}$$

$$H_{-1} * H_1 = \delta(x)\delta(y), \qquad \text{(IV-3b)}$$

then operator $\mathbf{A}$ can be expressed as

$$\mathbf{A} = \mathbf{L}\Lambda\mathbf{L}^{-1}, \qquad \text{(IV-4a)}$$

with

$$\mathbf{L} = \begin{bmatrix} d_o * & d_o * \\ \frac{-j}{\rho}H_1 * & \frac{j}{\rho}H_1 * \end{bmatrix}, \quad \Lambda = \begin{bmatrix} -jH_1 * & o \\ o & jH_1 * \end{bmatrix}, \quad \mathbf{L}^{-1} = \tfrac{1}{2}\begin{bmatrix} d_o * & jH_{-1} * \rho d_o * \\ d_o * & -jH_{-1} * \rho d_o * \end{bmatrix} \qquad \text{(IV-4b,c,d)}$$

Furthermore we define P^+ and P^- such that

$$P = P^+ + P^-, \qquad \text{(IV-5a)}$$

$$\frac{1}{\rho}\frac{\partial P}{\partial z} = -\frac{j}{\rho}H_1 * (P^+ - P^-), \qquad \text{(IV-5b)}$$

or, in matrix notation,

$$\vec{Q} = \mathbf{L}\vec{P} \qquad \text{(IV-5c)}$$

or, equivalently,

$$\vec{P} = \mathbf{L}^{-1}\vec{Q} \qquad \text{(IV-5d)}$$

with

$$\vec{P} = \begin{bmatrix} P^+ \\ P^- \end{bmatrix}. \qquad \text{(IV-5e)}$$

Substitution of relation (IV-5c) into two-way equation (IV-2a), using property (IV-4a), yields

$$\frac{\partial \vec{P}}{\partial z} = \mathbf{B}\vec{P} \qquad \text{(IV-6a)}$$

with

$$\mathbf{B} = \mathbf{A} - \mathbf{L}^{-1}\frac{\partial \mathbf{L}}{\partial z}, \qquad \text{(IV-6b)}$$

or

$$\frac{\partial P^+}{\partial z} = -jH_1 * P^+ - \tfrac{1}{2}H_{-1} * [\rho\frac{\partial}{\partial z}(\frac{1}{\rho}H_1)] * (P^+ - P^-), \qquad \text{(IV-6c)}$$

and

$$\frac{\partial P^-}{\partial z} = +jH_1 * P^- + \tfrac{1}{2}H_{-1} * [\rho\frac{\partial}{\partial z}(\frac{1}{\rho}H_1)] * (P^+ - P^-). \qquad \text{(IV-6d)}$$

Apparently P^+ and P^- satisfy the coupled one-way wave equations for downgoing and upgoing waves, which were derived on physical grounds in section III.4. Recall that in the conventional one-way approach it is assumed that $|P^-| << |P^+|$ in (IV-6c) and $|P^+| << |P^-|$ in (IV-6d), which means that multiple reflections, or critical angle events (in continuously layered media), are not considered, hence

$$\frac{\partial P^+}{\partial z} \approx -jH_1^+ * P^+, \qquad \text{(IV-7a)}$$

$$\frac{\partial P^-}{\partial z} \approx +jH_1^- * P^-, \qquad \text{(IV-7b)}$$

where the operators H_1^+ and H_1^- are defined as

$$jH_1^+ = jH_1 + \tfrac{1}{2}H_{-1} * [\rho\frac{\partial}{\partial z}(\frac{1}{\rho}H_1)], \qquad \text{(IV-7c)}$$

$$jH_1^- = jH_1 - \tfrac{1}{2}H_{-1} * [\rho\frac{\partial}{\partial z}(\frac{1}{\rho}H_1)]. \qquad \text{(IV-7d)}$$

Finally, recall that equations (IV-6c) and (IV-6d) **fully** decouple for media which are homogeneous along the z-coordinate, that is, when $\partial_z(\rho^{-1}H_1) = o$. Summarizing, by decomposing operator $\mathbf{A}$ we showed that two-way wave equation (IV-2a)

$$\frac{\partial\vec{Q}}{\partial z} = \mathbf{A}\vec{Q} \qquad \text{(IV-8)}$$

can be transformed into coupled one-way wave equations (IV-6c,d), or, assuming that critical angle events may be neglected, into decoupled one-way wave equations (IV-7a,b), in matrix notation given by

$$\frac{\partial\vec{P}}{\partial z} \approx j\mathbf{H}_1\vec{P}, \qquad \text{(IV-9a)}$$

with

$$\mathbf{H}_1 = \begin{bmatrix} -H_1^+* & o \\ o & H_1^-* \end{bmatrix}. \qquad \text{(IV-9b)}$$

For downward extrapolation, a solution of one-way wave equation (IV-9) is symbolically described by (see also relations (III-1a) and (III-1d))

$$\begin{bmatrix} P^+(z_i) \\ P^-(z_i) \end{bmatrix} = \begin{bmatrix} W^+(z_i,z_{i-1})* & o \\ o & F^-(z_i,z_{i-1})* \end{bmatrix} \begin{bmatrix} P^+(z_{i-1}) \\ P^-(z_{i-1}) \end{bmatrix}, \qquad \text{(IV-10a)}$$

or, in abbreviated form, by

$$\vec{P}(z_i) = \mathbf{V}(z_i,z_{i-1})\vec{P}(z_{i-1}). \qquad \text{(IV-10b)}$$

A similar relation holds for upward extrapolation.

With respect to these independent **one-way** solutions, notice the following:

- Critical angle events are not included because the underlying wave equation (IV-9) is a decoupled approximated version of (IV-6).
- In practical implementations for inhomogeneous media the solution is highly affected by numerical inaccuracy (limited dip angle performance)

because the underlying wave equation is based on the implicitly defined **one-way square-root operator** H_1 (see relation (IV-3a)).

- In recursive applications additional effort is required with respect to the boundary conditions between the consecutive extrapolation steps, because downgoing and upgoing waves are not continuous at layer interfaces. In practical implementations these boundary conditions are often neglected, which means that transmission effects and multiple reflections are not incorporated.

On the other hand, a solution of two-way wave equation (IV-8) is symbolically described by (see also relation (IV-1d))

$$\vec{Q}(z_i) = \mathbf{W}(z_i, z_{i-1})\vec{Q}(z_{i-1}). \qquad \text{(IV-11)}$$

Notice that for media which are homogeneous along the z-coordinate, as well as for **small dip angle** applications in arbitrarily inhomogeneous media, two-way wave field extrapolation, as described by (IV-11), could be replaced by three sub-processes as follows:

i. **Decomposition** of the total wave field $\vec{Q} = [P, \rho^{-1}\partial_z P]^T$ into downgoing and upgoing waves $\vec{P} = [P^+, P^-]^T$, according to (IV-5d):

$$\vec{P}(z_{i-1}) = \mathbf{L}^{-1}(z_{i-1})\vec{Q}(z_{i-1}). \qquad \text{(IV-12a)}$$

ii. Independent **one-way wave field extrapolation** of downgoing and upgoing waves, according to (IV-10b):

$$\vec{P}(z_i) = \mathbf{V}(z_i, z_{i-1})\vec{P}(z_{i-1}). \qquad \text{(IV-12b)}$$

iii. **Composition** of the total wave field from its downgoing and upgoing constituents, according to (IV-5c):

$$\vec{Q}(z_i) = \mathbf{L}(z_i)\vec{P}(z_i). \qquad \text{(IV-12c)}$$

Combination of these three steps yields

$$\vec{Q}(z_i) = \left[\mathbf{L}(z_i)\mathbf{V}(z_i, z_{i-1})\,\mathbf{L}^{-1}(z_{i-1})\right]\vec{Q}(z_{i-1}). \qquad \text{(IV-13)}$$

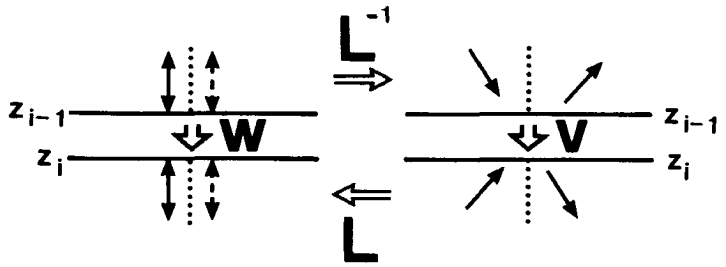

Figure IV-3: Diagram showing the relationship between two-way and one-way wave field extrapolation.

This total process is visualized in Figure IV-3. It is important to realize, however, that direct **two-way** wave field extrapolation, as described by (IV-11), is preferred above forementioned one-way processes for the following reasons:

- Critical angle events are included in (IV-11) because the underlying wave equation (IV-8) is exact.
- In practical implementations for inhomogeneous media the solution may be very accurate (90 degrees dip angle performance, see section IV.6) because the underlying wave equation is based on the explicitly defined **two-way operator** H_2 (see relation IV-2d).
- In recursive applications **no** additional effort is required with respect to the boundary conditions, because the total wave field $\vec{Q} = [P, \rho^{-1}\partial_z P]^T$ is continuous at layer interfaces. Hence, transmission effects and multiple reflections are automatically incorporated.

IV.3 TWO-WAY SOLUTION FOR 1-D INHOMOGENEOUS MEDIA, INCLUDING CRITICAL ANGLE EVENTS

In this section we start with a review of the two-way wave equation in the wavenumber-frequency domain, following Ursin (1983). Next, we give the solution for a homogeneous layer. Finally, we present two solutions for piece-wise continuously layered media.

Applying a double spatial Fourier transform, as defined by (III-10a), to relation (IV-2), yields the two-way wave equation in the wavenumber-frequency domain

$$\frac{\partial \tilde{\vec{Q}}}{\partial z} = \tilde{\mathbf{A}}\,\tilde{\vec{Q}}, \qquad \text{(IV-14a)}$$

where

$$\tilde{\mathbf{A}} = \begin{bmatrix} o & \rho \\ -\tilde{H}_2/\rho & o \end{bmatrix}, \quad \tilde{\tilde{Q}} = \begin{bmatrix} \tilde{P} \\ \frac{1}{\rho}\frac{\partial \tilde{P}}{\partial z} \end{bmatrix}, \tag{IV-14b,c}$$

and

$$\tilde{H}_2(k_x, k_y, z, \omega) = \omega^2/c^2 - k_x^2 - k_y^2. \tag{IV-14d}$$

Here it is assumed that the medium parameters c and ρ are functions of the depth coordinate only, that is, $c = c(z)$ and $\rho = \rho(z)$. When we define $\tilde{H}_1$ such that

$$\tilde{H}_1^2 = \tilde{H}_2, \tag{IV-15}$$

then the **eigenvalue decomposition** of operator $\tilde{\mathbf{A}}$ reads

$$\tilde{\mathbf{A}} = \tilde{\mathbf{L}}\,\tilde{\mathbf{\Lambda}}\,\tilde{\mathbf{L}}^{-1} \tag{IV-16a}$$

with

$$\tilde{\mathbf{L}} = \begin{bmatrix} 1 & 1 \\ -j\tilde{H}_1/\rho & j\tilde{H}_1/\rho \end{bmatrix}, \quad \tilde{\mathbf{\Lambda}} = \begin{bmatrix} -j\tilde{H}_1 & o \\ o & j\tilde{H}_1 \end{bmatrix}, \quad \tilde{\mathbf{L}}^{-1} = \tfrac{1}{2}\begin{bmatrix} 1 & j\rho/\tilde{H}_1 \\ 1 & -j\rho/\tilde{H}_1 \end{bmatrix}. \tag{IV-16b,c,d}$$

Notice that this relation represents the wavenumber domain equivalent of relation (IV-4). Similar as in (IV-5), we define downgoing waves $\tilde{\tilde{P}}^+$ and upgoing waves $\tilde{\tilde{P}}^-$ according to

$$\tilde{\tilde{Q}} = \tilde{\mathbf{L}}\,\tilde{\tilde{P}} \tag{IV-17a}$$

or

$$\tilde{\tilde{P}} = \tilde{\mathbf{L}}^{-1}\tilde{\tilde{Q}}, \tag{IV-17b}$$

with

$$\tilde{\tilde{P}} = \begin{bmatrix} \tilde{P}^+ \\ \tilde{P}^- \end{bmatrix}. \tag{IV-17c}$$

Notice that decomposition (IV-17b) breaks down for critical angle events, that is, when $\tilde{H}_1 \to o$. This phenomenon was already discussed in chapter III. Later in this section we present an alternative decomposition which is also valid for critical angle events.

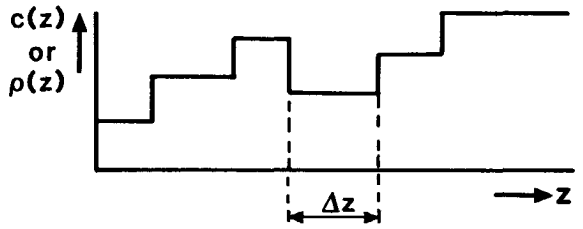

Figure IV-4: Subsurface model with homogeneous layers.

We now consider the case that both c and ρ are constant within a given depth interval (see Figure IV-4). Then the solution of equation (IV-14) is given by

$$\tilde{\vec{Q}}(z) = \tilde{\mathbf{W}}(z,z_o)\tilde{\vec{Q}}(z_o), \qquad \text{(IV-18a)}$$

where, symbolically,

$$\tilde{\mathbf{W}}(z,z_o) = \exp[\tilde{\mathbf{A}}\Delta z], \qquad \text{(IV-18b)}$$

with $\Delta z = z - z_o$. Using property (IV-16), relation (IV-18b) can be written as

$$\tilde{\mathbf{W}}(z,z_o) = \mathbf{I} + \tilde{\mathbf{L}}(\tilde{\mathbf{\Lambda}}\Delta z)\tilde{\mathbf{L}}^{-1} + \tilde{\mathbf{L}}(\tilde{\mathbf{\Lambda}}\Delta z)\tilde{\mathbf{L}}^{-1}\tilde{\mathbf{L}}(\tilde{\mathbf{\Lambda}}\Delta z)\tilde{\mathbf{L}}^{-1} + \ldots, \qquad \text{(IV-19a)}$$

or

$$\tilde{\mathbf{W}}(z,z_o) = \tilde{\mathbf{L}}\,[\mathbf{I} + (\tilde{\mathbf{\Lambda}}\Delta z) + (\tilde{\mathbf{\Lambda}}\Delta z)^2 + \ldots]\tilde{\mathbf{L}}^{-1}, \qquad \text{(IV-19b)}$$

or

$$\tilde{\mathbf{W}}(z,z_o) = \tilde{\mathbf{L}}(z)\tilde{\mathbf{V}}(z,z_o)\tilde{\mathbf{L}}^{-1}(z_o), \qquad \text{(IV-20a)}$$

with

$$\tilde{\mathbf{V}}(z,z_o) = \exp[\tilde{\mathbf{\Lambda}}\Delta z], \qquad \text{(IV-20b)}$$

or

$$\tilde{\mathbf{V}}(z,z_o) = \begin{bmatrix} \exp(-j\tilde{H}_1\Delta z) & o \\ o & \exp(j\tilde{H}_1\Delta z) \end{bmatrix}. \qquad \text{(IV-20c)}$$

Relation (IV-20) shows that for this special case of a homogeneous layer, two-way operator $\tilde{\mathbf{W}}(z,z_o)$ can be written in terms of one-way

sub-processes. This phenomenon was already discussed in the previous section (see relations (IV-12) and (IV-13)) and is visualized in Figure IV-3. On the other hand, if we define two-way operator $\tilde{\mathbf{W}}(z,z_o)$ as

$$\tilde{\mathbf{W}}(z,z_o) = \begin{bmatrix} \tilde{W}_I(z,z_o) & \tilde{W}_{II}(z,z_o) \\ \tilde{W}_{III}(z,z_o) & \tilde{W}_{IV}(z,z_o) \end{bmatrix}, \qquad \text{(IV-21a)}$$

then expressions for the sub-operators $\tilde{W}_I \ldots \tilde{W}_{IV}$ follow directly from relation (IV-20):

$$\tilde{W}_I(z,z_o) = \cos[\tilde{H}_1 \Delta z], \qquad \text{(IV-21b)}$$

$$\tilde{W}_{II}(z,z_o) = \frac{\rho}{\tilde{H}_1} \sin[\tilde{H}_1 \Delta z], \qquad \text{(IV-21c)}$$

$$\tilde{W}_{III}(z,z_o) = \tilde{Z}_2 \tilde{W}_{II}(z,z_o), \qquad \text{(IV-21d)}$$

$$\tilde{W}_{IV}(z,z_o) = \tilde{W}_I(z,z_o), \qquad \text{(IV-21e)}$$

with

$$\tilde{Z}_2 = -\frac{1}{\rho^2}\tilde{H}_2. \qquad \text{(IV-21f)}$$

Notice that the limit for $\tilde{H}_1 \to o$ exists. For evanescent waves $(k_x^2+k_y^2>\omega^2/c^2)$ the operator $\tilde{H}_1$ becomes imaginary. The goniometric functions should then preferably be replaced by hyperbolic functions of the real argument $j\tilde{H}_1\Delta z$.

For propagating waves $(k_x^2+k_y^2<\omega^2/c^2)$ sub-operator $\tilde{W}_I$ describes the real part of the phase-shift operator $\exp(-j\tilde{H}_1\Delta z)$, which represents the spatial Fourier transform of the Rayleigh II operator. In a similar way, operators $\tilde{W}_{II}$ and $\tilde{W}_{III}$ are related to the imaginary part of the transformed Rayleigh I and Rayleigh III operators. Hence, the spatially **band-limited** inverse Fourier transform of relation (IV-18a) is given by the following relation in the space-frequency domain

$$\vec{Q}(z) = \mathbf{W}(z,z_o)\vec{Q}(z_o), \qquad \text{(IV-22a)}$$

where

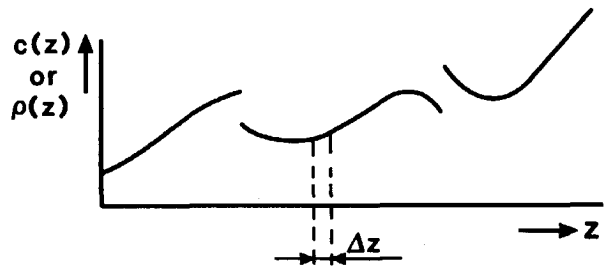

Figure IV-5: Piece-wise continuously layered subsurface model.

$$\mathbf{W}(z,z_o) = \begin{bmatrix} W_I(z,z_o)^* & W_{II}(z,z_o)^* \\ W_{III}(z,z_o)^* & W_{IV}(z,z_o)^* \end{bmatrix}, \qquad \text{(IV-22b)}$$

with

$$W_I(z,z_o) = \text{Real (Rayleigh II)}, \qquad \text{(IV-22c)}$$

$$W_{II}(z,z_o) = \frac{1}{\omega}\,\text{Imag (Rayleigh I)}, \qquad \text{(IV-22d)}$$

$$W_{III}(z,z_o) = -\omega\,\text{Imag (Rayleigh III)}, \qquad \text{(IV-22e)}$$

$$W_{IV}(z,z_o) = W_I(z,z_o). \qquad \text{(IV-22f)}$$

The three Rayleigh operators are extensively discussed by Berkhout (1982). Notice that relation (IV-22) describes stable two-way wave field extrapolation in the z-direction (the convolutions are carried out in the x- and y-directions).

When $c(z)$ and $\rho(z)$ are arbitrary continuous functions within a given depth interval (see Figure IV-5), then two-way wave equation (IV-14) cannot be solved as above. Suppose a solution is given by

$$\tilde{\tilde{Q}}(z) = \tilde{\mathbf{W}}(z,z_o)\tilde{\tilde{Q}}(z_o), \qquad \text{(IV-23a)}$$

then operator $\tilde{\mathbf{W}}(z,z_o)$ should satisfy the wave equation

$$\frac{\partial \tilde{\mathbf{W}}(z,z_o)}{\partial z} = \tilde{\mathbf{A}}(z)\tilde{\mathbf{W}}(z,z_o). \qquad \text{(IV-23b)}$$

Furthermore, when the gradients of c and ρ vanish, then $\tilde{\mathbf{W}}(z,z_o)$ should be equal to operator (IV-21). Assuming that the medium parameters may be linearized within a sufficiently thin layer, according to

$$c(z) = c_o[1 + q\Delta z] \tag{IV-24a}$$

and

$$\rho(z) = \rho_o[1 + r\Delta z], \tag{IV-24b}$$

with

$$\Delta z = z - z_o,$$

while

$$|q\Delta z| << 1 \tag{IV-24c}$$

and

$$|r\Delta z| << 1, \tag{IV-24d}$$

then it can be verified by substitution that operator $\tilde{\mathbf{W}}(z,z_o)$ is given by

$$\tilde{\mathbf{W}}(z,z_o) = \begin{bmatrix} \tilde{W}_I(z,z_o) & \tilde{W}_{II}(z,z_o) \\ \tilde{W}_{III}(z,z_o) & \tilde{W}_{IV}(z,z_o) \end{bmatrix}, \tag{IV-25a}$$

with

$$\tilde{W}_I(z,z_o) = (1+R)\tilde{\psi}_1 + (S-R)\tilde{\psi}_2 + S\tilde{\psi}_3, \tag{IV-25b}$$

$$\tilde{W}_{II}(z,z_o) = \rho_o\Delta z[(1+R)\tilde{\psi}_2 - S\tilde{\psi}_3], \tag{IV-25c}$$

$$\tilde{W}_{III}(z,z_o) = \tilde{Z}_2\tilde{W}_{II}(z,z_o), \tag{IV-25d}$$

$$\tilde{W}_{IV}(z,z_o) = (1-R)\tilde{\psi}_1 + (S+R)\tilde{\psi}_2 - S\tilde{\psi}_3, \tag{IV-25e}$$

$$\tilde{Z}_2 = \frac{-1}{\rho_o^2}[(1-r\Delta z)\tilde{H}_2(z_o) - q\Delta z\,\frac{\omega^2}{c_o^2}], \tag{IV-25f}$$

$$S = \frac{q\omega^2}{2c_o^2}\Delta z^3, \qquad R = \frac{r}{2}\Delta z. \tag{IV-25g,h}$$

For propagating waves, $\tilde{H}_2 > o$, the operators $\tilde{\psi}_1,\tilde{\psi}_2,\tilde{\psi}_3$ are given by

$$\tilde{\psi}_1 = \cos\tilde{\Phi}, \tag{IV-25i}$$

$$\tilde{\psi}_2 = (\sin\tilde{\Phi})/\tilde{\Phi}, \tag{IV-25j}$$

$$\tilde{\psi}_3 = (\cos\tilde{\Phi})/\tilde{\Phi}^2 - (\sin\tilde{\Phi})/\tilde{\Phi}^3, \qquad \text{(IV-25k)}$$

with

$$\tilde{\Phi} = \tilde{H}_1(z_o)\Delta z. \qquad \text{(IV-25l)}$$

Notice that the limit for $\tilde{H}_1(z_o) \to o$ exists. For evanescent waves the operator $\tilde{H}_1(z_o)$ becomes imaginary. The goniometric functions should then preferably be replaced by hyperbolic functions of the real argument $j\tilde{H}_1(z_o)\Delta z$. Notice that the only approximation is thin layer assumption (IV-24). This means that **critical angle events** are properly incorporated in operator $\tilde{\mathbf{W}}(z,z_o)$, given by relation (IV-25). For large extrapolation distances this operator must be applied recursively, such that in each recursion step thin layer assumption (IV-24) is satisfied.

In chapter III we have shown that decomposition of the total wave field into downgoing and upgoing waves is not uniquely defined. Based on the WKBJ approach for 1-D inhomogeneous media, we discussed an alternative choice of **decoupled** downgoing and upgoing propagating waves $\tilde{P}^+$ and $\tilde{P}^-$ in the vicinity of a turning point, which include critical angle events. In the following, italic type symbols refer to the incorporation of critical angle events in the one-way approach. The superposition of $\tilde{P}^+$ and $\tilde{P}^-$, given by

$$\tilde{P} = \tilde{P}^+ + \tilde{P}^- \qquad \text{(IV-26a)}$$

satisfies the wave equation

$$\frac{\partial^2}{\partial z^2}\left(\frac{\tilde{P}}{\sqrt{\rho}}\right) = -\tilde{H}_2\left(\frac{\tilde{P}}{\sqrt{\rho}}\right), \qquad \text{(IV-26b)}$$

whereas $\tilde{P}^+$ and $\tilde{P}^-$ satisfy the following decoupled one-way wave equations

$$\frac{\partial \tilde{P}^+}{\partial z} = -j\tilde{H}_1^+\tilde{P}^+, \qquad \text{(IV-26c)}$$

$$\frac{\partial \tilde{P}^-}{\partial z} = +j\tilde{H}_1^-\tilde{P}^-. \qquad \text{(IV-26d)}$$

Wave equation (IV-26b) represents the spatial Fourier transform of wave equation (III-9), assuming $|E_\rho| = |(2\rho)^{-1}\partial_z^2\rho - (3/4)(\rho^{-1}\partial_z\rho)^2| \ll k^2$. Furthermore it was assumed in chapter III that the operator $\tilde{H}_2$ is linearized in depth in the vicinity of the turning point z_t, according to

$$\tilde{H}_2(z) = (z-z_t)\chi. \qquad \text{(IV-26e)}$$

Hence, it is assumed that in the vicinity of z_t the propagation velocity c(z) satisfies

$$c^{-2}(z) = c^{-2}(z_t) + (z-z_t)\chi\omega^{-2}, \qquad \text{(IV-26f)}$$

or, if z_o is close to z_t

$$c^{-2}(z) = c_o^{-2}[1+c_o^2\omega^{-2}\chi\Delta z], \qquad \text{(IV-26g)}$$

with $c_o=c(z_o)$ and $\Delta z=z-z_o$. In one-way wave equations (IV-26c) and (IV-26d) the operators $\tilde{H}_1^+$ and $\tilde{H}_1^-$ are based on Airy functions, according to relations (III-54c,d). We may now construct a matrix formalism, based on relations (IV-26a,b,c,d). The total wave field $\tilde{\vec{Q}}=(\tilde{P},\rho^{-1}\partial_z\tilde{P})^T$ can be composed from the wave functions $\tilde{P}^+$ and $\tilde{P}^-$ according to

$$\tilde{\vec{Q}} = \tilde{\mathbf{L}}\tilde{\vec{P}}, \qquad \text{(IV-27a)}$$

where

$$\tilde{\mathbf{L}} = \begin{bmatrix} 1 & 1 \\ -j\tilde{H}_1^+/\rho & j\tilde{H}_1^-/\rho \end{bmatrix}, \qquad \tilde{\vec{P}} = \begin{bmatrix} \tilde{P}^+ \\ \tilde{P}^- \end{bmatrix}, \qquad \text{(IV-27b,c)}$$

and where $\tilde{\vec{Q}}$ satisfies two-way wave equation (IV-14a), assuming $|E_\rho|<<k^2$. Similarly, decomposition is described by

$$\tilde{\vec{P}} = \tilde{\mathbf{L}}^{-1}\tilde{\vec{Q}}, \qquad \text{(IV-27d)}$$

where

$$\tilde{\mathbf{L}}^{-1} = \frac{1}{\tilde{H}_1^+ + \tilde{H}_1^-}\begin{bmatrix} \tilde{H}_1^- & j\rho \\ \tilde{H}_1^+ & -j\rho \end{bmatrix}. \qquad \text{(IV-27e)}$$

Notice that $\tilde{\mathbf{L}}^{-1}$ defines a decomposition operator which is valid for sub-critical as well as critical angle events. Finally, the one-way wave equations (IV-26c) and (IV-26d) can be combined into the following matrix equation

$$\frac{\partial\tilde{\vec{P}}}{\partial z} = j\tilde{\mathbf{H}}_1\tilde{\vec{P}}, \qquad \text{(IV-28a)}$$

with

$$\tilde{\mathbf{H}}_1 = \begin{bmatrix} -\tilde{H}_1^{+} & o \\ o & \tilde{H}_1^{-} \end{bmatrix} \qquad \text{(IV-28b)}$$

For downward extrapolation, a solution of one-way wave equation (IV-28) is described by (see also relations (III-56) and (III-57))

$$\begin{bmatrix} \tilde{P}^{+}(z) \\ \tilde{P}^{-}(z) \end{bmatrix} = \begin{bmatrix} \tilde{W}^{+}(z,z_o) & o \\ o & \tilde{F}^{-}(z,z_o) \end{bmatrix} \begin{bmatrix} \tilde{P}^{+}(z_o) \\ \tilde{P}^{-}(z_o) \end{bmatrix}, \qquad \text{(IV-29a)}$$

or, in abbreviated form, by

$$\tilde{\vec{P}}(z) = \tilde{\mathbf{V}}(z,z_o)\tilde{\vec{P}}(z_o). \qquad \text{(IV-29b)}$$

A similar relation holds for upward extrapolation. Notice that relations (IV-27) and (IV-29) can be elegantly combined into one relation for downward extrapolation of the total wave field $\tilde{\vec{Q}}$:

$$\tilde{\vec{Q}}(z) = \left[\tilde{\mathbf{L}}(z)\tilde{\mathbf{V}}(z,z_o)\tilde{\mathbf{L}}^{-1}(z_o)\right]\tilde{\vec{Q}}(z_o). \qquad \text{(IV-30)}$$

Under thin layer assumption (IV-24), with $q=-\frac{1}{2}c_o^2\omega^{-2}\chi$, this solution is equivalent to

$$\tilde{\vec{Q}}(z) = \tilde{\mathbf{W}}(z,z_o)\tilde{\vec{Q}}(z_o), \qquad \text{(IV-31)}$$

with two-way operator $\tilde{\mathbf{W}}(z,z_o)$ given by relation (IV-25).

Hence, relation (IV-30) shows that also in the special case of a 1-D inhomogeneous medium, *two-way wave field extrapolation can be written in terms of one-way sub-processes which include* **critical angle events.** For practical implementations, however, two-way algorithm (IV-31) is preferred because it avoids the use of Airy functions. Two-way operator $\tilde{\mathbf{W}}(z,z_o)$, as defined by (IV-25), is fully based on simple goniometric functions, which provide the basis for recursive finite-difference schemes that include critical angle events, as is shown in section IV.5.

Summarizing, in this section we derived two-way wave field extrapolation operators for media with depth dependent properties $c(z)$ and $\rho(z)$, as shown in Figures IV-4 and IV-5. Both in modeling and migration schemes, the operators should be applied recursively, which is allowed because the extrapolated total

wave field $\tilde{\vec{Q}}$ is continuous for all depths. This means that transmission effects as well as multiple reflections are automatically incorporated when applying operator (IV-21) or (IV-22). In addition, critical angle events are incorporated when applying operator (IV-25). Modeling and migration schemes, based on the extrapolation operators (IV-21) and (IV-25), are discussed in sections IV.7 and IV.8. In addition, it is shown in these sections that the composition and decomposition algorithms (IV-17) and (IV-27) play an important role in two-way modeling and migration schemes.

IV.4 TWO-WAY SOLUTION FOR ARBITRARILY INHOMOGENEOUS MEDIA, INCLUDING CRITICAL ANGLE EVENTS

In this section we discuss two-way wave field extrapolation in arbitrarily inhomogeneous media. It is shown that in principle lateral derivatives of the medium parameters can be incorporated. In addition, the operator may include all propagation angles as well as evanescent waves.

Our starting point is two-way wave equation (IV-2a)

$$\frac{\partial \vec{Q}}{\partial z} = \mathbf{A}\vec{Q}, \tag{IV-32}$$

where $\mathbf{A}$ and $\vec{Q}$ are defined by relations (IV-2b,c). Assuming that the derivatives $\partial^m \vec{Q}/\partial z^m$ exist and are continuous between z_o and z, we can define two-way wave field extrapolation by means of the following Taylor series summation

$$\vec{Q}(z) = \sum_{m=0}^{\infty} \frac{\Delta z^m}{m!} \left[\frac{\partial^m \vec{Q}}{\partial z^m}\right]_{z_o}, \tag{IV-33}$$

with $\Delta z = z - z_o$. In practice the scheme should be applied recursively for small $|\Delta z|$. A similar approach for one-way wave field extrapolation was discussed by Berkhout (1982) and in chapter III. Notice that the total error per extrapolation step depends on two different sub-errors:

1. The error in the estimates of the derivatives with respect to z.
2. The error due to truncation of the Taylor series.

In one-way wave field extrapolation, the z-derivatives are based on the **implicit** square-root operator H_1, defined by relation (IV-3a). On the other hand, in two-way wave field extrapolation, the z-derivatives are based on the **explicit** operator H_2, defined by relation (IV-2d). They can be calculated

exactly within the seismic bandwidth, which means that sub-error 1 vanishes in case of two-way wave field extrapolation. In the next section we show that by assuming the lateral derivatives of the medium parameters may be neglected also sub-error 2 can be held to a minimum.

From equation (IV-32), the z-derivatives follow directly by recursively applying

$$\frac{\partial^m \vec{Q}}{\partial z^m} = \frac{\partial}{\partial z}\left[\frac{\partial^{m-1}\vec{Q}}{\partial z^{m-1}}\right], \qquad \text{(IV-34a)}$$

so

$$\frac{\partial \vec{Q}}{\partial z} = \mathbf{A}\vec{Q}, \qquad \text{(IV-34b)}$$

$$\frac{\partial^2 \vec{Q}}{\partial z^2} = [\mathbf{A}\,\mathbf{A} + \frac{\partial \mathbf{A}}{\partial z}]\vec{Q}, \qquad \text{(IV-34c)}$$

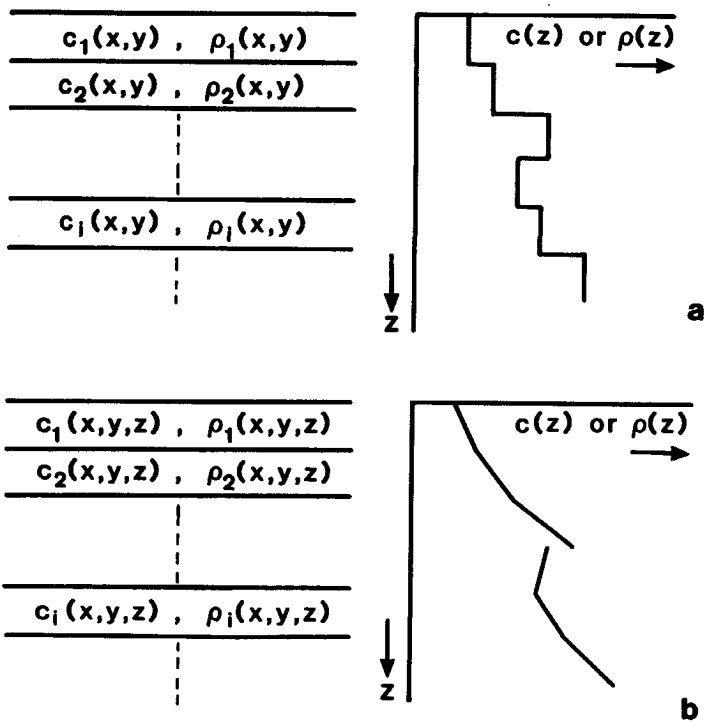

Figure IV-6: Computationally convenient acoustic subsurface models with thin inhomogeneous layers.

a. c and ρ constant in depth per layer.

b. c and ρ linearized in depth per layer.

$$\frac{\partial^3 \vec{Q}}{\partial z^3} = [\mathbf{A}\mathbf{A}\mathbf{A} + 2\frac{\partial \mathbf{A}}{\partial z}\mathbf{A} + \mathbf{A}\frac{\partial \mathbf{A}}{\partial z} + \frac{\partial^2 \mathbf{A}}{\partial z^2}]\vec{Q}, \qquad \text{(IV-34d)}$$

etc.

As in the previous section, we assume linearized medium parameters in the z-direction. This means that sufficiently small layers should be taken (see Figure IV-6b). For this situation the scheme is worked out in Appendix E. In this section we only show the principle, assuming the medium parameters are constant in depth, that is, $c=c(x,y)$ and $\rho=\rho(x,y)$ within each layer (see Figure IV-6a). In this case all derivatives of operator $\mathbf{A}$ with respect to z vanish, so relation (IV-33) can be written as

$$\vec{Q}(z) = \sum_{m=o}^{\infty} \frac{\Delta z^m}{m!} \mathbf{A}^m \vec{Q}(z_o). \qquad \text{(IV-35)}$$

This relation can be rewritten as

$$\vec{Q}(z) = \sum_{n=o}^{\infty} \left[\frac{\Delta z^{2n}}{(2n)!}\mathbf{A}^{2n} + \frac{\Delta z^{2n+1}}{(2n+1)!}\mathbf{A}^{2n+1}\right]\vec{Q}(z_o), \qquad \text{(IV-36a)}$$

where

$$\mathbf{A}^{2n} = (-1)^n \begin{bmatrix} H_{2n}^* & o \\ o & \frac{1}{\rho}H_{2n}^*\rho H_o^* \end{bmatrix}, \qquad \text{(IV-36b)}$$

$$\mathbf{A}^{2n+1} = (-1)^n \begin{bmatrix} o & H_{2n}^*\rho H_o^* \\ -\frac{1}{\rho}H_{2n+2}^* & o \end{bmatrix}, \qquad \text{(IV-36c)}$$

with H_{2n+2} recursively defined by

$$H_{2n+2} = H_2 * H_{2n}, \qquad \text{(IV-36d)}$$

$$H_{2n} = H_2 * H_{2n-2}, \qquad \text{(IV-36e)}$$

etc. and

$$H_o = d_o(x,y) = \delta(x)\delta(y). \qquad \text{(IV-36f)}$$

Notice that relation (IV-36) can be written as

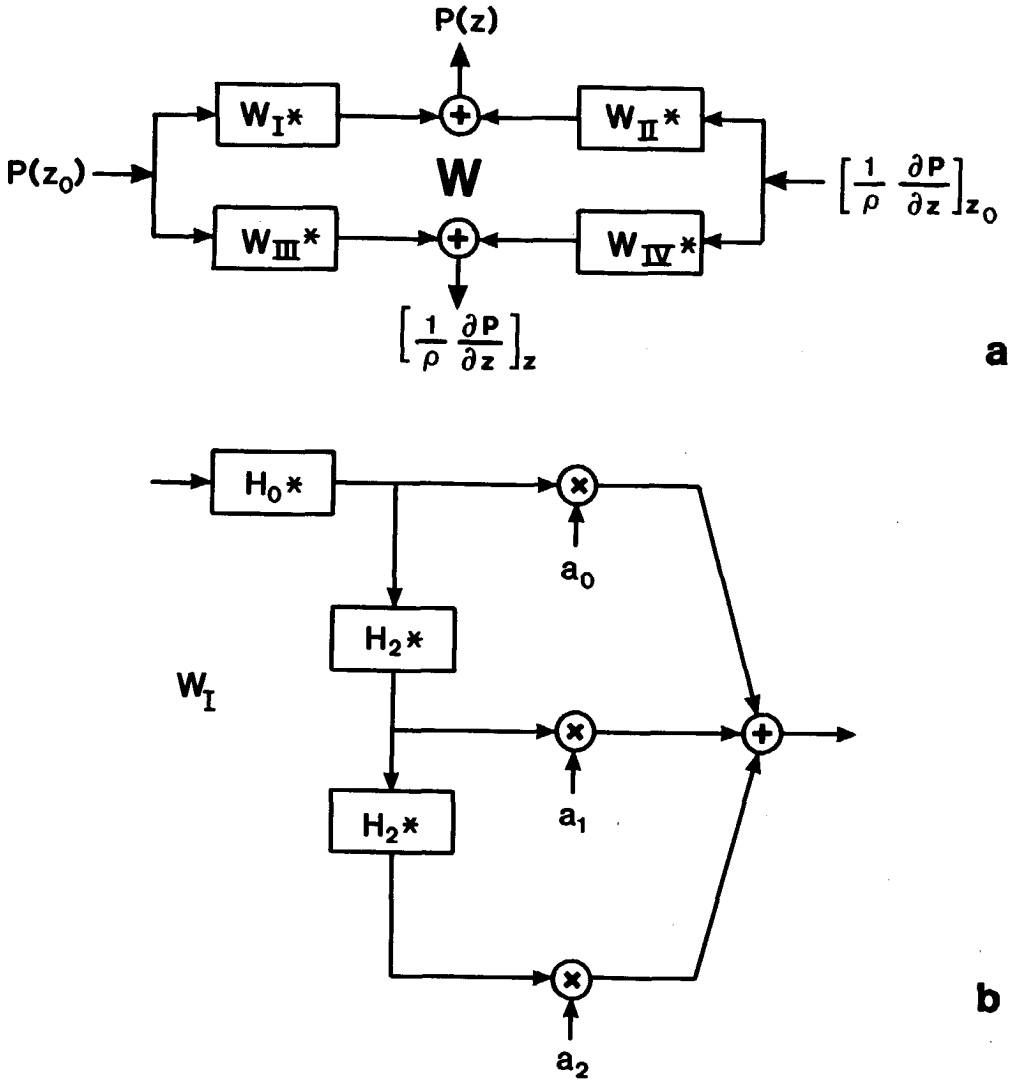

Figure IV-7: a. Two-way wave field extrapolation scheme.

b. Detailed diagram of the second order approximation of sub-operator W_I. For operators W_{II}, W_{III}, W_{IV}, operator H_o should be replaced by ρH_o, H_2, ρH_o respectively, while coefficients a_n should be replaced by b_n, $-b_n/\rho$, a_n/ρ respectively.

$$\vec{Q}(z) = \mathbf{W}(z,z_o)\vec{Q}(z_o), \qquad \text{(IV-37a)}$$

where

$$\mathbf{W}(z,z_o) = \begin{bmatrix} W_I(z,z_o)^* & W_{II}(z,z_o)^* \\ W_{III}(z,z_o)^* & W_{IV}(z,z_o)^* \end{bmatrix}, \qquad \text{(IV-37b)}$$

with

$$W_I(z,z_o) = \sum_{n=o}^{\infty} a_n H_{2n}, \qquad a_n = \frac{\Delta z^{2n}}{(2n)!}(-1)^n, \qquad \text{(IV-37c,d)}$$

$$W_{II}(z,z_o) = \sum_{n=o}^{\infty} b_n H_{2n}^* \rho H_o, \quad b_n = \frac{\Delta z^{2n+1}}{(2n+1)!}(-1)^n, \qquad \text{(IV-37e,f)}$$

$$W_{III}(z,z_o) = \sum_{n=o}^{\infty} -b_n \frac{1}{\rho} H_{2n+2}, \qquad \text{(IV-37g)}$$

$$W_{IV}(z,z_o) = \sum_{n=o}^{\infty} a_n \frac{1}{\rho} H_{2n}^* \rho H_o. \qquad \text{(IV-37h)}$$

For two-dimensional as well as three-dimensional applications, relation (IV-37) describes an explicit finite-difference two-way wave field extrapolation operator in the space-frequency domain, based on **one-dimensional** convolutions. The extrapolation scheme is shown in diagram in Figure IV-7.

In the special situation that c and ρ are constant in one layer, extrapolation may be carried out in the wavenumber-frequency domain, so H_{2n} may be replaced by $\tilde{H}_2^n$, with $\tilde{H}_2$ given by relation (IV-14d). Now the infinite series in (IV-37) can be summed to closed expressions, yielding operators (IV-21b,c,d,e).

Summarizing, in this section we derived a two-way wave field extrapolation operator for inhomogeneous media, assuming that in each layer the medium properties are constant in depth (see Figure IV-6a). Since no approximations were made, the operator (IV-37b) is exact. Of course, for practical applications this formal operator should be truncated. This is discussed in the following sections. In Appendix E we generalized the operator assuming that in each layer the medium properties may be linearized in depth (see Figure IV-6b) as described by (E-2). Operator (E-5b) takes properly into account sub-critical as well as critical angle events.

IV.5 A FAST CONVERGING TWO-WAY EXTRAPOLATION SCHEME FOR ARBITRARILY INHOMOGENEOUS MEDIA

In the previous section we have seen that one of the sub-errors in wave field extrapolation by means of Taylor series summation vanishes when the scheme is based on the two-way wave equation, since the z-derivatives of the total wave field can be calculated exactly within the seismic bandwidth. However, significant errors may arise in practice due to the truncation of the Taylor series, particularly for horizontal plane waves. For one-way wave field extrapolation, Claerbout (1976) introduced a floating time reference in order to improve the convergence speed. This actually means that the horizontal plane-wave phase-shift operator $\exp(-jk\Delta z)$ is kept out of the Taylor series expansion (Berkhout, 1982). In two-way wave field extrapolation the floating time reference concept cannot be followed, because downgoing and upgoing waves are considered simultaneously (see Figure IV-2). Instead we rearrange the Taylor series expansion such that the two-way horizontal plane-wave extrapolation operator can be kept out of the Taylor series expansion. In this section we only show the principle, assuming that c and ρ are constant in depth within each layer (see Figure IV-6a). In Appendix F we consider the case that c and ρ are linear functions of depth within each layer (see Figure IV-6b).

Assuming that the lateral derivatives of the medium parameters may be neglected, operator (IV-37b) can be written as

$$\mathbf{W}(z,z_o) = \sum_{n=o}^{\infty} \left[(\mathbf{E}_n + \mathbf{A}\,\mathbf{F}_n)\mathbf{H}_2^n \right], \qquad \text{(IV-38a)}$$

where

$$\mathbf{E}_n = \begin{bmatrix} a_n & o \\ o & a_n \end{bmatrix}, \quad \mathbf{F}_n = \begin{bmatrix} b_n & o \\ o & b_n \end{bmatrix}, \quad \mathbf{H}_2^n = \begin{bmatrix} H_{2n}^* & o \\ o & H_{2n}^* \end{bmatrix}, \qquad \text{(IV-38b,c,d)}$$

and $\mathbf{A}$ defined by (IV-2b). Applying a binomial expansion for $\mathbf{H}_2^n$ we may write

$$\mathbf{H}_2^n = (\mathbf{K} + \mathbf{D}_2)^n = \sum_{m=o}^{n} \left[\frac{1}{m!} \left(\frac{\partial^m}{\partial K^m} \mathbf{K}^n \right) \mathbf{D}_2^m \right], \qquad \text{(IV-39a)}$$

where

$$\mathbf{K} = \begin{bmatrix} \kappa & o \\ o & \kappa \end{bmatrix}, \quad \mathbf{D}_2 = \begin{bmatrix} D_2^* & o \\ o & D_2^* \end{bmatrix}, \tag{IV-39b,c}$$

$$\kappa = k^2, \quad D_2 = d_2(x) + d_2(y). \tag{IV-39d,e}$$

Substituting (IV-39a) in (IV-38a), changing the order of summations, and using the property $\partial_\kappa^m \kappa^n = o$ for $m > n$, yields

$$\mathbf{W}(z,z_o) = \sum_{m=o}^{\infty} \left[\frac{1}{m!} \left\{ \frac{\partial^m}{\partial \kappa^m} \mathbf{M} + \mathbf{A} \frac{\partial^m}{\partial \kappa^m} \mathbf{N} \right\} \mathbf{D}_2^m \right], \tag{IV-40a}$$

where

$$\mathbf{M} = \sum_{n=o}^{\infty} \left[\mathbf{E}_n \mathbf{K}^n \right], \quad \mathbf{N} = \sum_{n=o}^{\infty} \left[\mathbf{F}_n \mathbf{K}^n \right]. \tag{IV-40b,c}$$

Sofar we did nothing but rewriting operator $\mathbf{W}(z,z_o)$, assuming the lateral derivatives of the medium parameters may be neglected. In our next step, however, we replace the infinite series (IV-40b,c) by closed expressions, according to

$$\mathbf{M} = \begin{bmatrix} W_{I,o} & o \\ o & W_{I,o} \end{bmatrix}, \quad \mathbf{N} = \frac{1}{\rho} \begin{bmatrix} W_{II,o} & o \\ o & W_{II,o} \end{bmatrix}, \tag{IV-41a,b}$$

where

$$W_{I,o} = \cos(k\Delta z), \quad W_{II,o} = \frac{\rho}{k} \sin(k\Delta z). \tag{IV-41c,d}$$

Notice that $W_{I,o}$ and $W_{II,o}$ equal the operators $\tilde{W}_I$ and $\tilde{W}_{II}$, respectively, given by relations (IV-21b,c), for a horizontal plane-wave, that is, for $k_x^2 = k_y^2 = o$.

By substituting relation (IV-41) in relation (IV-40), it follows that operator $\mathbf{W}(z,z_o)$ is given by

$$\mathbf{W}(z,z_o) = \begin{bmatrix} W_I(z,z_o)^* & W_{II}(z,z_o)^* \\ W_{III}(z,z_o)^* & W_{IV}(z,z_o)^* \end{bmatrix}, \tag{IV-42a}$$

where

$$W_I(z,z_o) = \sum_{m=o}^{\infty} \alpha_m D_{2m}, \qquad \text{(IV-42b)}$$

$$W_{II}(z,z_o) = \sum_{m=o}^{\infty} \beta_m D_{2m}, \qquad \text{(IV-42c)}$$

$$W_{III}(z,z_o) = Z_2 * W_{II}(z,z_o), \qquad \text{(IV-42d)}$$

$$W_{IV}(z,z_o) = \sum_{m=o}^{\infty} \gamma_m D_{2m}, \qquad \text{(IV-42e)}$$

with

$$\alpha_m = \frac{1}{m!}\left(\frac{\partial^m}{\partial \kappa^m} W_{I,o}\right), \qquad \text{(IV-42f)}$$

$$\beta_m = \frac{1}{m!}\left(\frac{\partial^m}{\partial \kappa^m} W_{II,o}\right), \qquad \text{(IV-42g)}$$

$$\gamma_m = \alpha_m, \qquad \text{(IV-42h)}$$

$$Z_2 = -\frac{1}{\rho^2} H_2, \qquad \text{(IV-42i)}$$

and D_{2m} defined recursively by

$$D_{2m} = D_2 * D_{2m-2}, \qquad \text{(IV-42j)}$$

$$D_{2m-2} = D_2 * D_{2m-4}, \qquad \text{(IV-42k)}$$

etc. and

$$D_o = d_o(x,y) = \delta(x)\delta(y). \qquad \text{(IV-42l)}$$

For two-dimensional as well as three-dimensional applications, relation (IV-42) describes an explicit finite-difference two-way wave field extrapolation scheme based on one-dimensional convolutions. Operator D_{2m} represents space invariant spatial convolutions for all m, while α_m, β_m and γ_m represent space dependent coefficients:

$$\alpha_o = \gamma_o = \cos(k\Delta z), \quad \alpha_1 = \gamma_1 = -\frac{\Delta z}{2k}\sin(k\Delta z), \text{ etc.,} \qquad \text{(IV-43a,b)}$$

$$\beta_o = \frac{\rho}{k}\sin(k\Delta z), \quad \beta_1 = -\frac{\rho}{2k^3}[\sin(k\Delta z) - (k\Delta z)\cos(k\Delta z)], \qquad \text{(IV-43c,d)}$$

etc., with

$$k = \omega/c(x,y), \quad \rho = \rho(x,y). \qquad \text{(IV-43e,f)}$$

In practice only a finite number of terms can be used. We define the M'th order approximation of $\mathbf{W}(z,z_o)$ by

$$\mathbf{W}_M(z,z_o) = \begin{bmatrix} W_{I,M}(z,z_o)^* & W_{II,M}(z,z_o)^* \\ W_{III,M}(z,z_o)^* & W_{IV,M}(z,z_o)^* \end{bmatrix}, \qquad \text{(IV-44a)}$$

where

$$W_{I,M}(z,z_o) = \sum_{m=o}^{M} \alpha_m D_{2m} \qquad \text{(IV-44b)}$$

$$W_{II,M}(z,z_o) = \sum_{m=o}^{M} \beta_m D_{2m}, \qquad \text{(IV-44c)}$$

$$W_{III,M}(z,z_o) = Z_2 * W_{II,M}(z,z_o), \qquad \text{(IV-44d)}$$

$$W_{IV,M}(z,z_o) = \sum_{m=o}^{M} \gamma_m D_{2m}. \qquad \text{(IV-44e)}$$

Notice that for a horizontal plane-wave all lateral derivatives are zero, which means that the zeroth order scheme (M=o) already converges for this situation. We may conclude that the zeroth order terms represent the 'floating time reference for the two-way wave equation'.

Accuracy and stability properties for various orders are studied in the next section. The first order extrapolation scheme is shown in diagram in Figure IV-8. Notice that the operator D_2 is used efficiently in two sub-operators.

Summarizing, in this section we derived a fast converging two-way wave field extrapolation operator for inhomogeneous media, assuming that the medium parameters are constant in depth for each layer (see Figure IV-6a). In the derivation we assumed that the lateral **derivatives** of the medium parameters may be neglected. In Appendix F we generalized the operator, assuming that the medium parameters for each layer may be linearized in depth (see Figure IV-6b), as described by (E-2). Operator (F-5) is comparable to operator (IV-42); only Z_2 and the coefficients α_m, β_m and γ_m are defined differently. These coefficients are based on operators $\tilde{\psi}_1$, $\tilde{\psi}_2$ and $\tilde{\psi}_3$, given by relations (IV-25i,j,k), for $k_x^2=k_y^2=o$, and their derivatives with respect to κ. Operator (F-5) takes properly into account sub-critical as well as critical angle

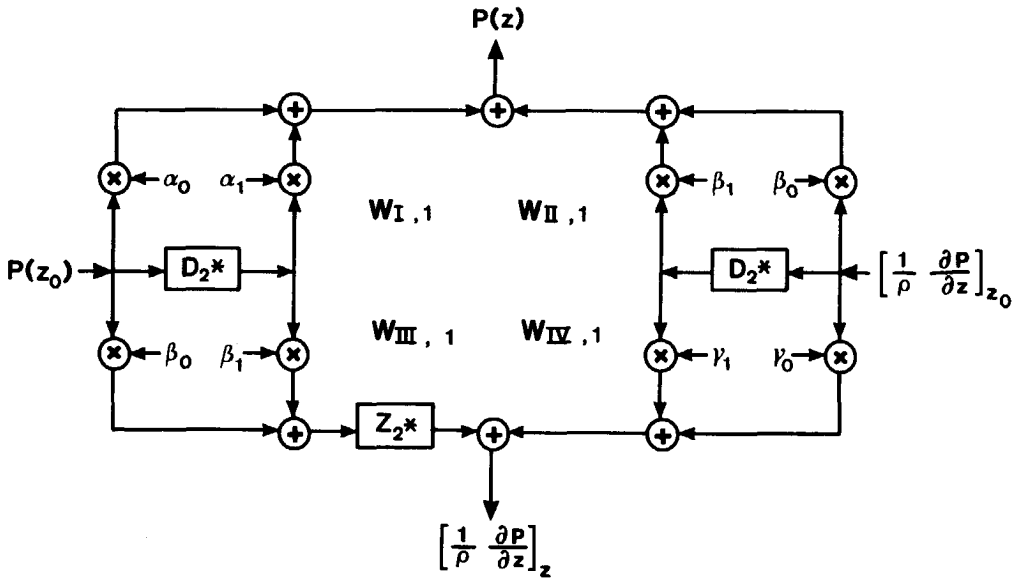

Figure IV-8: First order approximation of the fast converging two-way wave field extrapolation scheme for sub-critical as well as critical angle events.

events. Hence, the diagram in Figure IV-8 represents the first order approximation of the two-way wave field extrapolation scheme for sub-critical as well as critical angle events.

Finally, we present a two-term operator $W_M^{(2)}(z,z_0)$. Therefore we define a computational model as shown in Figure IV-9. In each layer the medium parameters c(x,y,z) and ρ(x,y,z) are written as the sum of homogeneous **reference**

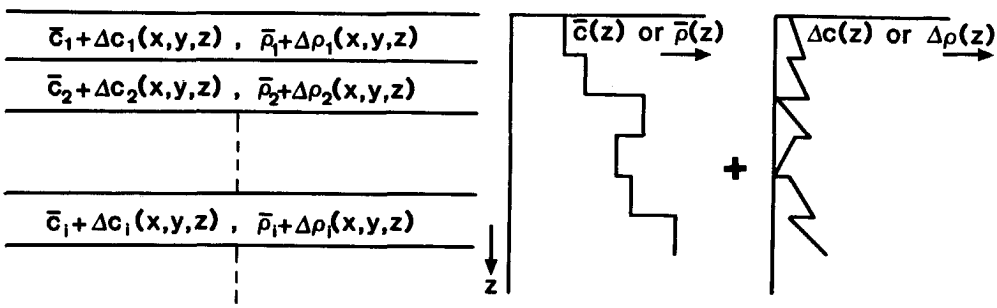

Figure IV-9: Computationally convenient subsurface model with inhomogeneous layers, used for the two-term operator.

parameters $\bar{c}$ and $\bar{\rho}$, and inhomogeneous **deviation** parameters $\Delta c(x,y,z)$ and $\Delta\rho(x,y,z)$. Notice that for migration applications the reference parameters and the deviation parameters **together** define the acoustic macro subsurface model. For this computational model, the two-term operator $\mathbf{W}_M^{(2)}(z,z_o)$ is defined as follows

$$\mathbf{W}_M^{(2)}(z,z_o) = \begin{bmatrix} W_{I,M}^{(2)}(z,z_o)^* & W_{II,M}^{(2)}(z,z_o)^* \\ W_{III,M}^{(2)}(z,z_o)^* & W_{IV,M}^{(2)}(z,z_o)^* \end{bmatrix}, \qquad \text{(IV-45a)}$$

where

$$W_{I,M}^{(2)}(z,z_o) = \bar{W}_I(z,z_o) + \Delta W_{I,M}(z,z_o), \qquad \text{(IV-45b)}$$

$$W_{II,M}^{(2)}(z,z_o) = \bar{W}_{II}(z,z_o) + \Delta W_{II,M}(z,z_o), \qquad \text{(IV-45c)}$$

$$W_{III,M}^{(2)}(z,z_o) = Z_2 * W_{II,M}^{(2)}(z,z_o), \qquad \text{(IV-45d)}$$

$$W_{IV,M}^{(2)}(z,z_o) = \bar{W}_{IV}(z,z_o) + \Delta W_{IV,M}(z,z_o). \qquad \text{(IV-45e)}$$

Operator Z_2 is defined by (F-1ℓ). The operators $\bar{W}_I$, $\bar{W}_{II}$ and $\bar{W}_{IV}$ describe two-way wave field extrapolation in the homogeneous reference layer. They should preferably be applied in the wavenumber-frequency domain. The double spatial Fourier transforms of these operators are given by relations (IV-21b,c,e), where c and ρ should be replaced by $\bar{c}$ and $\bar{\rho}$. The operators $\Delta W_{I,M}$, $\Delta W_{II,M}$ and $\Delta W_{IV,M}$ take into account the two-way propagation effects due to the deviation parameters. They are defined as follows

$$\Delta W_{I,M}(z,z_o) = \sum_{m=o}^{M} \Delta\alpha_m D_{2m}, \quad \Delta\alpha_m = \alpha_m - \bar{\alpha}_m, \qquad \text{(IV-46a,b)}$$

$$\Delta W_{II,M}(z,z_o) = \sum_{m=o}^{M} \Delta\beta_m D_{2m}, \quad \Delta\beta_m = \beta_m - \bar{\beta}_m, \qquad \text{(IV-46c,d)}$$

$$\Delta W_{IV,M}(z,z_o) = \sum_{m=o}^{M} \Delta\gamma_m D_{2m}, \quad \Delta\gamma_m = \gamma_m - \bar{\gamma}_m, \qquad \text{(IV-46e,f)}$$

where α_m, β_m and γ_m are defined by (F-5f,g,h) and where $\bar{\alpha}_m$, $\bar{\beta}_m$ and $\bar{\gamma}_m$ are defined by (IV-42f,g,h), with c and ρ replaced by $\bar{c}$ and $\bar{\rho}$.

A Born-type two-term wave field extrapolation operator was discussed by Kennett (1972). In his approach the deviation term describes the effects of a moderate inhomogeneity (10 per cent contrast with the surrounding medium) of small

lateral and vertical extent. For comparison, in two-term operator (IV-45) no assumptions are made with respect to the dimensions of the contrast. It is shown in the next section that the first oder scheme (M=1) converges for sub-critical as well as critical angle events, even when the contrast $\Delta c/\bar{c}$ is in the order of 25 per cent in the whole layer.

IV.6 ACCURACY AND STABILITY OF TWO-WAY EXTRAPOLATION

In this section we discuss the accuracy and stability properties of the M'th order finite-difference operators $\mathbf{W}_M(z,z_o)$ and $\mathbf{W}_M^{(2)}(z,z_o)$, given by relations (IV-44) and (IV-45), respectively, as a function of the propagation angle. Therefore it is convenient if we assume that c and ρ are functions of z only. First we consider operator $\mathbf{W}_M(z,z_o)$, in the wavenumber-frequency domain given by

$$\tilde{\mathbf{W}}_M(z,z_o) = \begin{bmatrix} \tilde{W}_{I,M}(z,z_o) & \tilde{W}_{II,M}(z,z_o) \\ \tilde{W}_{III,M}(z,z_o) & \tilde{W}_{IV,M}(z,z_o) \end{bmatrix}, \qquad \text{(IV-47a)}$$

where

$$\tilde{W}_{I,M}(z,z_o) = \sum_{m=o}^{M} \alpha_m \tilde{D}_2^m, \qquad \text{(IV-47b)}$$

$$\tilde{W}_{II,M}(z,z_o) = \sum_{m=o}^{M} \beta_m \tilde{D}_2^m, \qquad \text{(IV-47c)}$$

$$\tilde{W}_{III,M}(z,z_o) = \tilde{Z}_2 \tilde{W}_{II,M}(z,z_o), \qquad \text{(IV-47d)}$$

$$\tilde{W}_{IV,M}(z,z_o) = \sum_{m=o}^{M} \gamma_m \tilde{D}_2^m, \qquad \text{(IV-47e)}$$

$$\tilde{D}_2^m = (-k_x^2 - k_y^2)^m, \qquad \text{(IV-47f)}$$

with α_m, β_m and γ_m given by (F-5f,g,h) and $\tilde{Z}_2$ given by (IV-25f). Notice that

$$\lim_{M\to\infty} \tilde{\mathbf{W}}_M(z,z_o) = \tilde{\mathbf{W}}(z,z_o), \qquad \text{(IV-48)}$$

with $\tilde{\mathbf{W}}(z,z_o)$ given by (IV-25). In the following analysis, we compare the eigenvalues $\tilde{\mu}_M$ of $\tilde{\mathbf{W}}_M(z,z_o)$ with the eigenvalues $\tilde{\mu}$ of operator $\tilde{\mathbf{W}}(z,z_o)$:

$$\tilde{\mu}^{+}_{M} = \tfrac{1}{2}(\tilde{W}_{I,M}+\tilde{W}_{IV,M}) \mp j\sqrt{\det(\tilde{\mathbf{W}}_{M}) - \tfrac{1}{2}(\tilde{W}_{I,M}+\tilde{W}_{IV,M})^{2}}, \qquad \text{(IV-49a)}$$

$$\tilde{\mu}^{+}_{-} = \tfrac{1}{2}(\tilde{W}_{I} + \tilde{W}_{IV}) \mp j\sqrt{1 - \tfrac{1}{2}(\tilde{W}_{I} + \tilde{W}_{IV})^{2}}. \qquad \text{(IV-49b)}$$

Notice that $\tilde{\mu}^{+}_{M}\tilde{\mu}^{-}_{M} = \det(\tilde{\mathbf{W}}_{M})$ and $\tilde{\mu}^{+}\tilde{\mu}^{-} = 1$.
The angle dependent amplitude and phase errors we define as

$$\Delta\tilde{A} = \sqrt{\det(\tilde{\mathbf{W}}_{M})} - 1, \qquad \text{(IV-50a)}$$

$$\Delta\tilde{\Phi} = \pm[\arg(\tilde{\mu}^{+}_{M}) - \arg(\tilde{\mu}^{+}_{-})]. \qquad \text{(IV-50b)}$$

In order to specify the threshold values for these errors, we consider a homogeneous medium. Notice that in this case the eigenvalues of the exact operator, given by relation (IV-49b), simplify to

$$\tilde{\mu}^{+}_{-} = \exp[\mp j\tilde{H}_{1}\Delta z], \qquad \text{(IV-51)}$$

which is equivalent to the **phase-shift operator** for one-way wave field extrapolation. In recursive extrapolation, the total amplitude and phase errors after N extrapolation steps in a homogeneous medium read

$$\Delta\tilde{A}_{tot} = (1+\Delta\tilde{A})^{N} - 1 \approx N\Delta\tilde{A}, \qquad \text{(IV-52a)}$$

$$\Delta\tilde{\Phi}_{tot} = N\Delta\tilde{\Phi}. \qquad \text{(IV-52b)}$$

We define the following (arbitrary) accuracy criteria:

> At an extrapolation depth of $N\Delta z = 50\lambda$ the absolute amplitude error $N\Delta\tilde{A}$ should be smaller than 3 dB and the absolute phase error $N\Delta\tilde{\Phi}$ should be smaller than $\pi/10$.

Here $\Delta z = z - z_{o} > o$, while λ represents the wave length. Since $N = 100\pi/(k\Delta z)$, the **accuracy** criteria read

$$|\Delta\tilde{A}|/(k\Delta z) \leq 0.001, \qquad \text{(IV-53a)}$$

$$|\Delta\tilde{\Phi}|/(k\Delta z) \leq 0.001. \qquad \text{(IV-53b)}$$

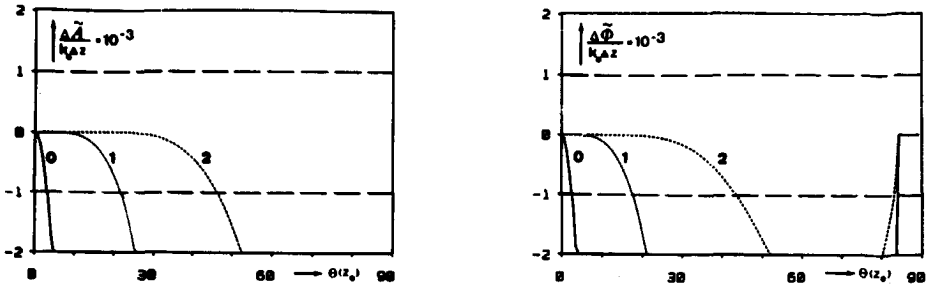

Figure IV-10: Error curves for the zeroth, first and second order finite difference two-way wave field extrapolation operator, with $k_o\Delta z = \pi/2$, $q\Delta z = 0.01$, $r\Delta z = 0$.

These requirements cannot always be met for all propagation angles. To avoid that the solution grows out of bounds, our **stability** criterion reads

$$\Delta\tilde{A}/(k\Delta z) \leq 0.001 \text{ for all propagation angles.} \qquad \text{(IV-53c)}$$

We adopt these criteria for the inhomogeneous situation. In this case k should be replaced by $k_o = k(z_o)$.
In Figure IV-10 the scaled amplitude and phase errors are shown as a function of θ, with

$$\sin^2\theta = (k_x^2 + k_y^2)/k^2(z_o). \qquad \text{(IV-54)}$$

Notice that θ represents the propagation angle at depth z_o, so $\theta=\theta(z_o)$. The extrapolation stepsize Δz equals $\lambda/4$, so $k_o\Delta z=\pi/2$. The parameter q (see relation (IV-24)) is chosen such that $q\Delta z=.01$, which means that the velocity at extrapolation depth $z_o+25\lambda$ equals twice the velocity at depth z_o (assuming the velocity function is linear also outside the considered depth interval Δz). The density is chosen constant, so r=o. Notice that thin layer condition (IV-24c,d) is satisfied. From Figure IV-10 we observe that the first order operator $\tilde{\mathbf{W}}_1$ is accurate upto 20° and that the second order operator $\tilde{\mathbf{W}}_2$ is accurate upto 45°. Notice that all operators are stable. For a proper incorporation of critical angle events ($\theta\to 90°$), higher order schemes are required, which is not very attractive from a computational point of view. Therefore we consider also the two-term operator $\tilde{\mathbf{W}}_M^{(2)}$. Similarly as above we can define the eigenvalues $\tilde{\mu}_M^{(2)}$ of the two-term operator in the wavenumber-frequency domain. The amplitude and phase errors for one extrapolation step we define as

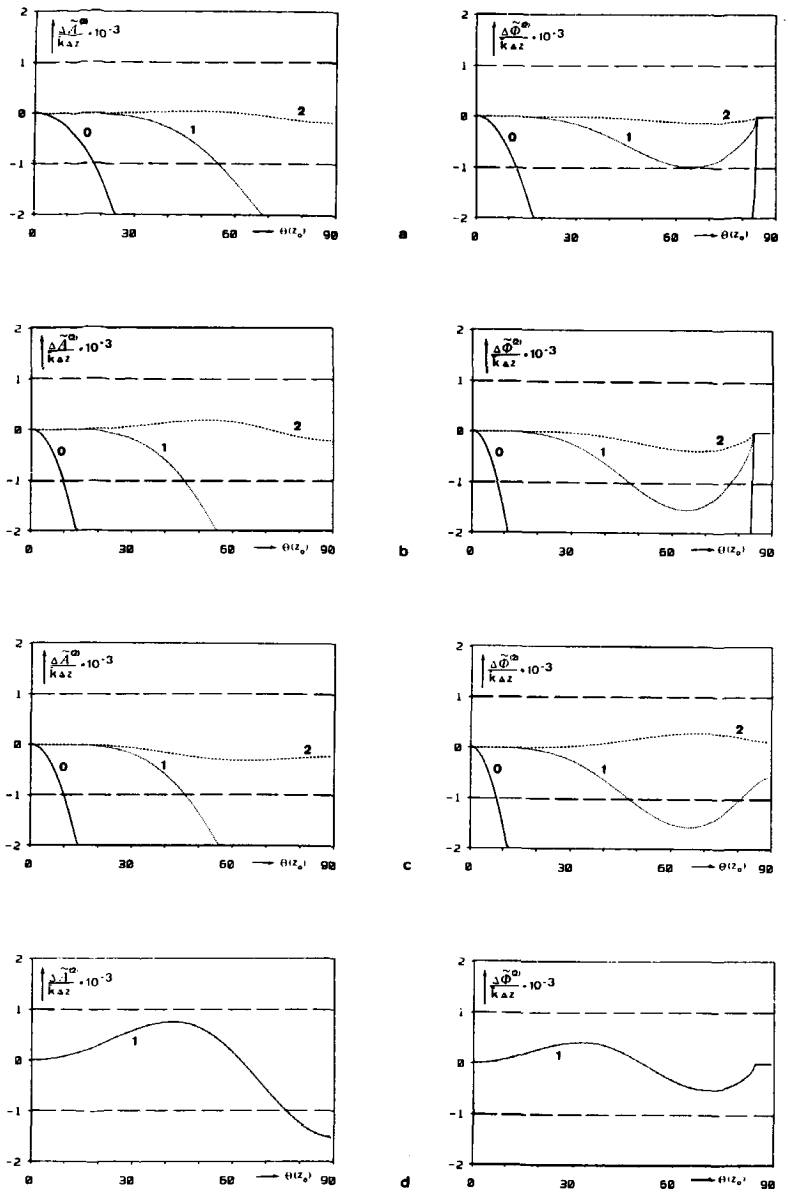

Figure IV-11: Error curves for the zeroth, first and second order finite difference two-term two-way wave field extrapolation operator, with $\bar{k}\Delta z = \pi/2$, $\rho(z_o) = \bar{\rho}$ and $r\Delta z = o$.

a. $[c(z_o) - \bar{c}]/\bar{c} = .05$, $q\Delta z = .01$.

b. $[c(z_o) - \bar{c}]/\bar{c} = .25$, $q\Delta z = .01$.

c. $[c(z_o) - \bar{c}]/\bar{c} = .25$, $q\Delta z = -.01$.

d. As in b, improved first order scheme, $\theta_1(z_o) = 60°$.

$$\Delta\tilde{A}^{(2)} = \sqrt{\det(\tilde{W}_M^{(2)})} - 1, \qquad \text{(IV-55a)}$$

$$\Delta\tilde{\Phi}^{(2)} = \pm\,[\arg(\tilde{\mu}_M^{(2)\pm}) - \arg(\tilde{\mu}^{\pm})]. \qquad \text{(IV-55b)}$$

In Figure IV-11 the scaled amplitude and phase errors are shown as a function of $\theta(z_o)$. In all examples Δz is chosen such that $\bar{k}\Delta z=\pi/2$, where $\bar{k}=\omega/\bar{c}$. Furthermore, $\rho(z_o)=\bar{\rho}$ and r=o. In Figure IV-11a the true velocity is chosen close to the reference velocity, according to $[c(z_o)-\bar{c}]/\bar{c}=.05$ and $q\Delta z=.01$. Notice that the first order two-term operator is accurate upto 55° and that the second order operator is accurate upto 90°. All operators are stable. For angles higher than 82° a turning point is present within the considered depth interval Δz. This accounts for the phase behaviour at high angles ($\theta\to 90°$), where the eigenvalues become purely real. (For comparison, the phase-shift operator for one-way wave field extrapolation becomes real for evanescent waves). In Figure IV-11b the true velocity differs significantly from the reference velocity, according to $[c(z_o)-\bar{c}]/\bar{c}=.25$, $q\Delta z=.01$. Notice that the first order operator is accurate upto 45° and that the second order operator is accurate upto 90°. All operators are stable. In Figure IV-11c, a decreasing velocity is chosen, according to $[c(z_o)-\bar{c}]/\bar{c}=.25$ and $q\Delta z=-.01$. The error curves are comparable with Figure IV-11b. Notice that no turning point is present within the considered depth interval Δz. In Figure IV-11d the same example is chosen as in Figure IV-11b, however, the operator D_4 is approximated by $-[k^2(z_o)\sin^2\theta_1(z_o)]D_2$ with $\theta_1(z_o)=60°$. This means that the second order scheme has been simplified to a first order scheme, without loss of accuracy at 60°. Notice that this improved first order scheme is accurate and stable upto 90°.

Summarizing, we formulated accuracy and stability conditions for the finite-difference approximation of the eigenvalues of the two-way wave field extrapolation operator. In the examples we studied the error curves for various orders, assuming a depth dependent velocity function. Since density variations do not account for critical angle events, the density was kept constant in all examples. From the examples it may be concluded that the finite-difference approximations are stable and that critical angle events are properly taken into account. Particularly the improved first order two-term operator is very attractive from a computational point of view. Notice that the analysis has

been performed in the wavenumber-frequency domain. It is assumed that the investigated accuracy and stability properties apply locally in a laterally varying medium.

IV.7 PRE-STACK MODELING SCHEME BASED ON THE ACOUSTIC TWO-WAY WAVE EQUATION

In chapter III we have seen that one-way wave equation modeling schemes are based on the simplified model

$$S^+ \rightarrow W^+ \rightarrow R \rightarrow W^- \rightarrow D \rightarrow P^-_{CSP}. \qquad \text{(IV-56)}$$

Also we discussed an extension of this model for the incorporation of critical angle events, according to

$$S^+ \rightarrow W^+ \rightarrow R \rightarrow W^- \rightarrow D \rightarrow P^-_{CSP}. \qquad \text{(IV-57)}$$

In this chapter (chapter IV) we discussed the two-way approach to wave field extrapolation, which is schematically represented by

$$\begin{bmatrix} P \\ \frac{1}{\rho}\frac{\partial P}{\partial z} \end{bmatrix}_{z_i} \rightarrow \mathbf{W} \rightarrow \begin{bmatrix} P \\ \frac{1}{\rho}\frac{\partial P}{\partial z} \end{bmatrix}_{z_{i-1}}. \qquad \text{(IV-58)}$$

Here $[P,\rho^{-1}\partial_z P]^T$ describes the **total** wave field (downgoing and upgoing waves), while $\mathbf{W}$ describes the two-way propagation effects between two depth levels. Relation (IV-58) holds for sub-critical as well as critical angle events in 1-D, 2-D and 3-D inhomogeneous media. Because **migration** is the main subject of this thesis, we discuss two-way modeling only for simple subsurface geometries. It is obvious that relation (IV-58) is not particularly suited for modeling purposes because it requires knowledge of the total wave field at a specific depth **before** modeling. In this section we show how this paradox can be solved for 1-D inhomogeneous media. Therefore we consider a horizontally layered computational model consisting of I (1-D inhomogeneous) thin layers, as is shown in Figure IV-12. We assume homogeneous half spaces for $z<z_0$ and $z \geq z_I$. In layer i, with $z_{i-1} \leq z < z_i$, the propagation velocity and density are given by $c_i(z)$ and $\rho_i(z)$, respectively. Because we consider thin layers we assume that these functions may be linearized in z.

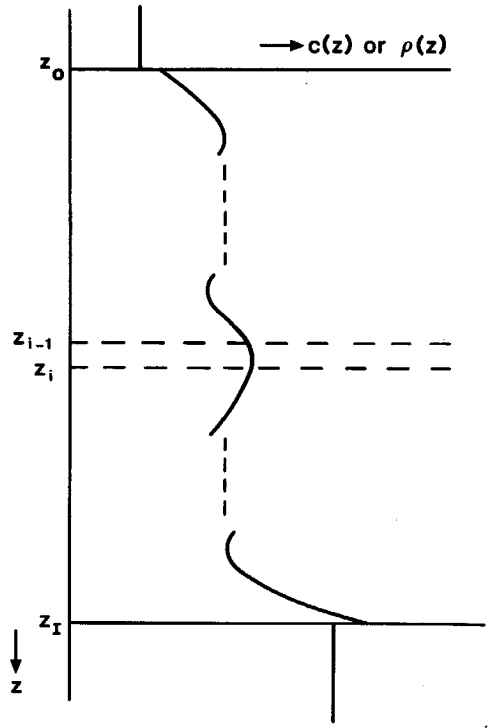

Figure IV-12: Acoustic model of the subsurface for the two-way wave equation modeling scheme which includes critical angle events.

In the wavenumber-frequency domain (k_x,k_y,ω), modeling consists of the following steps

1. Given the total field $\tilde{\tilde{Q}}(z_i)$, then **all propagation effects** for layer i can be modeled according to

$$\tilde{\tilde{Q}}(z_{i-1}) = \tilde{\tilde{W}}(z_{i-1},z_i)\tilde{\tilde{Q}}(z_i), \qquad \text{(IV-59)}$$

with $\tilde{\tilde{Q}}=[\tilde{P},\rho^{-1}\partial_z\tilde{P}]^T=[\tilde{P},-j\omega\tilde{V}_z]^T$, and $\tilde{\tilde{W}}$ being given by relation (IV-25).

Step 1, which describes the total modeling procedure for layer i, should be applied recursively, which is allowed because $\tilde{\tilde{Q}}$ is continuous for all depths.

2. The procedure (for each k_x, k_y and ω-value) starts at $z=z_I$ by specifying $\tilde{\tilde{Q}}(z_I)$, according to

$$\tilde{\underline{Q}}(z_I) = \tilde{\underline{L}}(z_I)\tilde{\underline{P}}(z_I), \qquad \text{(IV-60)}$$

with $\tilde{\underline{P}}=[\tilde{P}^+,\tilde{P}^-]^T$, and $\tilde{\underline{L}}$ being given by relation (IV-16b). Since the lower half space $z \geq z_I$ is homogeneous and source free, the upgoing wave $\tilde{P}^-(z_I)$ should be taken zero. The downgoing wave $\tilde{P}^+(z_I)$ is chosen arbitrarily.

3. When the surface $z=z_o$ has been reached, then the plane-wave (PW) impulse response can be calculated from $\tilde{\underline{Q}}(z_o)=[\tilde{P}(z_o),-j\omega\tilde{V}_z(z_o)]^T$. We consider two cases:
   i. Similar as in section III.8, we can define the impulse response $\tilde{X}(z_o)$ which describes the detected upgoing pressure wave due to an impulsive downgoing pressure source wave, according to

$$\tilde{\underline{P}}(z_o) = [\tilde{P}^+(z_o),\tilde{P}^-(z_o)]^T = \tilde{\underline{L}}^{-1}(z_o)\tilde{\underline{Q}}(z_o), \qquad \text{(IV-61a)}$$

$$\tilde{X}^{(o)}(z_o) = \tilde{P}^-(z_o)/\tilde{P}^+(z_o), \qquad \text{(IV-61b)}$$

$$\tilde{X}(z_o) = [1 - \tilde{X}^{(o)}(z_o)\tilde{R}^-(z_o)]^{-1}\tilde{X}^{(o)}(z_o), \qquad \text{(IV-61c)}$$

   where we assumed thin layer 1 to be homogeneous. Here operator $\tilde{\underline{L}}^{-1}$ is given by relation (IV-16d); operator $\tilde{R}^-(z_o)=-\tilde{R}(z_o)$ describes the reflectivity at the lower side of the surface z_o.
   ii. If z_o is a (pressure) free surface, we prefer an admittance impulse response $\tilde{Y}(z_o)$ which describes the detected total particle velocity due to an impulsive pressure source. We may simply write

$$\tilde{Y}(z_o) = \tilde{V}_z(z_o)/\tilde{P}(z_o), \qquad \text{(IV-62)}$$

   since at a free surface the total pressure is given by the source pressure only.

4. Next the source and detector properties can be included. Again we consider two cases.
   i. Similar as in section III.8 we may write for the detected upgoing pressure wave $\tilde{P}_{CSP}(z_o)$ in a common-shotpoint (CSP) gather in the wavenumber-frequency domain

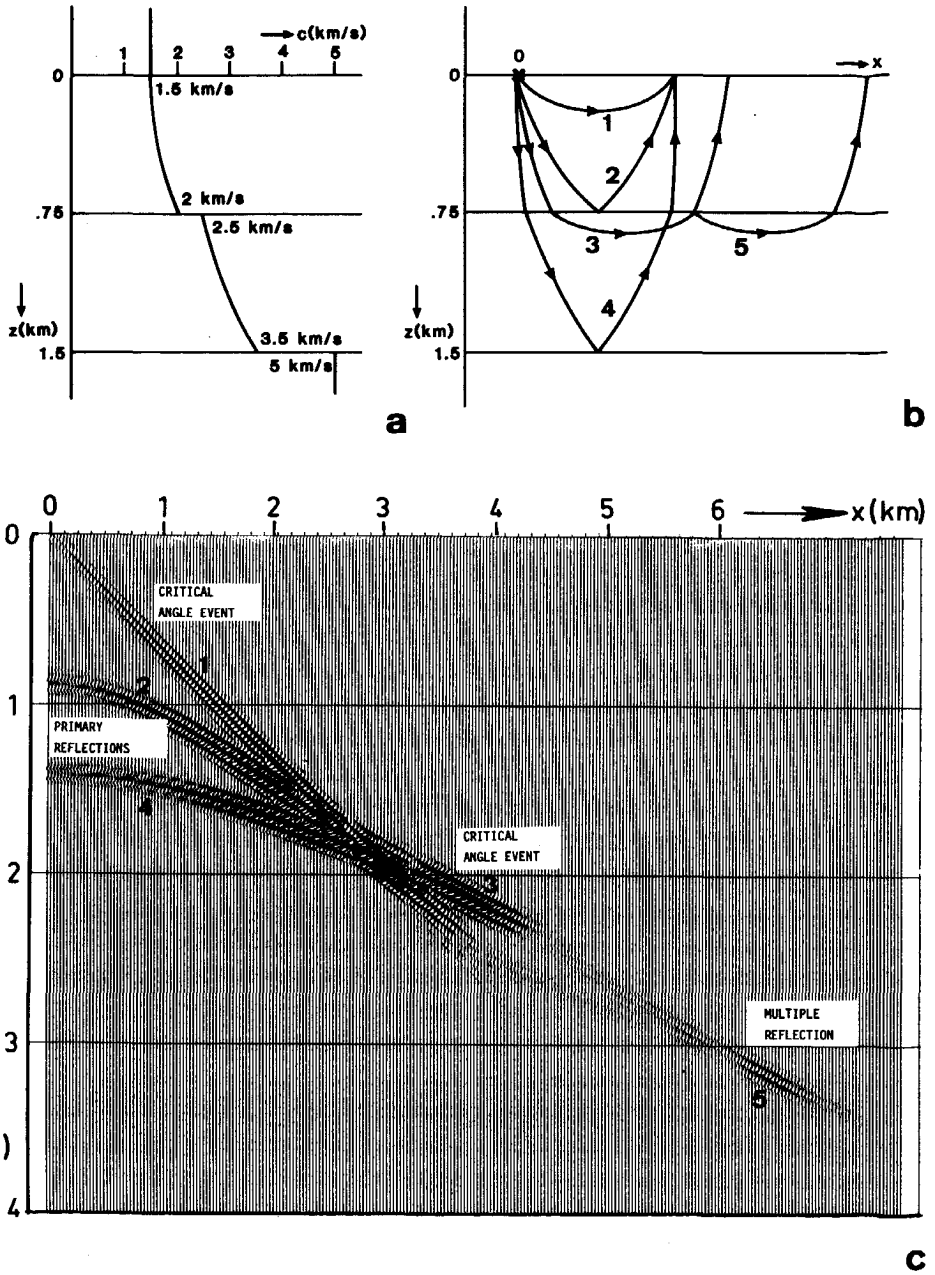

Figure IV-13: Critical angle data, modeled with the two-way wave equation.

a. Subsurface velocity model (density is constant).

b. Ray-representation of the main events.

c. CSP gather in the x,t-domain.

$$\tilde{P}^{-}_{CSP}(z_o) = \tilde{D}_P(z_o)\tilde{X}(z_o)\tilde{S}^{+}(z_o), \qquad \text{(IV-63)}$$

where $\tilde{S}^{+}(z_o)$ represents the downgoing source pressure wave and where $\tilde{D}_P(z_o)$ represents the pressure detector transfer function. Ideally, $\tilde{D}_P(z_o)$ is a function of ω only: $\tilde{D}_P(k_x,k_y,z_o,\omega) = D_P(\omega)$.

ii. For the detected particle velocity $\tilde{V}_{z,CSP}(z_o)$ in a CSP gather at a pressure free surface we may write

$$\tilde{V}_{z,CSP}(z_o) = \tilde{D}_v(z_o)\tilde{Y}(z_o)\tilde{S}(z_o), \qquad \text{(IV-64)}$$

where $\tilde{S}(z_o)$ represents the pressure source and where $\tilde{D}_v(z_o)$ represents the particle velocity detector transfer function. Ideally, $\tilde{D}_v(k_x,k_y,z_o,\omega) = D_v(\omega)$.

5. When this modeling procedure has been applied for all wavenumbers and frequencies, then the space-time data (one shot record) are obtained after inverse temporal and spatial Fourier transforms (see relations (III-3b) and (III-10b)).

Notice that in step 2 the downgoing wave $\tilde{P}^{+}(z_I)$ can be chosen arbitrarily, for example $\tilde{\vec{P}}(z_I)=[\tilde{P}^{+}(z_I),\tilde{P}^{-}(z_I)]^T=[1,0]^T$, because in step 3 the **ratios** $\tilde{P}^{-}/\tilde{P}^{+}$ or $\tilde{V}_z/\tilde{P}$ are considered.

Example.
A 2-D common-shotpoint gather was modeled for the 1-D inhomogeneous subsurface configuration shown in Figure IV-13a. Figure IV-13b shows the ray representation, while Figure IV-13c represents the CSP gather in the space-time domain (x,t). Notice that sub-critical angle events (2,4), as well as critical angle events (1,3) and multiple reflection (5) are clearly visible in Figure IV-13c. Of course more multiples are present. However, these are not visible due to their very low amplitudes.

The advantage of the scheme, introduced in this section, over the scheme introduced in section III.8, is that critical angle events, multiple reflections, transmission effects as well as evanescent energy are all included in the simple recursion algorithm (IV-59) and that arbitrary 1-D piece-wise continuously layered media can be handled (compare Figures III-7 and IV-12).

Based on the same concept, a two-way wave equation modeling scheme for **full elastic media** is presented in chapter V.

For 2-D and 3-D inhomogeneous media, modeling techniques based on two-way depth extrapolation become very complicated and two-way time extrapolation techniques are preferred (Kosloff and Baysal, 1982). An extensive discussion of modeling algorithms is beyond the scope of this thesis.

IV.8 PRE-STACK MIGRATION SCHEME BASED ON THE ACOUSTIC TWO-WAY WAVE EQUATION

Two-way wave equation migration is in principle based on inverting relation (IV-58), which is schematically represented by

$$\begin{bmatrix} P \\ \frac{1}{\rho}\frac{\partial P}{\partial z} \end{bmatrix}_{z_i} \leftarrow \mathbf{W} \leftarrow \begin{bmatrix} P \\ \frac{1}{\rho}\frac{\partial P}{\partial z} \end{bmatrix}_{z_{i-1}} . \qquad \text{(IV-65)}$$

It was argued already in section IV.1 that in two-way wave field extrapolation techniques upward and downward extrapolation are fundamentally equivalent.

i. In upward extrapolation (modeling), downgoing waves are inverse extrapolated, while upgoing waves are forward extrapolated simultaneously.

ii. In downward extrapolation (migration), downgoing waves are forward extrapolated, while upgoing waves are inverse extrapolated simultaneously.

This means that the two-way wave field extrapolation operators, which were discussed in this chapter, can be applied both for modeling and migration applications. Of course care must be taken with respect to evanescent energy. For migration in the presence of noise, spatially band-limited operators should be used. The two-way operators in the space-frequency domain, which were discussed in this chapter, are all band-limited operators. When applying the two-way operators in the wavenumber-frequency domain, then the evanescent energy should be suppressed for stability reasons.

It was argued in chapter I that for two-way wave equation migration a common-depthpoint (CDP) oriented technique should be chosen. In chapter II we have extensively discussed the principle of full pre-stack migration by single-shot record inversion (SSRI) and CDP stacking. The procedure can be summarized as follows

1. **Partly compensation for the acquisition limitations at the surface z_o.**
   The boundary condition $\bar{P}_{mn}(x,y,z_o,\omega)$ follows by inverting

$$P^{-}_{CSP,mn}(x,y,z_o,\omega) = [D_p(\omega)S(\omega)]P^{-}_{mn}(x,y,z_o,\omega) \qquad \text{(IV-66a)}$$

in a band-limited way (deconvolution). Here $P^{-}_{CSP,mn}$ represents the measured upgoing pressure wave in CSP gather mn. The boundary condition $S^{+}_{mn}(x,y,z_o,\omega)$ is simply given by

$$S^{+}_{mn}(x,y,z_o,\omega) = \delta(x-x_m)\delta(y-y_n). \qquad \text{(IV-66b)}$$

2. **Recursive downward wave field extrapolation of the downgoing source wave and the upgoing reflected waves,** according to

$$S^{+}_{mn}(z_i) = W^{+}(z_i,z_{i-1}) * S^{+}_{mn}(z_{i-1}), \qquad \text{(IV-67a)}$$

$$P^{-}_{mn}(z_i) = F^{-}(z_i,z_{i-1}) * P^{-}_{mn}(z_{i-1}). \qquad \text{(IV-67b)}$$

3. **Correlation** of the downgoing source wave and the upgoing reflected waves, yielding the single-fold ZO impulse response

$$\langle X_{ZO}(x,y,z_i,\omega)\rangle_{mn} = \frac{1}{s^2_{mn}} P^{-}_{mn}(x,y,z_i,\omega)[S^{+}_{mn}(x,y,z_i,\omega)]^{*}, \qquad \text{(IV-68a)}$$

where

$$s^2_{mn} = \iint S^{+}_{mn}(x,y,z_i,\omega)[S^{+}_{mn}(x,y,z_i,\omega)]^{*}dxdy. \qquad \text{(IV-68b)}$$

4. **Imaging** by summing over all frequencies, yielding the single-fold ZO reflectivity

$$\langle R_{ZO}(x,y,z_i)\rangle_{mn} = \frac{\Delta\omega}{2\pi} \sum_{\omega} \langle X_{ZO}(x,y,z_i,\omega)\rangle_{mn}. \qquad \text{(IV-69)}$$

5. **CDP stacking** by summing all single-fold ZO reflectivity functions, yielding the multi-fold wide-angle ZO reflectivity

$$\langle R^{CDP}_{ZO}(x,y,z_i)\rangle = \sum_{m} \sum_{n} \langle R_{ZO}(x,y,z_i)\rangle_{mn}. \qquad \text{(IV-70)}$$

The computational diagram is shown in Figure IV-14a. Notice that the scheme is based on one-way wave field extrapolation (relations IV-67a,b). However, the

scheme can be easily adapted for two-way wave field extrapolation. Therefore steps 1 and 2 must be modified as follows.

1. **Partly compensation for the acquisition limitations and composition of the total wave field at the surface z_o.** We consider two cases.

   i. At a reflection free surface the total wave field follows from

$$\vec{Q}_{mn}(z_o) = \mathbf{L}(z_o)\vec{P}_{mn}(z_o), \tag{IV-71a}$$

   where

$$\vec{P}_{mn}(z_o) = \begin{bmatrix} P^+_{mn}(z_o) \\ \\ P^-_{mn}(z_o) \end{bmatrix} = \begin{bmatrix} \delta(x-x_m)\delta(y-y_n) \\ \\ P^-_{mn}(x,y,z_o,\omega) \end{bmatrix}. \tag{IV-71b}$$

   The operator $\mathbf{L}$ is discussed below. P^-_{mn} follows from the measured data by inverting relation (IV-66a) in a band-limited way.

   ii. At a pressure free surface we may write for the total wave field

$$\vec{Q}_{mn}(z_o) = \begin{bmatrix} P_{mn}(z_o) \\ \\ \frac{1}{\rho}\frac{\partial P_{mn}}{\partial z}\Big|_{z_o} \end{bmatrix} = \begin{bmatrix} \delta(x-x_m)\delta(y-y_n) \\ \\ -j\omega V_{z,mn}(x,y,z_o,\omega) \end{bmatrix}, \tag{IV-72a}$$

   where $V_{z,mn}(x,y,z_o,\omega)$ follows from the detected particle velocity $V_{z,CSP,mn}$ in CSP gather mn by inverting

$$V_{z,CSP,mn}(x,y,z_o,\omega) = [D_v(\omega)S(\omega)]V_{z,mn}(x,y,z_o,\omega) \tag{IV-72b}$$

   in a band-limited way.

2a. **Recursive downward extrapolation of the total wave field,** according to

$$\begin{bmatrix} P_{mn}(z_i) \\ \\ \frac{1}{\rho}\frac{\partial P_{mn}}{\partial z}\Big|_{z_i} \end{bmatrix} = \begin{bmatrix} W_I(z_i,z_{i-1})^* & W_{II}(z_i,z_{i-1})^* \\ \\ W_{III}(z_i,z_{i-1})^* & W_{IV}(z_i,z_{i-1})^* \end{bmatrix} \begin{bmatrix} P_{mn}(z_{i-1}) \\ \\ \frac{1}{\rho}\frac{\partial P_{mn}}{\partial z}\Big|_{z_{i-1}} \end{bmatrix}, \tag{IV-73a}$$

   or, in abbreviated form

$$\vec{Q}_{mn}(z_i) \approx \mathbf{W}(z_i, z_{i-1})\vec{Q}_{mn}(z_{i-1}). \qquad \text{(IV-73b)}$$

The operator $\mathbf{W}$ is discussed below.

2b. **Decomposition of the total wave field into downgoing and upgoing waves,** according to

$$\vec{P}_{mn}(z_i) = \mathbf{L}^{-1}(z_i)\vec{Q}_{mn}(z_i), \qquad \text{(IV-74a)}$$

where

$$\vec{P}_{mn}(z_i) = \begin{bmatrix} P^{+}_{mn}(x,y,z_i,\omega) \\ P^{-}_{mn}(x,y,z_i,\omega) \end{bmatrix}. \qquad \text{(IV-74b)}$$

The operator $\mathbf{L}^{-1}$ is discussed below. The downgoing and upgoing waves at the current depth level are related to each other via a spatial convolution, according to

$$P^{-}_{mn}(x,y,z_i,\omega) = X(x,y,z_i,\omega) * P^{+}_{mn}(x,y,z_i,\omega), \qquad \text{(IV-74c)}$$

where $X(x,y,z_i,\omega)$ describes the impulse response of the subsurface. $P^{+}_{mn}(x,y,z_i,\omega)$ contains primary and multiple reflected downgoing waves, hence the spectrum may contain many dips, so inversion of (IV-74c) is unstable in the presence of noise. Instead we propose an inversion procedure analogous to the one-way procedure. Therefore, we first need to extract the downgoing source wave from the total downgoing wave field by means of a 'first arrival time window', yielding $S^{+}_{mn}(x,y,z_i,\omega)$. The procedure can now be continued by steps 3, 4 and 5 of the one-way scheme, described above.

The composition operator $\mathbf{L}$ in step 1i is given by relation (IV-4b). For many practical applications, operation (IV-71a) may be applied in the wavenumber-frequency domain, with $\tilde{\mathbf{L}}$ given by relation (IV-16b). Notice that at a pressure free surface the composition algorithm is not required (step 1ii).
For the computational macro subsurface model of Figure IV-9, operator $\mathbf{W}$ in step 2a represents the first order finite-difference two-term operator $\mathbf{W}_1^{(2)}$ in the space-frequency domain, given by relation (IV-45). For the special situation that lateral variations of the medium parameters may be neglected, step 2a should preferably be applied in the wavenumber-frequency domain, with operator $\tilde{\mathbf{W}}$ given by relation (IV-25).

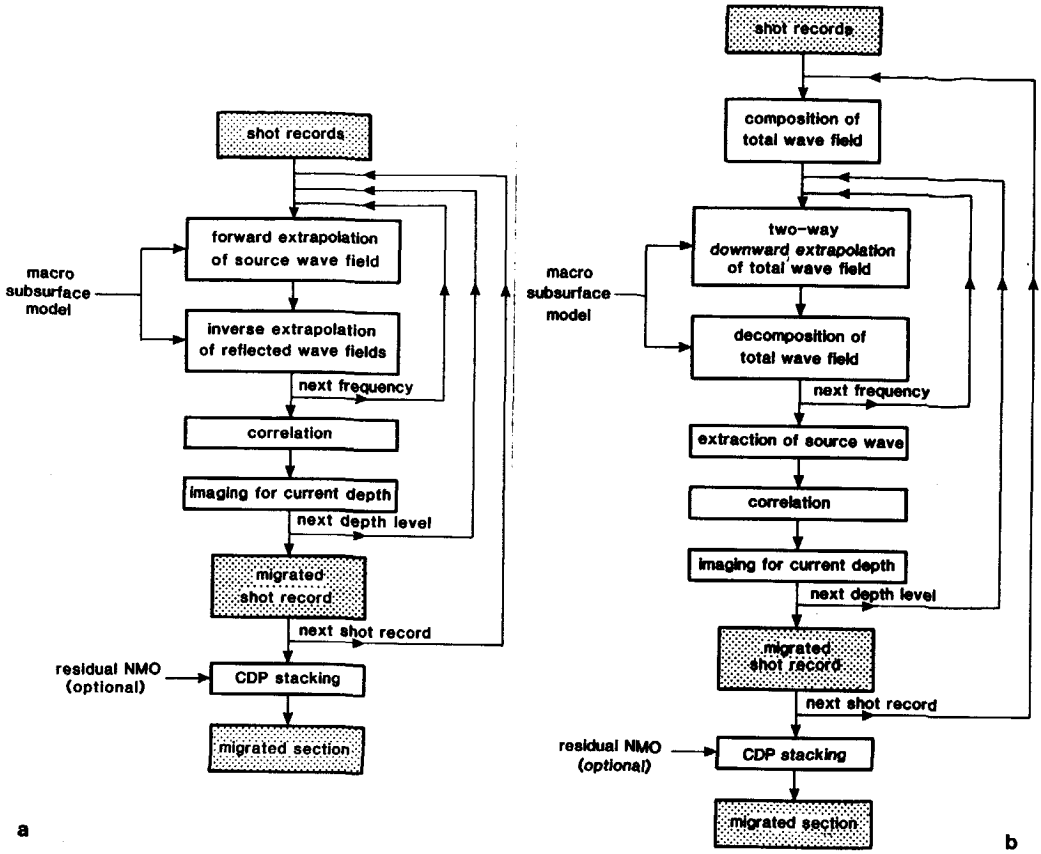

Figure IV-14: Computational diagrams for shot record oriented pre-stack migration. a. Scheme based on the one-way wave equations. b. Scheme based on the two-way wave equation.

The decomposition operator $\mathbf{L}^{-1}$ in step 2b is given by relation (IV-4d). Unfortunately this operator converges slowly and critical angle events are not incorporated. However, in practice it is often sufficient to apply the decomposition in the wavenumber-frequency domain for a reference medium only, with operator $\tilde{\mathbf{L}}^{-1}$ given by relation (IV-16d). When critical angle events must be incorporated in the decomposition as well, then operator $\tilde{\mathbf{L}}^{-1}$, given by relation (IV-27e) should be used. It should be noted that errors in the decomposed wave field $\vec{P}$ do not contribute to deeper depth levels, because the total field $\vec{Q}$ is downward extrapolated independently in step 2a.
In step 2b the downgoing source wave is resolved from the total downgoing wave in order to avoid imaging of **multiple reflections.** This is demonstrated in an example below.

With these modifications the total two-way scheme for full pre-stack migration by SSRI and CDP stacking can be summarized as follows:

1. Partly compensation for the acquisition limitations (deconvolution) and composition of the total wave field at the surface z_o.
2a. Recursive downward extrapolation of the total wave field.
2b. Decomposition of the total wave field into downgoing and upgoing waves and extraction of the downgoing source wave from the total downgoing wave field.
3. Correlation of the downgoing source wave and the upgoing reflected waves, yielding the single-fold ZO impulse response.
4. Imaging, yielding the single-fold ZO reflectivity.
5. CDP stacking, yielding the multi-fold wide-angle ZO reflectivity.

The computational diagram is shown in Figure IV-14b.

Examples.

The performance of the algorithm is demonstrated with two simple two-dimensional numerical examples. We consider horizontally layered 1-D inhomogeneous media. In this case the whole procedure can be applied in the wavenumber-frequency domain. As an alternative we replace the ZO imaging step by a PW imaging step, that is, we calculate

$$\langle \tilde{R}(p,z_i) \rangle = \frac{\Delta\omega}{2\pi} \sum_{\omega}{}' \tilde{X}(k_x,z_i,\omega), \qquad \text{(IV-75a)}$$

with

$$\tilde{X}(k_x,z_i,\omega) = \tilde{P}^-(k_x,z_i,\omega)/\tilde{S}^+(k_x,z_i,\omega), \qquad \text{(IV-75b)}$$

in some stable sense. The symbol $\sum'$ denotes that the summation is carried out for constant ray-parameter $p=k_x/\omega$ (constant propagation angle, see also section III.9).

Consider the medium shown in Figure IV-15a, which is bounded by a pressure free surface at z_o. The boundary condition $\tilde{\underline{Q}}(z_o)=[\tilde{P}(z_o),-j\omega\tilde{V}_z(z_o)]^T$ is shown in Figure IV-15b for one constant p-value (constant k_x/ω), such that $\sin\theta(z_o)=pc(z_o)=.5$, that is, for one oblique plane-wave with incidence angle $\theta(z_o)=30°$. For clarity the data are shown as a function of the intercept time

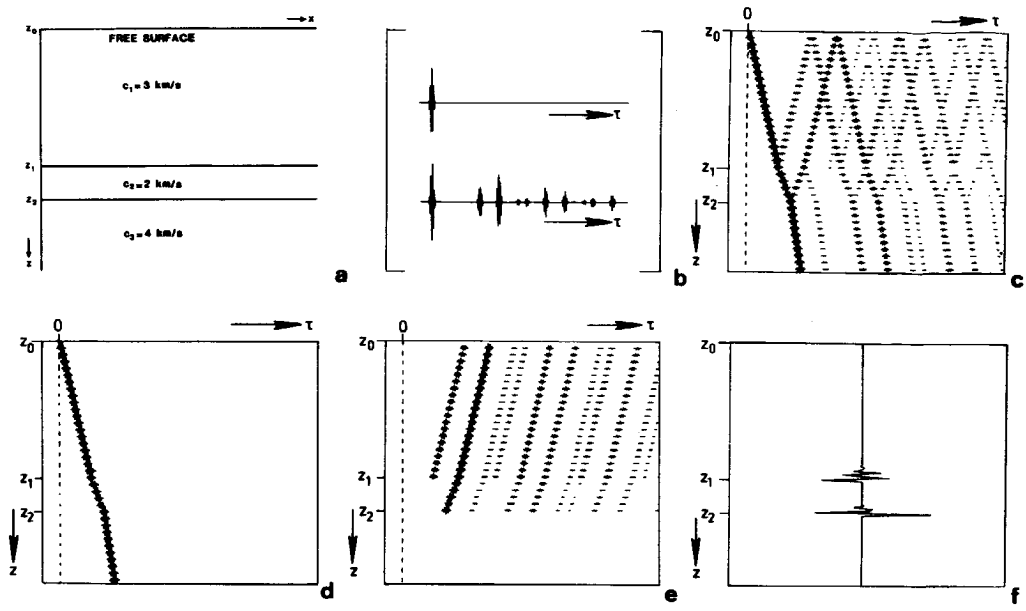

Figure IV-15: Example of pre-stack two-way wave equation migration.

a. Horizontally layered medium below a free surface.

b. Boundary condition.

c. Downward extrapolated data.

d. Downgoing source wave.

e. Upgoing reflected waves.

f. PW-imaged result.

τ, hence all reflection events related to this single plane-wave are visible. Notice that besides the primary reflections many multiples are present, which makes the trace difficult to interpret, even for this simple two-layer model. However, the interpretability improves significantly when the data are downward extrapolated, using a two-way wave field extrapolation operator. The downward extrapolated pressure data are shown in Figure IV-15c as a function of depth and intercept time, again for one p-value. A similar picture could be shown for the vertical component of the particle velocity. Notice that, similarly as in a vertical seismic profile (VSP) recorded in a vertical bore hole, all primary and multiple reflections can be clearly recognized. The decomposed data are shown in Figures IV-15d (downgoing source wave) and IV-15e (upgoing reflected

waves), again as a function of depth and intercept time for one p-value. Notice that the downward extrapolated upgoing waves are terminated at the reflectors; no upgoing waves are present in the lower (homogeneous and source free) half space. This is a typical property of the two-way approach. Figure IV-15f shows the PW image as a function of depth. Notice that this PW image shows the two reflectors only, in spite of the complex nature of the input trace (Figure IV-15b). Multiple energy is not imaged because the downgoing source wave and the upgoing multiple reflected waves do not correlate at zero intercept time.

Consider the continuously layered medium shown in Figures IV-16a,b with a reflection free surface at z_o. For one oblique plane-wave with incidence angle $\theta(z_o)=45°$, the downward extrapolated pressure data are shown in Figure IV-16c. The decomposed data $\tilde{P}^+$ and $\tilde{P}^-$ are shown in Figures IV-16d,e, respectively. Finally the PW imaged result is shown in Figure IV-16f. Notice that the image shows the turning point for the critical angle event under consideration.

Notice that in both examples the imaged results (Figures IV-15f and IV-16f) represent **one** angle of incidence only. If the procedure would be repeated for all angles of incidence then image representations similar to Figure III-10d would be obtained. Images for all angles of incidence are also shown in the next chapter for the more interesting case of full elastic two-way wave equation migration.
Finally notice that in both examples for 1-D inhomogeneous media PW imaging was carried out outside the depth extrapolation loop and that one shot record was considered only. For 2-D and 3-D inhomogeneous media ZO imaging should be carried out inside the depth extrapolation loop and the procedure should be repeated for all shot records, conformably to the computational diagram shown in Figure IV-14b.

Summarizing, in this section we proposed a CDP oriented pre-stack migration scheme based on the acoustic two-way wave equation. Notice the following advantages of this scheme in comparison with conventional one-way schemes

- use of the square-root operator is avoided,
- transmission effects are automatically included,
- critical angle events may be properly handled,
- multiple reflected waves may be properly handled.

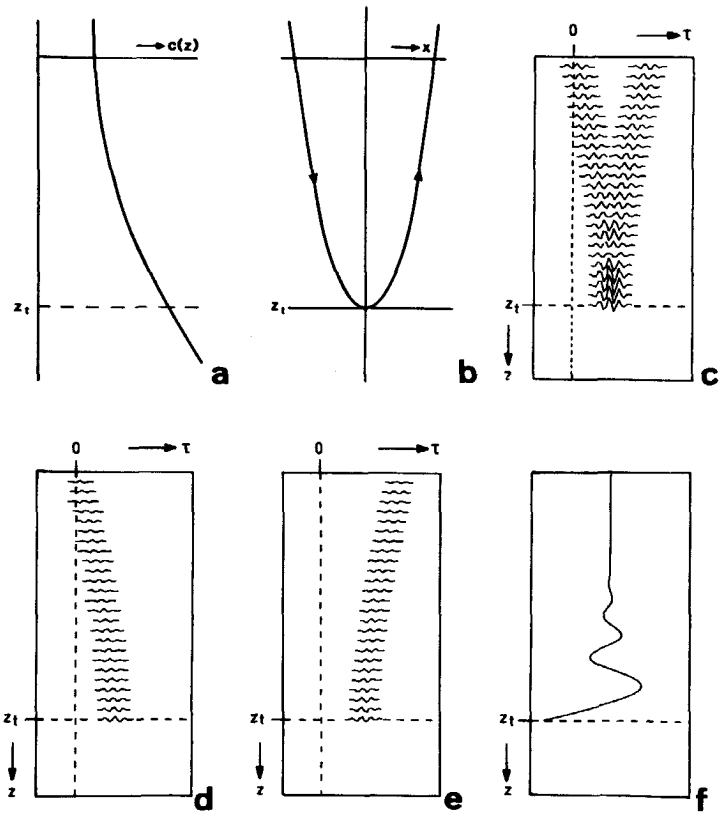

Figure IV-16: Example of pre-stack two-way wave equation migration, including critical angle events.

a. Depth dependent velocity function c(z).

b. Continuously layered medium with ray representation of a critical angle event.

c. Downward extrapolated data.

d. Downgoing wave.

e. Upgoing wave.

f. PW-imaged result.

For a proper handling of multiple reflected waves, accurate knowledge of the macro subsurface model is required. Similar as in conventional multiple elimination schemes, a small mis-positioning of the major reflecting boundaries may result in an increase of undesired reflection events, so the scheme should preferably be applied iteratively. Alternatively, the generation of undesired reflection events may be avoided by spatially filtering (smoothing) the abrupt changes in the macro subsurface model before migration. Of course multiple reflected waves will then not be properly handled anymore.

IV.9 CONCLUDING REMARKS

In principle there are two approaches to modify the acoustic wave equation such that wave field extrapolation operators along the depth coordinate can be derived:

i. Decomposition into two first order one-way wave equations for P^+ and P^-, respectively.
ii. Reformulation into a first order two-way matrix wave equation for $[P,\rho^{-1}\partial P/\partial z]^T$.

In this chapter we discussed methods using the two-way wave equation. We have shown the close relationship with the one-way wave equations which were discussed in chapter III. We have discussed several two-way solutions for increasing complexity of the medium:

A. The medium consists of a sequence of homogeneous layers. An exact solution for each layer can be formulated in the wavenumber-frequency domain. The recursive scheme is very simple because the total field is continuous for all depths. This means that the boundary conditions (reflection, transmission) for downgoing and upgoing waves are automatically fulfilled at the layer interfaces. This is advantageous with respect to a proper treatment of multiple reflections in modeling as well as migration schemes.
B. The medium consists of a sequence of layers where in each layer the medium parameters are functions of the depth coordinate only. An approximate solution can be formulated in the wavenumber-frequency domain, assuming the medium parameters may be linearized in depth within each thin layer. Critical angle events are properly incorporated. The solution is closely related to that of the decoupled WKBJ one-way wave equations, as discussed in chapter III. Again the recursive scheme is very simple.
C. The medium is arbitrarily inhomogeneous. A formal solution can be formulated in the space-frequency domain in terms of wave field extrapolation operators based on Taylor series summation, assuming that within each layer the medium parameters may be linearized in depth. Critical angle events are incorporated.
This formal solution can be reformulated as a fast converging explicit finite-difference scheme, if the lateral derivatives of the medium

parameters may be neglected. This two-way finite difference scheme is stable and converges already in the first order approximation, also for critical angle events.

Pre-stack migration based on the acoustic two-way wave equation is in principle founded on two-way downward extrapolation, schematically represented by

$$\begin{bmatrix} P \\ \frac{1}{\rho}\frac{\partial P}{\partial z} \end{bmatrix}_{z_i} \leftarrow \mathbf{W} \leftarrow \begin{bmatrix} P \\ \frac{1}{\rho}\frac{\partial P}{\partial z} \end{bmatrix}_{z_{i-1}}, \qquad \text{(IV-76a)}$$

followed by decomposition

$$\begin{bmatrix} S^+ \\ P^- \end{bmatrix}_{z_i} \xleftarrow{\text{window}} \begin{bmatrix} P^+ \\ P^- \end{bmatrix}_{z_i} \leftarrow \mathbf{L}^{-1} \leftarrow \begin{bmatrix} P \\ \frac{1}{\rho}\frac{\partial P}{\partial z} \end{bmatrix}_{z_i}, \qquad \text{(IV-76b)}$$

and imaging

$$S^+(z_i) \rightarrow \langle R(z_i) \rangle \leftarrow P^-(z_i). \qquad \text{(IV-76c)}$$

This CDP-oriented scheme is applicable for 1-D, 2-D and 3-D inhomogeneous macro subsurface models. It properly handles critical angle events and multiple reflections if the macro subsurface model is accurately known. For smoothed macro subsurface models a high dip angle performance for primary waves may be expected.

Note that we have addressed depth techniques only, that is, those algorithms which are based on extrapolating along the depth coordinate. An interesting alternative approach to two-way wave field extrapolation is discussed by Baysal et al. (1984). They present CMP oriented **post-stack** modeling and migration schemes, for 2-D inhomogeneous media, which make use of recursive traveltime steps rather than depth steps. The principle of time extrapolation can easily be used for pre-stack **modeling** in 1-D, 2-D and 3-D inhomogeneous media. A discussion is beyond the scope of this thesis. The reader is referred to Kosloff and Baysal (1982). However, for CDP oriented pre-stack **migration** in 1-D, 2-D and 3-D inhomogeneous macro subsurface models we prefer to make use of the depth extrapolation scheme, as discussed in this chapter, because it allows simultaneous forward and inverse extrapolation of downgoing and upgoing waves, respectively (primaries as well as multiples), which is essential for a proper imaging principle.

CHAPTER V

WAVE FIELD EXTRAPOLATION TECHNIQUES, INCLUDING WAVE CONVERSION, BASED ON THE FULL ELASTIC TWO-WAY WAVE EQUATION

V.1 INTRODUCTION

In chapter IV we discussed the acoustic approach to two-way wave field extrapolation. We discussed operators $\mathbf{W}_\ell$ which describe extrapolation of the total wave field from one depth level to another, according to

$$\vec{Q}_\ell(z_{i-1}) = \mathbf{W}_\ell(z_{i-1},z_i)\vec{Q}_\ell(z_i), \qquad \text{(V-1a)}$$

for upward extrapolation (see Figure IV-2a), and

$$\vec{Q}_\ell(z_i) = \mathbf{W}_\ell(z_i,z_{i-1})\vec{Q}_\ell(z_{i-1}), \qquad \text{(V-1b)}$$

for downward extrapolation (see Figure IV-2b). In this chapter we use the sub-script ℓ when the extrapolation takes place in a liquid. In relation (V-1), the wave vector $\vec{Q}_\ell$ contains the total pressure and its first derivative with respect to z, divided by the mass density, according to

$$\vec{Q}_\ell = \begin{bmatrix} P \\ \\ \frac{1}{\rho}\frac{\partial P}{\partial z} \end{bmatrix}. \qquad \text{(V-1c)}$$

It was shown that operator $\mathbf{W}_\ell$ may include all fundamental wave phenomena (primary waves, multiple reflected waves, critical angle events) in arbitrarily inhomogeneous liquids. The acoustic approach breaks down, however, in

arbitrarily inhomogeneous solids, where wave conversion may not be neglected. Therefore, in this chapter we generalize two-way algorithms (V-1a) and (V-1b) for wave field extrapolation in 2-D inhomogeneous solids, according to

$$\vec{Q}_s(z_{i-1}) = \mathbf{W}_s(z_{i-1},z_i)\vec{Q}_s(z_i), \qquad \text{(V-2a)}$$

for upward extrapolation, and

$$\vec{Q}_s(z_i) = \mathbf{W}_s(z_i,z_{i-1})\vec{Q}_s(z_{i-1}), \qquad \text{(V-2b)}$$

for downward extrapolation. Here the sub-script s denotes that the extrapolation takes place in a solid. The wave vector $\vec{Q}_s$, given by

$$\vec{Q}_s = \begin{bmatrix} j\omega V_z \\ Z_x \\ Z_z \\ j\omega V_x \end{bmatrix}, \qquad \text{(V-2c)}$$

describes the total wave field in terms of the stress vector $\vec{Z}$ and the particle velocity vector $\vec{V}$, with

$$\vec{Z} = \begin{bmatrix} Z_x \\ \\ Z_z \end{bmatrix}, \quad \vec{V} = \begin{bmatrix} V_x \\ \\ V_z \end{bmatrix}. \qquad \text{(V-2d,e)}$$

Various expressions for the operator $\mathbf{W}_s$ are derived further on in this chapter. It is shown that primary as well as multiple reflected dilatational P waves and distortional SV waves in inhomogeneous solids are all included. Applications in modeling and CDP-oriented migration schemes are also discussed in this chapter.

V.2 THE FULL ELASTIC TWO-WAY WAVE EQUATION

In this section we introduce the matrix formulation of the full elastic wave equation for P and SV waves in solids. A rigorous discussion on wave phenomena in inhomogeneous anisotropic solids is given in several textbooks. Amongst others we mention Aki and Richards (1980) and Pilant (1979). For most seismic applications anisotropy is a second order effect in comparison with

inhomogeneity. Therefore we start our discussion with the equation of motion for inhomogeneous isotropic solids, in the frequency domain given by

$$\nabla[(\lambda+2\mu)\nabla.\vec{V}] - \nabla\times(\mu\nabla\times\vec{V}) + \rho\omega^2\vec{V} = \tag{V-3}$$

$$= -2[(\nabla\mu.\nabla)\vec{V} - (\nabla\mu)\nabla.\vec{V} + (\nabla\mu)\times(\nabla\times\vec{V})],$$

where $\vec{V}=[V_x,V_y,V_z]^T$ represents the particle velocity. The Lamé coefficients λ and μ are related to the bulk compression modulus K and Poisson's ratio σ according to

$$K = \lambda + 2\mu/3, \tag{V-4a}$$

$$\sigma = \tfrac{1}{2}\lambda/(\lambda+\mu). \tag{V-4b}$$

In the following we consider 2-D inhomogeneous media, that is, we assume that the medium parameters are given by $\lambda=\lambda(x,z)$, $\mu=\mu(x,z)$ and $\rho=\rho(x,z)$; the modifications required for the 3-D inhomogeneous case are briefly outlined in section V.6. Furthermore we assume that the normals to the wave fronts lie in the x,z-plane. Under these assumptions, shear waves with horizontal polarization (SH waves, with $V_x=V_z=o$), propagate independently from compressional waves and shear waves with vertical* polarization (P and SV waves, with $V_y=o$). In the following we only consider waves with vertical polarization (the solution for waves with horizontal polarization is very similar to the solution for acoustic waves in liquids and is therefore not handled here). With these assumptions, the x and z-component of equation (V-3) read

$$\frac{\partial}{\partial x}\left[(\lambda+2\mu)\left(\frac{\partial V_x}{\partial x}+\frac{\partial V_z}{\partial z}\right)\right] - 2\left(\frac{\partial\mu}{\partial x}\right)\left(\frac{\partial V_z}{\partial z}\right)$$
$$+\frac{\partial}{\partial z}\left[\mu\left(\frac{\partial V_x}{\partial z}-\frac{\partial V_z}{\partial x}\right)\right] + 2\left(\frac{\partial\mu}{\partial z}\right)\left(\frac{\partial V_z}{\partial x}\right) + \rho\omega^2 V_x = o, \tag{V-5a}$$

and

$$\frac{\partial}{\partial z}\left[(\lambda+2\mu)\left(\frac{\partial V_x}{\partial x}+\frac{\partial V_z}{\partial z}\right)\right] - 2\left(\frac{\partial\mu}{\partial z}\right)\left(\frac{\partial V_x}{\partial x}\right)$$
$$-\frac{\partial}{\partial x}\left[\mu\left(\frac{\partial V_x}{\partial z}-\frac{\partial V_z}{\partial x}\right)\right] + 2\left(\frac{\partial\mu}{\partial x}\right)\left(\frac{\partial V_x}{\partial z}\right) + \rho\omega^2 V_z = o. \tag{V-5b}$$

*) In this thesis "vertical" polarization means: polarization in the vertical (x,z) plane.

Relations (V-5a) and (V-5b) represent two coupled second order differential equations which require four boundary conditions. Similar as in the acoustic case, we want to arrive at a first order matrix differential equation, from which wave field extrapolation operators can be derived. Therefore we also consider the following two stress-strain relations

$$j\omega Z_x = \mu(\partial V_x/\partial z + \partial V_z/\partial x), \tag{V-6a}$$

$$j\omega Z_z = \lambda(\partial V_x/\partial x + \partial V_z/\partial z) + 2\mu(\partial V_z/\partial z), \tag{V-6b}$$

where Z_x and Z_z represent two components of the stress tensor. We use the same notation as Brekhovskikh (1980), so stress vector $\vec{Z}$ refers to the stress on a plane normal to the z-axis, whereas its components Z_x and Z_z represent the shear stress and the normal stress respectively. (Notice that in liquids the shear modulus μ vanishes, so Z_x=o, Z_z=-P). Equations (V-5) and (V-6) can be rearranged such that the derivatives with respect to depth z are expressed in terms of lateral convolution operators (see also section III.2), according to

$$\frac{\partial}{\partial z}(j\omega V_z) = -\left(\frac{\omega^2}{\lambda+2\mu}\right)d_o(x) * Z_z - \left(\frac{\lambda}{\lambda+2\mu}\right)d_1(x) * (j\omega V_x), \tag{V-7a}$$

$$\frac{\partial}{\partial z}Z_x = -\left(\frac{\lambda}{\lambda+2\mu}\right)d_1(x) * Z_z + \left[\rho d_o(x) + \frac{4\mu}{\omega^2}\left(\frac{\lambda+\mu}{\lambda+2\mu}\right)d_2(x)\right] * (j\omega V_x), \tag{V-7b}$$

$$\frac{\partial}{\partial z}Z_z = \rho d_o(x) * (j\omega V_z) - d_1(x) * Z_x, \tag{V-7c}$$

$$\frac{\partial}{\partial z}(j\omega V_x) = -d_1(x) * (j\omega V_z) - \frac{\omega^2}{\mu} d_o(x) * Z_x. \tag{V-7d}$$

Here (V-7a) and (V-7d) represent the stress-strain relations (V-6b) and (V-6a), respectively, while (V-7b) and (V-7c) are obtained after substituting the stress-strain relations into equations (V-5a) and (V-5b), respectively. Notice that we neglected the lateral derivatives of the medium parameters. Relations (V-7a,b,c,d) can be elegantly combined into one matrix differential equation, according to

$$\frac{\partial \vec{Q}_s}{\partial z} = \mathbf{A}_s \vec{Q}_s, \tag{V-8a}$$

with

$$\vec{Q}_s = \begin{bmatrix} j\omega V_z \\ Z_x \\ Z_z \\ j\omega V_x \end{bmatrix}, \qquad \text{(V-8b)}$$

and where 4x4 matrix operator $\mathbf{A}_s$ is given by relation (G-1) in Appendix G. (Notice that equation (V-8) cannot be applied in liquids because operator $\mathbf{A}_s$ is singular for $\mu=0$. In liquids the quantities Z_z and $j\omega V_z$ may be replaced by $-P$ and $-\rho^{-1}\partial_z P$, respectively, which represent the two components of the wave vector $-\vec{Q}_\ell$. This explains our choice of the factor $j\omega$ in the wave vector $\vec{Q}_s$). The operator $\mathbf{A}_s$ can be decomposed according to

$$\mathbf{A}_s = \mathbf{L}_s \mathbf{\Lambda}_s \mathbf{L}_s^{-1}, \qquad \text{(V-9)}$$

with operators $\mathbf{L}_s$, $\mathbf{\Lambda}_s$ and $\mathbf{L}_s^{-1}$ given by relations (G-2b,c,d). Let us now define the Lamé potentials Φ and $\vec{\psi}$ for the particle velocity:

$$\vec{V} = \nabla\Phi + \nabla \times \vec{\psi}, \qquad \text{(V-10)}$$

where Φ represents the scalar potential for dilatational or compressional waves and where $\vec{\psi}$ represents the vector potential for distortional or shear waves. In the general inhomogeneous case the potentials Φ and $\vec{\psi}$ are coupled, which can be easily seen when relation (V-10) is substituted into the equation of motion (V-3).

With the assumptions made before, the vector potential $\vec{\psi}=[\psi_x,\psi_y,\psi_z]^T$ can be chosen such that $\psi_x=\psi_z=0$. We define $\psi=\psi_y$. Furthermore we define Φ^+, Φ^-, ψ^+ and ψ^- such that

$$\Phi = \Phi^+ + \Phi^-, \qquad \text{(V-11a)}$$

$$\frac{\partial\Phi}{\partial z} = -jH_1^{(P)} * [\Phi^+ - \Phi^-], \qquad \text{(V-11b)}$$

$$\psi = \psi^+ + \psi^-, \qquad \text{(V-11c)}$$

$$\frac{\partial\psi}{\partial z} = -jH_1^{(SV)} * [\psi^+ - \psi^-], \qquad \text{(V-11d)}$$

with $H_1^{(P)}$ and $H_1^{(SV)}$ defined by relations (G-2ℓ,p). These definitions can be

combined with (V-6) and (V-10) in the following matrix equations

$$\vec{Q}_s = \mathbf{L}_s \vec{P}_s \tag{V-12a}$$

and

$$\vec{P}_s = \mathbf{L}_s^{-1} \vec{Q}_s, \tag{V-12b}$$

with

$$\vec{P}_s = \begin{bmatrix} \Phi^+ \\ \psi^+ \\ -\Phi^- \\ \psi^- \end{bmatrix} . \tag{V-12c}$$

Substitution of relation (V-12a) into two-way wave equation (V-8), using property (V-9), yields a set of coupled one-way wave equations, according to

$$\frac{\partial \vec{P}_s}{\partial z} = \mathbf{B}_s \vec{P}_s, \tag{V-13a}$$

with

$$\mathbf{B}_s = \mathbf{\Lambda}_s - \mathbf{L}_s^{-1} \frac{\partial \mathbf{L}_s}{\partial z}. \tag{V-13b}$$

Notice that these equations fully decouple for media which are homogeneous along the z-coordinate ($\partial \mathbf{L}_s / \partial z = \mathbf{O}$):

$$\frac{\partial \Phi^+}{\partial z} = -jH_1^{(P)} * \Phi^+, \tag{V-14a}$$

$$\frac{\partial \psi^+}{\partial z} = -jH_1^{(SV)} * \psi^+, \tag{V-14b}$$

$$\frac{\partial \Phi^-}{\partial z} = jH_1^{(P)} * \Phi^-, \tag{V-14c}$$

$$\frac{\partial \psi^-}{\partial z} = jH_1^{(SV)} * \psi^-, \tag{V-14d}$$

where Φ^+ and Φ^- represent the potentials for downgoing and upgoing P waves, respectively, while ψ^+ and ψ^- represent the potentials for downgoing and upgoing SV waves, respectively. Notice also that for this situation Φ and ψ satisfy the following wave equations

$$\frac{\partial^2 \Phi}{\partial z^2} = -H_2^{(P)} * \Phi, \tag{V-15a}$$

where

$$H_2^{(P)} = H_1^{(P)} * H_1^{(P)} = k_P^2 d_o(x) + d_2(x), \qquad \text{(V-15b)}$$

with

$$k_P^2 = \omega^2/c_P^2, \qquad \text{(V-15c)}$$

$$c_P^2 = (\lambda+2\mu)/\rho, \qquad \text{(V-15d)}$$

and

$$\frac{\partial^2\psi}{\partial z^2} = -H_2^{(SV)} * \psi, \qquad \text{(V-16a)}$$

where

$$H_2^{(SV)} = H_1^{(SV)} * H_1^{(SV)} = k_{SV}^2\, d_o(x) + d_2(x), \qquad \text{(V-16b)}$$

with

$$k_{SV}^2 = \omega^2/c_{SV}^2, \qquad \text{(V-16c)}$$

$$c_{SV}^2 = \mu/\rho. \qquad \text{(V-16d)}$$

Above equations, which are well known among geophysicists, exhibit a strong resemblance with the acoustic wave equation. Notice that c_P and c_{SV} represent the P and SV wave propagation velocity, respectively, with $c_P > c_{SV}$.

Summarizing, the full elastic two-way wave equation for inhomogeneous solids can be elegantly described by the first order matrix differential equation (V-8). By decomposing operator $\mathbf{A}_s$, given by (G-1), we showed the close relationship between the **full elastic two-way wave equation** (V-8) and the **full elastic one-way wave equations** (V-13). According to relation (V-12b) the total wave field $\vec{Q}_s$ is decomposed into coupled downgoing and upgoing P and SV waves by means of decomposition operator $\mathbf{L}_s^{-1}$, given by (G-2d). This operator plays an important role in full elastic pre-stack modeling and migration schemes. Equation (V-8) is solved in the next section.

V.3 FULL ELASTIC TWO-WAY WAVE FIELD EXTRAPOLATION

In this section we discuss the solution of the full elastic two-way wave equation. For convenience we consider 2-D waves in a homogeneous medium. We also discuss the extension of the solution for inhomogeneous media.

For homogeneous media we may consider the full elastic two-way wave equation in the wavenumber-frequency domain

$$\frac{\partial \tilde{\tilde{Q}}_s}{\partial z} = \tilde{\tilde{A}}_s \tilde{\tilde{Q}}_s, \tag{V-17a}$$

where

$$\tilde{\tilde{Q}}_s = \begin{bmatrix} j\omega\tilde{V}_z \\ \tilde{Z}_x \\ \tilde{Z}_z \\ j\omega\tilde{V}_x \end{bmatrix} \tag{V-17b}$$

and where operator $\tilde{\tilde{A}}_s$ represents the spatial Fourier transform of operator $\mathbf{A}_s$, given by relation (G-1). The eigenvalue decomposition of operator $\tilde{\tilde{A}}_s$ reads

$$\tilde{\tilde{A}}_s = \tilde{\tilde{L}}_s \tilde{\Lambda}_s \tilde{\tilde{L}}_s^{-1} \tag{V-18}$$

where operators $\tilde{\tilde{L}}_s$, $\tilde{\Lambda}_s$ and $\tilde{\tilde{L}}_s^{-1}$ represent the spatial Fourier transforms of operators $\mathbf{L}_s$, $\mathbf{\Lambda}_s$ and $\mathbf{L}_s^{-1}$, given by relations (G-2b,c,d). Notice that this decomposition breaks down for $\tilde{H}_1^{(P)} \to o$ and for $\tilde{H}_1^{(SV)} \to o$. Following Ursin (1983), a solution of (V-17) can be given by

$$\tilde{\tilde{Q}}_s(z) = \tilde{\tilde{W}}_s(z,z_o)\tilde{\tilde{Q}}_s(z_o), \tag{V-19a}$$

where, symbolically,

$$\tilde{\tilde{W}}_s(z,z_o) = \exp[\tilde{\tilde{A}}_s \Delta z], \tag{V-19b}$$

with $\Delta z = z - z_o$. Using property (V-18), relation (V-19b) can be written as

$$\tilde{\tilde{W}}_s(z,z_o) = \mathbf{I} + \tilde{\tilde{L}}_s(\tilde{\Lambda}_s\Delta z)\tilde{\tilde{L}}_s^{-1} + \tilde{\tilde{L}}_s(\tilde{\Lambda}_s\Delta z)\tilde{\tilde{L}}_s^{-1}\tilde{\tilde{L}}_s(\tilde{\Lambda}_s\Delta z)\tilde{\tilde{L}}_s^{-1} + \ldots, \tag{V-20a}$$

or

$$\tilde{\tilde{W}}_s(z,z_o) = \tilde{\tilde{L}}_s\left[\mathbf{I} + (\tilde{\Lambda}_s\Delta z) + (\tilde{\Lambda}_s\Delta z)^2 + \ldots\right]\tilde{\tilde{L}}_s^{-1}, \tag{V-20b}$$

or

$$\tilde{\tilde{W}}_s(z,z_o) = \tilde{\tilde{L}}_s(z)\tilde{\tilde{V}}_s(z,z_o)\tilde{\tilde{L}}_s^{-1}(z_o), \tag{V-21a}$$

with

$$\tilde{\mathbf{V}}_s(z,z_o) = \exp[\tilde{\mathbf{\Lambda}}_s \Delta z], \qquad \text{(V-21b)}$$

or

$$\tilde{\mathbf{V}}_s(z,z_o) = \begin{bmatrix} \exp[-j\tilde{H}_1^{(P)}\Delta z] & 0 & 0 & 0 \\ 0 & \exp[-j\tilde{H}_1^{(SV)}\Delta z] & 0 & 0 \\ 0 & 0 & \exp[j\tilde{H}_1^{(P)}\Delta z] & 0 \\ 0 & 0 & 0 & \exp[j\tilde{H}_1^{(SV)}\Delta z] \end{bmatrix}. \qquad \text{(V-21c)}$$

Relation (V-21) shows that for this special case of a homogeneous medium, full elastic two-way operator $\tilde{\mathbf{W}}_s(z,z_o)$ can be written in terms of one-way sub-processes. This phenomenon was already discussed for the acoustic case in chapter IV and is visualized in Figure IV-3. On the other hand, if we define full-elastic two-way operator $\tilde{\mathbf{W}}_s(z,z_o)$ as

$$\tilde{\mathbf{W}}_s(z,z_o) = \begin{bmatrix} \tilde{\mathbf{W}}_I(z,z_o) & \tilde{\mathbf{W}}_{II}(z,z_o) \\ \tilde{\mathbf{W}}_{III}(z,z_o) & \tilde{\mathbf{W}}_{IV}(z,z_o) \end{bmatrix}, \qquad \text{(V-22a)}$$

then expressions for the sub-matrices $\tilde{\mathbf{W}}_I \ldots \tilde{\mathbf{W}}_{IV}$ follow directly from relation (V-21) and Appendix G:

$$\tilde{\mathbf{W}}_I(z,z_o) = \tilde{\mathbf{L}}_1[\cosh\tilde{\mathbf{\Lambda}}\Delta z]\,\tilde{\mathbf{L}}_1^{-1}, \quad \tilde{\mathbf{W}}_{II} = \tilde{\mathbf{L}}_1[\sinh\tilde{\mathbf{\Lambda}}\Delta z]\,\tilde{\mathbf{L}}_2^{-1}, \qquad \text{(V-22b,c)}$$

$$\tilde{\mathbf{W}}_{III}(z,z_o) = \tilde{\mathbf{L}}_2[\sinh\tilde{\mathbf{\Lambda}}\Delta z]\,\tilde{\mathbf{L}}_1^{-1}, \quad \tilde{\mathbf{W}}_{IV} = \tilde{\mathbf{L}}_2[\cosh\tilde{\mathbf{\Lambda}}\Delta z]\,\tilde{\mathbf{L}}_2^{-1}, \qquad \text{(V-22d,e)}$$

where operators $\tilde{\mathbf{L}}_1$, $\tilde{\mathbf{L}}_1^{-1}$, $\tilde{\mathbf{L}}_2$, $\tilde{\mathbf{L}}_2^{-1}$ and $\tilde{\mathbf{\Lambda}}$ are given by the spatial Fourier transforms of operators $\mathbf{L}_1$, $\mathbf{L}_1^{-1}$, $\mathbf{L}_2$, $\mathbf{L}_2^{-1}$ and $\mathbf{\Lambda}$, given by relations (G-2e,f,g,h,i). Finally, if we define operator $\tilde{\mathbf{W}}_s(z,z_o)$ as

$$\tilde{\mathbf{W}}_s(z,z_o) = \begin{bmatrix} \tilde{W}_{11}(z,z_o) & \tilde{W}_{12}(z,z_o) & \tilde{W}_{13}(z,z_o) & \tilde{W}_{14}(z,z_o) \\ \tilde{W}_{21}(z,z_o) & \tilde{W}_{22}(z,z_o) & \tilde{W}_{23}(z,z_o) & \tilde{W}_{24}(z,z_o) \\ \tilde{W}_{31}(z,z_o) & \tilde{W}_{32}(z,z_o) & \tilde{W}_{33}(z,z_o) & \tilde{W}_{34}(z,z_o) \\ \tilde{W}_{41}(z,z_o) & \tilde{W}_{42}(z,z_o) & \tilde{W}_{43}(z,z_o) & \tilde{W}_{44}(z,z_o) \end{bmatrix}, \qquad \text{(V-23a)}$$

then expressions for the sub-operators $\tilde{W}_{11} \ldots \tilde{W}_{44}$ follow directly from relation (V-22) and Appendix G:

$$\tilde{W}_{11}(z,z_o) = (1-2k_x^2/k_{SV}^2)\tilde{W}_I^{(P)}(z,z_o) + (2k_x^2/k_{SV}^2)\tilde{W}_I^{(SV)}(z,z_o), \quad \text{(V-23b)}$$

$$\tilde{W}_{12}(z,z_o) = (-jk_x/\rho)\tilde{W}_I^{(P)}(z,z_o) + (jk_x/\rho)\tilde{W}_I^{(SV)}(z,z_o), \quad \text{(V-23c)}$$

$$\tilde{W}_{13}(z,z_o) = \tilde{W}_{III}^{(P)}(z,z_o) - (k_x^2/\rho^2)\tilde{W}_{II}^{(SV)}(z,z_o), \quad \text{(V-23d)}$$

$$\vdots$$

$$\tilde{W}_{44}(z,z_o) = (2k_x^2/k_{SV}^2)\tilde{W}_I^{(P)}(z,z_o) + (1-2k_x^2/k_{SV}^2)\tilde{W}_I^{(SV)}(z,z_o), \quad \text{(V-23e)}$$

where

$$\tilde{W}_I^{(P)}(z,z_o) = \cos[\tilde{H}_1^{(P)}\Delta z], \quad \text{(V-23f)}$$

$$\tilde{W}_I^{(SV)}(z,z_o) = \cos[\tilde{H}_1^{(SV)}\Delta z], \quad \text{(V-23g)}$$

$$\tilde{W}_{II}^{(P)}(z,z_o) = \frac{\rho}{\tilde{H}_1^{(P)}} \sin[\tilde{H}_1^{(P)}\Delta z], \quad \text{(V-23h)}$$

$$\tilde{W}_{II}^{(SV)}(z,z_o) = \frac{\rho}{\tilde{H}_1^{(SV)}} \sin[\tilde{H}_1^{(SV)}\Delta z], \quad \text{(V-23i)}$$

$$\tilde{W}_{III}^{(P)}(z,z_o) = -\frac{1}{\rho^2}\tilde{H}_2^{(P)}\tilde{W}_{II}^{(P)}(z,z_o), \quad \text{(V-23j)}$$

$$\tilde{W}_{III}^{(SV)}(z,z_o) = -\frac{1}{\rho^2}\tilde{H}_2^{(SV)}\tilde{W}_{II}^{(SV)}(z,z_o), \quad \text{(V-23k)}$$

and

$$\tilde{H}_1^{(P)} = \sqrt{\tilde{H}_2^{(P)}} = \sqrt{k_P^2 - k_x^2}, \quad \text{(V-23l)}$$

$$\tilde{H}_1^{(SV)} = \sqrt{\tilde{H}_2^{(SV)}} = \sqrt{k_{SV}^2 - k_x^2}. \quad \text{(V-23m)}$$

Operator $\tilde{\mathbf{W}}_s$, given by relation (V-23), describes full elastic two-way wave field extrapolation in the wavenumber-frequency domain. Notice that the limits for $\tilde{H}_1^{(P)} \to o$ and for $\tilde{H}_1^{(SV)} \to o$ exist.

It can be easily verified that all sub-operators $\tilde{W}_{11} \ldots \tilde{W}_{44}$ can be written as linear combinations of operators $\tilde{W}_I^{(P)} \ldots \tilde{W}_{III}^{(P)}$ and $\tilde{W}_I^{(SV)} \ldots \tilde{W}_{III}^{(SV)}$, given by relations (V-23f,g,h,i,j,k). Notice that these operators represent the acoustic two-way sub-operators $\tilde{W}_I \ldots \tilde{W}_{III}$, given by relations (IV-21b,c,d), with $\tilde{H}_1$ replaced by $\tilde{H}_1^{(P)}$ or $\tilde{H}_1^{(SV)}$, respectively.

The band-limited inverse spatial Fourier transform of relation (V-19a) we define as

$$\vec{Q}_s(z) = \mathbf{W}_s(z,z_o)\vec{Q}_s(z_o), \tag{V-24}$$

where

$$\mathbf{W}_s(z,z_o) = \begin{bmatrix} W_{11}(z,z_o)^* & W_{12}(z,z_o)^* & W_{13}(z,z_o)^* & W_{14}(z,z_o)^* \\ W_{21}(z,z_o)^* & W_{22}(z,z_o)^* & W_{23}(z,z_o)^* & W_{24}(z,z_o)^* \\ W_{31}(z,z_o)^* & W_{32}(z,z_o)^* & W_{33}(z,z_o)^* & W_{34}(z,z_o)^* \\ W_{41}(z,z_o)^* & W_{42}(z,z_o)^* & W_{43}(z,z_o)^* & W_{44}(z,z_o)^* \end{bmatrix}, \tag{V-25a}$$

where the sub-operators $W_{11}\ldots W_{44}$ follow directly from the sub-operators $\tilde{W}_{11}\ldots\tilde{W}_{44}$, given above, according to

$$W_{11}(z,z_o) = [d_o(x)+2k_{SV}^{-2}d_2(x)] * W_I^{(P)}(z,z_o) - [2k_{SV}^{-2}d_2(x)] * W_I^{(SV)}(z,z_o), \tag{V-25b}$$

$$W_{12}(z,z_o) = [\rho^{-1}d_1(x)] * W_I^{(P)}(z,z_o) - [\rho^{-1}d_1(x)] * W_I^{(SV)}(z,z_o), \tag{V-25c}$$

$$W_{13}(z,z_o) = W_{III}^{(P)}(z,z_o) + [\rho^{-2}d_2(x)] * W_{II}^{(SV)}(z,z_o), \tag{V-25d}$$

$$\vdots$$

$$W_{44}(z,z_o) = -[2k_{SV}^{-2}d_2(x)] * W_I^{(P)}(z,z_o) + [d_o(x)+2k_{SV}^{-2}d_2(x)] * W_I^{(SV)}(z,z_o). \tag{V-25e}$$

Here the sub-operators $W_I^{(P)}\ldots W_{III}^{(P)}$ and $W_I^{(SV)}\ldots W_{III}^{(SV)}$ represent the acoustic sub-operators $W_I\ldots W_{III}$, given by relations (IV-42b,c,d), with α_m, β_m replaced by $\alpha_m^{(P)}$, $\beta_m^{(P)}$ or $\alpha_m^{(SV)}$, $\beta_m^{(SV)}$, respectively:

$$W_I^{(P)}(z,z_o) = \sum_{m=o}^{\infty} \alpha_m^{(P)} d_{2m}(x), \tag{V-25f}$$

$$W_I^{(SV)}(z,z_o) = \sum_{m=o}^{\infty} \alpha_m^{(SV)} d_{2m}(x), \tag{V-25g}$$

$$W_{II}^{(P)}(z,z_o) = \sum_{m=o}^{\infty} \beta_m^{(P)} d_{2m}(x), \tag{V-25h}$$

$$W_{II}^{(SV)}(z,z_o) = \sum_{m=o}^{\infty} \beta_m^{(SV)} d_{2m}(x), \tag{V-25i}$$

$$W_{III}^{(P)}(z,z_o) = -\frac{1}{\rho^2} H_2^{(P)} * W_{II}^{(P)}(z,z_o), \tag{V-25j}$$

$$W_{III}^{(SV)}(z,z_o) = -\frac{1}{\rho^2} H_2^{(SV)} * W_{II}^{(SV)}(z,z_o), \qquad \text{(V-25k)}$$

with

$$\alpha_o^{(P)} = \cos k_P\Delta z,\ \alpha_1^{(P)} = -\frac{\Delta z}{2k_P} \sin k_P\Delta z, \text{ etc.,} \qquad \text{(V-25l,m)}$$

$$\alpha_o^{(SV)} = \cos k_{SV}\Delta z,\ \alpha_1^{(SV)} = -\frac{\Delta z}{2k_{SV}} \sin k_{SV}\Delta z, \text{ etc.,} \qquad \text{(V-25n,o)}$$

$$\beta_o^{(P)} = \frac{\rho}{k_P} \sin k_P\Delta z,\ \beta_1^{(P)} = -\frac{\rho}{2k_P^3} [\sin k_P\Delta z - k_P\Delta z \cos k_P\Delta z], \text{ etc.,} \qquad \text{(V-25p,q)}$$

$$\beta_o^{(SV)} = \frac{\rho}{k_{SV}} \sin k_{SV}\Delta z,\ \beta_1^{(SV)} = -\frac{\rho}{2k_{SV}^3} [\sin k_{SV}\Delta z - k_{SV}\Delta z \cos k_{SV}\Delta z], \text{ etc.,} \qquad \text{(V-25r,s)}$$

If the medium parameters are written as the sum of reference parameters and deviation parameters then sub-operators $W_I^{(P)} \ldots W_{III}^{(P)}$ and $W_I^{(SV)} \ldots W_{III}^{(SV)}$, given by (V-25f,g,h,i,j,k) can be rewritten as rapidly converging two-term operators, conformable to relations (IV-45b,c,d). The excellent dip-angle performance of the acoustic two-way wave field extrapolation operators has been discussed in chapter IV (see also Figure IV-11). Because operator (V-25) contains the same sub-operators, as is shown above, full elastic two-way extrapolation algorithm (V-24) also exhibits a very good dip-angle performance.

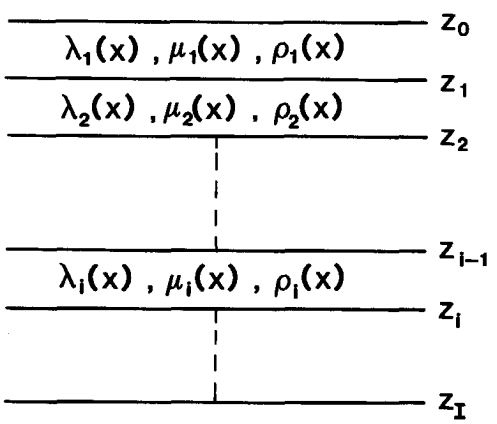

Figure V-1: A computationally convenient subsurface model for recursive full elastic two-way wave field extrapolation in 2-D inhomogeneous solids, based on algorithm (V-24). The pre-stack migration scheme, described in section V.5, is based on this model.

Notice that operator (V-25) has been derived via the wavenumber-frequency domain, hence it may be applied in homogeneous media. Let us now consider the computationally convenient subsurface model, as is shown in Figure V-1. This model consists of a sequence of thin layers, where the medium parameters in the i'th layer ($z_{i-1} \leq z < z_i$) are given by $\lambda_i(x)$, $\mu_i(x)$ and $\rho_i(x)$. For this subsurface model a full elastic two-way wave field extrapolation operator should be derived in the space-frequency domain, based on Taylor series summation, in a similar way as was discussed for the acoustic case in sections IV.4 and IV.5. A discussion of the derivation for the full elastic case is beyond the scope of this thesis. The result of the derivation, assuming that the lateral derivatives of the medium parameters may be neglected, is given by, not surprisingly, operator (V-25), with space dependent coefficients $\alpha_m^{(P)}(x)$, $\alpha_m^{(SV)}(x)$, $\beta_m^{(P)}(x)$ and $\beta_m^{(SV)}(x)$, based on $\lambda_i(x)$, $\mu_i(x)$ and $\rho_i(x)$. Hence, full elastic two-way extrapolation algorithm (V-24) may be applied recursively in inhomogeneous media, as shown in Figure V-1. Notice that at the layer boundaries the boundary conditions are automatically fulfilled, because the extrapolated total wave field $\vec{Q}_s$ is continuous for all depths. This means that transmission effects, multiple reflections and wave conversion are properly incorporated. Finally we remark that critical angle events (related to vertical variations of the medium parameters within the layers) were not considered in this section. The matrix formulation (V-8) of the full elastic two-way wave equation properly includes vertical variations of the medium parameters λ, μ and ρ, hence, full elastic two-way extrapolation operators which include critical angle events can be derived in a similar way as discussed in chapter IV for the acoustic case. A further discussion of critical angle events in solids is beyond the scope of this thesis.

V.4 PRE-STACK MODELING SCHEME BASED ON THE FULL ELASTIC TWO-WAY WAVE EQUATION

An elegant analytical derivation of the exact seismic response of a plane fluid-solid interface to an impulsive monopole line source is given by De Hoop and Van der Hijden (1983). Their approach is very well suited for full elastic modeling applications. In the preceding sections we discussed a relatively easy manageable matrix formalism which describes the full elastic wave propagation effects between two depth levels. This is schematically represented by

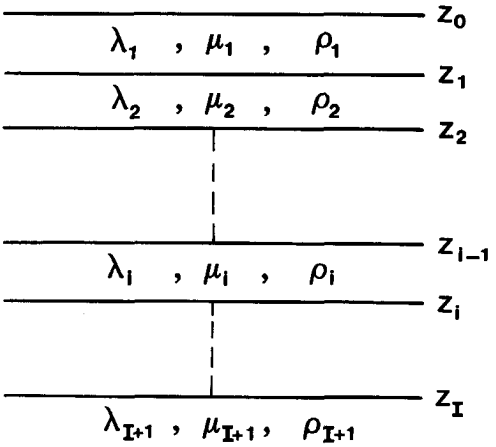

Figure V-2: Subsurface model for the modeling scheme based on the full elastic two-way wave equation. The shear modulus μ_i may be zero for arbitrary i.

$$\begin{bmatrix} j\omega V_z \\ Z_x \\ Z_z \\ j\omega V_x \end{bmatrix}_{z_i} \rightarrow \mathbf{W}_s \rightarrow \begin{bmatrix} j\omega V_z \\ Z_x \\ Z_z \\ j\omega V_x \end{bmatrix}_{z_{i-1}} . \qquad \text{(V-26)}$$

This approach is suited for **modeling** as well as **migration** applications. Because migration is the main subject of this thesis, we discuss full elastic modeling only for simple subsurface geometries. Therefore we consider a horizontally layered medium consisting of I homogeneous layers, as is shown in Figure V-2. We assume homogeneous half spaces for $z<z_0$ and $z \geq z_I$. In layer i, with $z_{i-1} \leq z < z_i$, the medium parameters are given by the Lamé constants λ_i and μ_i and the mass density ρ_i. We consider an arbitrary sequence of liquid layers and solid layers, which means that the shear modulus μ_i may be zero for arbitrary i. We have seen that operator $\mathbf{A}_s$ is singular when $\mu=0$. Therefore special attention must be paid to the behaviour of the total wave field within the different type of layers and particularly at liquid-solid interfaces.
As long as no boundary conditions are specified, then

- within a liquid layer the total wave field $\vec{Q}_\ell=[P,\rho^{-1}\partial_z P]^T=-[Z_z, j\omega V_z]^T$ can be expressed as a linear combination of two arbitrary linearly independent basic wave fields $\vec{Q}_\ell^{(1)}$ and $\vec{Q}_\ell^{(2)}$,
- within a solid layer the total wave field $\vec{Q}_s=[j\omega V_z, Z_x, Z_z, j\omega V_x]^T$ can be expressed as a linear combination of four arbitrary linearly independent basic wave fields $\vec{Q}_s^{(1)}$, $\vec{Q}_s^{(2)}$, $\vec{Q}_s^{(3)}$ and $\vec{Q}_s^{(4)}$.

Due to the radiation condition at $z=z_I$, the number of linearly independent basic wave fields reduces to one in liquid layers ($\vec{Q}_\ell$), and to two in solid layers ($\vec{Q}_s^{(1)}$ and $\vec{Q}_s^{(2)}$), see also step 3.

In the wavenumber-frequency domain (k_x,ω), modeling of P and SV waves consists of the following steps.

1. **Solution of the Boundary Conditions**

   Given the basic wave fields at z_i, then the basic wave fields at $z_i-\varepsilon$, $\varepsilon\to o$, follow easily from the boundary conditions. We consider four cases.

i. At liquid-liquid interfaces, $\tilde{\vec{Q}}_\ell$ is continuous.

ii. At solid-solid interfaces, $\tilde{\vec{Q}}_s^{(1)}$ and $\tilde{\vec{Q}}_s^{(2)}$ are continuous.

iii. Going from solid to fluid, the shear stress $\tilde{Z}_x(z_i)$ vanishes. A linear combination of $\tilde{\vec{Q}}_s^{(1)}$ and $\tilde{\vec{Q}}_s^{(2)}$ should be chosen such that

$$[\,j\omega\tilde{V}_z,\tilde{Z}_x=o,\tilde{Z}_z,j\omega\tilde{V}_x]^T_{z_i} = \nu_1\tilde{\vec{Q}}_s^{(1)} + \nu_2\tilde{\vec{Q}}_s^{(2)}. \qquad \text{(V-27a)}$$

   Now the basic wave field at $z_i-\varepsilon,\varepsilon\to o$, reads

$$\lim_{\varepsilon\to o}\tilde{\vec{Q}}_\ell(z_i-\varepsilon) = -[\tilde{Z}_z,j\omega\tilde{V}_z]^T_{z_i}. \qquad \text{(V-27b)}$$

iv. Going from fluid to solid, the tangential particle velocity $\tilde{V}_x(z_i-\varepsilon)$, $\varepsilon\to o$, can be chosen freely. The basic wave fields at $z_i-\varepsilon,\varepsilon\to o$, can be specified according to

$$\lim_{\varepsilon\to o}\tilde{\vec{Q}}_s^{(1)}(z_i-\varepsilon) = [\,j\omega\tilde{V}_z,\tilde{Z}_x=o,\tilde{Z}_z,j\omega\tilde{V}_x=o]^T_{z_i}, \qquad \text{(V-28a)}$$

$$\lim_{\varepsilon\to o}\tilde{\vec{Q}}_s^{(2)}(z_i-\varepsilon) = [\,j\omega\tilde{V}_z,\tilde{Z}_x=o,\tilde{Z}_z,j\omega\tilde{V}_x=1]^T_{z_i}, \qquad \text{(V-28b)}$$

   where $j\omega\tilde{V}_z(z_i)$ and $\tilde{Z}_z(z_i)$ follow from the basic wave field $\tilde{\vec{Q}}_\ell(z_i)$.

2. **Wave Field Extrapolation**

   Given the basic wave fields at $z_i-\varepsilon,\varepsilon\to o$, then the basic wave fields at z_{i-1} can be found by applying a two-way wave field extrapolation operator for layer i. We consider two cases.

i. In liquid layers the extrapolation algorithm reads

$$\tilde{\mathbf{Q}}_\ell(z_{i-1}) = \tilde{\mathbf{W}}_\ell(z_{i-1},z_i)\tilde{\mathbf{Q}}_\ell(z_i-\varepsilon),\ \varepsilon\to o, \tag{V-29}$$

with extrapolation operator $\tilde{\mathbf{W}}_\ell$ given by relation (IV-21).

ii. In solid layers the extrapolation algorithm reads

$$\tilde{\mathbf{Q}}_s^{(1)}(z_{i-1}) = \tilde{\mathbf{W}}_s(z_{i-1},z_i)\tilde{\mathbf{Q}}_s^{(1)}(z_i-\varepsilon),\ \varepsilon\to o, \tag{V-30a}$$

$$\tilde{\mathbf{Q}}_s^{(2)}(z_{i-1}) = \tilde{\mathbf{W}}_s(z_{i-1},z_i)\tilde{\mathbf{Q}}_s^{(2)}(z_i-\varepsilon),\ \varepsilon\to o, \tag{V-30b}$$

with extrapolation operator $\tilde{\mathbf{W}}_s$ given by relation (V-23).

Above two steps (solution of the boundary conditions and wave field extrapolation), which describe the total modeling procedure for layer i, should be applied recursively.

3. Specification of the Radiation Condition

The procedure (for each k_x and ω-value) starts at $z=z_I$ by specifying the basic wave fields, assuming only downgoing waves are present in the homogeneous lower half space $z\geq z_I$. We consider two cases.

i. For a liquid lower half space we define

$$\tilde{\mathbf{Q}}_\ell(z_I) = \tilde{\mathbf{L}}_\ell(z_I)\tilde{\mathbf{P}}_\ell(z_I), \tag{V-31a}$$

with

$$\tilde{\mathbf{P}}_\ell(z_I) = [\tilde{P}^+=1,\ \tilde{P}^-=o]^T, \tag{V-31b}$$

and $\tilde{\mathbf{L}}_\ell$ being given by relation (IV-16b).

ii. For a solid lower half space we define

$$\tilde{\mathbf{Q}}_s^{(1)}(z_I) = \tilde{\mathbf{L}}_s(z_I)\tilde{\mathbf{P}}_s^{(1)}(z_I), \tag{V-32a}$$

$$\tilde{\mathbf{Q}}_s^{(2)}(z_I) = \tilde{\mathbf{L}}_s(z_I)\tilde{\mathbf{P}}_s^{(2)}(z_I), \tag{V-32b}$$

with

$$\tilde{\mathbf{P}}_s^{(1)}(z_I) = [\tilde{\Phi}^+=1,\ \tilde{\psi}^+=o,\ -\tilde{\Phi}^-=o,\ \tilde{\psi}^-=o]^T, \tag{V-32c}$$

$$\tilde{\mathbf{P}}_s^{(2)}(z_I) = [\tilde{\Phi}^+=o,\ \tilde{\psi}^+=1,\ -\tilde{\Phi}^-=o,\ \tilde{\psi}^-=o]^T, \tag{V-32d}$$

and $\tilde{\mathbf{L}}_s$ being the spatial Fourier transform of $\mathbf{L}_s$, given by (G-2b).

4. **Computation of the Impulse Response**

When the surface $z=z_0$ has been reached, then the plane-wave (PW) impulse response of the subsurface can be calculated. We consider six cases.

i. Layer 1 is a liquid, surface z_0 is reflection free (so the homogeneous upper half space is a liquid as well, with the same properties as layer 1). Because at a reflection free surface the total downgoing wave is given by the downgoing source wave only, an impulse response $\tilde{X}^{(o)}(z_0)$ may be defined according to

$$\tilde{X}^{(o)}(z_0) = \tilde{P}^{-}(z_0)/\tilde{P}^{+}(z_0), \qquad \text{(V-33a)}$$

where $\tilde{P}^{+}(z_0)$ and $\tilde{P}^{-}(z_0)$ follow from

$$\tilde{\underline{P}}_{\ell}(z_0) = [\tilde{P}^{+}(z_0), \tilde{P}^{-}(z_0)]^T = \tilde{\mathbf{L}}_{\ell}^{-1}(z_0)\tilde{\underline{Q}}_{\ell}(z_0), \qquad \text{(V-33b)}$$

$\tilde{\mathbf{L}}_{\ell}^{-1}$ being given by relation (IV-16d).

ii. Layer 1 is a liquid, surface z_0 is characterized by $\tilde{R}^{-}(z_0)$, which describes the pressure reflectivity at the lower side of surface z_0. An impulse response $\tilde{X}(z_0)$ may be defined according to

$$\tilde{X}(z_0) = [1 - \tilde{X}^{(o)}(z_0)\tilde{R}^{-}(z_0)]^{-1}\tilde{X}^{(o)}(z_0), \qquad \text{(V-34)}$$

with $\tilde{X}^{(o)}(z_0)$ given by (V-33). Surface related multiple generation, as described by (V-34), is schematically represented by the feed-back system in Figure V-3.

iii. Layer 1 is a liquid, surface z_0 is pressure free (the upper half space is vacuum). This situation can be handled as above, with $\tilde{R}^{-}(z_0)=-1$. As an alternative we may define an admittance impulse response $\tilde{Y}(z_0)$ which

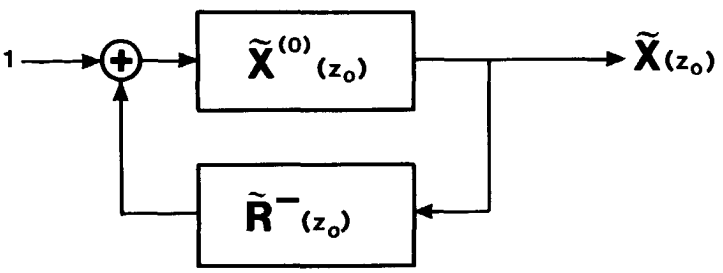

Figure V-3: Feed-back system for surface related multiple generation.

describes the detected total particle velocity due to an impulsive pressure source. Because at a 'pressure free' surface the total pressure is given by the source pressure only, we may write

$$\tilde{Y}(z_o) = \tilde{V}_z(z_o)/\tilde{P}(z_o), \tag{V-35a}$$

where $\tilde{P}(z_o)$ and $\tilde{V}_z(z_o)$ follow from

$$\tilde{\mathbf{Q}}_\ell(z_o) = [\tilde{P}(z_o), -j\omega\tilde{V}_z(z_o)]^T. \tag{V-35b}$$

iv. Layer 1 is a solid, surface z_o is reflection free (the homogeneous upper half space is a solid as well, with the same properties as layer 1). Because at a reflection free surface the total downgoing waves are given by the source waves only, an impulse response $\tilde{\mathbf{X}}^{(o)}(z_o)$ may be defined according to

$$\tilde{\mathbf{X}}^{(o)}(z_o) = \begin{bmatrix} \tilde{X}^{(o)}_{P,P} & \tilde{X}^{(o)}_{P,SV} \\ \tilde{X}^{(o)}_{SV,P} & \tilde{X}^{(o)}_{SV,SV} \end{bmatrix}_{z_o} = \begin{bmatrix} \tilde{\Phi}^-_1 & \tilde{\Phi}^-_2 \\ \tilde{\psi}^-_1 & \tilde{\psi}^-_2 \end{bmatrix}_{z_o} \begin{bmatrix} \tilde{\Phi}^+_1 & \tilde{\Phi}^+_2 \\ \tilde{\psi}^+_1 & \tilde{\psi}^+_2 \end{bmatrix}^{-1}_{z_o} \tag{V-36a}$$

where $\tilde{\Phi}^+_{1,2}(z_o)$ and $\tilde{\psi}^+_{1,2}(z_o)$ follow from

$$\tilde{\mathbf{P}}^{(1)}_s(z_o) = [\tilde{\Phi}^+_1, \tilde{\psi}^+_1, -\tilde{\Phi}^-_1, \tilde{\psi}^-_1]^T_{z_o} = \tilde{\mathbf{L}}^{-1}_s(z_o)\tilde{\mathbf{Q}}^{(1)}_s(z_o), \tag{V-36b}$$

$$\tilde{\mathbf{P}}^{(2)}_s(z_o) = [\tilde{\Phi}^+_2, \tilde{\psi}^+_2, -\tilde{\Phi}^-_2, \tilde{\psi}^-_2]^T_{z_o} = \tilde{\mathbf{L}}^{-1}_s(z_o)\tilde{\mathbf{Q}}^{(2)}_s(z_o), \tag{V-36c}$$

$\tilde{\mathbf{L}}^{-1}_s$ being the spatial Fourier transform of $\mathbf{L}^{-1}_s$, given by (G-2d).
The sub-scripts in matrix $\tilde{\mathbf{X}}^{(o)}$ should be read from right to left. For instance, $\tilde{X}^{(o)}_{SV,P}$ denotes the P-SV impulse response.
Notice that when the shear modulus μ_1 tends to zero, then $\tilde{X}^{(o)}_{P,P}(z_o)$ tends to $\tilde{X}^{(o)}(z_o)$ as defined by (V-33a).

v. Layer 1 is a solid, surface z_o is characterized by $\tilde{\mathbf{R}}^-(z_o)$, which represents the reflectivity matrix (Aki and Richards, 1980) for the lower side of surface z_o. An impulse response $\tilde{\mathbf{X}}(z_o)$ may be defined according to

$$\tilde{\mathbf{X}}(z_o) = [\mathbf{I} - \tilde{\mathbf{X}}^{(o)}(z_o)\tilde{\mathbf{R}}^-(z_o)]^{-1}\tilde{\mathbf{X}}^{(o)}(z_o), \tag{V-37}$$

with $\tilde{\mathbf{X}}^{(o)}(z_o)$ given by (V-36) and where $\mathbf{I}$ represents a 2x2 identity matrix.

vi. Layer 1 is a solid, surface z_o is stress free (the upper half space is vacuum). This situation can be handled as above. Note that in this case $\det[\tilde{\mathbf{R}}^-(z_o)]=1$. As an alternative we may define an admittance impulse response $\tilde{\mathbf{Y}}(z_o)$ which describes the detected total particle velocities due to impulsive stress sources. Because at a 'stress free' surface the total stresses are given by the source stresses only, we may write

$$\tilde{\mathbf{Y}}(z_o) = \begin{bmatrix} \tilde{Y}_{x,x} & \tilde{Y}_{x,z} \\ \tilde{Y}_{z,x} & \tilde{Y}_{z,z} \end{bmatrix}_{z_o} = -\begin{bmatrix} \tilde{V}_x^{(1)} & \tilde{V}_x^{(2)} \\ \tilde{V}_z^{(1)} & \tilde{V}_z^{(2)} \end{bmatrix}_{z_o} \begin{bmatrix} \tilde{Z}_x^{(1)} & \tilde{Z}_x^{(2)} \\ \tilde{Z}_z^{(1)} & \tilde{Z}_z^{(2)} \end{bmatrix}^{-1}_{z_o}, \qquad \text{(V-38a)}$$

where $\tilde{V}_{x,z}^{(1,2)}(z_o)$ and $\tilde{Z}_{x,z}^{(1,2)}(z_o)$ follow from

$$\tilde{Q}_s^{(1)}(z_o) = [j\omega\tilde{V}_z^{(1)}, \tilde{Z}_x^{(1)}, \tilde{Z}_z^{(1)}, j\omega\tilde{V}_x^{(1)}]^T_{z_o}, \qquad \text{(V-38b)}$$

$$\tilde{Q}_s^{(2)}(z_o) = [j\omega\tilde{V}_z^{(2)}, \tilde{Z}_x^{(2)}, \tilde{Z}_z^{(2)}, j\omega\tilde{V}_x^{(2)}]^T_{z_o}. \qquad \text{(V-38c)}$$

Notice that when the shear modulus μ_1 tends to zero, then $\tilde{Y}_{z,z}(z_o)$ tends to $\tilde{Y}(z_o)$ as defined by (V-35a).

5. Specification of the Source and Detector Properties

Next the source and detector properties can be included. Again we consider six cases.

i. Layer 1 is a liquid, surface z_o is reflection free. We may write for the detected upgoing pressure wave $\tilde{P}^-_{CSP}(z_o)$ in a common-shotpoint gather (CSP) in the wavenumber-frequency domain

$$\tilde{P}^-_{CSP}(z_o) = \tilde{D}_P(z_o)\tilde{X}^{(o)}(z_o)\tilde{S}^+(z_o), \qquad \text{(V-39)}$$

where $\tilde{S}^+(z_o)$ represents the downgoing source pressure wave, $\tilde{X}^{(o)}(z_o)$ represents the PW impulse response, given by (V-33) and $\tilde{D}_P(z_o)$ represents the pressure detector transfer function. (Ideally $\tilde{D}_P(z_o)$ is a function of ω only: $\tilde{D}_P(z_o)=D_P(\omega)$).

ii. Layer 1 is a liquid, surface z_o is characterized by $\tilde{R}^-(z_o)$. Again we may apply (V-39), with $\tilde{X}^{(o)}(z_o)$ replaced by $\tilde{X}(z_o)$, given by (V-34).

iii. Layer 1 is a liquid, surface z_o is pressure free. For the detected

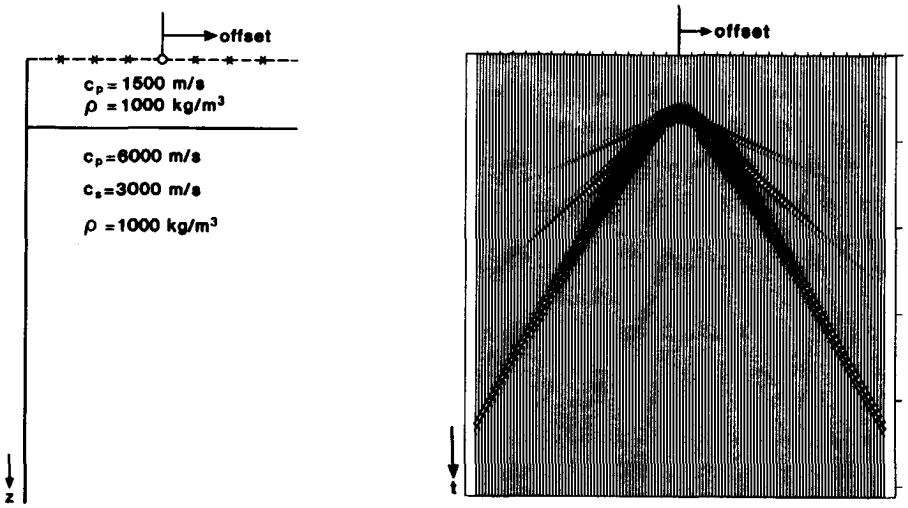

Figure V-4: Marine data modeled with the full elastic two-way wave equation.
a. Subsurface model
b. CSP gather in x,t-domain

particle velocity $\tilde{V}_{z,CSP}(z_o)$ in a CSP gather we may write

$$\tilde{V}_{z,CSP}(z_o) = \tilde{D}_V(z_o)\tilde{Y}(z_o)\tilde{S}(z_o), \qquad \text{(V-40)}$$

where $\tilde{S}(z_o)$ represents the pressure source, $\tilde{Y}(z_o)$ represents the admittance impulse response, given by (V-35) and $\tilde{D}_V(z_o)$ represents the particle velocity detector transfer function. (Ideally, $\tilde{D}_V(z_o)=D_V(\omega)$).

iv. Layer 1 is a solid, surface z_o is reflection free. For the upgoing reflected P and SV waves $\tilde{\mathcal{P}}^-_{refl}=[\tilde{\Phi}^-_{refl},\tilde{\Psi}^-_{refl}]^T$ due to downgoing incident P and SV waves $\tilde{\mathcal{P}}^+_{inc}=[\tilde{\Phi}^+_{inc},\tilde{\Psi}^+_{inc}]^T$ we may write

$$\tilde{\mathcal{P}}^-_{refl}(z_o) = \tilde{\mathbf{X}}^{(o)}(z_o)\tilde{\mathcal{P}}^+_{inc}(z_o), \qquad \text{(V-41)}$$

where $\tilde{\mathbf{X}}^{(o)}(z_o)$ represents the impulse response, given by (V-36). Notice that, unlike in (V-39), we did not introduce source functions and detector transfer functions because sources and detectors for individual P and SV waves do not exist.

v. Layer 1 is a solid, surface z_o is characterized by $\tilde{\mathbf{R}}^-(z_o)$. Again we may apply (V-41), with $\tilde{\mathbf{X}}^{(o)}(z_o)$ replaced by $\tilde{\mathbf{X}}(z_o)$, given by (V-37).

vi. Layer 1 is a solid, surface z_o is stress free. For the detected particle velocity $\tilde{\mathbf{V}}_{CSP}(z_o)=[\tilde{V}_{x,CSP},\tilde{V}_{z,CSP}]^T$ in a CSP gather we may write

$$\tilde{\mathbf{V}}_{CSP}(z_o) = -\tilde{\mathbf{D}}_V(z_o)\tilde{\mathbf{Y}}(z_o)\tilde{\mathbf{Z}}_{SRC}(z_o), \qquad (V\text{-}42)$$

where $\tilde{\mathbf{Z}}_{SRC}(z_o)=[\tilde{Z}_{x,SRC},\tilde{Z}_{z,SRC}]^T_{z_o}$ represents the stress source, $\tilde{\mathbf{Y}}(z_o)$ represents the impulse response, given by (V-38), and $\tilde{\mathbf{D}}_V(z_o)$ represents the particle velocity detector transfer function. (Ideally, $\tilde{\mathbf{D}}_V(z_o)$ is a function of ω only: $\tilde{\mathbf{D}}_V(z_o)=D_V(\omega)\,\mathbf{I}$).

6. **Inverse Fourier transforms**

When this modeling procedure has been applied for all wavenumbers and frequencies, then the space-time data (one shot record) are obtained after inverse temporal and spatial Fourier transforms.

Examples

A CSP gather was modeled for the marine subsurface configuration shown in Figure V-4a. The surface is assumed reflection free, the first layer is a liquid (sea water), while the lower half space is a solid. Figure V-4b shows the CSP gather in the space-time domain (x,t). Notice that an ordinary reflected P wave, as well as P and SV head-waves are clearly visible.

Also a CSP gather was modeled for the land subsurface configuration shown in Figure V-5a. A vertical stress is imposed in one point at the free surface. The resulting particle velocity at the surface is shown in the x,t domain in Figures V-5b (vertical component) and V-5c (horizontal component). Notice that primary P and SV waves, as well as many multiple reflected and converted waves are visible in these figures. Also notice the opposite polarities of the horizontal component of the particle velocity at both sides of the vertical stress source.

The advantage of the modeling scheme, introduced in this section, is that all primary and multiple P as well as SV waves are included in the simple recursion algorithms (V-29) and (V-30), while the boundary conditions at the layer interfaces are solved very easy. For 2-D and 3-D inhomogeneous media, modeling techniques based on full elastic two-way depth extrapolation become very complicated and two-way time extrapolation techniques are preferred. A 2-D application is presented by Reshef and Kosloff (1985). An extensive discussion of modeling algorithms, however, is beyond the scope of this thesis.

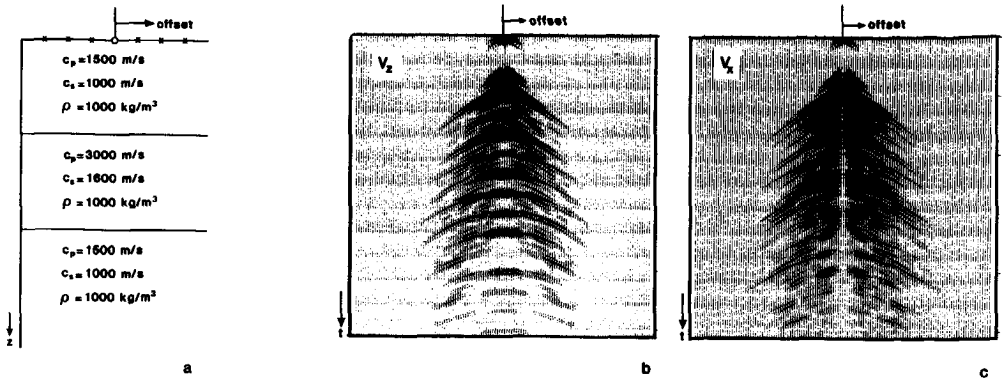

Figure V-5: Land data, modeled with the full elastic two-way wave equation.
a. Subsurface model
b. Vertical component of the particle velocity in the x,t-domain
c. Horizontal component of the particle velocity in the x,t-domain

V.5 PRE-STACK MIGRATION SCHEME BASED ON THE FULL ELASTIC TWO-WAY WAVE EQUATION

It was argued in chapter I that for full elastic two-way wave equation migration a common-depthpoint (CDP) oriented technique should be chosen. In chapter II we have extensively discussed the principle of full pre-stack migration by single-shot record inversion (SSRI) and CDP stacking and in chapter IV we have discussed the acoustic two-way approach to full pre-stack migration by SSRI and CDP stacking. It was shown that the scheme is in principle based on inverting relation (IV-58), which is schematically represented by

$$\begin{bmatrix} P \\ \frac{1}{\rho}\frac{\partial P}{\partial z} \end{bmatrix}_{z_i} \leftarrow \mathbf{W}_\ell \leftarrow \begin{bmatrix} P \\ \frac{1}{\rho}\frac{\partial P}{\partial z} \end{bmatrix}_{z_{i-1}} . \qquad \text{(V-43)}$$

In this section we discuss the full elastic approach to full pre-stack migration by SSRI and CDP stacking. The scheme is in principle based on inverting relation (V-26), which is schematically represented by

$$\begin{bmatrix} j\omega V_z \\ Z_x \\ Z_z \\ j\omega V_x \end{bmatrix}_{z_i} \leftarrow \mathbf{W}_s \leftarrow \begin{bmatrix} j\omega V_z \\ Z_x \\ Z_z \\ j\omega V_x \end{bmatrix}_{z_{i-1}}, \qquad \text{(V-44)}$$

and is very similar to the acoustic scheme. The total scheme consists of the following steps:

1. **Partly compensation for the acquisition limitations and composition of the total wave vector $\vec{Q}_s$ at the surface z_o.**
We consider a stress free surface and assume that the detected particle velocity vector $\vec{V}_{CSP,m}$ in the m'th CSP gather is related to the m'th source stress vector $\vec{Z}_{SRC,m}$ according to

$$\vec{V}_{CSP,m}(z_o) = -\mathbf{D}_v(z_o)\,\mathbf{Y}(z_o)\vec{Z}_{SRC,m}(z_o), \qquad \text{(V-45a)}$$

or

$$\begin{bmatrix} V_{x,CSP,m}(x,z_o,\omega) \\ V_{z,CSP,m}(x,z_o,\omega) \end{bmatrix} = \qquad \text{(V-45b)}$$

$$-\begin{bmatrix} D_v(\omega)\delta(x)^* & o \\ o & D_v(\omega)\delta(x)^* \end{bmatrix} \begin{bmatrix} Y_{x,x}(x,z_o,\omega)^* & Y_{x,z}(x,z_o,\omega)^* \\ Y_{z,x}(x,z_o,\omega)^* & Y_{z,z}(x,z_o,\omega)^* \end{bmatrix} \begin{bmatrix} \delta(x-x_m)S(\omega)Z_x(z_o) \\ \delta(x-x_m)S(\omega)Z_z(z_o) \end{bmatrix}.$$

Acquisition parameters and medium parameters can be separately described as follows

$$\begin{bmatrix} V_{x,CSP,m}(x,z_o,\omega) \\ V_{z,CSP,m}(x,z_o,\omega) \end{bmatrix} = [D_v(\omega)S(\omega)] \begin{bmatrix} V_{x,m}(x,z_o,\omega) \\ V_{z,m}(x,z_o,\omega) \end{bmatrix}, \qquad \text{(V-46a)}$$

where

$$\begin{bmatrix} V_{x,m}(x,z_o,\omega) \\ V_{z,m}(x,z_o,\omega) \end{bmatrix} = -\mathbf{Y}(z_o) \begin{bmatrix} \delta(x-x_m)Z_x(z_o) \\ \delta(x-x_m)Z_z(z_o) \end{bmatrix}. \qquad \text{(V-46b)}$$

Notice that $V_{x,m}(x,z_o,\omega)$ and $V_{z,m}(x,z_o,\omega)$ can be resolved from the measured data by inverting (V-46a) in a band-limited way (deconvolution). Relation (V-46b) describes the m'th seismic experiment, corrected for the source and detector spectra $S(\omega)$ and $D_v(\omega)$, respectively. According to this relation the total wave field at the surface reads

$$\vec{Q}_{s,m}(z_o) = \begin{bmatrix} j\omega V_{z,m}(x,z_o,\omega) \\ \delta(x-x_m)Z_x(z_o) \\ \delta(x-x_m)Z_z(z_o) \\ j\omega V_{x,m}(x,z_o,\omega) \end{bmatrix} . \qquad \text{(V-47)}$$

2a. **Recursive downward extrapolation of the total wave field,** according to

$$\vec{Q}_{s,m}(z_i) = \mathbf{W}_s(z_i,z_{i-1})\vec{Q}_{s,m}(z_{i-1}). \qquad \text{(V-48)}$$

For the computationally convenient macro subsurface model of Figure V-1, operator $\mathbf{W}_s$ represents a truncated version of the fast converging finite difference operator (V-25) in the space-frequency domain, optionally rewritten as a two-term operator. For the special situation that lateral variations of the medium parameters may be neglected, this step should preferably be applied in the wavenumber-frequency domain, with operator $\tilde{\mathbf{W}}_s$ given by relation (V-23).

2b. **Decomposition of the total wave field into downgoing and upgoing P and SV waves,** according to

$$\vec{P}_{s,m}(z_i) = \mathbf{L}_s^{-1}(z_i)\vec{Q}_{s,m}(z_i), \qquad \text{(V-49a)}$$

with

$$\vec{P}_{s,m}(z_i) = \begin{bmatrix} \Phi_m^+(x,z_i,\omega) \\ \psi_m^+(x,z_i,\omega) \\ -\Phi_m^-(x,z_i,\omega) \\ \psi_m^-(x,z_i,\omega) \end{bmatrix} , \qquad \text{(V-49b)}$$

and where decomposition operator $\mathbf{L}_s^{-1}$ is given by relation (G-2d). Unfortunately this operator converges slowly. However, in practice it is often sufficient to apply the decomposition in the wavenumber-frequency domain for a reference medium only, by means of operator $\tilde{\mathbf{L}}_s^{-1}$. It should

be noted that errors in the decomposed wave field $\vec{P}_{s,m}$ do not contribute to deeper depth levels, because the total wave field $\vec{Q}_{s,m}$ is downward extrapolated independently in step 2a. The downgoing and upgoing waves at the current depth level are related to each other according to

$$\vec{P}^{-}_{s,m}(z_i) = \mathbf{X}(z_i)\vec{P}^{+}_{s,m}(z_i), \tag{V-50a}$$

or

$$\begin{bmatrix} \Phi^{-}_m(x,z_i,\omega) \\ \psi^{-}_m(x,z_i,\omega) \end{bmatrix} = \begin{bmatrix} X_{P,P}(x,z_i,\omega)^* & X_{P,SV}(x,z_i,\omega)^* \\ X_{SV,P}(x,z_i,\omega)^* & X_{SV,SV}(x,z_i,\omega)^* \end{bmatrix} \begin{bmatrix} \Phi^{+}_m(x,z_i,\omega) \\ \psi^{+}_m(x,z_i,\omega) \end{bmatrix} \tag{V-50b}$$

where $\mathbf{X}(z_i)$ describes the impulse response of the subsurface. Inversion of this relation requires at least one more independent seismic experiment being carried out at the same source location x_m, such that the vectors $\vec{P}^{+}_{s,m}$ and $\vec{P}^{-}_{s,m}$ can be extended to matrices. This is not very attractive from a practical point of view and therefore we propose an inversion procedure analogous to the one-way procedure described in chapter II. Therefore we first need to extract the downgoing source wave from the total downgoing wave field. Because $c_P > c_{SV}$ we may extract the dilatational part (P wave) of the downgoing source wave from the downgoing wave $\Phi^{+}_m(x,z_i,\omega)$ by means of a first arrival time window, yielding $\Phi^{+}_{SRC,m}(x,z_i,\omega)$. This actually means that multiple reflected waves are excluded from the imaging procedure, as is demonstrated in an example below.

3. **Correlation** of the downgoing source P wave and the upgoing reflected P and SV waves, yielding the single-fold ZO P-P and P-SV impulse responses

$$\langle X_{ZO;P,P}(x,z_i,\omega)\rangle_m = \frac{1}{s_m^2}\,\Phi^{-}_m(x,z_i,\omega)[\Phi^{+}_{SRC,m}(x,z_i,\omega)]^*, \tag{V-51a}$$

$$\langle X_{ZO;SV,P}(x,z_i,\omega)\rangle_m = \frac{1}{s_m^2}\,\psi^{-}_m(x,z_i,\omega)[\Phi^{+}_{SRC,m}(x,z_i,\omega)]^*, \tag{V-51b}$$

where

$$s_m^2 = \int \Phi^{+}_{SRC,m}(x,z_i,\omega)[\Phi^{+}_{SRC,m}(x,z_i,\omega)]^* dx. \tag{V-51c}$$

Notice that we cannot define the SV-P and the SV-SV impulse responses because we do not have an expression for the downgoing SV source wave. The fact that only two out of four impulse responses can be resolved is in agreement with an observation we made before: proper inversion requires additional information obtained from an extra independent seismic experiment, carried out at the same source location.
Notice that, with definition (V-51a), $\langle X_{ZO;P,P} \rangle_m$ may still contain multiple reflected and converted waves. These are eliminated by the imaging step. A similar remark holds for $\langle X_{ZO;SV,P} \rangle_m$, given by relation (V-51b).

4. **Imaging** by summing over all frequencies, yielding the single-fold ZO P-P and P-SV reflectivities:

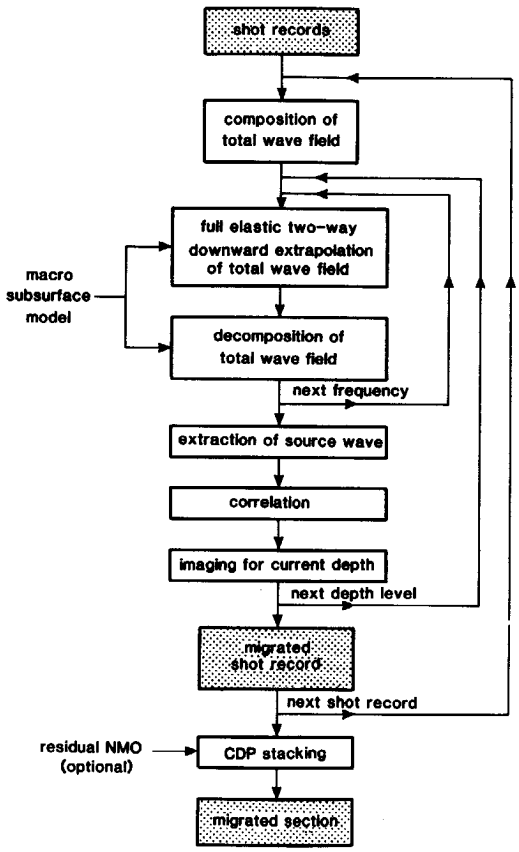

Figure V-6: Computational diagram of the shot record oriented pre-stack migration scheme, based on the full elastic two-way wave equation.

$$\langle R_{ZO;P,P}(x,z_i)\rangle_m = \frac{\Delta\omega}{2\pi}\sum_{\omega}\langle X_{ZO;P,P}(x,z_i,\omega)\rangle_m, \qquad \text{(V-52a)}$$

$$\langle R_{ZO;SV,P}(x,z_i)\rangle_m = \frac{\Delta\omega}{2\pi}\sum_{\omega}\langle X_{ZO;SV,P}(x,z_i,\omega)\rangle_m. \qquad \text{(V-52b)}$$

5. **CDP stacking** by summing all single-fold ZO reflectivity functions, yielding the multi-fold wide-angle ZO P-P and P-SV reflectivities

$$\langle R^{CDP}_{ZO;P,P}(x,z_i)\rangle = \sum_m \langle R_{ZO;P,P}(x,z_i)\rangle_m, \qquad \text{(V-53a)}$$

$$\langle R^{CDP}_{ZO;SV,P}(x,z_i)\rangle = \sum_m \langle R_{ZO;SV,P}(x,z_i)\rangle_m. \qquad \text{(V-53b)}$$

The computational diagram is shown in Figure V-6.

Example

The performance of the algorithm is demonstrated with a simple numerical example. We consider a horizontally layered 1-D inhomogeneous medium. In this case the whole procedure can be applied in the wavenumber-frequency domain. As an alternative we replace the ZO imaging step by a plane-wave (PW) imaging step, according to

$$\langle \tilde{R}_{P,P}(p,z_i)\rangle = \frac{\Delta\omega}{2\pi}\sum_{\omega}{}' \tilde{X}_{P,P}(k_x,z_i,\omega), \qquad \text{(V-54a)}$$

$$\langle \tilde{R}_{SV,P}(p,z_i)\rangle = \frac{\Delta\omega}{2\pi}\sum_{\omega}{}' \tilde{X}_{SV,P}(k_x,z_i,\omega), \qquad \text{(V-54b)}$$

where

$$\tilde{X}_{P,P}(k_x,z_i,\omega) \triangleq \tilde{\Phi}^{-}(k_x,z_i,\omega)/\tilde{\Phi}^{+}_{SRC}(k_x,z_i,\omega), \qquad \text{(V-54c)}$$

$$\tilde{X}_{SV,P}(k_x,z_i,\omega) \triangleq \tilde{\psi}^{-}(k_x,z_i,\omega)/\tilde{\Phi}^{+}_{SRC}(k_x,z_i,\omega) \qquad \text{(V-54d)}$$

in some stable sense. The symbol $\sum'$ denotes that the summation is carried out for constant ray-parameter $p=k_x/\omega$ (constant propagation direction, see also section III.9).

Figure V-7a shows again the subsurface configuration of the second modeling example (Figure V-5a). The top frame of Figure V-7b shows one trace of a τ-p map of the vertical component of the particle velocity data (Figure V-5b) for one constant p-value (constant k_x/ω), such that $\sin\theta(z_o)=pc_P(z_o)=.47$, that

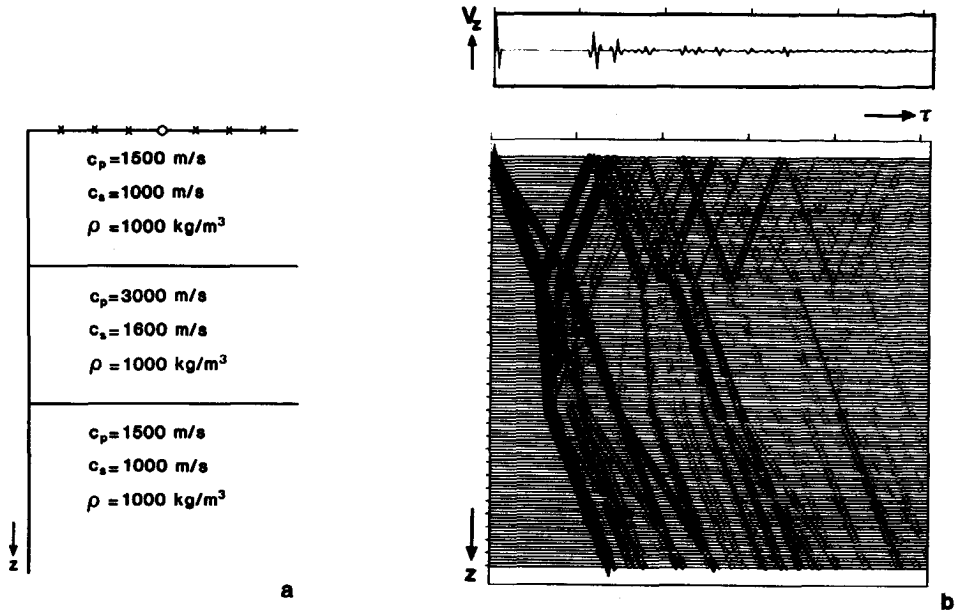

Figure V-7: Results of full elastic two-way wave equation migration for a horizontally layered medium.

a. Subsurface model.

b. Vertical component of the particle velocity as a function of intercept time registered at the surface (top frame) and downward extrapolated (bottom frame).

is, for one oblique plane-wave with incidence angle $\theta(z_o)$=28°. Because the data are presented as a function of the intercept time τ, all reflection events related to this single plane-wave are visible. Notice that besides primary P waves many multiple reflected and converted waves are present, which makes the trace difficult to interpret, even for this simple two-layer model. However, the interpretability improves significantly when the data are downward extrapolated, using the full elastic two-way wave field extrapolation operator. The downward extrapolated vertical component of the particle velocity is shown in the bottom frame of Figure V-7b as a function of depth and intercept time, again for one p-value. Similar pictures could be shown for the horizontal component of the particle velocity and for the two components of the stress tensor. Notice that, similarly as in a vertical seismic profile (VSP) recorded in a vertical bore hole, all wave types can be clearly recognized. The decomposed data are shown in Figure V-7c, again as a function of depth and intercept time for one p-value. Notice that the downward extrapolated upgoing

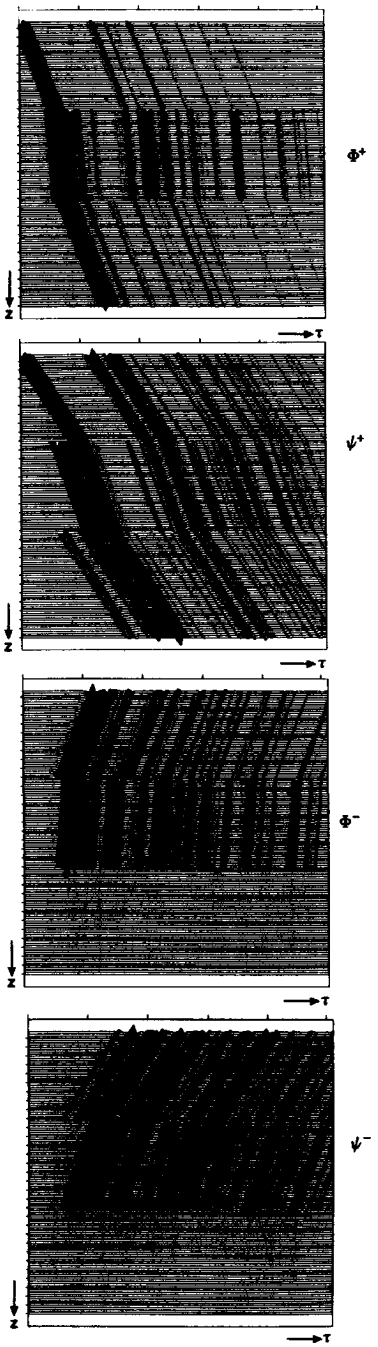

Figure V-7: (continued) c. Decomposed data: from top to bottom: downgoing compressional waves, downgoing shear waves, upgoing compressional waves, upgoing shear waves.

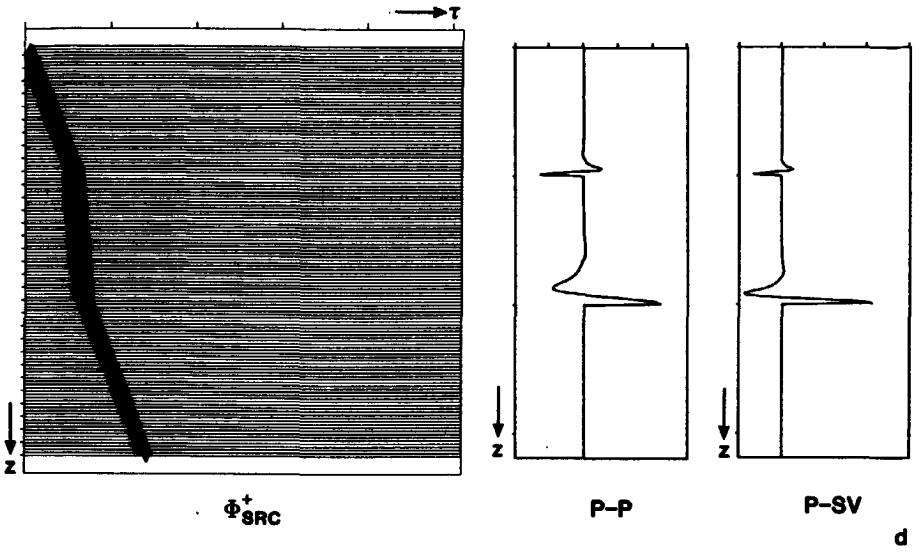

Figure V-7: (continued) d. Downgoing compressional source wave (left frame), PW imaged P-P reflectivity (middle frame) and PW imaged P-SV reflectivity (right frame).

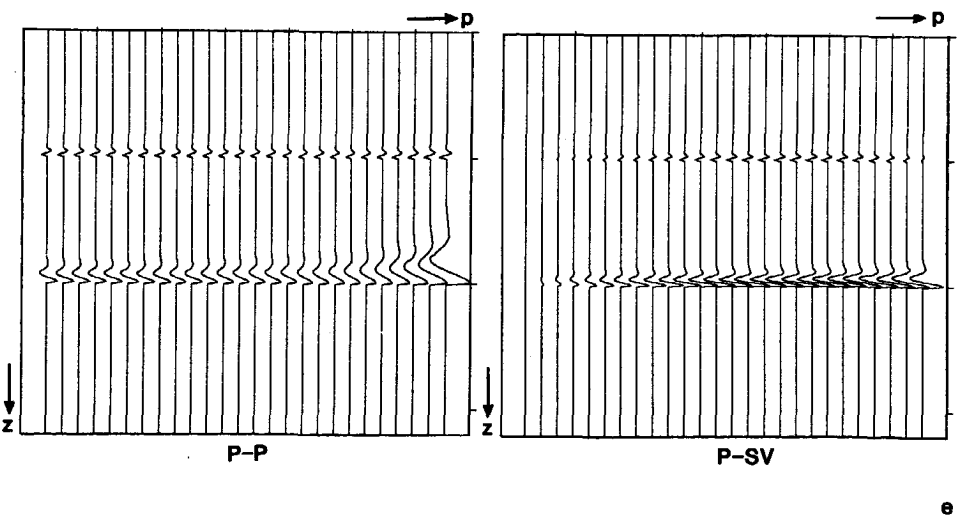

Figure V-7: (continued) e. PW imaged results for all incidence angles; P-P reflectivity (left frame) and P-SV reflectivity (right frame).

waves are terminated at the reflectors, which is a typical property of the two-way approach. The left frame of Figure V-7d shows the compressional down-going source wave which has been retrieved from the upper frame of Figure V-7c by means of a first arrival time window. Also in Figure V-7d the PW imaged P-P and P-SV reflectivities are presented as a function of depth. Notice that these PW images show the two reflectors only, in spite of the complex nature of the input trace (top frame of Figure V-7b). Sofar we showed the migration procedure for one plane-wave only. The procedure can be repeated for all angles of incidence. In Figure V-7e the PW imaged P-P and P-SV reflectivities are shown as a function of depth for various ray-parameters. Notice that the angle dependent reflection behaviour is clearly visible in these data.
For this 1-D inhomogeneous medium PW imaging was carried out outside the depth extrapolation loop and one shot record was considered only. For 2-D inhomogeneous media ZO imaging should be carried out inside the depth extrapolation loop and the procedure should be repeated for all shot records, conformably to the computational diagram shown in Figure V-6.

Summarizing, in this section we introduced a CDP oriented pre-stack migration scheme based on the full elastic two-way wave equation. Notice the following advantages of this scheme in comparison with conventional acoustic one-way schemes

- use of the square-root operator is avoided,
- transmission effects are automatically included,
- multiple reflected waves may be properly handled,
- converted waves may be properly handled.

The transmission effects, multiple reflected and converted waves are properly handled because the extrapolated total wave field $\vec{Q}_s$ is continuous for all depths as long as only solid layers are considered. Problems occur if the macro subsurface model consists of liquid as well as solid layers because the horizontal component V_x of the particle velocity may be discontinuous at liquid-solid interfaces. Of course, given the source configuration as well as a complete description of the subsurface, V_x just below a liquid-solid interface is uniquely defined. However, it cannot be obtained from V_x just above the liquid-solid interface. For this reason full elastic migration of, for instance, marine data is impracticable.

For a proper handling of multiple reflected and converted waves (in case of land data), accurate knowledge of the macro subsurface model is required. Similar as in conventional multiple elimination schemes, a small mis-positioning of the major reflecting boundaries may result in an increase of undesired reflection events, so the migration scheme should preferably be applied iteratively. On the other hand, the generation of undesired reflection events may be avoided by spatially filtering (smoothing) the abrupt changes in the macro subsurface model before migration. Of course multiple reflected and converted waves will then not be properly handled anymore.

Another approach to full elastic migration is proposed by Kennet (1984). In his approach **all** CSP gathers must be handled simultaneously. In addition, **two** independent seismic experiments are required for each source location. For comparison, the full elastic two-way pre-stack migration scheme, as proposed in this chapter, including multiple elimination, is carried out on **single**-shot records, similar as the acoustic one-way pre-stack primary migration scheme, as discussed in chapter II.

V.6 CONCLUDING REMARKS

In chapter IV we have discussed the following matrix representation of the acoustic wave equation

$$\frac{\partial \vec{Q}_\ell}{\partial z} = \mathbf{A}_\ell \vec{Q}_\ell \qquad \text{(V-55a)}$$

and

$$\frac{\partial \vec{P}_\ell}{\partial z} = \mathbf{B}_\ell \vec{P}_\ell, \qquad \text{(V-55b)}$$

where the sub-script ℓ refers to liquids. Expression (V-55a) represents the **two-way** wave equation for the total wave field $\vec{Q}_\ell=[P,\rho^{-1}\partial_z P]^T$. Expression (V-55b) represents the **one-way** wave equations for the decomposed wave field $\vec{P}_\ell=[P^+,P^-]^T$. This decomposition is described by

$$\vec{P}_\ell = \mathbf{L}_\ell^{-1}\vec{Q}_\ell. \qquad \text{(V-55c)}$$

In this chapter we discussed the following matrix representation of the full elastic wave equation

$$\frac{\partial \vec{Q}_s}{\partial z} = \mathbf{A}_s \vec{Q}_s \qquad \text{(V-56a)}$$

and

$$\frac{\partial \vec{P}_s}{\partial z} = \mathbf{B}_s \vec{P}_s, \qquad \text{(V-56b)}$$

where the sub-scipt s refers to solids. Expression (V-56a) represents the two-way wave equation for the total wave field $\vec{Q}_s=[j\omega V_z, Z_x, Z_z, j\omega V_x]^T$. Expression (V-56b) represents the one-way wave equations for the decomposed wave field $\vec{P}_s=[\Phi^+,\psi^+,-\Phi^-,\psi^-]^T$. This decomposition is described by

$$\vec{P}_s = \mathbf{L}_s^{-1}\vec{Q}_s. \qquad \text{(V-56c)}$$

Because the square-root operator is avoided in the two-way wave equations (V-55a) and (V-56a), explicit finite-difference two-way wave field extrapolation operators $\mathbf{W}_\ell$ and $\mathbf{W}_s$ for $\vec{Q}_\ell$ and $\vec{Q}_s$, respectively, converge rapidly. These operators can be used recursively in inhomogeneous media, assuming that the lateral derivatives of the medium parameters may be neglected.

Pre-stack migration based on the full elastic two-way wave equation is in principle founded on two-way downward extrapolation, which is schematically represented by

$$\begin{bmatrix} j\omega V_z \\ Z_x \\ Z_z \\ j\omega V_x \end{bmatrix}_{z_i} \leftarrow \mathbf{W}_s \leftarrow \begin{bmatrix} j\omega V_z \\ Z_x \\ Z_z \\ j\omega V_x \end{bmatrix}_{z_{i-1}}, \qquad \text{(V-57a)}$$

followed by decomposition

$$\begin{bmatrix} \Phi^+ \\ \psi^+ \\ -\Phi^- \\ \psi^- \end{bmatrix}_{SRC,z_i} \xleftarrow{\text{window}} \begin{bmatrix} \Phi^+ \\ \psi^+ \\ -\Phi^- \\ \psi^- \end{bmatrix}_{z_i} \leftarrow \mathbf{L}_s^{-1} \leftarrow \begin{bmatrix} j\omega V_z \\ Z_x \\ Z_z \\ j\omega V_x \end{bmatrix}_{z_i}, \qquad \text{(V-57b)}$$

and imaging

$$\Phi^{+}_{SRC}(z_i) \rightarrow \langle R_{P,P}(z_i) \rangle \leftarrow \Phi^{-}(z_i), \qquad \text{(V-57c)}$$

$$\Phi^{+}_{SRC}(z_i) \rightarrow \langle R_{SV,P}(z_i) \rangle \leftarrow \psi^{-}(z_i). \qquad \text{(V-57d)}$$

This CDP oriented scheme assumes 2-D wave propagation in 1-D or 2-D inhomogeneous macro subsurface models. It properly handles multiple reflections and wave conversion if the macro subsurface model is accurately known. For smoothed macro subsurface models a high dip angle performance for primary waves may be expected. For 3-D wave propagation in 1-D, 2-D and 3-D inhomogeneous macro subsurface models the scheme is not valid because the conversion between P and SV waves on one hand and SH waves on the other hand cannot be longer neglected. Hence, for the 3-D case the scheme should be based on a modified full elastic two-way wave equation which describes all wave types (P, SV and SH) simultaneously. Therefore the wave vector $\vec{Q}_s$ should also contain the y-components of the particle velocity vector $\vec{V}$ and the stress vector $\vec{Z}$. Analogous to the derivation in section V.2 it can be shown that for this extended wave vector the following full elastic two-way wave equation holds:

$$\frac{\partial \vec{Q}_s}{\partial z} = \mathbf{A}_s \vec{Q}_s, \qquad \text{(V-58a)}$$

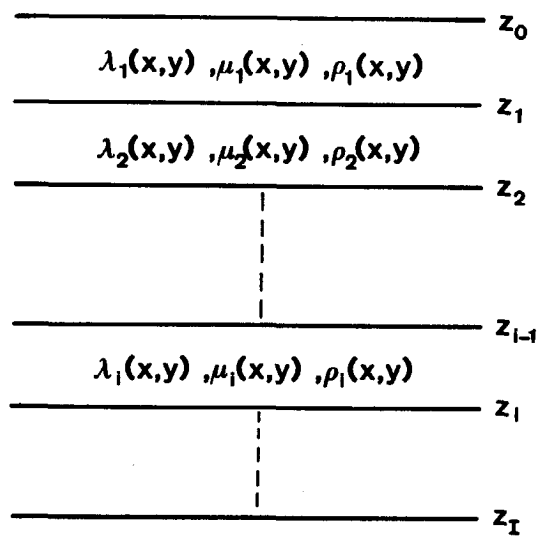

Figure V-8: A computationally convenient subsurface model for recursive full elastic two-way wave field extrapolation in 3-D inhomogeneous solids.

with

$$\vec{Q}_s = \begin{bmatrix} j\omega V_z \\ Z_x \\ Z_y \\ Z_z \\ j\omega V_x \\ j\omega V_y \end{bmatrix}, \qquad \text{(V-58b)}$$

and 6x6 matrix operator $\mathbf{A}_s$ given in Appendix H. The solution for 1-D inhomogeneous media is given by Ursin (1983), assuming constant medium parameters in a certain depth interval. The solution for 2-D and 3-D inhomogeneous media can be found in a similar way as described in section V.3, assuming the computationally convenient macro subsurface model, as shown in Figure V-8. Based on this solution, a full elastic pre-stack migration scheme for 3-D inhomogeneous macro subsurface models can be designed in a similar way as described in section V.5. A further discussion is beyond the scope of this thesis.

CHAPTER VI

PRACTICAL ASPECTS OF 3-D PRE-STACK MIGRATION

VI.1 INTRODUCTION

In the preceding chapters theoretical aspects of pre-stack migration have been discussed. It may be concluded that the ideal pre-stack migration scheme should be based on 3-D single-shot record inversion (SSRI), followed by common-depth-point (CDP) stacking. Furthermore, in the ideal scheme it should be assumed that all wave propagation effects, including multiple reflections and wave conversions, are governed by the full elastic two-way wave equation for a 3-D geologically oriented elastic macro model of the subsurface. By properly eliminating these propagation effects per common-shotpoint (CSP) gather, the reflectivity properties of the elastic micro and macro subsurface model can be optimumly resolved. It is obvious that the practical implementation of this ideal pre-stack migration scheme is far beyond reach of nowadays vector computers. This is easily appreciated if one considers the 3-D version of the full elastic two-way wave equation, as described by relation (V-58). The solution of this equation is given by a full elastic two-way wave field extrapolation matrix consisting of 36 sub-operators. However, even in the acoustic one-way approach, where the number of operators reduces to two (one operator for forward extrapolation of the downgoing source wave and one operator for inverse extrapolation of the reflected upgoing waves), full 3-D pre-stack migration still requires a computational power much stronger than what is available today. Finally, the ideal 3-D pre-stack migration scheme assumes an extensive areal data acquisition configuration, which is seldom realized in practice. For instance, a 3-D marine survey merely consists of a number of 2-D

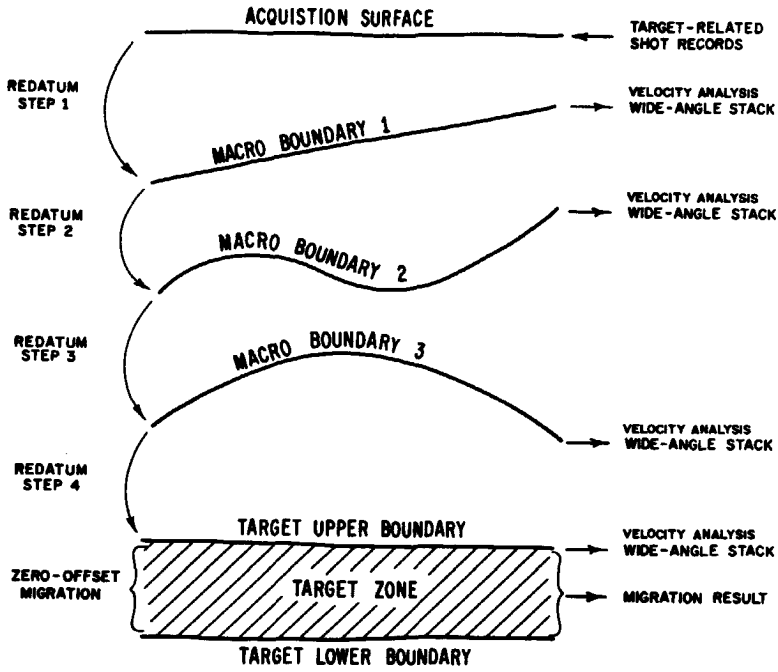

Figure VI-1: Principle of target oriented 3-D pre-stack migration.

surveys (seismic lines), as is visualized in Figure I-1a. Particularly for the (acoustic or full elastic) two-way approach to 3-D pre-stack migration these incomplete 'boundary conditions' represent a serious drawback.

It is obvious that, given the limitations of nowadays computational power, a more practical approach to 3-D pre-stack migration is required. In many practical situations seismic interpreters are mainly interested in a high resolution image of a pre-specified target zone. Hence, much work can be saved by applying 'target-oriented' 3-D pre-stack migration without the need to simplify the underlying principles of the algorithm. The details of target oriented 3-D processing are discussed in this chapter. It is shown with the aid of a synthetic data example as well as a scale-model data example that high quality images can be obtained in realistic processing times. Furthermore it is shown that the method can cope with pseudo 3-D acquisition techniques when use is made of the acoustic one-way wave equations.

VI.2 PRINCIPLE OF TARGET ORIENTED 3-D PRE-STACK MIGRATION

In this section we discuss the three basic steps of target oriented 3-D pre-stack migration (see also Figure VI-1):

1. **Pre-stack redatuming**
   Target-related CSP gathers at the surface are downward extrapolated in a 3-D sense via the boundaries of the macro subsurface model to the upper boundary of the target zone.
2. **Wide-angle CDP stacking**
   At the macro layer boundaries and at the upper boundary of the target zone single-fold ZO gathers are formed by correlating the downgoing source wave and the upgoing reflected waves. Genuine multi-fold ZO gathers are obtained by combining the individual results (wide-angle CDP stacking). Optionally, these data can be used for velocity analysis based on model verification. A further discussion of velocity analysis is beyond the scope of this thesis.
3. **ZO migration**
   Full 3-D wide-angle ZO migration is applied within the target zone.

The computational diagram is shown in Figure VI-2. In the following we discuss the different steps in more detail.

Pre-stack redatuming (step 1) may be based on the acoustic one-way wave equations, the acoustic two-way wave equation, or the full elastic two-way wave equation. We briefly consider all cases.

i. **Acoustic one-way** downward extrapolation of a CSP gather is formally described by

$$S^{+}(x,y,\sigma_i,\omega) = W^{+}(x,y,\sigma_i,\sigma_{i-1},\omega) * S^{+}(x,y,\sigma_{i-1},\omega), \qquad \text{(VI-1a)}$$

$$P^{-}(x,y,\sigma_i,\omega) = F^{-}(x,y,\sigma_i,\sigma_{i-1},\omega) * P^{-}(x,y,\sigma_{i-1},\omega). \qquad \text{(VI-1b)}$$

Relation (VI-1a) describes forward extrapolation of the downgoing source wave, relation (VI-1b) describes inverse extrapolation of the upgoing reflected waves. The symbol * denotes a two-dimensional space dependent generalized spatial convolution along the x and y coordinates. The symbols σ_{i-1} and σ_i

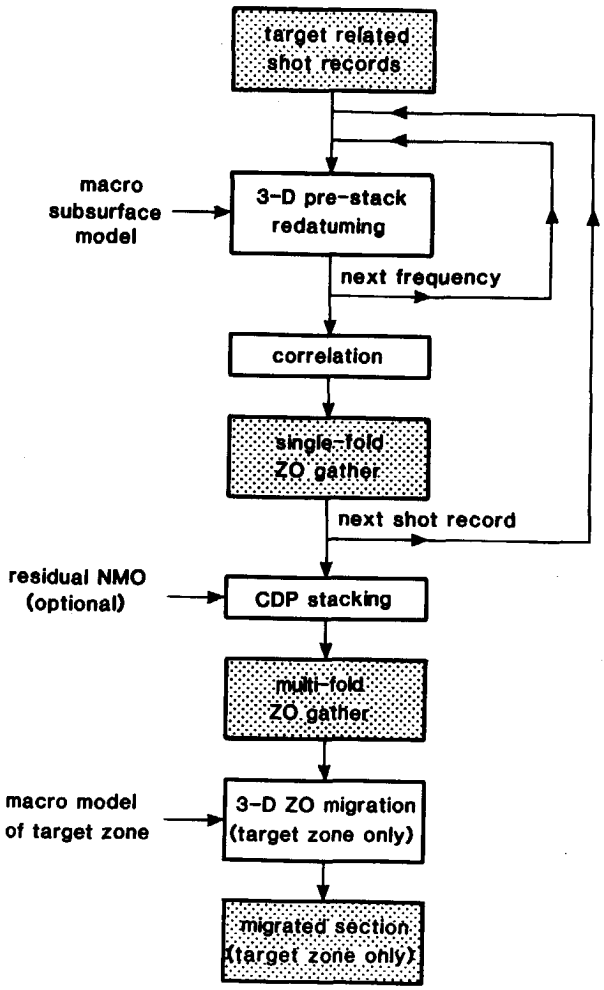

Figure VI-2: Computational diagram for target oriented 3-D pre-stack migration.

refer to arbitrarily curved macro layer boundaries. Explicit expressions for the operators W^+ and F^- cannot be generally given. Assuming that the medium parameters of macro layer i are homogeneous and that this macro layer is bounded by plane, horizontal surfaces σ_{i-1} and σ_i (Figure VI-3a), then relations (VI-1a) and (VI-1b) are identical to relations (III-19a) and (III-19d), respectively, hence operator W^+ represents the Rayleigh II operator, while operator F^- represents the complex conjugated of the Rayleigh II operator. In case of an inhomogeneous macro layer recursive finite-difference operators should be used, as described by

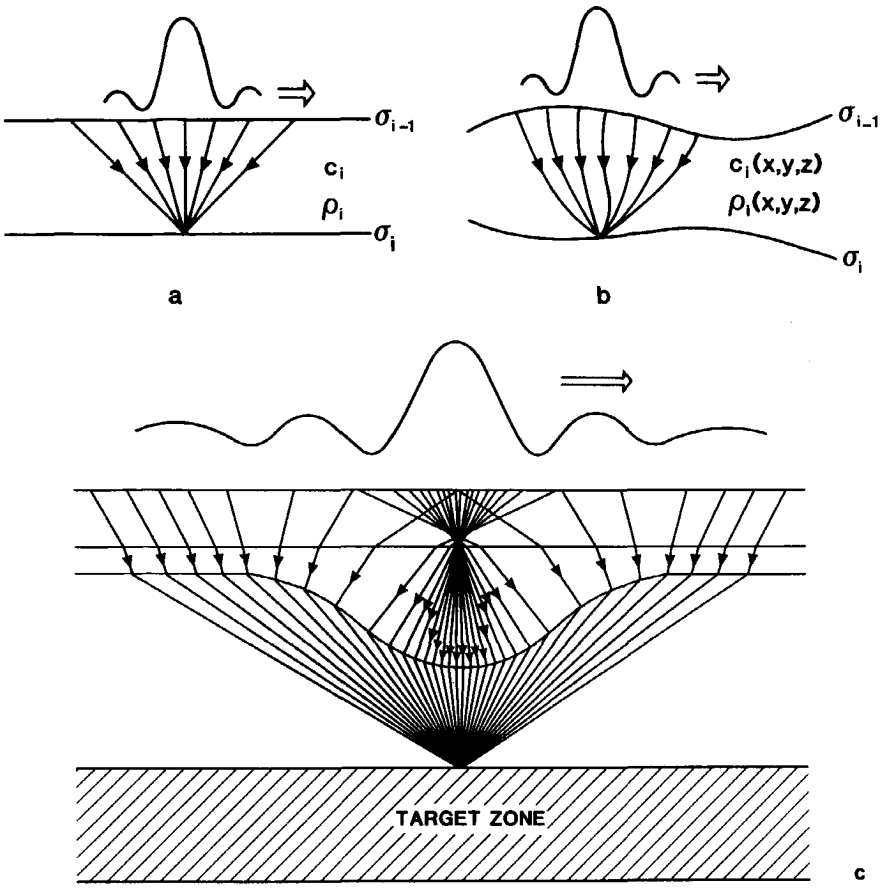

Figure VI-3: Acoustic one-way wave field extrapolation by means of the Rayleigh II operator merely consists of a weighted summation of input samples for each output sample.

a. Theoretically, plane interfaces and homogeneous medium parameters are assumed.

b. Practically, the operator may be modified for curved interfaces and slightly inhomogeneous medium parameters.

c. For non-recursive extrapolation the operator can be generated by ray-tracing or finite-difference modeling.

relations (III-29) to (III-31). However, in the 3-D pre-stack scheme, application of these operators is too computationally intensive. Instead we prefer to apply a **modified** Rayleigh II operator which accounts for the curvature of surfaces σ_{i-1} and σ_i as well as for slight inhomogeneities

of the medium parameters of the macro layer. The principle is visualized in Figure VI-3b. It is important to realize that amplitudes are not accurately handled by the modified Rayleigh II operator. However, the operator properly handles non-hyperbolic traveltimes. Notice that application of the modified Rayleigh II operator is significantly less computationally intensive than above mentioned finite-difference operators, because it extrapolates the wave field from macro layer boundary σ_{i-1} to macro layer boundary σ, in one single step. An ideal combination of accuracy and efficiency can be obtained by optimumly designing the geologically oriented macro subsurface model: smaller macro layers yield a higher accuracy for the cost of a lower efficiency; on the other hand, if the total overburden is considered as one macro layer (Figure VI-3c), then a high efficiency is obtained for the cost of a degradation of the amplitude accuracy. A further discussion of the modified Rayleigh II operator is beyond the scope of this thesis.

ii. **Acoustic two-way** downward extrapolation of a CSP gather is formally described by

$$\begin{bmatrix} P(\sigma_i) \\ \frac{1}{\rho}\frac{\partial P}{\partial \vec{n}}\Big|_{\sigma_i} \end{bmatrix} = \begin{bmatrix} W_I(\sigma_i,\sigma_{i-1})^* & W_{II}(\sigma_i,\sigma_{i-1})^* \\ W_{III}(\sigma_i,\sigma_{i-1})^* & W_{IV}(\sigma_i,\sigma_{i-1})^* \end{bmatrix} \begin{bmatrix} P(\sigma_{i-1}) \\ \frac{1}{\rho}\frac{\partial P}{\partial \vec{n}}\Big|_{\sigma_{i-1}} \end{bmatrix} . \quad \text{(VI-2)}$$

The symbol $\partial/\partial\vec{n}$ denotes differentiation in the direction of the normal to the surface. For notational convenience the arguments x, y and ω are deleted. Explicit expressions for the operators W_I, W_{II}, W_{III} and W_{IV} cannot be generally given. Assuming that the medium parameters of macro layer i are homogeneous and that this macro layer is bounded by plane, horizontal surfaces σ_{i-1} and σ_i, then relation (VI-2) is identical to relation (IV-22), hence operators $W_I \ldots W_{IV}$ are given by

$$W_I = \text{Real (Rayleigh II)}, \quad \text{(VI-3a)}$$

$$W_{II} = \frac{1}{\omega}\,\text{Imag (Rayleigh I)}, \quad \text{(VI-3b)}$$

$$W_{III} = -\omega\,\text{Imag (Rayleigh III)}, \quad \text{(VI-3c)}$$

$$W_{IV} = \text{Real (Rayleigh II)}. \quad \text{(VI-3d)}$$

In case of an inhomogeneous macro layer recursive finite-difference operators should be used, as described by relation (IV-45). However, for reasons of efficiency we prefer to apply operators $W_I \ldots W_{IV}$, as defined by (VI-3), based on modified Rayleigh operators which account for the curvature of surfaces σ_{i-1} and σ_i as well as for slight inhomogeneities of the medium parameters of the macro layer. If the macro layer is accurately defined, then these operators properly handle 'long period' multiples between the main reflecting boundaries σ_{i-1} and σ_i.

iii. **Full elastic two-way** downward extrapolation of a CSP gather is formally described by

$$\begin{bmatrix} j\omega V_n \\ Z_{t1} \\ Z_{t2} \\ Z_n \\ j\omega V_{t1} \\ j\omega V_{t2} \end{bmatrix}_{\sigma_i} = \begin{bmatrix} W_{11}(\sigma_i,\sigma_{i-1})^* & \cdots & W_{16}(\sigma_i,\sigma_{i-1})^* \\ \vdots & & \vdots \\ W_{61}(\sigma_i,\sigma_{i-1})^* & \cdots & W_{66}(\sigma_i,\sigma_{i-1})^* \end{bmatrix} \begin{bmatrix} j\omega V_n \\ Z_{t1} \\ Z_{t2} \\ Z_n \\ j\omega V_{t1} \\ j\omega V_{t2} \end{bmatrix}_{\sigma_{i-1}} . \qquad \text{(VI-4)}$$

Here $\vec{V} = [V_{t1}, V_{t2}, V_n]^T$ represents the particle velocity and $\vec{Z} = [Z_{t1}, Z_{t2}, Z_n]^T$ represents the stress at the macro layer boundary. The normal components of $\vec{V}$ and $\vec{Z}$ are denoted by the sub-script n, whereas the two orthogonal tangential components are denoted by the sub-scripts t_1 and t_2. Explicit expressions for the operators $W_{11} \ldots W_{66}$ cannot be generally given. Again for reasons of efficiency, these operators should be based on modified Rayleigh operators. If the macro layer is accurately defined, then these operators properly handle 'long period' multiples as well as wave conversions at the main reflecting boundaries σ_{i-1} and σ_i.

Wide-angle CDP stacking (step 2) takes place at the macro layer boundaries σ_i and at the upper boundary σ_I of the target zone. Notice that a plane 'reference' boundary σ_I may be chosen which does not necessarily coincide with one of the macro layer boundaries. Again we consider three cases based on the acoustic one-way wave equations, the acoustic two-way wave equation and the full elastic two-way wave equation, respectively.

i. In the **acoustic one-way** case the downgoing source waves $S^+_{mn}(x,y,\sigma_i,\omega)$ and the upgoing reflected waves $P^-_{mn}(x,y,\sigma_i,\omega)$ are available at the macro layer boundaries σ_i and at the upper boundary σ_I of the target zone. Here the sub-scripts mn denote that the wave fields are related to

CSP gather mn, generated by a (unit) source located at (x_m, y_n, z_o) at the surface. According to relation (II-37), the single-fold ZO impulse response at boundary σ_i is obtained by correlating the downgoing and upgoing waves at σ_i as follows

$$\langle X_{ZO}(x,y,\sigma_i,\omega)\rangle_{mn} = \frac{1}{s_{mn}^2} P^-_{mn}(x,y,\sigma_i,\omega)[S^+_{mn}(x,y,\sigma_i,\omega)]^*, \qquad \text{(VI-5a)}$$

where

$$s^2_{mn} = \iint S^+_{mn}(x,y,\sigma_i,\omega)[S^+_{mn}(x,y,\sigma_i,\omega)]^* dxdy. \qquad \text{(VI-5b)}$$

According to relations (II-38) and (II-39) the multi-fold ZO **reflectivity** at σ_i could now be obtained by imaging (summing over all frequencies) and CDP stacking (summing over all shots). In the present procedure the imaging step is deleted, hence the multi-fold ZO **impulse response** is obtained by CDP stacking, according to

$$X^{CDP}_{ZO}(x,y,\sigma_i,\omega) = \sum_m \sum_n \langle X_{ZO}(x,y,\sigma_i,\omega)\rangle_{mn}. \qquad \text{(VI-6)}$$

Notice that high quality ZO traces can be obtained by applying an inverse Fourier transform from the frequency domain to the time domain. If the inverse Fourier transform is carried out **before** CDP stacking, then residual NMO corrections can be applied when the macro subsurface model, used in the pre-stack redatuming step, was slightly in error.

ii. In the **acoustic two-way** case the total wave fields $P_{mn}(x,y,\sigma_i,\omega)$ and $\rho^{-1}\partial_{\vec{n}}P_{mn}(x,y,\sigma_i,\omega)$ are available at the macro layer boundaries σ_i and at the upper boundary σ_I of the target zone. According to relation (IV-74) the total wave fields can be decomposed into downgoing and upgoing waves $P^+_{mn}(x,y,\sigma_i,\omega)$ and $P^-_{mn}(x,y,\sigma_i,\omega)$, respectively. (Strictly speaking this decomposition is correct only at the plane upper boundary σ_I of the target zone; at the curved macro layer boundaries σ_i errors are made).

The downgoing source wave $S^+_{mn}(x,y,\sigma_i,\omega)$ can be extracted from the total downgoing wave field $P^+_{mn}(x,y,\sigma_i,\omega)$ by means of a 'first arrival time window'. Having determined the downgoing source waves and the upgoing reflected wave fields the procedure can now be continued as described above for the acoustic one-way case. Again the final result (after correlation and CDP stacking) is a set of high quality ZO gathers at all σ_i. In addition, when an accurate macro subsurface model was used in the

(acoustic two-way) pre-stack redatuming step, all 'long period' multiples of the overburden have been properly eliminated. Finally, if no major reflecting interfaces occur in the target zone, that is, if the target zone completely lies inside a macro layer, then the constructed ZO data (related to the target zone) at σ_I are free from 'long period' multiples.

iii. In the **full elastic two-way** case the total wave fields $\vec{Z}_{mn}(x,y,\sigma_I,\omega)$ and $\vec{V}_{mn}(x,y,\sigma_I,\omega)$ are available at the macro layer boundaries σ_i and at the upper boundary σ_I of the target zone. The total wave fields can be decomposed into Lamé potentials for downgoing and upgoing P, SV and SH waves. The Lamé potentials for downgoing and upgoing P waves are represented by $\Phi^+_{mn}(x,y,\sigma_i,\omega)$ and $\Phi^-_{mn}(x,y,\sigma_i,\omega)$, respectively. The dilatational part (P wave) of the downgoing source wave can be extracted from the downgoing wave $\Phi^+_{mn}(x,y,\sigma_i,\omega)$ by means of a first arrival time window, yielding $\Phi^+_{SRC,mn}(x,y,\sigma_i,\omega)$. The procedure can now be continued as described above for the acoustic one-way case, with S^+_{mn} and P^-_{mn} replaced by $\Phi^+_{SRC,mn}$ and Φ^-_{mn}, respectively. Again the final result (after correlation and CDP stacking) is a set of high quality ZO gathers at all σ_i. In addition, when an accurate macro subsurface model was used in the (full elastic two-way) pre-stack redatuming step, all 'long period' multiples as well as 'major' converted waves at the main reflecting boundaries in the overburden have been properly eliminated. Finally, if no major reflecting interfaces occur in the target zone, then the constructed ZO data (related to the target zone) at σ_I are free from 'long period' multiples and 'major' converted waves.

ZO migration (step 3)

In all above described cases (acoustic one-way, acoustic two-way, full elastic two-way), high quality ZO data are constructed at the upper boundary σ_I of the target zone. Because true CDP stacking was applied **after** downward extrapolation, these ZO data contain diffraction energy as well as wide-angle information related to the target zone. Therefore it is important to apply a **full 3-D wide-angle** ZO migration algorithm in order to obtain a high resolution image of the target zone. If the medium parameters of the macro subsurface model in the target zone are arbitrarily 3-D inhomogeneous functions of the spatial coordinates, then preferably use should be made of a full 3-D 'local operator' ZO migration algorithm: band-limited 3-D Rayleigh II operators are generated in advance for a wide range of (ω/c)-values; next, for each extrapolation step the proper operator is chosen in accordance with the local

propagation velocity. Because generally small depth-steps are made, the operators should be designed with utmost care via the wavenumber-frequency domain in order to avoid 'operator aliasing'. A further discussion of this wide-angle 3-D ZO migration algorithm is beyond the scope of this thesis.

VI.3 PRACTICAL ASPECTS OF TARGET ORIENTED 3-D PRE-STACK MIGRATION

In the previous section we discussed the principle of target oriented 3-D pre-stack migration. The computational diagram, shown in Figure VI-2, can be seen as a modification of the computational diagram for full pre-stack migration by SSRI and CDP stacking (Figures II-6, IV-14 or V-6). The target oriented scheme, however, is much less computationally intensive, while the CDP-principle is fully preserved. Therefore, for practical implementation, target oriented 3-D pre-stack migration is preferred above full 3-D pre-stack migration by SSRI and CDP stacking. No attention has been paid sofar to the practical aspects of data management during processing.

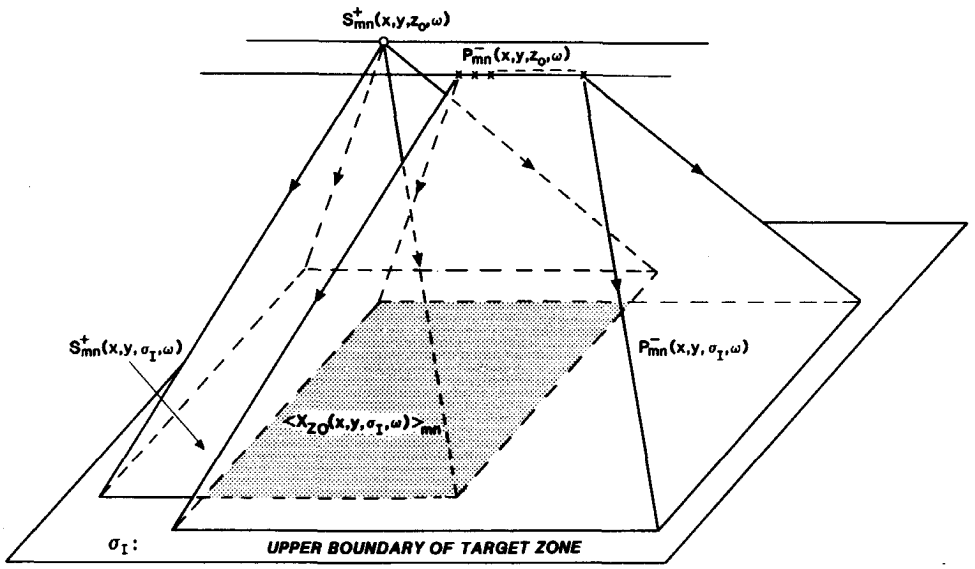

Figure VI-4: Downward extrapolation of one single-shot record to the upper boundary of the target zone and generation of single-fold ZO-data in the overlap area.

Therefore we consider the data flow for a pre-stack marine dataset (see also Figure I-1), which typically consists of

200 seismic lines,
200 seismic experiments (shot records) per seismic line,
100 traces (detectors) per seismic experiment,
2000 samples per trace,
4 bytes per sample,

hence, the total survey contains 32 Gbyte of data. According to the computational diagram of Figure VI-2, each shot record is downward extrapolated to the upper boundary of the target zone, where per shot record a single-fold ZO gather is generated by correlating the downgoing and upgoing waves. For one monochromatic shot record this procedure is visualized in Figure VI-4. Notice that the source and detector data, which are represented at the acquisition surface by one (complex) scalar and one (complex) 1-D array, respectively, are both spread out over a 2-D area at the upper boundary of the target zone. Consequently, the monochromatic single-fold ZO-data, which are constructed in the overlap area with the aid of relation (VI-5), are represented by a (complex) 2-D array. Hence, the amount of single-fold ZO **output** data after redatuming is much larger than the amount of single-shot record **input** data. Typically, for one broad-band single-shot input record, which contains 0.8 Mbyte of data (see above), the broad-band single-fold ZO output gather consists of

200x200 traces,
500 samples per trace (target zone only),
4 bytes per sample,

or 80 Mbyte in total, so the amount of data increases by a factor **one hundred.** Assuming that all shot records are involved in the process, then the total amount of data just before CDP stacking equals hundred times the amount of input data, hence 100x32 Gbyte = 3200 Gbyte! Of course the next step in the process (CDP stacking) involves again an enormous data reduction. However, the huge amount of tape I/O that would be required makes the computational diagram of Figure VI-2 impracticable. If CDP stacking would be carried out inside the 'shot record loop', then the tape I/O problem would be evaded. However, for the residual NMO correction, which is required when the macro subsurface model was slightly in error, it is essential that CDP stacking is carried out outside the shot record loop. An attractive compromise of efficiency (with respect to tape I/O) on one hand and flexibility (with respect to CDP stacking) on the other hand is outlined by the modified computational diagram of Figure VI-5. Notice

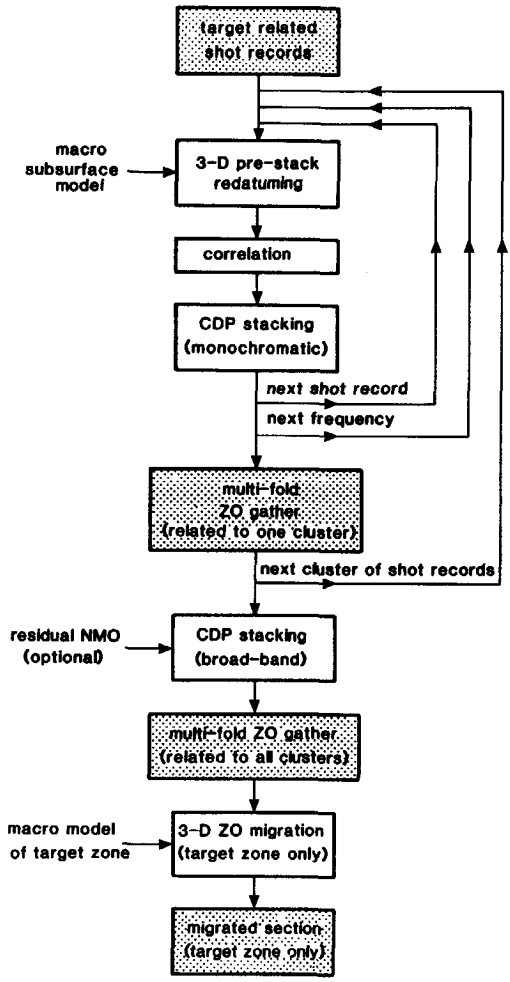

Figure VI-5: Modified computational diagram for target oriented 3-D pre-stack migration.

that according to this diagram, the processing is carried out per **cluster** of shot records. A cluster consists of, typically, one hundred shot records (for instance all shot records on one tape). **CDP stacking for all shot records in one cluster** is carried out efficiently inside the shot record loop (without the possibility for residual NMO corrections). Hence, the amount of data just before the final **CDP stacking for all clusters** is of the same order as the amount of input data (typically 32 Gbyte). This means a significant improvement compared with the scheme discussed before (Figure VI-2).

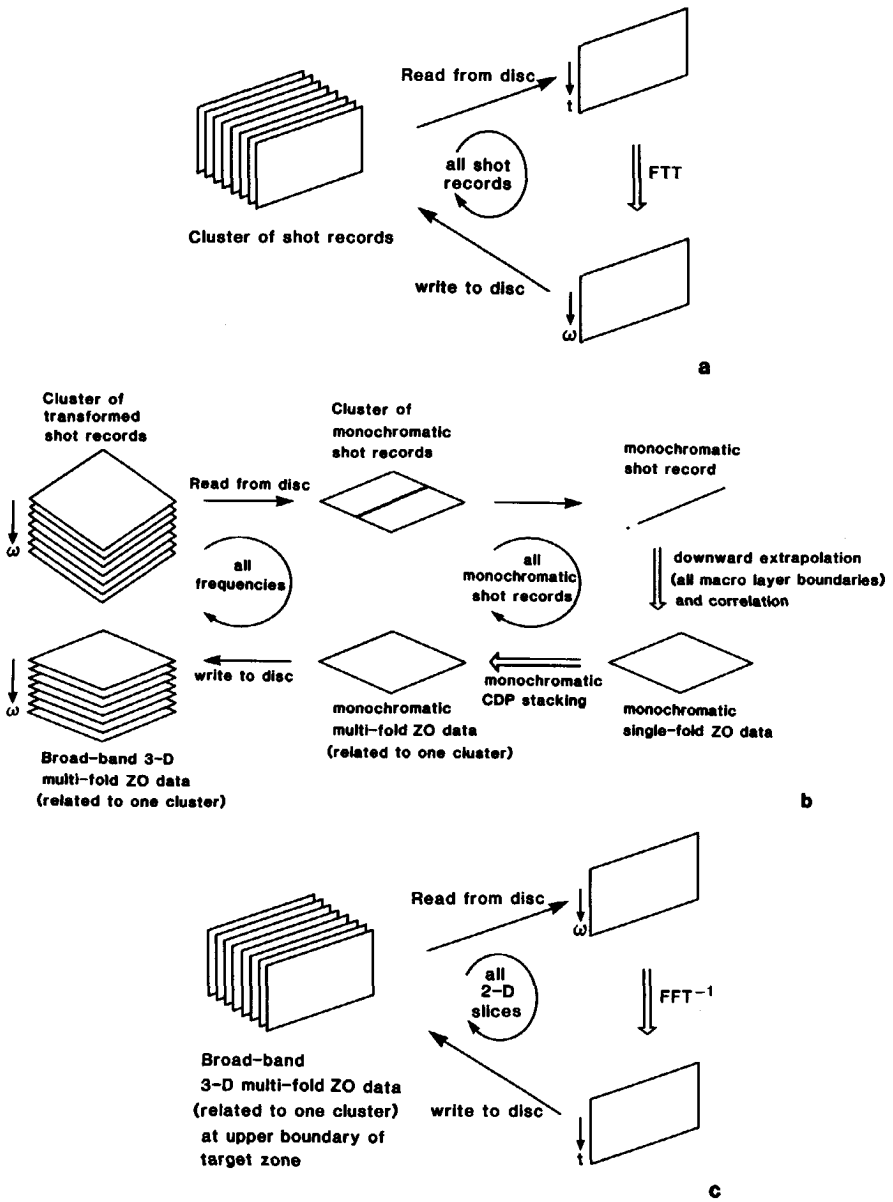

Figure VI-6: The data-flow for one cluster of shot records in target oriented 3-D pre-stack migration.

a. Transformation from time to frequency domain.

b. The actual processing (only the output data at the upper boundary of the target zone are shown; similar broad-band data sets may be generated at various macro layer boundaries).

c. Transformation from frequency to time domain.

Notice that the final CDP stacking (for all clusters) takes place outside the 'cluster loop'. Hence, in this stage residual NMO corrections can be applied if the macro subsurface model was slightly in error.
Another important practical aspect, which has not been discussed sofar, is the amount of required disc I/O. A cluster of shot records typically contains 80 Mbyte of data (see above). Processing of these data requires a memory overhead of typically 400 Mbyte, which is much larger than the internal computer memory. Hence, the required memory space should be reserved on disc and the algorithm should be designed efficiently with respect to disc I/O. Since in target oriented 3-D pre-stack migration no imaging (summing over all frequencies) is performed, there is no longer any reason to choose the 'frequency loop' as the inner loop (see Figures II-6, IV-14, V-6 and VI-2). Much disc I/O can be avoided if (for each cluster of shot records) the processing (redatuming and CDP stacking) is carried out per frequency component (see Figure VI-5). For one cluster of shot records the data-flow is visualized in Figure VI-6. As shown in Figure VI-6a, the data are first prepared by transforming from the time domain to the frequency domain (this step is not shown in the computational diagram of Figure VI-5). The actual processing (per frequency component) is visualized in Figure VI-6b. Notice the optimum efficiency with respect to disc I/O: each frequency component is transported from disc to memory (and vice versa) only once. Finally, as is shown in Figure VI-6c, the output data are transformed back from the frequency domain to the time domain (this step is not shown in the computational diagram of Figure VI-5).

VI.4 AN EFFICIENT SIMPLIFIED TARGET ORIENTED 3-D PRE-STACK MIGRATION SCHEME

In the previous sections the principle as well as the practical aspects of a target oriented 3-D pre-stack migration scheme have been discussed. The practical implementation of the scheme can be realized on nowadays vector computers. However, at this moment still much software development is required before large real datasets can be processed, particularly in case of complicated acoustic or full elastic macro subsurface models.

To demonstrate that the principle of target oriented 3-D pre-stack migration is correct, we implemented a simplified version on a powerful seismic work-station as well as on a Cray XMP vector computer. The computational diagram and the

data-flow for the version we implemented is in principle shown in Figures VI-5 and VI-6 in the previous section. The main simplification concerns the 3-D pre-stack downward extrapolation step (redatuming). We replaced the recursive procedure, in which the data are downward extrapolated via the boundaries of the macro subsurface model, by a non-recursive procedure. In this non-recursive procedure a CSP gather is downward extrapolated from the acquisition surface to the upper boundary of the target zone in one single step. In this section we discuss the non-recursive extrapolation operators and show that they can be implemented very efficiently. In the following sections we discuss results of the method obtained with synthetic data as well as scale model data.

Consider the acoustic macro subsurface model, shown in Figure VI-7. This model consists of a homogeneous overburden (propagation velocity c, mass density ρ) between the acquisition surface z_o and depth level z_I, and a target zone below depth level z_I. Because the overburden is homogeneous, a CSP gather can be downward extrapolated by means of the Rayleigh II operator. Forward extrapolation of the downgoing source wave is described by

$$S^+_{mn}(x,y,z_I,\omega) = W^+(x,y,z_I,z_o,\omega) * S^+_{mn}(x,y,z_o,\omega), \qquad \text{(VI-7a)}$$

or

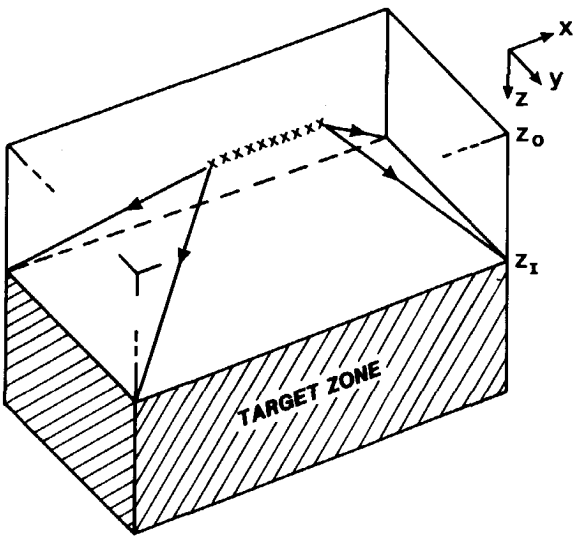

Figure VI-7: Simplified acoustic macro subsurface model.

$$S^+_{mn}(x,y,z_I,\omega) = \iint_{-\infty}^{\infty} W^+(x-x',y-y',z_I,z_o,\omega)S^+_{mn}(x',y',z_o,\omega)dx'dy'. \quad \text{(VI-7b)}$$

Here the 3-D Rayleigh II operator W^+ is given by (Berkhout, 1982)

$$W^+(x,y,z_I,z_o,\omega) = \frac{1}{2\pi}\frac{1+jkr}{r^2}\cos\phi\ e^{-jkr}, \quad \text{(VI-7c)}$$

with

$$r = \sqrt{x^2 + y^2 + \Delta z^2}, \quad \text{(VI-7d)}$$

$$\Delta z = z_I - z_o, \quad \text{(VI-7e)}$$

$$\cos\phi = \Delta z/r, \quad \text{(VI-7f)}$$

$$k = \omega/c. \quad \text{(VI-7g)}$$

Assuming that $S^+_{mn}(x,y,z_o,\omega)$ represents a unit source at (x_m,y_n,z_o) according to

$$S^+_{mn}(x,y,z_o,\omega) = \delta(x-x_m)\delta(y-y_n), \quad \text{(VI-8a)}$$

we may write

$$S^+_{mn}(x,y,z_I,\omega) = \iint_{-\infty}^{\infty} W^+(x-x',y-y',z_I,z_o,\omega)\delta(x'-x_m)\delta(y'-y_n)dx'dy', \quad \text{(VI-8b)}$$

or

$$S^+_{mn}(x,y,z_I,\omega) = W^+(x-x_m,y-y_n,z_I,z_o,\omega). \quad \text{(VI-8c)}$$

Hence, the downward extrapolated source wave is simply given by the Rayleigh II operator. Notice that the scaling factor s^2_{mn}, defined according to relation (VI-5b) by

$$s^2_{mn} = \iint_{-\infty}^{\infty} S^+_{mn}(x,y,z_I,\omega)[S^+_{mn}(x,y,z_I,\omega)]^* dxdy, \quad \text{(VI-8d)}$$

approaches unity. Hence, in the correlation step scaling need not be applied.

Extrapolation of the detected upgoing wave $P^{-}_{mn}(x,y,z_o,\omega)$ can be carried out most efficiently in the mixed wavenumber-space-frequency domain. We consider the wave equation in the k_x,y,z,ω domain

$$\frac{\partial^2 P}{\partial y^2} + \frac{\partial^2 P}{\partial z^2} + \kappa^2 P = 0, \qquad \text{(VI-9a)}$$

where

$$\kappa^2 = k^2 - k_x^2. \qquad \text{(VI-9b)}$$

Notice that, for each k_x, relation (VI-9) represents a 2-D wave equation, which is solved by the following 2-D Rayleigh II integral

$$\tilde{P}^{+}(k_x,y,z_I,\omega) = \int_{-\infty}^{\infty} \tilde{W}^{+}(k_x,y-y',z_I,z_o,\omega)\tilde{P}^{+}(k_x,y',z_o,\omega)dy', \qquad \text{(VI-10a)}$$

where

$$\tilde{W}^{+}(k_x,y,z_I,z_o,\omega) = -\frac{j\kappa}{2}\cos\phi_o\, H_1^{(2)}(\kappa r_o), \qquad \text{(VI-10b)}$$

with

$$r_o = \sqrt{y^2 + \Delta z^2}, \qquad \text{(VI-10c)}$$

$$\cos\phi_o = \Delta z / r_o \qquad \text{(VI-10d)}$$

and κ being given by (VI-9b). $H_1^{(2)}$ represents the first order Hankel function of the second kind. (Operator $\tilde{W}^{+}$, given by relation (VI-10b), represents the **single** spatial Fourier transform of operator W^{+}, given by relation (VI-7c)). Notice that relation (VI-10) describes forward extrapolation of downgoing waves. For inverse extrapolation of upgoing waves the matched filter approach may be applied, according to

$$\tilde{P}^{-}(k_x,y,z_I,\omega) = \int_{-\infty}^{\infty} \tilde{F}^{-}(k_x,y-y',z_I,z_o,\omega)\tilde{P}^{-}(k_x,y',z_o,\omega)dy', \qquad \text{(VI-11a)}$$

where operator $\tilde{F}^{-}$ is the complex conjugated of $\tilde{W}^{+}$:

$$\tilde{F}^{-}(k_x,y,z_I,z_o,\omega) = [\tilde{W}^{+}(k_x,y,z_I,z_o,\omega)]^{*}. \qquad \text{(VI-11b)}$$

Assuming that the reflected upgoing wave $P^{-}_{mn}(x,y,z_o,\omega)$ is detected for $y=y_n$ only, then the spatially Fourier transformed CSP gather can be written as a scaled delta function, according to

$$\tilde{P}^{-}_{mn}(k_x,y,z_o,\omega) = \tilde{P}^{-}_{mn}(k_x,y_n,z_o,\omega)\delta(y-y_n), \qquad \text{(VI-12a)}$$

so relation (VI-11) may be written as

$$\tilde{P}^{-}_{mn}(k_x,y,z_I,\omega) = \tilde{P}^{-}_{mn}(k_x,y_n,z_o,\omega)\int_{-\infty}^{\infty}\tilde{F}^{-}(k_x,y-y',z_I,z_o,\omega)\delta(y'-y_n)dy', \qquad \text{(VI-12b)}$$

or

$$\tilde{P}^{-}_{mn}(k_x,y,z_I,\omega) = \tilde{F}^{-}(k_x,y-y_n,z_I,z_o,\omega)\tilde{P}^{-}_{mn}(k_x,y_n,z_o,\omega). \qquad \text{(VI-12c)}$$

Hence, downward extrapolation of the detected upgoing wave to the upper boundary of the target zone involves 1-D spatial Fourier transforms and vectorized multiplications (along the k_x coordinate) only.

Finally, notice that the implemented operators, as discussed above, are approximately valid for 1-D inhomogeneous macro subsurface models if the velocity c is replaced by the root-mean-square velocity (Δz should then be replaced by the apparent depth).

VI.5 RESULTS OF TARGET ORIENTED 3-D PRE-STACK MIGRATION ON SYNTHETIC DATA

In this section we demonstrate the mechanism of the target oriented 3-D pre-stack migration scheme. In section VI.3 we argued that the practical implementation of this scheme requires that the processing is carried out per **cluster** of shot records. Here we discuss some results obtained per cluster of **synthetic** shot records and show the CDP stack of these results, being a multi-fold ZO gather at the upper boundary of the target zone. Finally we show the migrated data in the target zone. The main steps are summarized in the computational diagram of Figure VI-8.

We consider again the 2-D example which was given in the final section of chapter II. The subsurface configuration is given in Figure VI-9a. It consists of a homogeneous overburden (c_1 = 1000 m/s), overlying a target zone

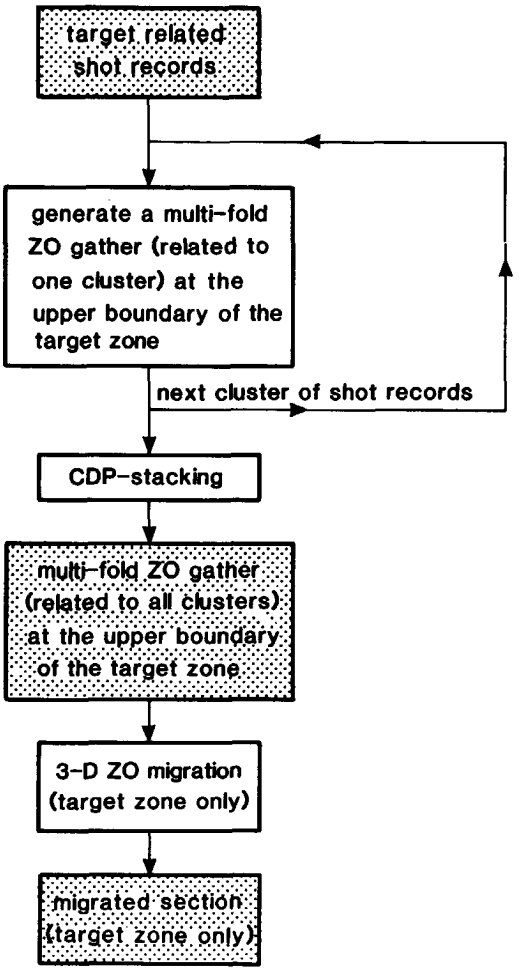

Figure VI-8: Computational diagram for the main steps in target oriented 3-D pre-stack migration.

(c_2 = 2000 m/s). Three diffractors are present at the upper boundary of the target zone; one diffractor is present at the lower boundary. At the acquisition surface 64 CSP experiments are simulated, which form together one seismic line. These CSP gathers are downward extrapolated to the upper boundary of the target zone, where ZO data are generated. Some single-fold ZO gathers are shown in section II.5. The final 2-D result, that is, a 64-fold ZO gather at the upper boundary of the target zone, is shown in the left frame of

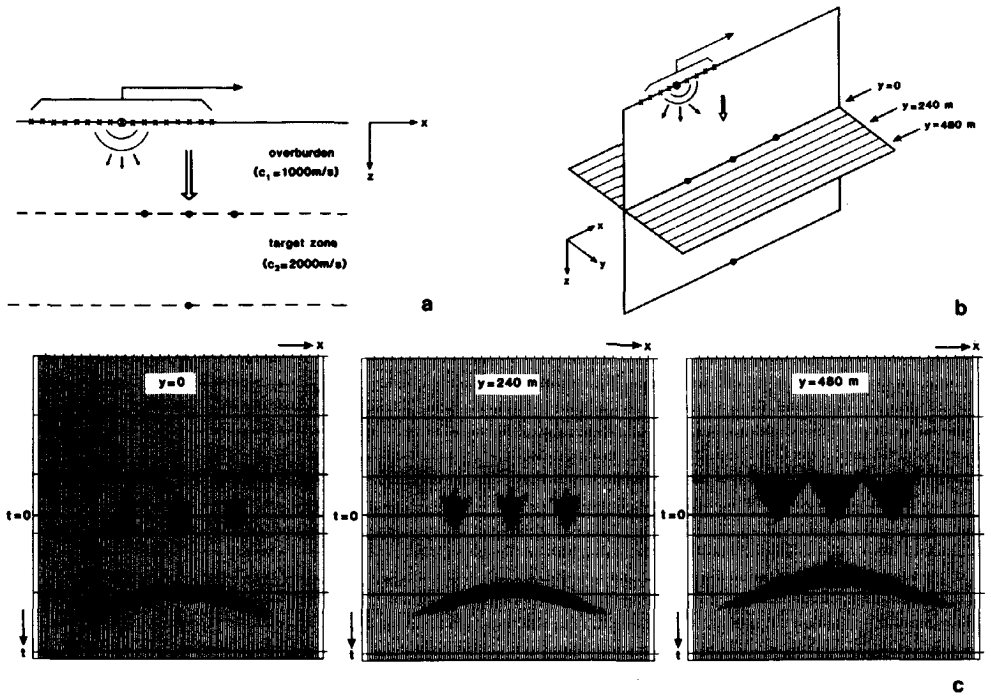

Figure VI-9: Example of target oriented 3-D pre-stack downward extrapolation and CDP stacking.

a. 2-D subsurface configuration, used for the example in chapter II.

b. 3-D subsurface configuration, containing the 2-D slice of Figure a.

c. Three 2-D slices of a 3-D multi-fold ZO section (related to one seismic line) at different lines (indicated by arrows in b) at the upper boundary of the target zone).

Figure VI-9c. Notice that the diffractors at the upper boundary of the target zone are well resolved, while the diffractor at the lower boundary is properly represented by a hyperbola. (The artefacts, which are visible because the amplitudes are clipped at -32 dB relative to the maximum amplitude, are due to the limited temporal and spatial bandwidth). Notice that this 2-D experiment can also be seen as one step in a target oriented 3-D pre-stack migration procedure. In the latter case, the 2-D seismic line represents one cluster of shot records in a 3-D seismic survey, while the subsurface configuration of Figure VI-9a represents one 2-D slice of a 3-D subsurface, as shown in

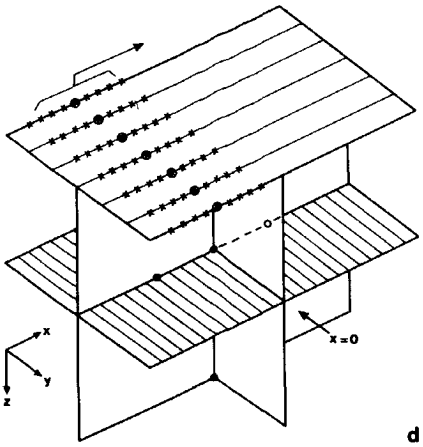

d

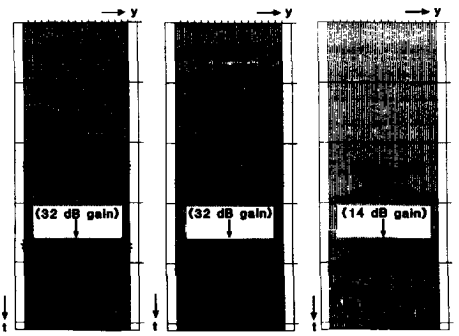

e

Figure VI-9: (continued)

d. 3-D marine acquisition configuration above the subsurface configuration of Figure b,

e. Cross-section (at x=o, indicated by the arrow in d) of the 3-D multi-fold ZO section at the upper boundary of the target zone.
Left frame: result obtained from one seismic line
Middle frame: result obtained from eight seismic lines
Right frame: result obtained from 64 seismic lines

Figure VI-9b. In the 3-D case, however, the cluster of shot records should not only be downward extrapolated to the central line at the upper boundary of the target zone (that is the line in Figure VI-9b which contains the three point diffractors), but to all parallel lines which together form the upper boundary of the target zone. Of course this downward extrapolation should be carried out in a 3-D sense. Figure VI-9c shows three 2-D slices of 3-D multi-fold ZO data (related to one cluster of shot records, that is, the original 2-D seismic line), generated at three different lines (indicated by arrows in Figure VI-9b) at the upper boundary of the target zone. It is interesting to note that the three point diffractors at the central line (y=o) also appear at other lines at this boundary. In other words, the diffractors are not resolved in the cross-direction (perpendicular to the acquisition direction). This lack of resolution in the cross-direction, which is even better seen in the left frame of Figure VI-9e, can be well understood if one keeps in mind that only one seismic line was involved in the downward extrapolation process. If the procedure is repeated for eight clusters of shot records (eight seismic lines, see also Figure VI-9d), followed by CDP stacking, then the resolution in the

cross-direction improves somewhat. The middle frame of Figure VI-9e shows a cross-section of the multi-fold ZO data (related to eight lines) at the upper boundary of the target zone. Notice that the results of all individual seismic lines can be distinguished in this figure. This effect is also known as spatial aliasing: the line spacing at the surface is significantly larger than a quarter of the dominant wavelength (remember that no offsets are measured in the cross-direction; therefore a ZO anti-aliasing criterion should be satisfied in the cross-direction). If the procedure is carried out for 64 clusters of shot records (64 seismic lines), then the line-spacing at the surface reduces. The right frame of Figure VI-9e shows an aliasing-free cross-section of wide-angle multi-fold ZO data at the upper boundary of the target zone. Notice that the upper diffractor is properly focussed and that the lower diffractor is clearly represented by a (cross-section of a) hyperboloid.

Finally, the ZO data for the target zone are migrated by a true 3-D ZO migration algorithm (recursive 3-D phase-shift and imaging). Figure VI-10a shows the in-line section at y=o and Figure VI-10b shows the cross-section at x=o, both after 3-D migration. Notice that the hyperboloid related to the lower point-diffractor has been collapsed. Constant-depth sections for the upper and lower boundary of the target zone are shown in Figures VI-10c and VI-10d, respectively. Notice that the resolution in the line-direction (x-direction) is much better than the resolution in the cross-direction (y-direction). This big difference of resolution in both directions is of course directly related to the orientation of the seismic lines at the surface.

Two important conclusions can be drawn from this experiment:

1. Target oriented 3-D pre-stack migration properly handles diffraction energy. This means a significant improvement over conventional 3-D migration, where diffraction energy is suppressed by CMP stacking.
2. Target oriented 3-D pre-stack migration yields resolution and proper positioning in the line-direction as well as in the cross-direction. This means a significant improvement over 2-D pre-stack migration, where resolution is obtained only in the line-direction and where 'out of plane events' are imaged in the wrong plane.

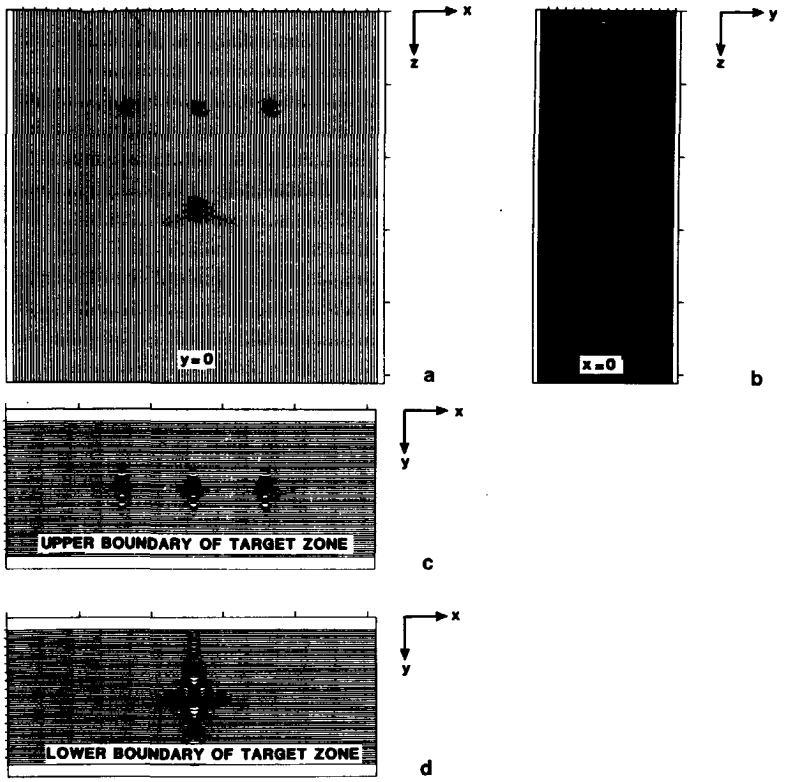

Figure VI-10: Data of Figure VI-9, after 3-D ZO migration.

a. In-line section at y=o.

b. Cross-section at x=o.

c. Constant-depth section (upper boundary of target zone).

d. Constant-depth section (lower boundary of target zone).

Finally, to give an impression of the practical feasibility, we give the required computation time. In this experiment the following amount of data was involved:

64 seismic lines,
64 shot records per seismic line,
256 traces per shot record,
256 samples per trace,
4 bytes per sample,

which is 1 Gbyte of data. The total procedure requires 100 minutes CPU time on a Cray XMP. This time can be reduced to approximately 30 minutes wall clock time on a Cray XMP-4 (four parallel processors).

VI.6 RESULTS OF TARGET ORIENTED 3-D PRE-STACK MIGRATION ON SCALE MODEL DATA

In this final section we demonstrate the validity of the target oriented migration concept and show how target oriented 3-D pre-stack migration compares with target oriented 2-D pre-stack migration. Therefore we generated 3-D multi-experiment, multi-offset data by physical modeling in a water tank. On the bottom of the water tank we placed the well known 'French model' (French, 1975), see Figure VI-11. The measurements were done just below the water surface, using two axial-symmetric piezo-electric transducers in a x_s,x_r,y-positioning system (x_s = in-line coordinate of source, x_r = in-line coordinate of receiver, y = cross-line coordinate of source and receiver). By carrying out 32 experiments for a fixed source position and a variable receiver position a 32 channel common-shotpoint gather can be simulated.

In total we modeled 64 seismic lines with 64 CSP gathers each, thus simulating a 3-D marine survey with 64x64x32 = 131,072 traces. The line spacing equals 20 m (throughout this section we give the simulated dimensions, the scaling factor being 20,000). The 32nd CSP gather of line 25 is shown in Figure VI-12a.

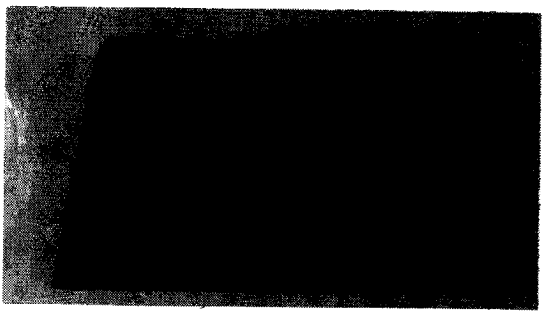

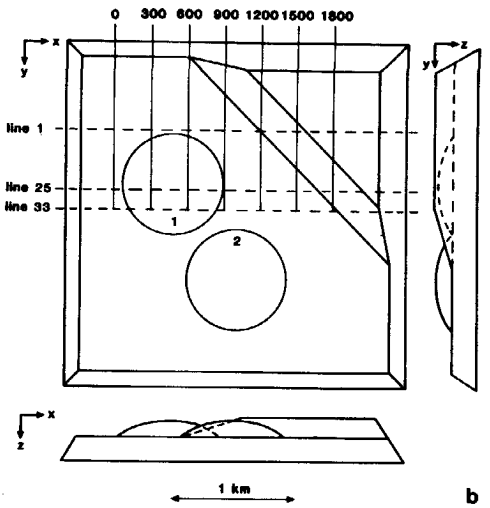

a b

Figure VI-11: The 'French model' (five centimeters in the model simulate one kilometer).
a. Perspective view.
b. Top-view and two-side views.

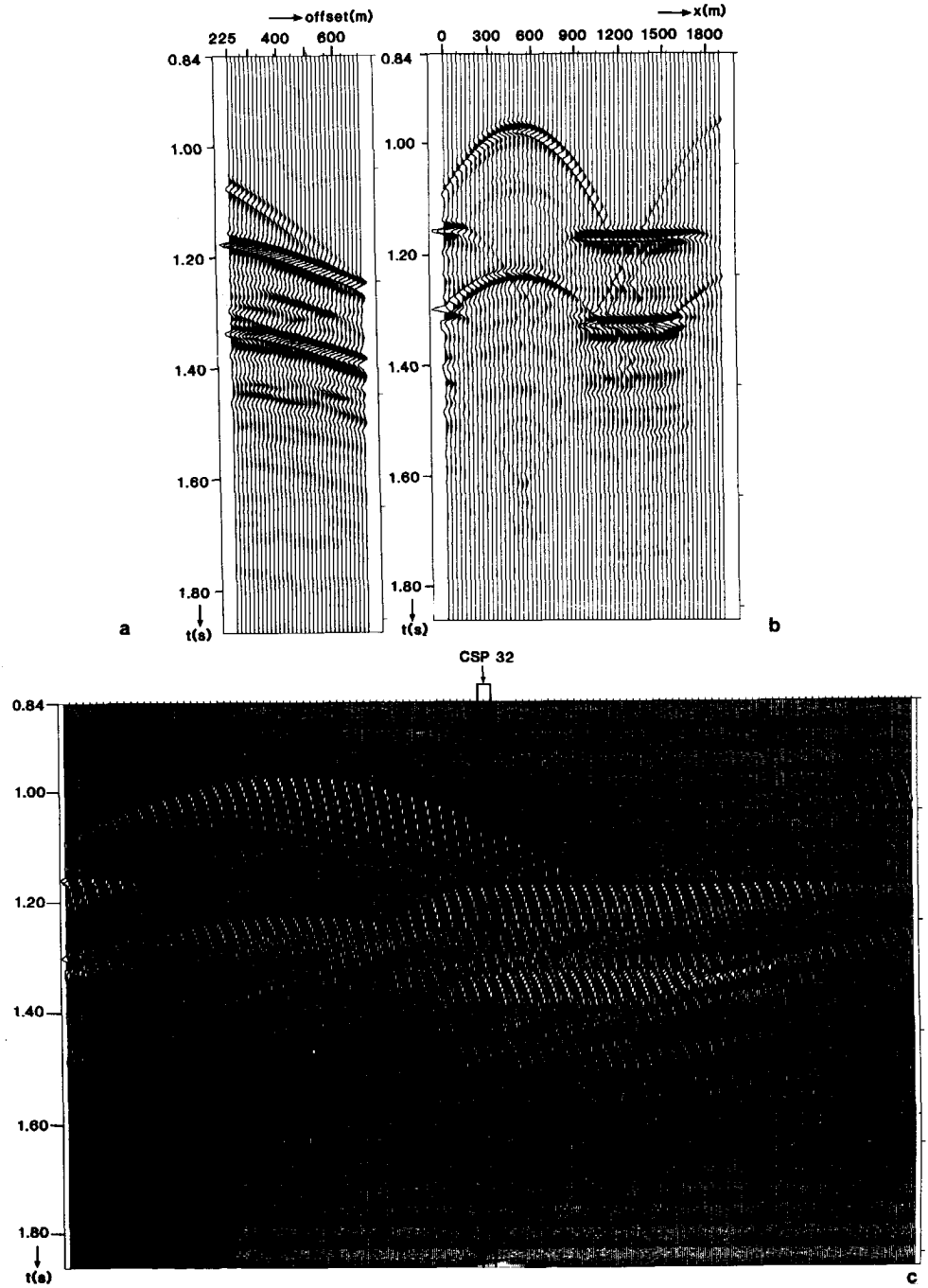

Figure VI-12: 3-D marine survey simulated by physical modeling.

a. CSP gather (line 25, shotpoint 32).

b. CO gather (line 25, offset 225 m).

c. Seismic line 25 (64 CSP gathers).

The smallest source-receiver offset equals 225 m and the receiver spacing equals 15 m. The time traces start at 0.84 s, the time sampling interval is 4 ms and the total trace-length is 256 samples. The frequency content ranges from approximately 20 Hz to 100 Hz. A common-offset gather, selected from line 25, is shown in Figure VI-12b. The offset equals 225 m and the midpoint spacing equals 30 m. Figure VI-12c shows all 64 CSP gathers of line 25, plotted next to each other (every fourth trace is plotted only). The shot spacing equals 30 m.

Vertical 2-D slices of the subsurface below lines 25 and 33, respectively, are shown in Figure VI-13. The upper boundary of the target zone is defined at a depth of 600 m and the lower boundary at 1000 m. **Two-dimensional** redatuming of line 25 to the upper boundary of the target zone, followed by 2-D wide-angle CDP stacking and 2-D ZO migration in the target zone yields the depth section shown in Figure VI-14a. Notice that the first dome is correctly positioned (the top of this dome lies almost vertically below line 25). However, two other events are easily mis-interpreted: a side-swipe reflection from the second dome is imaged just below the left end of the horizontal reflector and a side-swipe reflection from the sloping edge intersects the right end of the horizontal reflector. The same procedure applied to line 33 yields the depth section shown in Figure VI-14b. Apart from forementioned artefacts notice that also the first dome is mispositioned and that side-swipe diffractions from the dome-edge are imaged below the dome. For clarity the erroneously positioned 'out of plane

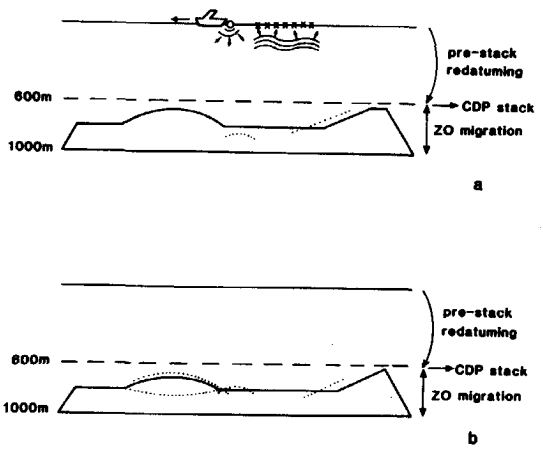

Figure VI-13: Vertical 2-D slices of the subsurface below lines 25 and 33, respectively. (The dotted lines indicate mis-positioned events after 2-D processing, see also Figure VI-14).

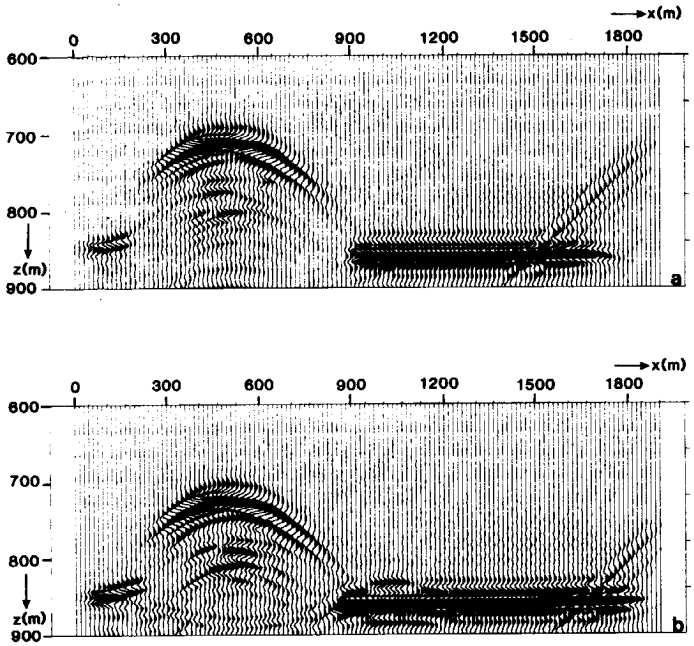

Figure VI-14: Results after 2-D redatuming, wide-angle CDP stacking and ZO migration.
a. Line 25
b. Line 33

events' are indicated by dotted lines in Figure VI-13. Notice that these false images are due to the invalidity of the 2-D assumption (the 'coherent noise' just below the dome is mainly due to imperfections of the physical model and the noise above the horizontal reflector is due to spatial under-sampling).

Three-dimensional redatuming to the upper boundary of the target zone, followed by 3-D wide-angle CDP stacking and 3-D ZO migration in the target zone, yields a 3-D depth section. 2-D slices of this section vertically below lines 25 and 33 are shown in Figures VI-15a and VI-15b, respectively. To avoid spatial aliasing related to the line spacing, we used an operator angle of 15 degrees in the cross-line direction. Therefore a high spatial **resolution** may not be expected in the cross-line direction. However, the **positioning** of most events is now correct, in spite of the small operator angle: all above mentioned side-swipe reflections and diffractions disappeared completely, which improved for instance the lateral continuity below the horizontal reflector. The limited

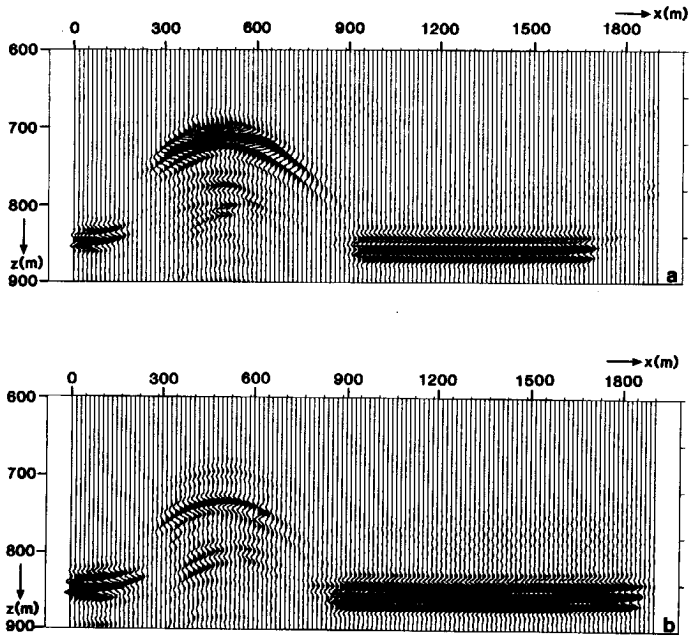

Figure VI-15: Results after 3-D redatuming, wide-angle CDP stacking and ZO migration.
a. Line 25.
b. Line 33.

cross-line operator angle accounts for the fact that the algorithm did not produce a new image of the sloping edge at the correct position.

Therefore we did another experiment, using a finer line spacing (10 m instead of 20 m) and a wider cross-line operator angle (30 degrees instead of 15 degrees). Also we reduced the detector interval (12 m instead of 15 m) to suppress the aliasing noise above the horizontal reflector. A vertical 2-D slice of the subsurface below line 1 is shown in Figure VI-16a. The result after 2-D redatuming, wide-angle CDP stacking and ZO migration of line 1 is shown in Figure VI-16b. Note the strong side-swipe reflection of dome 1 and the mis-positioned sloping edge. A 2-D slice below line 1 of the result after 3-D redatuming, wide-angle CDP stacking and ZO migration is shown in Figure VI-16c. Note that the side-swipe reflection of dome 1 disappeared for the greater part and that the sloping edge is positioned correctly.

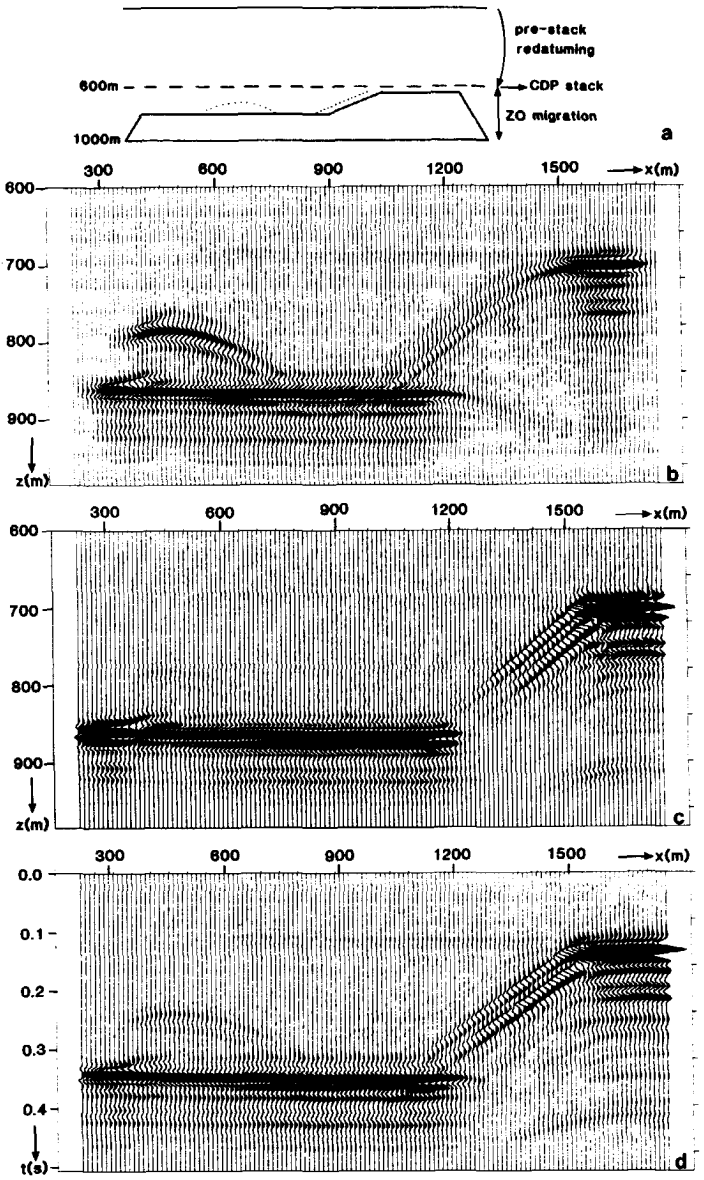

Figure VI-16: Results of a new experiment, using a finer line spacing.

a. A vertical 2-D slice of the subsurface below line 1 (the dotted lines indicate mis-positioned events after 2-D processing, see also Figure b).

b. Result after 2-D redatuming, wide-angle CDP stacking and ZO migration (line 1).

c. Result after 3-D redatuming, wide-angle CDP stacking and ZO migration (line 1).

d. **Unmigrated** result after 3-D redatuming and wide-angle CDP stacking (line 1).

Finally, in Figure VI-16d we show a 2-D slice of the **unmigrated** 3-D wide-angle CDP stack (after 3-D redatuming) at the upper boundary of the target zone. Notice that these ZO data in the **time domain** can be easily interpreted because they are simulated at a level just above the zone of interest. In fact these unmigrated data are very similar to the migrated data in Figure VI-16c! Hence, 3-D pre-stack redatuming and wide-angle CDP stacking at the upper boundary of the target zone represents a more costly but far superior alternative to conventional CMP stacking at the acquisition surface. It may be expected that the combination of redatuming and CDP stacking will play a key role in future seismic processing.

APPENDICES

APPENDIX A

In this appendix we give the mathematical proof of relations (II-50) and (II-51). We use the following notation convention: the elements of matrix **capital** $\mathbf{Q}$ are denoted by **lower case** q^{ij}. Furthermore we delete the super-scripts + and - as well as the argument z_i.

First we prove that $\mathbf{G}$, defined according to (II-47a) as

$$\mathbf{G} = \mathbf{S}^{*T}\mathbf{S} = \left[\sum_m \mathbf{S}_m^{*T}\right]\left[\sum_m \mathbf{S}_m\right], \tag{A-1}$$

may be written as

$$\mathbf{G} = \sum_m \mathbf{G}_m = \sum_m \left[\mathbf{S}_m^{*T}\mathbf{S}_m\right] \tag{A-2}$$

assuming $\mathbf{G}$ is a diagonal matrix. According to (A-1) the elements of $\mathbf{G}$ read

$$g^{ij} = \sum_k \left[\left(\sum_m (s_m^{ki})^*\right)\left(\sum_m s_m^{kj}\right)\right], \tag{A-3a}$$

or, since by definition $s_m^{uv} = o$ if $v \neq m$:

$$g^{ij} = \sum_k \left[(s_i^{ki})^* s_j^{kj}\right], \tag{A-3b}$$

or, since it is assumed that $g^{ij} = o$ if $i \neq j$:

$$g^{ii} = \sum_k \left[(s_i^{ki})^* \, s_i^{ki} \right]. \qquad \text{(A-3c)}$$

On the other hand, according to (A-2) the elements of $\mathbf{G}$ read

$$g^{ij} = \sum_m \left[\sum_k \left((s_m^{ki})^* \, s_m^{kj} \right) \right], \qquad \text{(A-4a)}$$

or, changing the order of summation and taking into account that $s_m^{uv} = o$ if $v \neq m$:

$$g^{ij} = \sum_k \left[(s_i^{ki})^* \, s_i^{kj} \right]. \qquad \text{(A-4b)}$$

According to this expression $g^{ij} = o$ if $i \neq j$, while the diagonal elements g^{ii} are given by

$$g^{ii} = \sum_k \left[(s_i^{ki})^* \, s_i^{ki} \right]. \qquad \text{(A-4c)}$$

Notice that g^{ii} in (A-3c) equals g^{ii} in (A-4c), which completes the proof of (II-50).

Next we prove that $\mathbf{X}$, defined according to (II-51a) as

$$\mathbf{X} = \left[\sum_m \mathbf{P}_m \right] \left[\sum_m \mathbf{C}_m \right] \left[\sum_m \mathbf{S}_m^{*T} \right], \qquad \text{(A-5)}$$

may be written as

$$\mathbf{X} = \sum_m \left[\mathbf{P}_m \mathbf{C}_m \mathbf{S}_m^{*T} \right], \qquad \text{(A-6)}$$

which is the equivalent of relation (II-51b).

According to (A-5) the elements of $\mathbf{X}$ read

$$x^{ij} = \sum_k \sum_l \left[\left(\sum_m p_m^{ik} \right) \left(\sum_m c_m^{kl} \right) \left(\sum_m (s_m^{jl})^* \right) \right], \qquad \text{(A-7a)}$$

or, since $p_m^{uv} = o$, $c_m^{uv} = o$ and $s_m^{uv} = o$ if $v \neq m$:

$$x^{ij} = \sum_k \sum_l \left[p_k^{ik} \, c_l^{kl} \, (s_l^{jl})^* \right], \qquad \text{(A-7b)}$$

or, since $c_v^{uv} = o$ if $u \neq v$:

$$x^{ij} = \sum_k \left[p_k^{ik} \, c_k^{kk} \, (s_k^{jk})^* \right]. \qquad \text{(A-7c)}$$

On the other hand, according to (A-6) the elements of $\mathbf{X}$ read

$$x^{ij} = \sum_m \left[\sum_k \sum_l \left(p_m^{ik} \, c_m^{kl} \, (s_m^{jl})^* \right) \right], \qquad \text{(A-8a)}$$

or, changing the order of summation and taking into account that $p_m^{uv} = o$ if $v \neq m$:

$$x^{ij} = \sum_k \sum_l \left[p_k^{ik} \, c_k^{kl} \, (s_k^{jl})^* \right], \qquad \text{(A-8b)}$$

or, since $c_v^{uv} = o$ if $u \neq v$:

$$x^{ij} = \sum_k \left[p_k^{ik} \, c_k^{kk} \, (s_k^{jk})^* \right]. \qquad \text{(A-8c)}$$

Notice that x^{ij} in (A-7c) equals x^{ij} in (A-8c), which completes the proof of (II-51).

APPENDIX B

In this appendix we study the relations (III-32c) and (III-32d) for $\Delta z \to 0$.

$$\lim_{\Delta z \to o} \tilde{W}^{+}(z_m, z_o) = \lim_{\Delta z \to o} \left[\left(\prod_{i=1}^{m-1} \tilde{T}^{+}(z_i) \right) \left(\prod_{i=1}^{m} \tilde{W}^{+}(z_i, z_{i-1}) \right) \right], \qquad \text{(B-1a)}$$

$$\lim_{\Delta z \to o} \tilde{W}^{-}(z_o, z_m) = \lim_{\Delta z \to o} \left[\left(\prod_{i=1}^{m-1} \tilde{T}^{-}(z_i) \right) \left(\prod_{i=1}^{m} \tilde{W}^{-}(z_{i-1}, z_i) \right) \right], \qquad \text{(B-1b)}$$

with $\Delta z = z_i - z_{i-1}$.
Notice that z_m is fixed, so $m \to \infty$ when $\Delta z \to 0$. Here we consider relation (B-1a), for propagating waves only ($\tilde{H}_1^2 \geq 0$). According to relation (III-16d) operator $\tilde{W}^{+}(z_i, z_{i-1})$ is given by

$$\tilde{W}^{+}(z_i, z_{i-1}) = \exp[-j\tilde{H}_1(z_{i-1})\Delta z]. \qquad \text{(B-2)}$$

By solving the boundary conditions at $z = z_i$ ($\tilde{P}$ continuous, $\tilde{V}_z$ continuous), it follows easily that the transmission operator $\tilde{T}^{+}(z_i)$ is given by (Berkhout, 1982)

$$\tilde{T}^{+}(z_i) = 1 + \tilde{R}(z_i), \qquad \text{(B-3a)}$$

with

$$\tilde{R}(z_i) = \frac{\rho(z_i)\tilde{H}_1(z_{i-1}) - \rho(z_{i-1})\tilde{H}_1(z_i)}{\rho(z_i)\tilde{H}_1(z_{i-1}) + \rho(z_{i-1})\tilde{H}_1(z_i)}. \qquad \text{(B-3b)}$$

Assuming a continuously layered medium, we may rewrite $\tilde{T}^{+}(z_i)$ when $\Delta z = z_i - z_{i-1} \to 0$, according to

$$\lim_{\Delta z \to o} \tilde{T}^{+}(z_i) = 1 + \left[\frac{1}{2\rho} \frac{\partial \rho}{\partial z}\bigg|_{z_i} - \frac{1}{2\tilde{H}_1} \frac{\partial \tilde{H}_1}{\partial z}\bigg|_{z_i} \right] \Delta z, \qquad \text{(B-4)}$$

assuming $\tilde{H}_1(z_i) \neq 0$.
Substitution of (B-2) and (B-4) in relation (B-1a), assuming $\tilde{H}_1^2(z) > 0$ for $z_o < z < z_m$, yields

$$\lim_{\Delta z\to o}\tilde{W}^{+}(z_m,z_o) = \exp\left[\lim_{\Delta z\to o}\left\{\sum_{i=1}^{m-1}\ln\tilde{T}^{+}(z_i)+\sum_{i=1}^{m}\ln\tilde{W}^{+}(z_i,z_{i-1})\right\}\right]$$

$$= \exp\int_{z_o}^{z_m}\left\{\frac{1}{2\rho}\frac{\partial\rho}{\partial z}-\frac{1}{2\tilde{H}_1}\frac{\partial\tilde{H}_1}{\partial z}-j\tilde{H}_1\right\}dz$$

$$= \exp\int_{z_o}^{z_m}\left[-\frac{\partial}{\partial z}\ln\sqrt{\frac{\tilde{H}_1}{\rho}}\right]dz\ \exp\int_{z_o}^{z_m}-j\tilde{H}_1\,dz,$$

from which relation (III-33a) follows immediately. Relation (III-33b) can be derived accordingly. Similar relations can be derived for evanescent waves ($\tilde{H}_1^2<0$ for $z_o<z<z_m$). This is beyond the scope of this appendix.

APPENDIX C

Solutions of Airy equation (III-43) are given by Airy functions (see Figure III-6). Here we summarize the results tabulated by Abramowitz and Stegun (1970). A pair of independent solutions is $Ai(\zeta)$, $Bi(\zeta)$, which can be expressed in terms of Bessel functions I and J of fractional order.

1. $\zeta>0$, $\vartheta = \frac{2}{3}\zeta^{3/2}$: $Ai(\zeta) = \frac{1}{3}\sqrt{\zeta}\,[I_{-1/3}(\vartheta) - I_{1/3}(\vartheta)]$, (C-1a)

$$Ai'(\zeta) = -\frac{1}{3}\zeta[I_{-2/3}(\vartheta) - I_{2/3}(\vartheta)], \quad \text{(C-1b)}$$

$$Bi(\zeta) = \sqrt{\frac{1}{3}\zeta}\,[I_{-1/3}(\vartheta) + I_{1/3}(\vartheta)], \quad \text{(C-1c)}$$

$$Bi'(\zeta) = \zeta\sqrt{\frac{1}{3}}\,[I_{-2/3}(\vartheta) + I_{2/3}(\vartheta)], \quad \text{(C-1d)}$$

where the primes denote differentiation with respect to ζ.

2. $\zeta<0$, $\vartheta = \frac{2}{3}(-\zeta)^{3/2}$: $Ai(\zeta) = \frac{1}{3}\sqrt{-\zeta}\,[J_{-1/3}(\vartheta) + J_{1/3}(\vartheta)]$, (C-2a)

$$Ai'(\zeta) = \frac{1}{3}\zeta\,[J_{-2/3}(\vartheta) - J_{2/3}(\vartheta)], \quad \text{(C-2b)}$$

$$Bi(\zeta) = \sqrt{-\frac{1}{3}\zeta}\,[J_{-1/3}(\vartheta) - J_{1/3}(\vartheta)], \quad \text{(C-2c)}$$

$$Bi'(\zeta) = -\zeta\sqrt{\frac{1}{3}}\,[J_{-2/3}(\vartheta) + J_{2/3}(\vartheta)]. \quad \text{(C-2d)}$$

3. $$Ai(\zeta)Bi'(\zeta) - Ai'(\zeta)Bi(\zeta) = \pi^{-1}. \quad \text{(C-3)}$$

4. $$Ai(0) = Bi(0)/\sqrt{3} = 3^{-2/3}/\Gamma(\tfrac{2}{3}) = .355028053887817, \quad \text{(C-4a)}$$

$$-Ai'(0) = Bi'(0)/\sqrt{3} = 3^{-1/3}/\Gamma(\tfrac{1}{3}) = .258819403792807. \quad \text{(C-4b)}$$

5. $\zeta\to\infty$, $\vartheta = \frac{2}{3}\zeta^{3/2}$: $Ai(\zeta) = \frac{1}{2\sqrt{\pi}}\zeta^{-\frac{1}{4}}\,e^{-\vartheta}$, (C-5a)

$$Ai'(\zeta) = (-\zeta^{\frac{1}{2}} - \tfrac{1}{4}\zeta^{-1})Ai(\zeta), \quad \text{(C-5b)}$$

$$Bi(\zeta) = \frac{1}{\sqrt{\pi}}\,\zeta^{-\frac{1}{4}}\,e^{\vartheta}, \quad \text{(C-5c)}$$

$$Bi'(\zeta) = (\zeta^{\frac{1}{2}} - \tfrac{1}{4}\zeta^{-1})Bi(\zeta). \quad \text{(C-5d)}$$

6. $\zeta \to -\infty$, $\vartheta = \frac{2}{3}(-\zeta)^{3/2}$:

$$\mathrm{Ai}(\zeta) = \frac{1}{\sqrt{\pi}}(-\zeta)^{-\frac{1}{4}} \sin(\vartheta + \tfrac{\pi}{4}), \tag{C-6a}$$

$$\mathrm{Ai}'(\zeta) = -(-\zeta)^{\frac{1}{2}}\mathrm{Bi}(\zeta) + \tfrac{1}{4}(-\zeta)^{-1}\mathrm{Ai}(\zeta), \tag{C-6b}$$

$$\mathrm{Bi}(\zeta) = \frac{1}{\sqrt{\pi}}(-\zeta)^{-\frac{1}{4}} \cos(\vartheta + \tfrac{\pi}{4}), \tag{C-6c}$$

$$\mathrm{Bi}'(\zeta) = (-\zeta)^{\frac{1}{2}}\mathrm{Ai}(\zeta) + \tfrac{1}{4}(-\zeta)^{-1}\mathrm{Bi}(\zeta). \tag{C-6d}$$

Notice that in chapter III the arguments ζ and ϑ for propagating waves read

$$\zeta = -\chi^{-2/3}\tilde{H}_2 = -\chi^{1/3}(z-z_t), \tag{C-7a}$$

$$\vartheta = \tfrac{2}{3}|\chi|^{-1}\tilde{H}_2^{3/2}. \tag{C-7b}$$

APPENDIX D

In this appendix, we discuss the details of step 2ii of the inversion scheme presented in section III-10. We assume that the data are downward extrapolated to z_m and we abbreviate $c_{m+1}(z)$ and $c_{m+1}(z_m)$ to $c(z)$ and c_o respectively. According to Aki and Richards (1980), the intercept time τ, corresponding to a critical angle event described by ray-parameter p, can be expressed as

$$\tau(p) = 2 \int_0^{z_t(p)} \sqrt{c^{-2}(z) - p^2}\, dz, \qquad \text{(D-1)}$$

where the turning point depth $z_t(p)$ follows from $p=1/c(z_t)$. Migrating critical angle data, using an estimated velocity profile $c'(z)$, yields an apparent turning point depth $z_t''(p)$ which satisfies the following integral equation

$$2 \int_0^{z_t(p)} \sqrt{c^{-2}(z) - p^2}\, dz = 2 \int_0^{z_t''(p)} \sqrt{\{c'(z)\}^{-2} - p^2}\, dz. \qquad \text{(D-2)}$$

The underlying philosophy for this equation is that the turning point image is obtained when the intercept time τ is consumed by means of downward extrapolation of the data. In the following we present a solution of (D-2), assuming

$$c^{-2}(z) = c_o^{-2}[1 - az], \qquad a>0. \qquad \text{(D-3a)}$$

Futhermore, we assume that the data are migrated, using migration velocity $c'(z)$, such that

$$\{c'(z)\}^{-2} = c_o^{-2}[1 - a'z], \qquad 0<a' \leq a. \qquad \text{(D-3b)}$$

Finally we assume that the output velocity profile $c''(z)$ satisfies

$$\{c''(z)\}^{-2} = c_o^{-2}[1 - a''z], \qquad a'' \geq a. \qquad \text{(D-3c)}$$

Notice that, with $p=1/c(z_t)$, the corresponding turning point depths follow from

$$z_t(p) = [1 - c_o^2 p^2]/a, \tag{D-4a}$$

$$z_t'(p) = [1 - c_o^2 p^2]/a', \tag{D-4b}$$

$$z_t''(p) = [1 - c_o^2 p^2]/a''. \tag{D-4c}$$

Given the input and output parameters **a'** and **a"** respectively, then the true value **a** follows from (D-2) - (D-4), according to

$$a = a'/[1 - (1 - \frac{a'}{a''})^{3/2}]. \tag{D-5}$$

Now the true velocity is obtained by substituting this value in relation (D-3a).

Notice that even for $|1-a'/a''|<<1$ we may **not** write $a \approx \frac{1}{2}(a'+a'')$, so relation (III-76a) is biased, even for small gradients, which follows from rewriting (D-3) for small gradients.

APPENDIX E

In this appendix, we derive a two-way wave field extrapolation operator for arbitrarily inhomogeneous media. We follow the same procedure as in section IV.4, however, here we take into account the first derivative of the medium properties with respect to z.

Our starting point is relation (IV-33)

$$\vec{Q}(z) = \sum_{m=0}^{\infty} \frac{(z-z_o)^m}{m!} \left[\frac{\partial^m \vec{Q}}{\partial z^m}\right]_{z_o}, \tag{E-1a}$$

where

$$\frac{\partial^m \vec{Q}}{\partial z^m} = \frac{\partial}{\partial z}\left[\frac{\partial^{m-1}\vec{Q}}{\partial z^{m-1}}\right], \tag{E-1b}$$

with

$$\frac{\partial \vec{Q}}{\partial z} = \mathbf{A}\vec{Q}, \tag{E-1c}$$

$\mathbf{A}$ and $\vec{Q}$ being defined by relations (IV-2b,c). In the following we assume linearized medium properties, according to

$$c(x,y,z) = c_o(x,y)[1+q(x,y)\Delta z] \tag{E-2a}$$

and

$$\rho(x,y,z) = \rho_o(x,y)[1+r(x,y)\Delta z], \tag{E-2b}$$

with

$$\Delta z = z-z_o,$$

while

$$|q(x,y)\Delta z| << 1 \tag{E-2c}$$

and

$$|r(x,y)\Delta z| << 1. \tag{E-2d}$$

Now operator $\mathbf{A}$ can be linearized, according to

$$\mathbf{A} = \mathbf{A}_o + \partial_z \mathbf{A}_o \Delta z, \tag{E-3a}$$

with

$$\mathbf{A}_o = \begin{bmatrix} o & \rho_o d_o^* \\ -\frac{1}{\rho_o} L_2^* & o \end{bmatrix}, \quad \partial_z \mathbf{A}_o = \begin{bmatrix} o & \rho_o r d_o^* \\ \frac{1}{\rho_o} G_2^* & o \end{bmatrix}, \qquad \text{(E-3b,c)}$$

$$L_2 = H_2(z_o), \quad G_2 = \rho_o [\frac{\partial}{\partial z}(-\frac{1}{\rho} H_2)]_{z_o}. \qquad \text{(E-3d,e)}$$

In the following we assume that lateral derivatives of q(x,y) and r(x,y) may be neglected. In this case we obtain

$$G_2 = rL_2 + (2q\omega^2/c_o^2)d_o, \qquad \text{(E-3f)}$$

while $[\partial_z^m \vec{Q}]_{z_o}$ can be approximated for even m (m=2n) by

$$[\partial_z^{2n} \vec{Q}]_{z_o} = [\mathbf{A}_o^{2n} + n^2 \mathbf{A}_o^{2n-2}(\partial_z \mathbf{A}_o) + n(n-1)\mathbf{A}_o^{2n-3}(\partial_z \mathbf{A}_o)\mathbf{A}_o]\vec{Q}(z_o), \qquad \text{(E-4a)}$$

and for odd m (m=2n+1) by

$$[\partial_z^{2n+1} \vec{Q}]_{z_o} = [\mathbf{A}_o^{2n+1} + n^2 \mathbf{A}_o^{2n-1}(\partial_z \mathbf{A}_o) + n(n+1)\mathbf{A}_o^{2n-2}(\partial_z \mathbf{A}_o)\mathbf{A}_o]\vec{Q}(z_o), \qquad \text{(E-4b)}$$

where

$$\mathbf{A}_o^{2n} = (-1)^n \begin{bmatrix} L_{2n}^* & o \\ o & \frac{1}{\rho_o} L_{2n}^* \rho_o L_o^* \end{bmatrix}, \mathbf{A}_o^{2n+1} = (-1)^n \begin{bmatrix} o & L_{2n}^* \rho_o L_o^* \\ -\frac{1}{\rho_o} L_{2n+2}^* & o \end{bmatrix}, \qquad \text{(E-4c,d)}$$

$$\mathbf{A}_o^{2n-2}(\partial_z \mathbf{A}_o) = -(-1)^n \begin{bmatrix} o & \rho_o r L_{2n-2}^* \\ \frac{1}{\rho_o} G_2^* L_{2n-2}^* & o \end{bmatrix}, \mathbf{A}_o^{2n-1}(\partial_z \mathbf{A}_o) = -(-1)^n \begin{bmatrix} G_2^* L_{2n-2}^* & o \\ o & -r L_{2n}^* \end{bmatrix}$$

$$\text{(E-4e,f)}$$

$$\mathbf{A}_o^{2n-3}(\partial_z \mathbf{A}_o)\mathbf{A}_o = (-1)^n \begin{bmatrix} o & \rho_o G_2^* L_{2n-4}^* \\ \frac{r}{\rho_o} L_{2n}^* & o \end{bmatrix}, \mathbf{A}_o^{2n-2}(\partial_z \mathbf{A}_o)\mathbf{A}_o = -(-1)^n \begin{bmatrix} -r L_{2n}^* & o \\ o & G_2^* L_{2n-2}^* \end{bmatrix},$$

with L_{2n+2} defined recursively, according to $\qquad \text{(E-4g,h)}$

$$L_{2n+2} = L_2 * L_{2n}, \quad L_o = d_o(x,y) = \delta(x)\delta(y). \qquad \text{(E-4i,j)}$$

With these relations we finally find

$$\vec{Q}(z) = \mathbf{W}(z,z_o)\vec{Q}(z_o), \tag{E-5a}$$

where

$$\mathbf{W}(z,z_o) = \begin{bmatrix} W_I(z,z_o)^* & W_{II}(z,z_o)^* \\ W_{III}(z,z_o)^* & W_{IV}(z,z_o)^* \end{bmatrix}, \tag{E-5b}$$

$$W_I(z,z_o) = \sum_{n=o}^{\infty}\left[a_n L_{2n} + 2nb_n\left\{-nq\,\frac{\omega^2}{c_o^2} + \frac{r}{2}\,L_2^*\right\}L_{2n-2}\right], \tag{E-5c}$$

$$W_{II}(z,z_o) = \sum_{n=o}^{\infty}\left[b_n L_{2n}^*\rho_o L_o + 2\rho_o n a_n\left\{(n-1)q\,\frac{\omega^2}{c_o^2} - \frac{r}{2}L_2^*\right\}L_{2n-4}\right], \tag{E-5d}$$

$$W_{III}(z,z_o) = \sum_{n=o}^{\infty}\left[-b_n\,\frac{1}{\rho_o}L_{2n+2} + \frac{2}{\rho_o}na_n\left\{-nq\,\frac{\omega^2}{c_o^2} - \frac{r}{2}L_2^*\right\}L_{2n-2}\right], \tag{E-5e}$$

$$W_{IV}(z,z_o) = \sum_{n=o}^{\infty}\left[a_n\,\frac{1}{\rho_o}L_{2n}^*\rho_o L_o + 2nb_n\left\{-(n+1)q\,\frac{\omega^2}{c_o^2} - \frac{r}{2}L_2^*\right\}L_{2n-2}\right], \tag{E-5f}$$

with a_n and b_n defined by relations (IV-37d,f). Notice that for q=r=o, relation (IV-37) is obtained. On the other hand, if the medium properties c and ρ are functions of z only, then extrapolation may be carried out in the wavenumber–frequency domain, so operator L_{2n} may be replaced by $\tilde{L}_2^n = \tilde{H}_2^n(z_o)$. Now the infinite series in (E-5) can be summed to closed expressions, yielding operators (IV-25b,c,d,e).

APPENDIX F

In this appendix, we derive a fast converging two-way wave field extrapolation operator for arbitrarily inhomogeneous media. We follow the same procedure as in section IV.5, however, here we take into account the first derivative of the medium properties with respect to z.

Our starting point is operator (E-5b). Neglecting the lateral derivatives of the medium parameters, this operator can be rewritten as

$$\mathbf{W}(z,z_o) = \sum_{n=o}^{\infty}\left[\left\{ \mathbf{R}\mathbf{E}_n + (\mathbf{S} + \mathbf{J}\mathbf{U})\mathbf{F}_n + (\mathbf{T} + \mathbf{J}\mathbf{V})\mathbf{G}_n\right\}\mathbf{L}_2^n\right] \qquad \text{(F-1a)}$$

where

$$\mathbf{R} = \begin{bmatrix} 1+R & o \\ o & 1-R \end{bmatrix}, \quad \mathbf{S} = \begin{bmatrix} S-R & o \\ o & S+R \end{bmatrix}, \quad \mathbf{T} = \begin{bmatrix} S & o \\ o & -S \end{bmatrix}, \qquad \text{(F-1b,c,d)}$$

$$\mathbf{J} = \rho_o \Delta z \begin{bmatrix} o & d_o^* \\ Z_2^* & o \end{bmatrix}, \quad \mathbf{U} = \begin{bmatrix} 1+R & o \\ o & 1+R \end{bmatrix}, \quad \mathbf{V} = \begin{bmatrix} -S & o \\ o & -S \end{bmatrix}, \qquad \text{(F-1e,f,g)}$$

$$\mathbf{E}_n = \begin{bmatrix} a_n & o \\ o & a_n \end{bmatrix}, \quad \mathbf{F}_n = \begin{bmatrix} b_n/\Delta z & o \\ o & b_n/\Delta z \end{bmatrix}, \qquad \text{(F-1h,i)}$$

$$\mathbf{G}_n = \frac{1}{\Delta z^2}\left[\mathbf{E}_{n+1} - \mathbf{F}_{n+1}\right], \quad \mathbf{L}_2^n = \begin{bmatrix} L_{2n}^* & o \\ o & L_{2n}^* \end{bmatrix}, \qquad \text{(F-1j,k)}$$

$$Z_2 = -\frac{1}{\rho_o^2}\left[(1-r\Delta z)L_2 - q\Delta z\,\frac{\omega^2}{c_o^2}\,d_o\right], \qquad \text{(F-1l)}$$

$$S = \frac{q\omega^2}{2c_o^2}\Delta z^3, \quad R = \frac{r}{2}\Delta z, \qquad \text{(F-1m,n)}$$

with $c_o(x,y)$, $\rho_o(x,y)$, $q(x,y)$, $r(x,y)$ given by (E-2), L_{2n} given by (E-4i) and a_n, b_n given by relations (IV-37d,f). In relation (F-1) we made use of the property $\Delta z a_n = (2n+1)b_n$.

Similar as in section IV.5, we may write for $\mathbf{L}_2^n$:

$$\mathbf{L}_2^n = \sum_{m=o}^{n} \left[\frac{1}{m!} \left(\frac{\partial^m}{\partial \kappa^m} \mathbf{K}^n \right) \mathbf{D}_2^m \right], \quad \kappa = \omega^2/c_o^2, \tag{F-2}$$

with $\mathbf{K}$ and $\mathbf{D}_2$ given by relations (IV-39b,c). Substitution in (F-1), changing the order of summations, and using the property $\partial_\kappa^m \kappa^n = o$ for $m>n$, yields

$$\mathbf{W}(z,z_o) = \sum_{m=o}^{\infty} \left[\frac{1}{m!} \left\{ \mathbf{R} \left(\frac{\partial^m}{\partial \kappa^m} \mathbf{M} \right) + (\mathbf{S} + \mathbf{J}\,\mathbf{U}) \left(\frac{\partial^m}{\partial \kappa^m} \mathbf{N} \right) \right.\right.$$

$$\left.\left. + (\mathbf{T} + \mathbf{J}\,\mathbf{V}) \left(\frac{\partial^m}{\partial \kappa^m} \mathbf{P} \right) \right\} \mathbf{D}_2^m \right], \tag{F-3a}$$

where

$$\mathbf{M} = \sum_{n=o}^{\infty} \left[\mathbf{E}_n \mathbf{K}^n \right], \quad \mathbf{N} = \sum_{n=o}^{\infty} \left[\mathbf{F}_n \mathbf{K}^n \right], \quad \mathbf{P} = \sum_{n=o}^{\infty} \left[\mathbf{G}_n \mathbf{K}^n \right]. \tag{F-3b,c,d}$$

The infinite expansions for $\mathbf{M}$, $\mathbf{N}$ and $\mathbf{P}$ can be replaced by closed expressions, according to

$$\mathbf{M} = \begin{bmatrix} \psi_{1,o} & o \\ o & \psi_{1,o} \end{bmatrix}, \quad \mathbf{N} = \begin{bmatrix} \psi_{2,o} & o \\ o & \psi_{2,o} \end{bmatrix}, \quad \mathbf{P} = \begin{bmatrix} \psi_{3,o} & o \\ o & \psi_{3,o} \end{bmatrix}, \tag{F-4a,b,c}$$

where

$$\psi_{1,o} = \cos\Phi_o, \quad \psi_{2,o} = \frac{\sin\Phi_o}{\Phi_o}, \quad \psi_{3,o} = \frac{\cos\Phi_o}{\Phi_o^2} - \frac{\sin\Phi_o}{\Phi_o^3}, \tag{F-4d,e,f}$$

with

$$\Phi_o = \sqrt{\kappa}\Delta z = \frac{\omega}{c_o} \Delta z. \tag{F-4g}$$

Notice that $\psi_{1,o}$, $\psi_{2,o}$ and $\psi_{3,o}$ equal the operators $\tilde{\psi}_1$, $\tilde{\psi}_2$ and $\tilde{\psi}_3$, respectively, given by relations (IV-25i,j,k) for horizontal plane waves, that is, for $k_x^2 = k_y^2 = o$.

By substituting relation (F-4) in relation (F-3), it follows that operator $\mathbf{W}(z,z_o)$ is given by

$$\mathbf{W}(z,z_o) = \begin{bmatrix} W_I(z,z_o)^* & W_{II}(z,z_o)^* \\ W_{III}(z,z_o)^* & W_{IV}(z,z_o)^* \end{bmatrix}, \tag{F-5a}$$

where

$$W_I(z,z_o) = \sum_{m=o}^{\infty} \alpha_m D_{2m}, \quad W_{II}(z,z_o) = \sum_{m=o}^{\infty} \beta_m D_{2m}, \tag{F-5b,c}$$

$$W_{III}(z,z_o) = Z_2 * W_{II}(z,z_o), \quad W_{IV}(z,z_o) = \sum_{m=o}^{\infty} \gamma_m D_{2m}, \tag{F-5d,e}$$

with

$$\alpha_m = (1+R)\zeta_m + \frac{(S-R)}{\rho_o \Delta z}\eta_m + S\vartheta_m, \tag{F-5f}$$

$$\beta_m = (1+R)\eta_m - \rho_o \Delta z S \vartheta_m, \tag{F-5g}$$

$$\gamma_m = (1-R)\zeta_m + \frac{(S+R)}{\rho_o \Delta z}\eta_m - S\vartheta_m, \tag{F-5h}$$

$$\zeta_m = \frac{1}{m!}\left(\frac{\partial^m}{\partial \kappa^m}\psi_{1,o}\right), \quad \eta_m = \rho_o \Delta z \frac{1}{m!}\left(\frac{\partial^m}{\partial \kappa^m}\psi_{2,o}\right), \quad \vartheta_m = \frac{1}{m!}\left(\frac{\partial^m}{\partial \kappa^m}\psi_{3,o}\right). \tag{F-5i,j,k}$$

For m=o, 1 etc., we find

$$\zeta_o = \cos\Phi_o, \quad \zeta_1 = -\frac{1}{2\kappa}\Phi_o \sin\Phi_o, \text{ etc.}, \tag{F-6a,b}$$

$$\eta_o = \rho_o \Delta z \frac{\sin\Phi_o}{\Phi_o}, \quad \eta_1 = -\frac{\rho_o \Delta z}{2\kappa}\left[\frac{\sin\Phi_o}{\Phi_o} - \cos\Phi_o\right], \text{ etc.} \tag{F-6c,d}$$

$$\vartheta_o = \frac{\cos\Phi_o}{\Phi_o^2} - \frac{\sin\Phi_o}{\Phi_o^3}, \quad \vartheta_1 = -\frac{1}{2\kappa}\left[\frac{\sin\Phi_o}{\Phi_o} + \frac{3\cos\Phi_o}{\Phi_o^2} - \frac{3\sin\Phi_o}{\Phi_o^3}\right], \text{ etc.} \tag{F-6e,f}$$

Notice that for q=r=o, operator (F-5) equals operator (IV-42). On the other hand, if the medium properties c and ρ are functions of z only, then extrapolation may be carried out in the wavenumber-frequency domain, so D_{2m} may be replaced by $\tilde{D}_2^m = (-k_x^2 - k_y^2)^m$. Now the infinite series in (F-5) can be summed to closed expressions, yielding operators (IV-25b,c,d,e).

APPENDIX G

Operator $\mathbf{A}_s$ in relation (V-8) is given by

$$\mathbf{A}_s = \begin{bmatrix} \mathbf{O} & \mathbf{A}_1 \\ \mathbf{A}_2 & \mathbf{O} \end{bmatrix}, \tag{G-1a}$$

$$\mathbf{O} = \begin{bmatrix} 0 & 0 \\ 0 & 0 \end{bmatrix}, \tag{G-1b}$$

$$\mathbf{A}_1 = \begin{bmatrix} -\left(\frac{\omega^2}{\lambda+2\mu}\right) d_o(x)^* & -\left(\frac{\lambda}{\lambda+2\mu}\right) d_1(x)^* \\ -\left(\frac{\lambda}{\lambda+2\mu}\right) d_1(x)^* & \left\{\rho d_o(x) + \frac{4\mu}{\omega^2}\left(\frac{\lambda+\mu}{\lambda+2\mu}\right) d_2(x)\right\}^* \end{bmatrix}, \tag{G-1c}$$

$$\mathbf{A}_2 = \begin{bmatrix} \rho d_o(x)^* & -d_1(x)^* \\ -d_1(x)^* & -\frac{\omega^2}{\mu} d_o(x)^* \end{bmatrix}. \tag{G-1d}$$

This operator can be decomposed as follows

$$\mathbf{A}_s = \mathbf{L}_s \mathbf{\Lambda}_s \mathbf{L}_s^{-1} \tag{G-2a}$$

with

$$\mathbf{L}_s = \begin{bmatrix} \mathbf{L}_1 & \mathbf{L}_1 \\ \mathbf{L}_2 & -\mathbf{L}_2 \end{bmatrix}, \tag{G-2b}$$

$$\mathbf{\Lambda}_s = \begin{bmatrix} \mathbf{\Lambda} & \mathbf{O} \\ \mathbf{O} & -\mathbf{\Lambda} \end{bmatrix}, \tag{G-2c}$$

$$\mathbf{L}_s^{-1} = \tfrac{1}{2} \begin{bmatrix} \mathbf{L}_1^{-1} & \mathbf{L}_2^{-1} \\ \mathbf{L}_1^{-1} & -\mathbf{L}_2^{-1} \end{bmatrix}, \tag{G-2d}$$

$$\mathbf{L}_1 = \begin{bmatrix} \omega H_1^{(P)*} & j\omega d_1(x)* \\ -2\frac{\mu}{\omega} d_1(x) * H_1^{(P)*} & -\left[j\rho\omega d_o(x) + 2j\frac{\mu}{\omega} d_2(x)\right]* \end{bmatrix}, \tag{G-2e}$$

$$\mathbf{L}_2 = \begin{bmatrix} [j\rho\omega d_o(x) + 2j\frac{\mu}{\omega} d_2(x)]* & -2\frac{\mu}{\omega} d_1(x) * H_1^{(SV)*} \\ j\omega d_1(x)* & -\omega H_1^{(SV)*} \end{bmatrix}, \tag{G-2f}$$

$$\mathbf{\Lambda} = \begin{bmatrix} -jH_1^{(P)*} & o \\ o & -jH_1^{(SV)*} \end{bmatrix}, \tag{G-2g}$$

$$\mathbf{L}_1^{-1} = -\frac{1}{\rho\omega^2} \mathbf{\Lambda}^{-1} \mathbf{L}_2^T, \tag{G-2h}$$

$$\mathbf{L}_2^{-1} = -\frac{1}{\rho\omega^2} \mathbf{\Lambda}^{-1} \mathbf{L}_1^T, \tag{G-2i}$$

$$\mathbf{\Lambda}^{-1} = \begin{bmatrix} jH_{-1}^{(P)*} & o \\ o & jH_{-1}^{(SV)*} \end{bmatrix}, \tag{G-2j}$$

$$H_{-1}^{(P)} * H_1^{(P)} = \delta(x), \tag{G-2k}$$

$$H_1^{(P)} * H_1^{(P)} = H_2^{(P)}, \tag{G-2l}$$

$$H_2^{(P)} = \left(\frac{\omega^2\rho}{\lambda+2\mu}\right) d_o(x) + d_2(x), \tag{G-2m}$$

$$H_{-1}^{(SV)} * H_1^{(SV)} = \delta(x), \tag{G-2n}$$

$$H_1^{(SV)} * H_1^{(SV)} = H_2^{(SV)}, \tag{G-2p}$$

$$H_2^{(SV)} = \left(\frac{\omega^2\rho}{\mu}\right) d_o(x) + d_2(x). \tag{G-2q}$$

APPENDIX H

From the equation of motion (V-3) for inhomogeneous isotropic solids

$$\nabla[(\lambda+2\mu)\nabla.\vec{V}] - \nabla\times(\mu\nabla\times\vec{V}) + \rho\omega^2\vec{V} =$$

$$= -2[(\nabla\mu.\nabla)\vec{V} - (\nabla\mu)\nabla.\vec{V} + (\nabla\mu)\times(\nabla\times\vec{V})] \qquad \text{(H-1a)}$$

and the following three stress-strain relations

$$j\omega Z_x = \mu(\partial V_x/\partial z + \partial V_z/\partial x), \qquad \text{(H-1b)}$$

$$j\omega Z_y = \mu(\partial V_y/\partial z + \partial V_z/\partial y), \qquad \text{(H-1c)}$$

$$j\omega Z_z = \lambda\nabla.\vec{V} + 2\mu(\partial V_z/\partial z), \qquad \text{(H-1d)}$$

the matrix formulation of the full elastic two-way wave equation for 3-D inhomogeneous solids can be derived in a similar way as described in section V.2 for the 2-D inhomogeneous case. Assuming the lateral derivatives of the medium parameters λ, μ and ρ may be neglected, we find

$$\frac{\partial\vec{Q}_s}{\partial z} = \mathbf{A}_s\vec{Q}_s, \qquad \text{(H-2a)}$$

where

$$\vec{Q}_s = [j\omega V_z, Z_x, Z_y, Z_z, j\omega V_x, j\omega V_y]^T, \qquad \text{(H-2b)}$$

and

$$\mathbf{A}_s = \begin{bmatrix} \mathbf{O} & \mathbf{A}_1 \\ \mathbf{A}_2 & \mathbf{O} \end{bmatrix}, \qquad \text{(H-2c)}$$

where

$$\mathbf{O} = \begin{bmatrix} o & o & o \\ o & o & o \\ o & o & o \end{bmatrix}, \qquad \text{(H-2d)}$$

$$\mathbf{A}_1 = \begin{bmatrix} -\left(\frac{\omega^2}{\lambda+2\mu}\right) d_o(x,y)^* & -\left(\frac{\lambda}{\lambda+2\mu}\right) d_1(x)^* & -\left(\frac{\lambda}{\lambda+2\mu}\right) d_1(y)^* \\ -\left(\frac{\lambda}{\lambda+2\mu}\right) d_1(x)^* & [\rho d_o(x,y) + \frac{4\mu}{\omega^2}\alpha d_2(x) + \frac{\mu}{\omega^2} d_2(y)]^* & \frac{\mu}{\omega^2}\beta d_1(x)^* d_1(y)^* \\ -\left(\frac{\lambda}{\lambda+2\mu}\right) d_1(y)^* & \frac{\mu}{\omega^2}\beta d_1(x)^* d_1(y)^* & [\rho d_o(x,y) + \frac{\mu}{\omega^2} d_2(x) + \frac{4\mu}{\omega^2}\alpha d_2(y)]^* \end{bmatrix}, \tag{H-2e}$$

$$\mathbf{A}_2 = \begin{bmatrix} \rho d_o(x,y)^* & -d_1(x)^* & -d_1(y)^* \\ -d_1(x)^* & -\frac{\omega^2}{\mu} d_o(x,y)^* & o \\ -d_1(y)^* & o & -\frac{\omega^2}{\mu} d_o(x,y)^* \end{bmatrix}, \tag{H-2f}$$

$$\alpha = \left(\frac{\lambda+\mu}{\lambda+2\mu}\right), \tag{H-2g}$$

$$\beta = \left(\frac{3\lambda+2\mu}{\lambda+2\mu}\right). \tag{H-2h}$$

REFERENCES

Abramowitz, M., and Stegun, I.A., 1970, Handbook of mathematical functions: Dover, New York

Aki, K., and Richards, P.G., 1980, Quantitative seismology: Freeman and Co., San Francisco

Baysal, E., Kosloff, D.D., and Sherwood, J.W.C., 1984, A two-way non-reflecting wave equation: Geophysics, **49**, 132-141

Berkhout, A.J., 1977, Least-squares inverse filtering and wavelet deconvolution: Geophysics, **42**, 1369-1383

Berkhout, A.J., 1982, Seismic migration, Volume A, Theoretical aspects: Elsevier, Amsterdam - New York

Berkhout, A.J., 1984a, Seismic migration, Volume B, Practical aspects: Elsevier, Amsterdam - New York

Berkhout, A.J., 1984b, Multidimensional linearized inversion and seismic migration: Geophysics, **49**, 1881-1895

Berkhout, A.J., 1986, Seismic inversion in terms of pre-stack migration and multiple elimination: proceedings of IEEE, march issue on inversion.

Bolondi, G., Loinger, E., and Rocca, F., 1984, Offset continuation in theory and practice: Geophys. Prosp., **32**, 1045-1073.

Brekhovskikh, L.M., 1980, Waves in layered media: Academic Press, New York

Bremmer, H., 1951, The WKB approximation as the first term of a geometric-optical series: Commun. Pure Appl. Math., **4**, 105

Brillouin, L., 1926, Remarques sur la mécanique ondulatoire: J. Phys. Radium, **6**, 353-368

Chapman, C.H., 1976, Exact and approximate generalized ray theory in vertically inhomogeneous media: Geophys. J.R. astr. Soc., **46**, 201-233

Cheng, G., and Coen, S., 1984, The relationship between Born inversion and migration for common-midpoint stacked data: Geophysics, **49**, 2117-2131

Claerbout, J.F., 1976, Fundamentals of geophysical data processing: McGraw-Hill, New York

Clayton, R.W., and McMechan, G.A., 1981, Inversion of refraction data by wave field continuation: Geophysics, **46**, 860-868

Clayton, R.W., and Stolt, R.H., 1981, A Born WKBJ inversion method for acoustic reflection data: Geophysics, **46**, 1559-1567

Cohen, J.K., and Bleistein, N., 1979, Velocity inversion for acoustic waves: Geophysics, **44**, 1077-1088

De Graaff, M.P., 1984, Pre-stack migration by single shot record inversion: Doctoral thesis, Delft University of Technology, Delft

De Hoop, A.T., and Van der Hijden, J.H.M.T., 1983, Generation of acoustic waves by an impulsive line source in a fluid/solid configuration with a plane boundary: J. Acoust. Soc. Am., **74**, 333-342

Diebold, J.B., and Stoffa, P.L., 1981, The traveltime equation, tau-p mapping, and inversion of common midpoint data: Geophysics, **46**, 238-254

Dix, C.H., 1955, Seismic velocities from surface measurements: Geophysics, **20**, 68-86

French, W.S., 1975, Computer migration of oblique seismic reflection profiles: Geophysics, **40**, 961-980

Gardner, G.H.F., McDonald, J.A., Watson, T.H., and Kotcher, J.S., 1978, An innovative 3-D marine seismic survey: Presented at the 40th EAEG Meeting, Dublin

Gazdag, J., 1978, Wave equation migration with the phase shift method: Geophysics, **43**, 1342-1351

Gibson, B., Larner, K., and Levin, S., 1983, Efficient 3-D migration in two steps: Geophys. Prosp., **31**, 1-31

Gjøystdal, H., and Ursin, B., 1981, Inversion of reflection times in three dimensions: Geophysics, **46**, 972-983

Green, G., 1837, On the motion of waves in a variable canal of small depth and width: Trans. Cambridge Philos. Soc., **6**, 457-462

Hale, D., 1983, Dip-moveout by Fourier transform: Ph.D. dissertation, Stanford University, Stanford

Hale, D., 1984, Dip-moveout by Fourier transform: Geophysics, **49**, 741-757

Hubral, P., 1976, Interval velocities from surface measurements in the three-dimensional plane layer case: Geophysics, **41**, 233-242

Jakubowicz, H., and Levin, S., 1983, A simple exact method of 3-D migration theory: Geophys. Prosp., **31**, 34-56

Jeffreys, H., 1924, On certain approximate solutions of linear differential equations of the second order: Proc. London Math. Soc., **2**, 428-436

Kennett, B.L.N., 1972, Seismic waves in laterally inhomogeneous media: Geophys. J. R. astr. Soc., **27**, 301-325

Kennett, B.L.N., 1984, An operator approach to forward modeling, data processing and migration: Geophys. Prosp., **32**, 1074-1090

Kennett, B.L.N., and Illingworth, M.R., 1981, Seismic waves in a stratified half space-III, Piecewise smooth models: Geophys. J.R. astr. Soc., **66**, 633-675

Kosloff, D.D., and Baysal, E., 1982, Forward modeling by a Fourier method: Geophysics, **47**, 1402-1412

Kosloff, D.D., and Baysal, E., 1983, Migration with the full acoustic wave equation: Geophysics, **48**, 677-687

Kramers, H.A., 1926, Wellenmechanik und halbzahlige Quantisierung: Z. Physik, **39**, 828-840

Krey, Th., 1976, Computation of interval velocities from common reflection point move-out times for n layers with arbitrary dips and curvatures in three dimensions when assuming small shot-geophone distances: Geophys. Prosp., **24**, 91-111

Liouville, J., 1837, Sur le développement des fonctions on parties de fonctions en séries: J. Math. Pures Appl., **1**, 16-35

Loewenthal, D., Lu, L., Roberson, R., and Sherwood, J., 1974, The wave equation applied to migration: Geophys. Prosp., **24**, 380

McHugh, J.A.M., 1971, An historical survey of ordinary linear differential equations with a large parameter and turning points: Arch. History Exact Sci., **7**, 277-324

McMechan, G.A., 1983, Migration by extrapolation of time-dependent boundary values: Geophys. Prosp., **31**, 413-420

Olver, F.W.J., 1974, Asymptotics and special functions: Academic Press, New York

Pilant, W.L., 1979, Elastic waves in the earth: Elsevier, New York

Raz, S., 1981, Three-dimensional velocity profile inversion from finite offset scattering data: Geophysics, **46**, 837-843

Reshef, M., and Kosloff, D., 1985, Applications of elastic forward modeling to seismic interpretation: Geophysics, **50**, 1266-1272

Ristow, D., 1980, 3D Downward extrapolation of seismic data, in particular by finite difference methods: Doctoral thesis, University of Utrecht, Utrecht

Robinson, E.A., 1984, Seismic inversion and deconvolution: Geophys. Press, Amsterdam

Robinson, E.A., and Treitel, S., 1980, Geophysical signal analysis: Prentice-Hall, Englewood Cliffs, N.J

Schneider, W.A., 1978, Integral formulation in two and three dimensions: Geophysics, **43**, 49-76

Sheriff, R.E., and Geldart, L.P., 1983, Exploration seismology, Volume 2, Data processing and interpretation: Cambridge University Press, Cambridge

Shultz, P.S., and Lau, A., 1984, Poststack estimation of three-dimensional crossline statics: Geophysics, **49**, 227-236

Taner, M.T., and Koehler, F., 1969, Velocity spectra-digital computer derivation and applications of velocity functions: Geophysics, **34**, 859-881

Tarantola, A., 1984, Linearized inversion of seismic reflection data: Geophys. Prosp., **32**, 998-1015

Treitel, S., and Lines, L.R., 1982, Linear inverse theory and deconvolution: Geophysics, **47**, 1153-1159

Ursin, B., 1983, Review of elastic and electromagnetic wave propagation in horizontally layered media: Geophysics, **48**, 1063-1081

Van der Made, P.M., Van Riel, P., and Berkhout, A.J., 1984, Velocity and subsurface geometry inversion by parameter estimation in complex inhomogeneous media: Presented at the 54th Annual International SEG Meeting, Atlanta, December 3rd

Van Riel, P., and Berkhout, A.J., 1985, Resolution in seismic trace inversion by parameter estimation: Geophysics, **50**, 1440-1455

Wapenaar, C.P.A., and Berkhout, A.J., 1985, Velocity determination in layered systems with arbitrarily curved interfaces by means of wave field extrapolation of CMP-data: Geophysics, **50**, 63-76

Wapenaar, C.P.A., and Berkhout, A.J., 1986a, Wave field extrapolation techniques for inhomogeneous media which include critical angle events, Part I, Methods using the one-way wave equations: accepted for publication in Geophys. Prosp.

Wapenaar, C.P.A., and Berkhout, A.J., 1986b, Wave field extrapolation techniques for inhomogeneous media which include critical angle events, Part II, Methods using the two-way wave equation: accepted for publication in Geophys. Prosp.

Wapenaar, C.P.A., and Berkhout, A.J., 1986c, Wave field extrapolation techniques for inhomogeneous media which include critical angle events, Part III, Applications in modeling, migration and inversion: accepted for publication in Geophys. Prosp.

Wapenaar, C.P.A., Kinneging, N.A., and Berkhout, A.J., 1986, Principle of pre-stack migration based on the full elastic two-way wave equation: accepted for publication in Geophysics

Wasow, W., 1965, Asymptotic expansions for ordinary differential equations: Wiley, New York

Weglein, A.B., 1982, Near-field inverse scattering formalism for the three-dimensional wave equation: The inclusion of a priori velocity information: J. Acoust. Soc. Am., **71**, 1179-1183

Wentzel, G., 1926, Eine Verallgemeinerung der Quantenbedingungen für die Zwecke der Wellenmechanik: Z. Physik, **38**, 518-529

Wiener, N., 1949, Extrapolation, interpolation and smoothing of stationary time series: MIT Press, Cambridge

Yilmaz, O., and Claerbout, J.F., 1980, Prestack partial migration: Geophysics, **45**, 1753-1779

Ziolkowski, A., 1984, Deconvolution: IHRDC publ., Boston

SUMMARY

This thesis deals with theoretical and practical aspects of an important seismic inversion technique, generally referred to as **pre-stack migration.** As opposed to post-stack migration, which inverts stacked (pseudo zero-offset) data, pre-stack migration inverts multi-experiment, multi-offset seismic data, assuming known macro features of the earth's subsurface (geologically oriented 'macro subsurface model'). The output consists of a detailed **two-dimensional** (2-D) or **three-dimensional** (3-D) structural image of the subsurface ('micro subsurface model') in terms of the wide-angle zero-offset reflectivity.

In chapter I some **general aspects of seismic inversion** are briefly reviewed. It is argued on theoretical and practical grounds that pre-stack migration should be applied to shot records (no common-midpoint or common-offset compromises), followed by genuine common-depthpoint stacking.

In chapter II the proposed **shot record migration** technique is discussed in more detail. It is shown that

- non-hyperbolic move-out curves are allowed,
- true amplitude migration may be accomplished,
- any data acquisition configuration is allowed,
- small errors in the macro subsurface model can be compensated for,
- any type of wave equation can be used (one-way, two-way, full elastic, etc.),
- many variants can be designed, depending of the migration objective (angle dependent reflectivity, full response data sets at the major interfaces, etc.).

In chapter III various theoretical aspects of the **acoustic one-way wave equations** are reviewed and applications in pre-stack migration are discussed. It is concluded that the one-way approach is valid for sub-critical primary events in 1-D, 2-D and 3-D inhomogeneous macro subsurface models. In addition, it is shown that pre-stack migration based on the acoustic **WKBJ** one-way wave equations is valid for sub-critical as well as critical 'primary' events (turning point effects) in 1-D inhomogeneous macro subsurface models.

In chapter IV various theoretical aspects of the **acoustic two-way wave equation** are reviewed and applications in pre-stack migration are discussed. It is concluded that the two-way approach is valid for 1-D, 2-D and 3-D inhomogeneous macro subsurface models. Acoustic two-way wave equation migration properly handles critical angle events and multiple reflections if the macro subsurface model is accurately known. For smoothed macro subsurface models a high dip-angle performance for primary waves may be expected.

In chapter V various theoretical aspects of the **full elastic two-way wave equation** are reviewed and applications in pre-stack migration are discussed. It is concluded that the full elastic two-way approach is valid for 1-D and 2-D inhomogeneous macro subsurface models and that it can be extended for 3-D inhomogeneous macro subsurface models. Full elastic wave equation migration properly handles multiple reflections and wave conversion if the (full elastic) macro subsurface model is accurately known. For smoothed macro subsurface models a high dip-angle performance for primary waves may be expected.

In chapter VI various **practical aspects of 3-D pre-stack migration** are discussed. In many practical situations seismic interpreters are mainly interested in a high resolution image of a pre-specified target zone. Hence, realistic processing times can be obtained by applying 'target-oriented' 3-D pre-stack migration, without the need to make compromises with respect to the underlying principles. The target-oriented shot record migration algorithm is tested on simulated 3-D marine surveys (both synthetic and scale model data) for simple subsurface models. The results illustrate the good imaging properties for the cross-line direction and the excellent imaging properties for the in-line direction.

SAMENVATTING

Dit proefschrift behandelt theoretische en praktische aspekten van een belangrijke seismische inversietechniek, de zogenaamde **pre-stack migratie** (letterlijk: migratie vóór stapelen). In tegenstelling tot post-stack migratie, waarin na stack pseudo zero-offset metingen geïnverteerd worden, worden in pre-stack migratie de originele seismische experimenten met meervoudige offsets geïnverteerd, uitgaande van een globale beschrijving van de ondergrond (het geologische 'makro model'). Het resultaat bestaat uit een gedetailleerde **twee-dimensionale** (2-D) of **drie-dimensionale** (3-D) struktuur-afbeelding van de ondergrond (het 'mikro model'), uitgedrukt in de 'groothoek' zero-offset reflektiviteit.

In hoofdstuk I worden in het kort enkele **algemene aspekten van seismische inversie** besproken. Op theoretische en praktische gronden wordt geargumenteerd dat pre-stack migratie dient te worden uitgevoerd per seismisch experiment (dus géén 'gemeenschappelijk-middelpunt' of 'gemeenschappelijke-offset' kompromissen), gevolgd door een echte stack (stapeling) per gemeenschappelijk afbeeldingspunt.

In hoofdstuk II wordt de voorgestelde methode, te weten, **migratie per seismisch experiment**, uitgebreider besproken. Er wordt aangetoond dat

- niet-hyperbolische responsie-krommen zijn toegestaan,
- korrekte amplitudes kunnen worden verkregen,
- iedere data-acquisitie konfiguratie is toegestaan,
- kleine fouten in het makro model van de ondergrond kunnen worden gekompenseerd,
- ieder type golfvergelijking kan worden toegepast (éénweg, tweeweg, volledig elastisch, enz.),
- vele varianten kunnen worden ontworpen, afhankelijk van het migratie-doel (hoekafhankelijke reflektie, volledige datasets op geologische grenslagen, enz.).

In hoofdstuk III wordt een overzicht gegeven van verscheidene theoretische aspekten van de **akoestische éénweg golfvergelijkingen.** Tevens worden toepassingen in pre-stack migratie besproken. Er wordt gekonkludeerd dat de éénweg-methode geldig is voor sub-kritische primaire golven in 1-D, 2-D en

3-D inhomogene makro modellen. Tevens wordt aangetoond dat pre-stack migratie, gebaseerd op de akoestische **WKBJ** éénweg golfvergelijkingen, geldig is voor zowel sub-kritische als kritische 'primaire' golven ('keerpunt' effekten) in 1-D inhomogene makro modellen.

In hoofdstuk IV wordt een overzicht gegeven van verscheidene theoretische aspekten van de **akoestische tweeweg golfvergelijking.** Tevens worden toepassingen in pre-stack migratie besproken. Er wordt gekonkludeerd dat de tweeweg-methode geldig is voor 1-D, 2-D en 3-D inhomogene makro modellen van de ondergrond. Pre-stack migratie, gebaseerd op de akoestische tweeweg golfvergelijking, behandelt op juiste wijze kritische effekten en meervoudige reflekties indien het makro model van de ondergrond nauwkeurig bekend is. Voor geëffende makro modellen mag tot grote openingshoeken een goede behandeling van primaire golven verwacht worden.

In hoofdstuk V wordt een overzicht gegeven van verscheidene theoretische aspekten van de **volledig elastische tweeweg golfvergelijking.** Tevens worden toepassingen in pre-stack migratie besproken. Er wordt gekonkludeerd dat de volledig elastische tweeweg methode geldig is voor 1-D en 2-D inhomogene makro modellen en dat de methode kan worden uitgebreid voor 3-D inhomogene makro modellen. Pre-stack migratie, gebaseerd op de volledig elastische golf-vergelijking, behandelt op juiste wijze meervoudige reflekties en golf-konversie indien het (volledig elastische) makro model van de ondergrond nauwkeurig bekend is. Voor geëffende makro modellen mag tot grote openings-hoeken een goede behandeling van primaire golven verwacht worden.

In hoofdstuk VI worden verscheidene **praktische aspekten van 3-D pre-stack migratie** besproken. In vele praktische situaties zijn seismische interpreta-toren vooral geïnteresseerd in een hoge resolutie afbeelding van een specifiek 'doelgebied'. Dit betekent dat realistische verwerkingstijden kunnen worden verkregen door 'doelgerichte' 3-D pre-stack migratie toe te passen, zonder dat hiervoor kompromissen met betrekking tot de onderliggende principes gesloten hoeven te worden. Het 'doelgerichte' migratie algoritme, toegepast per seis-misch experiment, is getest aan de hand van gesimuleerde 3-D zee-datasets (zowel syntetische- als schaalmodel-metingen) voor eenvoudige ondergrond-modellen. De resultaten illustreren de goede afbeeldingseigenschappen in de richting loodrecht op de seismische lijnen en de uitstekende afbeeldings-eigenschappen in de richting parallel aan de seismische lijnen.

CURRICULUM VITAE

van Kees Wapenaar

7 februari 1956	: Geboren te Vlaardingen
1962-1967	: Lager onderwijs te Vlaardingen
1968-1974	: Middelbare schoolopleiding te Vlaardingen (Atheneum)
1974-1981	: Studie voor natuurkundig ingenieur aan de Technische Hogeschool te Delft
1978-1979	: Kandidaatsonderzoek op het gebied van buitenlucht-akoestiek. (verslag: Geveldiffraktie; de invloed van gevelhoogte en gevelstruktuur op de reflektie van geluid).
1979-1981	: Afstudeeronderzoek op het gebied van echo-akoestiek. (verslag: Rekonstruktie van de geluidsnelheid-verdeling van een gelaagd systeem bestaande uit meerdere niet-plan-parallelle lagen); student-assistent bij het natuurkundig praktikum.
1981-1982	: Gesubsidieerd onderzoek (in het verlengde van het afstudeeronderwerp) te Delft en Houston.
1982-1985	: Promotie-onderzoek aan de Technische Hogeschool te Delft.
vanaf 1986	: Wetenschappelijk medewerker bij het "TRITON" projekt (onderzoeksprojekt op het gebied van drie-dimensionale pre-stack migratie) aan de Technische Hogeschool te Delft.

STELLINGEN

behorende bij het proefschrift

"Pre-stack migration in two and three dimensions"

1. Migratie per fysisch experiment is een veelbelovende seismische inversie-techniek. Met name de drie-dimensionale toepassing biedt perspektief.

2. Tweeweg golfveldextrapolatie langs de diepte-koördinaat (zowel akoestisch als volledig elastisch) is meer geschikt voor inversie dan voor simulatie van seismische data.

3. De akoestische tweeweg golfveldextrapolatie-operator kan na een eenvoudige modifikatie ook worden toegepast in laminair stromende media.

4. Voor extrapolatie van menselijk gedrag is geen eenduidig bemonsterings-kriterium vast te stellen.

5. De vraag of er in het heelal een tweede beschaving bestaat is prematuur: het bestaan van de eerste is nog niet bewezen.

6. Van de betrokkenen bij het zogenaamde 'Star Wars' projekt valt nauwelijks te verwachten dat zij tot inkeer zullen komen. De hoop dient gevestigd te worden op de in ruime mate in dit projekt toegepaste kunstmatige intelligentie.

7. Een cycloop met encyclopedische kennis heeft een ruimere blik dan men op grond van zijn uiterlijk zou vermoeden.

8. Ons model van de wereld is sterker verfijnd sinds Einstein dan ons begrip sinds de batavieren.

9. De mogelijkheden der techniek zijn begrensd. Zo valt er niet te verwachten dat er voor de piano een korrektietoets zal worden uitgevonden.

10. Een promovendus kan in zijn of haar vakantie volstaan met een 40-urige werkweek.

11. Descartes had aan zijn stelling: 'ik denk, dus ik besta' nog kunnen toevoegen: 'ik schrijf, dus ik blijf'.

6 februari 1986

Kees Wapenaar